EVOLUTION AND PALEOBIOLOGY OF CENOZOIC PLANKTONIC FORAMINIFERA AND COCCOLITHOPHORES

by

WEIMIN SI

A dissertation submitted to the

School of Graduate Studies

Rutgers, The State University of New Jersey

In partial fulfillment of the requirements

For the degree of

Doctor of Philosophy

Graduate Program in Geological Sciences

Written under the direction of

Marie-Pierre Aubry

And approved by

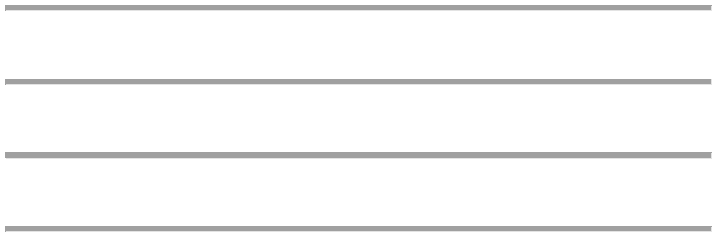

New Brunswick, New Jersey

October 2018

ABSTRACT OF THE DISSERTATION

EVOLUTION AND PALEOBIOLOGY OF CENOZOIC PLANKTONIC FORAMINIFERA AND COCCOLITHOPHORES, PALEOCEANOGRPAHIC APPLICATIONS

by

WEIMIN SI

Dissertation Directors:

Marie-Pierre Aubry

William A. Berggren

In this study, I have examined the micro- and macroevolutionary changes in planktonic foraminifera and coccolithophores on different timescales. I first studied the taxonomy, stratigraphy and evolution of the Middle Miocene planktonic foraminifera *Fohsella*, an iconic example of gradual morphologic evolution in marine planktonic species. In contrast to earlier studies that have focused on the gross morphology as embodied by the projection of the edge view of tests, I have analyzed multiple phenotypic traits of the evolving lineage and found that traits did not evolve in concert. The evolution of the lineage is a mosaic combination of different evolutionary modes for different traits, suggesting that interpretations based on "pure" morphologic and "overall shape" measurements, may significantly underestimate the dynamics of foraminiferal evolution. On shorter timescales, microfossils provide empirical evidence on adaptations of species to rapid ocean warming and acidification. I examined changes in vital effects in

photosymbiont-bearing planktonic foraminifera during the Paleocene-Eocene Thermal Maximum (ca. 56 Ma). The $\delta^{13}C$-size data indicate divergent changes in $\delta^{13}C$ vital effects in high- versus mid-latitude populations, due likely to different responses in photosymbiotic activities. Combined $\delta^{18}O$-size data and isotopic ranking indicates that some surface dwellers may have experienced depth migrations due to extreme sea surface temperatures. Species with flexible depth distribution were capable of adapting to rapid warming by vertical migration in the upper ocean, while populations restricted to near surface may have undergone temporal and/or regional collapse during peak warming. From a paleo-proxy perspective, biologic responses during the PETM have obscured palaeoceanographic signatures both regionally and globally. On multi-Myr scale, macro-evolutionary changes in planktonic calcifiers may have also affected the ocean's carbonate budget. I examined the changes in carbonate accumulation, production and dissolution of planktonic foraminifera and coccoliths. Mass Accumulation Rate shows that carbonate accumulation has decreased significantly over the last 15 Myr even though carbonate preservation has improved. A further separation of the bulk carbonate into foraminiferal and coccolith fractions indicates relatively constant foraminiferal contribution over time but significantly higher coccolith production in the Miocene. Given the constraint of relatively small changes in the carbonate compensation depth, carbonate accumulation in the deep-sea has decreased, suggesting reduced alkalinity input to the ocean since the Middle Miocene.

Acknowledgements

I wish to thank fellow graduate students, Firat Gocmenoglu, David Bord, Christian Putra, Chris Lombardi, César Sequeira, and Linda Martin, and micropaleontology lab assistant Sarah Klingler. Without your help, I would not know how to fill out a tax form and how to resolve my health insurance issues. Without your friendship, I would not have enjoyed life at Rutgers as I have experienced it.

I give special thanks to David Bord for helpful discussion throughout my graduate studies. Thanks for helping me build up the universal stage for morphometric measurements and for discussions on coccolith taxonomy and stratigraphy.

I also wish to thank Prof. James D. Wright and Kenneth G. Miller for discussions on the PETM study and on stable isotope analyses. Without your help, I would not have been able to finish my study on the PETM planktonic foraminifera. I also thank Jim Browning and Rick Mortlock who provided essential assistance in the lab and in sampling. I would like to thank Luc Beaufort for participation as committee members and providing critical reviews of this thesis.

Finally, my special thanks go to Professors Marie-Pierre Aubry, William Berggren, and Yair Rosenthal. Without their constant guidance and encouragements, I would not have completed this dissertation. Much of the content of this thesis came as a result of lengthy, and enjoyable conversations with them.

Table of Contents

List of Figures

Chapter 2

Chapter 3

Chapter 4

Chapter 5

List of tables

Chapter 2

Chapter 3

Chapter 4

Chapter 5

List of Plates

Chapter 4

Chapter 1

Introduction to the Dissertation

1.1 Objective

Microfossils form invaluable archives of the biologic and geochemical evolution of the ocean. Shells of planktonic foraminifera and coccolithophores accumulate on the seafloor over millions of years and, despite their small size, have built up the most continuous and extended paleontological and geochemical Cenozoic records. Shape study on these planktonic calcifiers (Arnold, 1983; Bralower and Parrow, 1996; Hull and Norris, 2009; Lazarus et al., 1995; Malmgren et al., 1983; Pearson and Ezard, 2016) answer questions as to which mode (Phyletic Gradualism, Random Walk, Punctuated Equilibria) best describe morphologic evolution of fossil species on timescales of several hundreds of thousands years (Eldredge and Gould, 1972; Grey et al., 2008; Hopkins and Lidgard, 2012; Hunt et al., 2015). On timescales of a few thousands of years, microfossil records have the potential to provide empirical evidence on adaptations of species to rapid climatic changes that may serve as analogues to the current ocean warming and acidification (Gibbs et al., 2006; Kelly et al., 1996; Speijer et al., 2012). On multi-Myr timescales, coccoliths and foraminiferal shells act as the major alkalinity sink of the ocean (Dunne et al., 2012; Milliman, 1993; Ridgwell and Zeebe, 2005) and therefore the production, preservation and accumulation of their shells on the seafloor inform long-term evolution of the carbonate cycle. Studies on microfossils, therefore, allow a synthetic approach to understand the co-evolution of organisms and their surroundings.

Introduced 43 years ago as an alternative to phyletic gradualism, the theory of Punctuated Equilibrium proposes that most morphologic traits in the fossil record are relatively stable over the course of a lineage's existence except for geologically rapid speciation events called cladogenetic events (Eldredge and Gould, 1972). Many aspects of this claim have remained contentious. In fact, the same datasets have supported opposite interpretations (Eldredge and Gould, 1988; Sheldon, 1987; Smith, 1987; Van Bocxlaer et al., 2008; Williamson, 1981). These debates, however, have brought to the paleontologists' attention the possibility that different evolutionary modes may have contributed to the evolution of species, whose relative importance has to be resolved (Hunt, 2007; Hunt et al., 2015).

Early studies on the morphologic evolution of fossil species have primarily focused on gross morphology, i.e. summarized as the principal component of multivariate measurements (Kellogg and Hays, 1975; Lazarus et al., 1995; Lohmann, 1983; Malmgren et al., 1983), implicitly assuming that this is a reliable representation of the evolutionary history of a lineage. Recent studies based on statistical analyses of multiple traits have discovered, however, that evolutionary modes within a lineage, such as directional trends, random walk, and stasis, can vary among morphologic traits (Hopkins and Lidgard, 2012; Hunt et al., 2015) as well as over geographic and temporal ranges (Grey et al., 2008). These findings raise the concern that gross morphology may be insufficient to describe the evolutionary history of a species.

In Chapters 2 and 3, I examine the taxonomy, stratigraphy and evolution of the Middle Miocene planktonic foraminifera *Fohsella*, an iconic example of gradual evolution. In contrast to earlier studies that have mainly focused on outline of the edge view of the test, I analyze multiple phenotypic traits including shell size, shape of spiral view, coiling direction and habitat depth (as inferred from isotopic data). These traits are selected in this study because their taxonomic, biologic and/or ecologic properties are better understood than the edge-view outline is. Quantifying changes in these traits should provide more readily interpretable information on evolutionary patterns, while the sources of evolutionary variations are more easily diagnosed. In general, the data suggest that traits did not evolve in concert. The timing and pattern of different traits are different. The evolution of the *Fohsella* lineage consists in a mosaic combination of different evolutionary modes for different traits, implying that interpretations based on "overall shape" significantly underestimate the dynamics of foraminiferal evolution.

The study on Middle Miocene *Fohsella* also suggests that the evolution of certain traits (i.e. changes in coiling direction) can occur in a geologic instant (below the sampling resolution of ~10 kyrs) even in stable open ocean environments. If so, one important question is how rapidly can planktonic species adapt to future climatic changes and what strategies will they develop? Studies on past climatic perturbations such as the Paleocene-Eocene Thermal Maximum event (PETM) may provide some insight into these questions.

The PETM is regarded as a possible geologic analogue of current anthropogenic climate change. It consists of an abrupt global warming of ~6˚C (Thomas et al., 2002; Zachos et

al., 2007) due to the rapid introduction of a large mass (>1200~4500 GtC) of greenhouse gas (Dickens et al., 1995; Zachos et al., 2005) within probably a few thousand years (Zeebe et al., 2016). Paleontological studies show that evolution and migrations occurred in both terrestrial and marine realms during the PETM in association with the environmental perturbations (Aubry, 1998; Bujak and Brinkhuis, 1998; Gibbs et al., 2006; Gingerich, 2006; Kelly et al., 1998; Kelly et al., 1996; McInerney and Wing, 2011; Speijer et al., 2012; Thomas, 1998), providing opportunities to evaluate the adaptive limitations and strategies of species to abrupt global warming.

In Chapter 4, I present evidence of changes in vital effects in photosymbiont-bearing planktonic foraminifera during the PETM (ca. 56 Ma). The $\delta^{13}C$-size data of four surface-dwelling lineages indicate divergent changes in $\delta^{13}C$ vital effects in high- versus mid-latitude populations, due likely to different responses in photosymbiotic activity. Combined $\delta^{18}O$-size data and isotopic ranking indicates that some surface dwellers may have experienced depth migrations, due to extreme surface temperatures. Species with flexible depth distribution were capable of adapting to rapid warming by vertical migration in the water column, while populations restricted to the near surface waters may have undergone temporal and/or regional collapse during peak warming. From a paleo-proxy perspective, biologic responses during the PETM have obscured paleoceanographic signatures both regionally and globally. The long-held view of low latitudinal temperature gradient during the PETM (Zachos et al., 2007) may be an artefact of a temperature threshold set by the upper-thermal limit of planktonic foraminifera.

In contrast to the microevolutionary processes that I have focused on in Chapters 2, 3 and 4, potential macroevolutionary changes in planktonic species not only matter to the survival of species, but also play a critical role in global geochemical cycles. The rise and ecological success of pelagic calcifiers during the Mesozoic have shifted the locus of carbonate accumulation from shallow water platforms and continental shelves to the open ocean. The result is that biologically driven carbonate production and subsequent deposition in the deepsea exert a strong control over the ocean's carbonate chemistry (Broecker, 1971; Ridgwell and Zeebe, 2005). In Chapter 5, I investigate how coccolithophores carbonate production has changed since the Late Miocene, and how this change has affected our understanding of the carbonate cycle as the Earth descended into the Ice-house world of the late Neogene.

The late Neogene climate is characterized by cooling steps that culminated in bi-polar glaciations in the Pleistocene (2.7–0 Ma). The origin of this long-term cooling, however, remains unresolved. One hypothesis suggests that active orogeny such as the uplift of the Himalayas has resulted in broad exposures of fresh rocks to weathering, leading to the drawdown of pCO_2 through enhanced weathering (Raymo, 1991; Raymo et al., 1988). The weathering hypothesis, however, raises a critical debate — enhanced weathering over multi-Myr, as interpreted from the $\delta^{87}Sr$ isotopes of marine carbonates, could have depleted the atmospheric CO_2 (Berner and Caldeira, 1997). This therefore challenges the widely-accepted view that the weathering process acts as a negative feedback for the long-term stabilization of Earth's climate (Walker et al., 1981).

In a steady state ocean, weathering alkalinity input to the ocean should be balanced by carbonate burial in the deepsea (Broecker, 2003). As a result, the Carbonate Compensation Depth (CCD) has been conventionally used to constrain the burial flux of carbonate. A deeper CCD is interpreted as enhanced carbonate burial, implying higher weathering alkalinity input (Raymo et al., 1988). This interpretation of the CCD, however, implicitly assumes that carbonate production in the surface ocean is constant over time.

In order to better constrain the biogenic $CaCO_3$ production in the euphotic zone and $CaCO_3$ dissolution at depth, I generate Mass Accumulation Rates of carbonate from 30 deepsea cores with a global coverage. Systematic comparison of pelagic sediments from shallow sites, where minimum dissolution is expected, to deep sites, where dissolution has taken its toll, suggests that MAR of carbonate have decreased significantly over the last 15 Myr even though carbonate preservation has improved. The apparent contradiction between higher $CaCO_3$ accumulation and stronger dissolution during the Late Miocene reflects high carbonate production at the time. A further separation of the bulk carbonate into foraminiferal and coccolith fractions indicates relatively constant foraminiferal contribution over time but significantly higher coccolith production in the Miocene. Most importantly, with the constraints of global averaged CCD records, the net accumulation of pelagic carbonate appears to have declined over the course of the late Neogene, suggesting reduced weathering alkalinity input ~15 Ma, as opposed to the weathering hypothesis (Raymo et al., 1988).

In summary, morphologic, ecologic and geochemical variations in planktonic foraminifera and coccolithophores have documented evolutionary changes of marine planktons on various timescales and revealed potential links of species evolution with changing climate and ocean chemistry. However, numerous questions remain to be answered. For instance, what has caused the coevolution of coccolithophores and carbonate during the late Neogene? From a paleobiologic perspective, was the forcing biotic or abiotic? If there was a long-term abiotic forcing, is it temperature or pCO_2 or other factors (Aubry, 2007; Bolton et al., 2016; Falkowski and Oliver, 2007; Schmidt et al., 2006)? From an oceanographic perspective, what is the significance of these alternatives? To probe into these questions, greater efforts must be made in the future to better integrate micropaleontological and chemical oceanographical understandings.

1.2 References

Arnold, A. J., 1983, Phyletic Evolution in the Globorotalia-Crassaformis (Galloway and Wissler) Lineage - a Preliminary-Report: Paleobiology, v. 9, no. 4, p. 390-397.

Aubry, M.-P., 1998, Early Paleogene calcareous nannoplankton evolution: a tale of climatic amelioration: Late Paleocene Early Eocene climatic and biotic events in the marine and terrestrial records, edited by: Aubry, MP, Lucas, SG, and Berggren, WA, p. 158-203.

Aubry, M. P., 2007, A major Pliocene coccolithophore turnover: Change in morphological strategy in the photic zone: Large Ecosystem Perturbations: Causes and Consequences, v. 424, p. 25-51.

Berner, R. A., and Caldeira, K., 1997, The need for mass balance and feedback in the geochemical carbon cycle: Geology, v. 25, no. 10, p. 955-956.

Bolton, C. T., Hernández-Sánchez, M. T., Fuertes, M.-A., González-Lemos, S., Abrevaya, L., Mendez-Vicente, A., Flores, J.-A., Probert, I., Giosan, L., and Johnson, J., 2016, Decrease in coccolithophore calcification and CO 2 since the middle Miocene: Nature communications, v. 7, p. 10284.

Bralower, T. J., and Parrow, M., 1996, Morphometrics of the Paleocene coccolith genera Cruciplacolithus, Chiasmolithus, and Sullivania: a complex evolutionary history: Paleobiology, v. 22, no. 3, p. 352-385.

Broecker, W., 2003, The oceanic CaCO3 cycle: Treatise on Geochemistry, v. 6, p. 625.

Broecker, W. S., 1971, A kinetic model for the chemical composition of sea water: Quaternary Research, v. 1, no. 2, p. 188-207.

Bujak, J. P., and Brinkhuis, H., 1998, Global warming and dinocyst changes across the Paleocene/Eocene Epoch boundary: Late Paleocene-early Eocene climatic and biotic events in the marine and terrestrial records, edited by: Aubry, M.-P., Lucas, S. G., and Berggren, W. A., Columbia University Press, New York, p. 277-295.

Dickens, G. R., Oneil, J. R., Rea, D. K., and Owen, R. M., 1995, Dissociation of Oceanic Methane Hydrate as a Cause of the Carbon-Isotope Excursion at the End of the Paleocene: Paleoceanography, v. 10, no. 6, p. 965-971.

Dunne, J. P., Hales, B., and Toggweiler, J. R., 2012, Global calcite cycling constrained by sediment preservation controls: Global Biogeochemical Cycles, v. 26, no. 3.

Eldredge, N., and Gould, S. J., 1972, Punctuated equilibria: an alternative to phyletic gradualism: Models in Paleobiology, p. 82-115.

Eldredge, N., and Gould, S. J., 1988, Punctuated equilibrium prevails: Nature, v. 332, no. 6161, p. 211.

Falkowski, P. G., and Oliver, M. J., 2007, Mix and match: how climate selects phytoplankton: Nature Reviews Microbiology, v. 5, no. 10, p. 813.

Gibbs, S. J., Bown, P. R., Sessa, J. A., Bralower, T. J., and Wilson, P. A., 2006, Nannoplankton extinction and origination across the Paleocene-Eocene Thermal Maximum: Science, v. 314, no. 5806, p. 1770-1773.

Gingerich, P. D., 2006, Environment and evolution through the Paleocene-Eocene thermal maximum: Trends Ecol Evol, v. 21, no. 5, p. 246-253.

Grey, M., Haggart, J. W., and Smith, P. L., 2008, Variation in evolutionary patterns across the geographic range of a fossil bivalve: Science, v. 322, no. 5905, p. 1238-1241.

Hopkins, M. J., and Lidgard, S., 2012, Evolutionary mode routinely varies among morphological traits within fossil species lineages: Proc Natl Acad Sci U S A, v. 109, no. 50, p. 20520-20525.

Hull, P. M., and Norris, R. D., 2009, Evidence for abrupt speciation in a classic case of gradual evolution: Proc Natl Acad Sci U S A, v. 106, no. 50, p. 21224-21229.

Hunt, G., 2007, The relative importance of directional change, random walks, and stasis in the evolution of fossil lineages: Proceedings of the National Academy of Sciences, v. 104, no. 47, p. 18404-18408.

Hunt, G., Hopkins, M. J., and Lidgard, S., 2015, Simple versus complex models of trait evolution and stasis as a response to environmental change: Proc Natl Acad Sci U S A, v. 112, no. 16, p. 4885-4890.

Kellogg, D. E., and Hays, J. D., 1975, Microevolutionary patterns in late Cenozoic Radiolaria: Paleobiology, v. 1, no. 2, p. 150-160.

Kelly, D. C., Bralower, T. J., and Zachos, J. C., 1998, Evolutionary consequences of the latest Paleocene thermal maximum for tropical planktonic foraminifera: Palaeogeography Palaeoclimatology Palaeoecology, v. 141, no. 1-2, p. 139-161.

Kelly, D. C., Bralower, T. J., Zachos, J. C., Silva, I. P., and Thomas, E., 1996, Rapid diversification of planktonic foraminifera in the tropical Pacific (ODP Site 865) during the late Paleocene thermal maximum: Geology, v. 24, no. 5, p. 423-426.

Lazarus, D., Hilbrecht, H., Spencercervato, C., and Thierstein, H., 1995, Sympatric Speciation and Phyletic Change in Globorotalia Truncatulinoides: Paleobiology, v. 21, no. 1, p. 28-51.

Lohmann, G., 1983, Eigenshape analysis of microfossils: a general morphometric procedure for describing changes in shape: Journal of the International Association for Mathematical Geology, v. 15, no. 6, p. 659-672.

Malmgren, B. A., Berggren, W. A., and Lohmann, G. P., 1983, Evidence for Punctuated Gradualism in the Late Neogene Globorotalia-Tumida Lineage of Planktonic-Foraminifera: Paleobiology, v. 9, no. 4, p. 377-389.

McInerney, F. A., and Wing, S. L., 2011, The Paleocene-Eocene Thermal Maximum: A perturbation of carbon cycle, climate, and biosphere with implications for the future: Annual Review of Earth and Planetary Sciences, v. 39, p. 489-516.

Milliman, J. D., 1993, Production and Accumulation of Calcium-Carbonate in the Ocean - Budget of a Nonsteady State: Global Biogeochemical Cycles, v. 7, no. 4, p. 927-957.

Pearson, P. N., and Ezard, T. H. G., 2016, Evolution and speciation in the Eocene planktonic foraminifer Turborotalia: Paleobiology, v. 40, no. 01, p. 130-143.

Raymo, M. E., 1991, Geochemical evidence supporting TC Chamberlin's theory of glaciation: Geology, v. 19, no. 4, p. 344-347.

Raymo, M. E., Ruddiman, W. F., and Froelich, P. N., 1988, Influence of Late Cenozoic Mountain Building on Ocean Geochemical Cycles: Geology, v. 16, no. 7, p. 649-653.

Ridgwell, A., and Zeebe, R. E., 2005, The role of the global carbonate cycle in the regulation and evolution of the Earth system: Earth and Planetary Science Letters, v. 234, no. 3-4, p. 299-315.

Schmidt, D. N., Lazarus, D., Young, J. R., and Kucera, M., 2006, Biogeography and evolution of body size in marine plankton: Earth-Science Reviews, v. 78, no. 3-4, p. 239-266.

Sheldon, P. R., 1987, Parallel gradualistic evolution of Ordovician trilobites: Nature, v. 330, no. 6148, p. 561-563.

Smith, J. M., 1987, Darwinism stays unpunctured: Nature, v. 330, no. 6148, p. 516-516.

Speijer, R. P., Scheibner, C., Stassen, P., and Morsi, A. M. M., 2012, Response of Marine Ecosystems to Deep-Time Global Warming: A Synthesis of Biotic Patterns across the Paleocene-Eocene Thermal Maximum (Petm): Austrian Journal of Earth Sciences, v. 105, no. 1, p. 6-16.

Thomas, D. J., Zachos, J. C., Bralower, T. J., Thomas, E., and Bohaty, S., 2002, Warming the fuel for the fire: Evidence for the thermal dissociation of methane hydrate during the Paleocene-Eocene thermal maximum: Geology, v. 30, no. 12, p. 1067-1070.

Thomas, E., 1998, Biogeography of the late Paleocene benthic foraminiferal extinction: Late Paleocene-Early Eocene climatic and biotic events in the marine and terrestrial records, p. 214-243.

Van Bocxlaer, B., Damme, D. V., and Feibel, C. S., 2008, Gradual versus punctuated equilibrium evolution in the Turkana basin molluscs: evolutionary events or biological invasions?: Evolution: International Journal of Organic Evolution, v. 62, no. 3, p. 511-520.

Walker, J. C., Hays, P., and Kasting, J. F., 1981, A negative feedback mechanism for the long-term stabilization of Earth's surface temperature: Journal of Geophysical Research: Oceans, v. 86, no. C10, p. 9776-9782.

Williamson, P., 1981, Palaeontological documentation of speciation in Cenozoic molluscs from Turkana Basin: Nature, v. 293, no. 5832, p. 437.

Zachos, J. C., Bohaty, S. M., John, C. M., McCarren, H., Kelly, D. C., and Nielsen, T., 2007, The Palaeocene-Eocene carbon isotope excursion: constraints from individual shell planktonic foraminifer records: Philos Trans A Math Phys Eng Sci, v. 365, no. 1856, p. 1829-1842.

Zachos, J. C., Rohl, U., Schellenberg, S. A., Sluijs, A., Hodell, D. A., Kelly, D. C., Thomas, E., Nicolo, M., Raffi, I., Lourens, L. J., McCarren, H., and Kroon, D., 2005, Rapid acidification of the ocean during the Paleocene-Eocene thermal maximum: Science, v. 308, no. 5728, p. 1611-1615.

Zeebe, R. E., Ridgwell, A., and Zachos, J. C., 2016, Anthropogenic carbon release rate unprecedented during the past 66 million years: Nature Geoscience, v. 9, no. 4, p. 325.

Chapter 2

Taxonomy, stratigraphy and phylogeny of the Middle Miocene *Fohsella* Lineage: geometric morphometric evidence

Paper chapter:

Si, W., and Berggren, W. A. (2017). Taxonomy, Stratigraphy and Phylogeny of the Middle Miocene Fohsella Lineage: Geometric Morphometric Evidence. Journal of Foraminiferal Research, 47(4), 310-324.

2.1 Abstract

The taxonomy and phylogeny of the planktonic foraminifera *Fohsella* lineage has been controversial for nearly 50 years despite its widespread application in Middle Miocene stratigraphy. We have re-examined type specimens of this lineage together with specimens from a continuous deep-sea record (Ocean Drilling Program Site 806, Ontong Java Plateau, western equatorial Pacific Ocean) with an astronomic chronology. Landmark-based geometric morphometry is employed to visualize and quantify morphologic variation within this lineage. Combined morphologic and stratigraphic data help clarify the evolutionary occurrence of diagnostic traits that characterize problematic species *praefohsi* and "*praefohsi*", resulting in a revised taxonomy and phylogeny of the lineage. We emphasize the importance of biometric studies of populations from continuous geologic records in establishing taxonomy and phylogeny of planktonic foraminifera. Over-emphasis on the importance of type specimens as reference points in

delineating various evolutionary stages of the *Fohsella* lineage in the past has resulted in inaccurate phylogenetic reconstructions.

2.2 Introduction

The *Fohsella* lineage evolved during the Early to Middle Miocene (~14.2–11.7 Ma, Wade et al., 2011, p. 132–133). The stratigraphic value of this lineage was first recognized by Cushman and Stainforth (1945) and exploited by Bolli (1950, 1957) and Blow and Banner (1966), based on stratigraphic sequences in Trinidad, the Gulf Coast, Venezuela and Barbados. According to Bolli and Saunders (1985), the principal morphologic changes that characterize the evolution of fohsellids include: 1) doubling in size from ~0.3 mm to ~0.7 mm; 2) development of a peripheral keel from the non-carinate taxon *peripheroacuta* Blow and Banner (Fig. 1.1) to partially keeled *praefohsi* Blow and Banner (Fig. 1.2), and to the fully keeled *fohsi* Cushman and Ellisor (Fig. 1.3), *lobata* Bermúdez (Fig. 1.4) and *robusta* Bolli (Figs. 1.5, 1.6); 3) distinct lobate periphery in *lobata*; and 4) increase in the number of chambers in the last whorl, from 5–6 in *peripheroacuta* and *fohsi* to 6 ½ –8 in *praefohsi*, *lobata* and *robusta*.

The taxonomy and phylogeny of this lineage remains controversial (Blow and Banner, 1966; Bolli and Saunders, 1985; Berggren, 1993; Wade et al., 2011) despite its widespread use in stratigraphic correlation for nearly a half century (Bolli, 1957; Berggren et al., 1995; Wade et al., 2011). Two phylogenies have been proposed for the morphologic transition from the early representative taxon *peripheroacuta* (FAD: 14.24

Ma, Wade et al., 2011) to the end-member *robusta* (FAD: 13.13 Ma, Wade et al., 2011) (Fig. 2A, B).

The two interpretations differ primarily in the phylogenetic position of *praefohsi*, a taxon that was originally erected by Blow and Banner (1966) as an intermediate form between non-carinate *peripheroacuta* and the keeled *fohsi*. This often-cited evolutionary scenario (Fig. 2A) suggests that the evolution of *peripheroacuta* without keel to (1) partially keeled margin on the final or last two chambers in *praefohsi* (2), followed by the development of a peripheral keel in the last whorl characteristic of *fohsi* (3), followed by the occurrence of the more advanced form *lobata*, which developed a strongly lobate cockscomb-like equatorial periphery. This phylogenetic scenario has been widely applied in biostratigraphy (e.g., Kennett and Srinivasan, 1983).

However, based on the study of the *praefohsi* holotype, Bolli and Saunders (1985, p. 215) commented that "the last two chambers of the fairly large holotype are already of the elongate cockscomb shape, typical of *lobata*." They therefore suggested that *praefohsi* represents a transitional form between *fohsi* and *lobata*, rather than being intermediate between *peripheroacuta* and *fohsi* (Fig. 2B).

This disagreement in taxonomic subdivision and phylogenetic classification, as we review below in detail, arose from 1) the somewhat subjective use of different morphologic traits as primary characters in taxonomic subdivision, and 2) the lack of robust age control on the stratigraphic occurrence of different morphotypes. Bolli (1950)

and Bolli and Saunders (1985) distinguished successive subspecies primarily based on chamber shape (from rounded to acute to lobate axial test periphery). In contrast Blow and Banner (1966) considered that "The stages of appearance and progressive development of the carina should be taken as the most important single morphocharacter for formal taxonomic distinction of the components of the lineage." (op. cit. p. 296).

In this paper, we try to clarify the taxonomy and phylogeny of the younger part of the *Fohsella* lineage (*perpheroacuta, praefohsi, fohsi*, *lobata* and r*obusta*) based on a continuous deep-sea record from the Western Pacific, using a newly developed astronomic chronology (Holbourn et al., 2013) that is largely independent of the planktonic foraminifera biostratigraphic interpretations. A new phylogeny is proposed (Fig. 2C) based on the stratigraphic occurrence of key morphologic characters (stratophenetics). We draw attention to our acceptance/usage of the formalization of subseries as a hierarchical category within series (and the consequent capitalization of subseries units, as Lower/Early, Upper/Late) as cogently argued with Cartesian clarity by Aubry (2016; see also Van Couvering et al., 2015).

2.3 Historical review of Fohsellid taxonomy and phylogeny

We begin by reviewing the historical discussion on fohsellid subspecies in Bolli (1950) and Blow and Banner (1966), the two primary studies that framed the taxonomy and phylogeny of fohsellids.

Bolli (1950) first included four successive subspecies now included in fohsellids: *Globorotalia fohsi barisanensis* LeRoy, *G. fohsi fohsi* (*sensu stricto*) Cushman and Ellisor, *G. fohsi lobata* Bermúdez, and *G. fohsi robusta* Bolli. The earliest representative *G. fohsi barisanensis* LeRoy is "rounded in the peripheral margin, sometimes subacute in the adult chambers" (op. cit. p. 88). This description is very similar to that of *peripheroronda* and *peripheroacuta* Blow and Banner (1996). The taxon *fohsi* was suggested to have evolved directly from *barisanensis* and "the periphery is slightly rounded to subacute in the early chambers and becomes acute but usually not keeled in the mature specimen" (op. cit. p. 88). At stratigraphically higher levels, Bolli (1950) recognized another more advanced form, *G. fohsi lobata*, in which "the peripheral margin is acute, the last chambers often with a faint keel" and with a "strongly lobate cockscomb-like" periphery (op. cit. p. 89).

This lineage delineation of Bolli (1950) was questioned by Blow and Banner (1966) in two respects. First, based on their examination of LeRoy's type material, Blow and Banner (1966) considered that *barisanensis* is a senior synonym that includes multiple fohsellid morphotypes. Second, they argued that "the degree of peripheral lobulation that developed within the *fohsi–lobata* series varies without direct relation to stratigraphic horizon" and "populations from stratigraphically earlier horizons are frequently just as lobate peripherally (or even more so) than those from stratigraphically later horizons" (op. cit. p. 286). Therefore, Blow and Banner (1966) established their taxonomic and stratigraphic subdivision based on the "progressive development of an imperforate keel,

without regard to the degree of lobulation exhibited by the last few chambers of the larger specimens" (op. cit. p. 286).

Blow and Banner (1966) recognized four taxa, in stratigraphic order: 1) *peripheroacuta* Blow and Banner, in which the later chambers in the adult develop an acute axial periphery and which have no deposit of imperforate shell material in the dorsal intercameral sutures or the spiral suture; 2) *praefohsi* Blow and Banner which possesses a characteristic keel on the last or later chambers of the last whorl only; 3) *fohsi* Cushman and Ellisor in which the axial periphery is acute and is furnished throughout the last whorl with an imperforate carina; and 4) *lobata* Bermúdez in which the carina is developed over the entire periphery of the last whorl of chambers and is particularly strongly developed on the early part of the final whorl.

Kennett and Srinivasan (1983) adapted Blow and Banner's (1966) taxonomic concept and selected representative specimens from the Deep Sea cores Site 289 (Western Pacific) to illustrate the stratigraphic occurrence of each morpotype. In their illustration (pl. 22, figs. 7–9, here re-illustrated in Fig. 1.7), *praefohsi* is a nonkeeled form, intermediate between nonkeeled *peripheroacuta* and keeled *fohsi*. Their illustration of fohsellides and Blow and Banner's taxonomic concept have generally been used by other authors (Hodell and Vayavananda, 1993, Chaisson and Leckie, 1993).

On the other hand, although Bolli and Saunders (1985) agreed with Blow and Banner's (1966) taxonomic subdivisions, they insisted that the test shape (peripheral lobulation) is

an important character in the interpretation of fohsellid evolution and phylogeny. They suggested that the holotype of *praefohsi* (Blow and Banner, 1966) is better interpreted as an intermediate form between *fohsi* and *lobata*.

Given these uncertainties in taxonomy and phylogeny, Pearson and Chaisson (1997) first used the name "*praefohsi*" in quotation marks to indicate the intermediate form between *peripheroacuta* and *fohsi* for practical application in stratigraphy. They proposed to provisionally retain the "*praefohsi*" concept of Blow and Banner (1966) so that its taxonomic concept as a transition between nonkeeled fohsellids and keeled ones can be used to refine stratigraphic subdivision and correlation. Wade et al. (2011) followed this strategy, suggesting at the same time that the holotype of *praefohsi* should be considered a subjective synonym of *lobata* as in Berggren et al. (1995).

Several recent studies (Norris et al., 1996, Eisenach and Kelly, 2006) have further investigated various aspects of the evolution of fohsellids, focusing on temporal patterns of individual traits (e.g., water depth distribution of the populations, coiling direction, size and angularity etc.). However, the evolution of these traits all postdate the evolution of two key taxonomic traits, namely the keel development and lobate periphery (see discussion). We see no necessity in naming more chronocline species based on the temporal pattern of these traits, therefore we do not further discuss them in the taxonomic study.

Finally, we review the generic assignment of *Fohsella*. The fohsellids are often considered as a short-lived clade of the genus *Globorotalia* which is defined on the base of apertural characteristic and includes virtually every late Neogene planktonic foraminiferal species with an extra-umbilical to peripheral aperture. However, it is clear that several groups of forms referred to as *Globorotalia* have distinct ancestry (Bandy, 1972, Kennett and Srinivasan, 1983, Cifelli and Scott, 1986), and the designation of these different phylogenetic lineages to *Globorotalia* is somewhat artificial.

Bandy (1972) and Fleisher (1974) therefore proposed several new subgenera to represent the different globorotaloid lineages based on phylogenetic considerations. The subgenus *Fohsella* was proposed to include the *G. peripheroacuta* to *G. robusta* series (Bandy, 1972) and later included members with round periphery such as *G. peripheroronda* and *G. kugleri* because they represent early members of the *Fohsella* lineage (Fleisher, 1974). This subgeneric designation was adopted subsequently (Kennett and Srinivasan, 1983; Hodell and Vayavananda, 1993; Norris et al., 1996).

The use of *Fohsella* as a separate genus from *Globorotalia* (Cifelli and Scott, 1986, Pearson and Chaisson, 1997) has received support in studies of Leckie et al. (submitted) who suggested that fohsellids had their origin in the spinose *Paragloborotalia* group of the Oligocene (*pseudokugler-kugleri*) and that the group lost their spines during the Early Miocene. If so, the fohsellids would have a phylogenetic origin totally different from Neogene globorotaliids. Therefore, we utilize the generic name *Fohsella* for this group, rather than *Globorotalia*.

2.4 Landmark-based geometric morphometrics

The morphology of foraminifera can be studied using multivariate methods and outline analysis. Both methods have been widely applied (e.g., Malmgren et al., 1983; Pearson and Ezard, 2014). In this study, we analyze instead the shape of fohsellids using the landmark-based morphometric method (Tabachnick and Bookstein, 1990; Zelditch et al., 2004).

The landmark-based method can extract spiral-view shape information more efficiently than multivariate or outline analysis. For example, outline analysis considers only the projection of a foraminiferal test; therefore, it does not include any shape information within the silhouettes of the projection (Fig. 3A). The multivariate analysis (exemplified in Fig. 3B) has proved to be useful in quantifying various aspects of morphologic evolution when measurements are carefully chosen (e.g., Pearson and Ezard, 2014), but it generally suffers from shortcomings such as: containing less information than it appears to hold because measurements (and measurement errors) are often not independent; shape information such as curvature may not be easily quantified; and shape variation quantified by the multivariate measurements is not as illustrative as the landmark methods (Zelditch et al., 2004).

By placing landmark and semi-landmark coordinates along the chamber periphery and sutures (Fig. 3C), we are able to extract shape information that is used in the taxonomic descriptions of *Fohsella* (e.g., lobate chamber and number of chambers in the last whorl).

A thorough overview of the landmark method and its advantages over other morphometric methods can be found in Zelditch et al., (2004).

It has been suggested that changes in edge view is also an important aspect of the fohsellid evolution and a critical trait to differentiate fohsellid species (Bolli and Saunders, 1985; Pearson per. com.). We also analyzed the edge view of two selected samples as well as holotype specimens to investigate the taxonomic significance of edge-view projection. A previous study (Hull and Norris, 2009) suggests that landmark analysis is more sensitive in recognizing different edge-view morphologies than the outline analysis. Hence, we analyze our edge-view data using the landmark method as well.

2.5 Data collection

Each specimen was glued on a slide with the spiral side up. A universal stage was used to ensure appropriate orientation of the specimens. To emphasize sutures and other fine structures, such as keels, most specimens were colored with green food dye before being photographed. All dextral coiling specimens were digitally mirrored and analyzed as sinistral coiling ones in shape analysis.

The selection of landmarks and semi-landmarks is a subject of debate (Zelditch et al., 2004). Here, eleven landmarks were placed where intercameral suture and periphery meet. Given that the number of chambers in the last whorl in fohsellids varies between five and seven, eleven landmarks allow a good coverage of the chambers exposed in the last whorl.

We placed the first landmark at the penultimate chamber and subsequent landmarks were placed back to the sixth chamber in the final whorl. Six curves of semi-landmarks were then placed between landmarks to capture intercameral suture and chamber shape information. The number of semi-landmarks of each segment is shown in Figure 3C.

We did not measure the final chamber in this study. The final chamber is thinner relative to early chambers and often broken (see also Bolli and Saunders, 1985). It has been impossible to obtain a sufficient number of fohsellid specimens with complete final chamber from our samples. Additionally, the size and shape of final tend to be highly variable in some specimens, in some instances larger, in other instances smaller, and in some cases dipping towards the umbilical side. Because the PCA analysis is very sensitive to outliers, including the shape information of the final chamber would introduce a large amount of uncertainties in the analysis in the appearance of a few abnormal forms.

For the study of the edge view, we re-orient the specimens with edge view vertical to the microscope. One landmark is placed at the uppermost point of the peripheral projection and followed by 50 semi-landmarks along the peripheral projection.

Ideally, all specimens should be appropriately oriented before data collection. However, in practice this is hard to achieve perfectly and consistently when numerous specimens are analyzed. Fohsellids are slightly convex on the spiral side, and the orthogonal

orientation is always made somewhat subjectively either in the spiral view or the edge view. This uncertainty in orientation may have added some noise to the data (see results).

We follow standard landmark methods (Zelditch et al., 2004) in collecting and processing shape variables using available toolkits (tpsDig, tpsUtil32 and tpsRelw created by F. James Rohlf, http://life.bio.sunysb.edu/ee/rohlf/software.html). Raw landmark data are stored in two TPS files (spiral-view.TPS and edge-view.TPS). The spiral-view and edge-view shape were then summarized as the first two principal components (PC1 and PC2) of shape variables, respectively.

2.6 Materials

Fifty-one samples of foraminifera-bearing nannofossil ooze from Ocean Drilling Program (ODP) Site 806 (Hole B) were analyzed (Lat. & Long. 0˚19.11'N, 159 ˚21.69'E; Water depth, 2519m; Ontong Java Plateau, western equatorial Pacific Ocean). Bulk samples were soaked in sodium metaphosphate overnight and then washed with tap water through a 63 μm sieve. About 30–150 fohsellid specimens were picked from the >150 μm size fraction of each sample, and the morphology of a total of 1285 specimens was analyzed. In addition to the ODP samples, we examined the holotypes and paratypes of the species of the lineage. The taxon *praefohsi* is archived at the British Museum (London). The taxa *fohsi*, *lobata*, *robusta* are curated at the U.S. National Museum of Nature History (Smithsonian Institution). With one exception, we focused on the shape analysis of the holotypes rather than the paratypes because the holotypes are central to taxonomic definition, not the paratypes. However, the holotype of *robusta* was not analyzed using

the landmark method because its spiral side is covered with clay and landmarks cannot be placed with confidence. Instead, the paratype of *robusta* was examined in this work.

2.7 Age model

An advantage of this study is that we were able to use published astronomically tuned benthic foraminiferal isotope records from the ODP Hole 806B (Holbourn et al., 2013) to calibrate the evolutionary sequence of fohsellids. For the lower part of our record (455–490 mbsf, Appendix Fig. A1), the Miocene isotope event 3 (Mi3, 13.9 Ma) was recognized at ~486 mbsf and numerical age of the sequence was assigned based on the correlation of $\delta^{18}O$ minima to constructed eccentricity-tilt-precession maxima (Holbourn et al., 2013). For the upper part of the studied section (435–455 mbsf, Appendix Fig. A1), no astronomical ages are available to date. The age of this section (435–455 mbsf) was determined through extrapolation of an average sedimentation rate of 5.5 cm/kyr, calculated for the interval of 455–480 mbsf.

2.8 Results

Figure 4 shows the PC1 distribution of the edge view of holotypes *peripheroacuta*, *praefohsi*, *fohsi*, *lobata*, *robusta*, "*praefohsi*" (Kennett and Srinivasan, 1983), and fohsellid populations from two samples between ~14.03–13.74 Ma (Hole 806B). The first principal components account for ~63% of the total variance. Note the two samples we analyzed show a bimodal distribution.

Figure 5 shows the distribution of spiral view of the holotypes (*peripheroacuta, praefohsi, fohsi, lobata*), paratype (*robusta*), "*praefohsi*" (Kennett and Srinivasan, 1983) together with fohsellid populations from the interval of 14–12.8 Ma (Hole 806B) in the PC1-PC2 space. The first two principal components account for ~90% of the total variance when only the types are analyzed. When the entire fohsellid population from Hole 806B is analyzed (Fig. 5), PC1 and PC2 account for ~45% and ~11% of the total variance, respectively. This decrease in explanatory power of the first two principal components as the sample size increases reflects the large within-population variation in shape. It may also reflect, to some extent, the degradation of the quality of the data due, for example, to uncertainties in orienting the specimens (see method). Nevertheless, we carefully selected our samples from photos taken for picked specimens and only use those we consider well oriented in an attempt to minimize this issue.

2.9 Discussion

2.9.1 Edge view and fohsellid taxonomy

It has been suggested that edge view is an important feature of the fohsellid evolution (Norris et al., 1993, 1996, Pearson, pers. com.) and is taxonomically important (Blow and Banner, 1966; Bolli and Saunders, 1985). However, our analysis of the edge view of selected samples and holotypes suggests that edge view only helps to differentiate *peripheroacuta* from other fohsellids. The edge view of the *peripheroacuta* holotype is more rounded but holotypes of all later forms are characterized by a compressed/pinched edge-view periphery (Fig. 4). In fact, it is hard/unlikely to identify *praefohsi, fohsi*, *lobata* and *robusta* holotypes from the edge view (Figs. 1.1b–1.6b). On the other hand, a

foraminifera specialist would have no difficulty in identifying *praefohsi*, *fohsi*, *lobata* and *robusta* based solely on spiral view and the keel development (Figs. 1.1c–1.6c).

The changes in edge view is captured at Site 806 between 489.1–478.3 mbsf (14.03 Ma and 13.74 Ma, Fig. 4), characterized by the replacement of *peripheroacuta* by later forms (dominantly non-keeled "*praefohsi*"). As we will show below, keels and lobate chamber shape also first occurred in this interval, although rarely. Because all these later forms ("*praefohsi*", *praefohsi*, *fohsi*, *lobata*, *robusta*) have acute and compressed edge-view periphery, the edge view will not be used to differentiate these later forms from each other. Norris et al. (1996) discussed the changes in the angularity of the periphery in edge view of these later forms at Site 806 from younger stratigraphic intervals (~13.2–12 Ma, ~450–417 mbsf). We suggest that Norris's study is more relevant to the discussion of evolutionary patterns, rather than taxonomic issues related to *Fohsella*. If edge-view angularity is going to be used to delineate species, then new species with various degree of angularity will be named, which is unnecessary.

2.9.2 Spiral-view PCs and Shape

Figure 6A–C illustrates shape changes corresponding to PC1 and PC2 for selected specimens in this study. The vectors (arrows) indicate shape changes of a specimen relative to the mean shape (hollow dot) in response to changes in PCs. Our analysis suggests that changes in PC1 primarily involve changes in angular growth rate of fohsellids in the last whorl. As the PC1 increases (Fig. 6D–F), landmarks and semi-landmarks on the penultimate chamber "rotate" dextrally towards the preceding chamber.

Meanwhile, landmarks and semi-landmarks on the sutures of juvenile chambers (fifth and sixth chambers in the last whorl) “rotate” sinistrally towards adult chambers. These deformations involved in juvenile and penultimate chambers in the last whorl indicate that the angle at which chambers are added to the test decreases. As a result, more chambers are exposed in the spiral view. In addition, as PC1 increases, the fourth and fifth chambers become smaller and “downsize” along the radial direction, probably due to increased overlap between successive chambers. This causes an increase of length/width ratio of the test (less rounded in spiral view).

The ordination of PC1 is very robust regardless of the configurations of landmarks and semi-landmarks. In our sensitivity test (see Appendix), we designed ten different scenarios in placing landmarks and semi-landmarks. However, the dominance of this PC1 is very robust as shown by the stable distribution of holotype specimens along the PC1 (Appendix Fig. A2). This robustness of the ordination suggests that PC1 is the primary variable that generates most spiral-view shape variation in fohsellids.

On the other hand, distribution of specimens along PC2 is less stable as sample size or the configuration of semi-landmarks varies. Generally speaking, when landmarks and semi-landmarks have a good coverage on the test and the sample size is large, PC2 corresponds to the enlargement of the penultimate chamber relative to early chambers in the last whorl (Fig. 6B).

2.9.3 The type specimen distribution

The type specimens essentially span the extent of PC1 (Fig. 5, 6D–F), with *robusta* and *lobata* holotypes occupying the two extreme ends of PC1 and the other forms distributed in-between. We show that there is a significant difference between the two advanced forms (*robusta* and *lobata*), as well as between *fohsi* and *lobata*. This distribution suggests that *robusta* (paratype) may be more similar to *fohsi* than to *lobata*, and that the *lobata* morphotype may represent a morpologic population that is distinct from *fohshi* and *robusta*.

Since the holotypes and paratype were collected from distant and poorly dated sedimentary sequences, it is difficult to test our hypothesis and competing phylogenetic schemes (Fig. 2) based on the type specimens alone. We therefore take a stratophenetic approach by looking for stratigraphic occurrences of key traits (lobate adult chambers and keels) in fohsellids.

2.9.4 Stratigraphic occurrence of lobate forms

As summarized above, a major controversy regarding fohsellid phylogeny is the stratigraphic and phylogenetic position of the holotype *praefohsi* and the "early lobate forms" (Blow and Banner, 1966). Our data suggest that the lobate/cockscomb-like chambers that characterize the *lobata* morphotype (Fig. 6C and Fig. 7.1–7.6) occurred as early as 13.74 Ma (478.4 mbsf). These early specimens have ~7 chambers in the last whorl and possess one to two lobate chambers in the final whorl. However, some specimens are not quite "*lobata*" yet (e.g., Figs. 7.1, 7.5), characterized by relatively large angle increments between successive chambers and overall rounded spiral-side

periphery. As a result, their PC1 plot is very close to that of *praefohsi* (Fig. 6C). In addition, these early "*lobata*" morphologies are distinct from true *lobata* found at higher stratigraphic levels in that: 1) they are smaller (~300–450 µm) than *lobata* (~600 µm), and 2) a perforate keel is developed in the last two chambers, but does not necessarily extend to the early chambers in the last whorl, which is different from *lobata* (Figs. 7.18–7.24). We consider these early lobate forms in Hole 806B as representatives of *praefohsi*.

2.9.5 Stratigraphic occurrence of keels

Blow and Banner (1966) remarked "The stages of appearance and progressive development of the carina should be taken as the most important single morphocharacter for formal taxonomic distinction of the components of the lineage." (op. cit. p. 286). Our data suggest a different scenario of keel evolution in fohsellids. To discuss the stratigraphic sequence of keel development in fohsellids, we first distinguish two types of keel development in this lineage. The first type is characterized by the occurrence of a perforate keel, mostly restricted along the peripheral margin (Figs. 7.1–7.20, Figs. 1.2–1.3). The second type, in contrast, is imperforate and occur along both the peripheral margin and dorsal intercameral sutures (Figs. 7.21–7.24, Figs. 1.4–1.6).

Keels of the first type occurred as early as 14.03~13.97 Ma (Figs. 7.7–7.8) in both lobate (Figs. 7.1–7.6) and non-lobate ones (Figs. 7.7–7.16). Some specimens exhibit a keel throughout the entire final whorl but others have a keel developed only in the last two or three chambers. These perforate keels are mostly restricted along the peripheral margin, as opposed to the second type (Figs. 7.21–7.24).

The second type of keel first occurs at ~450 mbsf (~13.2 Ma, Fig. 7.18) and becomes increasingly pronounced in younger samples. Specimens above ~432 mbsf (~12.89 Ma) exhibit distinct sutural and peripheral imperforate keels in the last whorl (e.g., Figs. 7.21–7.24). Pearson (per. com.) suggsted that an increase in spiral height or angularity (Norris et al, 1996) may be part of the reason keels become more pronounced over time (particularly along intercameral sutures). Another possibility is that the second type of keel represents a further development of the keel by adding additional layers of calcite on the perforate keels. Norris (1991) has shown that the keel developed in fohsellids by folding the periphery of the perforate wall flat and then layering calcite sheets over the flattened wall. The presence of the pores on the perforate keel indicates that the keel was generated by the same processes as for the chamber (Norris 1991). The occurrence of an imperforate band, therefore, suggests the ontogenetic development of an additional layer of calcite in advanced fohsellids.

2.10 *Fohsella* Taxonomy

We integrate observations on the holotypes (Fig. 1) and chronologically well-constrained fohsellid specimens from Hole 806B (Figs. 6–8) to address issues related to the taxonomy and the stratigraphy of different morphotypes. A revised phylogenetic model is proposed accordingly.

2.10.1 Fohsella peripheroacuta (Blow and Banner, 1966)

There is little argument about the taxonomic description and phylogenetic position of *peripheroacuta*. It is the immediate ancestral form of the fohsellids. This species is abundant at Hole 806B in our samples between 490–485 mbsf (~14.0–13.9 Ma). Specimens from Hole 806B (Figs. 8.1–8.7) are very similar to the holotype (Fig. 1.1). Diagnostic features of *peripheroacuta* include: the edge view of *peripheroacuta* is more inflated and rounded relative to later forms (more negative PC1 in Fig. 4). There are on average six chambers in the last whorl and the test is more rounded, due to relatively large angular increments and less overlapping between chambers in the final whorl (more negative PC1 in Figs. 5–6).

2.10.2 Fohsella praefohsi (Blow and Banner, 1966)

As Bolli and Saunders (1985) pointed out, the last two chambers of the fairly large holotype of *praefohsi* (Fig. 1.2c) already exhibits elongate cockscomb shape. However, it is still not quite *lobata* yet in our opinion. As shown in Figures 5 and 6, the morphology of *praefohsi* is intermediate between *peripheroacuta* and *lobata* when the last chamber is not included in the landmark analysis.

In Hole 806B, fohsellids with lobate adult chambers (Fig. 6C, Figs. 7.1–7.6) occurred as early as 13.74 Ma (478.4 mbsf, Fig. 7.1) and possess incipient perforate keels in the last few chambers, rather than the pronounced imperforate keels in *lobata*. Based on these observations on the holotype and lobate specimens from Hole 806B, we suggest that *praefohsi* is a transitional form between *peripheroacuta* and *lobata*, rather than a transitional form between *fohsi* and *lobata* as proposed by Bolli and Saunders (1985).

2.10.3 Fohsella "praefohsi" auct.

By "*praefohsi*", we refer to the taxonomic concept that is widely used in biostratigraphy (Kennett and Srinivasan, 1983, Pearson and Chaisson, 1997; Wade, et al., 2011) as a transitional form between *peripheroacuta* and *fohsi* (illustrated in Kennett and Srinivasan, 1983, p. 98, pl. 22, figs 7–9, here illustrated in Fig. 1.7). The SEM illustration of "*praefohsi*" in Kennett and Srinivasan (1983) is quite different from the *praefohsi* holotype (Fig. 1.2). It does not have the elongate last chamber and readily recognizable peripheral keel.

However, when the last chamber is not considered, *"praefohsi"* and *praefohsi* are similar in our morphometric analysis (Figs. 5, 6), suggesting their spiral growth is not very different until the final chamber. Indeed, since both *praefohsi* and "*praefohsi*" may have diverged from the same ancestral population, their pre-adult growth history should be similar and therefore morphologically close to each other when the adult chambers are not considered.

The *"praefohsi"* morphotype is also found in Hole 806B (Fig. 6F, Figs. 8.8–8.15) with the lowest occurrence at ~ 489.1 mbsf (14.03 Ma) and is readily recognizable in samples above ~485 mbsf (13.87 Ma). This slightly earlier occurrence of "*praefohsi*" (~14 Ma vs 13.77 Ma, Wade et al., 2011) seems to be consistent with the study from Eastern Equatorial Pacific Site U1338B with the LO of "*praefohsi*" at ~374.95 CCSF-A (m) (~

14 Ma, Hayashi et al, 2013; age is calculated based on the age model of Holbourn et al., 2014).

2.10.4 Fohsella fohsi (Cushman and Ellisor, 1939)

The taxon *fohsi* is not morphologically different from "*praefohsi*" (Figs. 5, 6, Fig. 1.3, Figs. 8.16–8.19). These two species together encompass the majority of fohsellid assemblages over the studied interval at Site 806, as indicated by the dense distribution of specimens around holotypes in Figure 5.

Kennett and Srinivasan (1983) emphasize that *fohsi* differs from "*praefohsi*" in exhibiting a *distinct* keel throughout the entire final whorl. We observe this difference between *fohsi* and "*praefohsi*" in our samples from Hole 806B. The *fohsi* individuals from ~460 mbsf (~13.4 Ma, Fig. 8.16) show pronounced peripheral keels. However, it is interesting that the holotype of *fohsi*, as seen in the SEM (Fig. 1.3), shows a rather faint and perforate peripheral keel (Fig. 1.3c). One possibility is that the edge of the spiral side of the holotype is covered by clay contamination and therefore the keel is not readily visible (Fig. 1.3b). Another possibility is that the keel development in the holotype of *fohsi* has been overemphasized in the literature due to our pre-conceived idea on fohsellid evolution (from unkeeled *praefohsi* to keeled *fohsi*). The holotype of *fohsi* indeed represents an intermediate form between unkeeled *praefohsi* and those strongly keeled later forms (Figs. 8.16–8.19).

In a discussion of Blow and Banner's revision, Bolli (1967) also questioned the drawings of the *Globorotalia fohsi* holotype. According to Bolli (1967, p. 505), the drawings are contradictory because no keel is shown on the early chambers in the spiral and umbilical views, although one is shown in the edge view. In response to this argument, Cifelli (1968, p. 360) reexamined the holotype and suggested that "the keel in the holotype does extend entirely around the periphery", and the inconsistency in the drawings are due to the projection. However, Cifelli (1968) also disclosed that the keel of *fohsi* is thin, particularly around the early chambers. In agreement with Cifelli, we emphasize that the recognition of a complete perforate peripheral keel in early fohsellid populations (Figs. 7.1–7.17, ~487–460 mbsf: ~13.97–13.4 Ma) is not easy and requires meticulous lab work including constant reorientation, wetting of the specimens, and coloring with food dye. In our Hole 806B records, forms with complete perforate peripheral keels occur as low as ~487.6 mbsf (~13.97 Ma, Fig. 7.7) but only becomes readily recognizable ~463.4–460 mbsf (13.45–13.4 Ma).

In stratigraphic practice, the recognition of the lowest occurrence of *fohsi* can be further complicated due to the transition from perforate keel into imperforate band (Fig. 8.19) up-section. If one recognizes *fohsi* based on the occurrence of an imperforate band (Chaisson and Leckie, 1993), the LO of *fohsi* can be very different (Table 1). Therefore, large variation in the keel development from faint perforate keel to robust imperforate keel introduces large uncertainties depending on the different understanding and judgment call of biostratigraphers.

2.10.5 Fohsella lobata (Bermúdez, 1949)

We agree with Bolli and Saunders (1985) that the *lobata* form is a further development of *praefohsi*. It has seven to eight chambers in the last whorl and a characteristic lobate equatorial periphery. The holotype and the specimens from Site 806 show that *lobata* developed a complete keel throughout the peripheral margin (Fig. 1.5, Figs. 7.18–7.24), distinct from *praefohsi* which has only a faint keel in the last two or three chambers. However, this evolution of the keel in *praefohsi–lobata* is gradual. Early *lobata* possesses a perforate peripheral keel and faint sutures keels (450 mbsf, ~13.2 Ma, Figs. 7.18–7.19, Fig. 7.20, ~442 mbsf, 13 Ma). Distinctive and imperforate keels occur later (e.g., Fig. 7.21, 432 mbsf, 12.9 Ma). This gradual development from perforate to imperfoate keel can actually be seen in the holotype specimen which has a perforate keel in the last chamber but early chambers are rimed by imperforate keels. Due to this variation in the keel development, the use of *lobata* in biostratigraphy should be cautious.

2.10.6 Fohsella robusta (Bolli, 1950)

The taxon *robusta* is neither carefully studied from the assemblages in Hole 806B nor for the holotype. In Hole 806B, *robusta* specimens are often partially broken, preventing us from further analysis. The one paratype specimen of *robusta* we analyzed suggests that *robusta* is very different from *lobata* in terms of spiral-view shape and more similar to *fohsi* and *peripheroacuta* (Fig. 5), characterized by larger angular increments and more uniform increase in size between successive chambers in the final whorl relative to *lobata* (more negative PC1). Thus, *robusta* has fewer number of chambers and more rounded spiral view that is somewhat similar to *peripheroacuta.* This similarity has also been

noticed by Cifelli and Scott (1986, op. cit. p.18, “this form also display a small reversal … a circular outline like the earlier *Fohsella* species rather than the radially elongate outline of *F. fohsi*”).

2.11 A new phylogeny for the Fohsellid linage

Based on our combined morphologic and stratigraphic study, we propose a revised phylogeny for the fohsellid lineage (Fig. 1C). We agree with Bolli and Saunders (1985) that *praefohsi* represents a transitional form between early non-lobate forms and *lobata*. We also agree with Wade et al. (2011) that the “*praefohsi*” concept of Blow and Banner (1966) is valid. Morphotypes that can be considered as intermediate between *peripheroacuta* and *fohsi* have been found in Hole 806B (Figs. 8.8–8.15). The taxon “*praefohsi*” and *fohsi* differ in the degree of keel development. The taxon “*praefohsi*” does not have a complete peripheral keel (Fig. 8.8s–8.15) but *fohsi* possesses a peripheral keel throughout the final whorl (Figs. 8.16–8.20).

The strongly keeled *robusta* morphotypes have long been considered to have evolved from *lobata*, primarily due to their similarity in pronounced keels, large test size as well as stratigraphic co-occurrences. However, our morphologic analysis suggests that *robusta* is more similar to *peripheroacuta-fohsi* than to *lobata* in terms of ontogenetic spiral growth. A parsimonious interpretation in consideration of growth history and keel development would be that *robusta* evolved from the *fohsi* type.

We suggest that the fohsellid lineage is actually composed of two evolving morphologic groups: the *praefohsi-lobata* and the "*praefohsi*"*-fohsi-robusta* groups. The two differ primarily in their spiral-ontogenetic growth in the adult stage, with *praefohsi-lobata* showing lower angular increments and lobate adult chambers, and with "*praefohsi*"*-fohsi-robusta* showing larger angular increments and non-lobate test. Both morphologic groups acquired their keels independently after they diverged from the common ancestor *peripheroacuta* and show convergent evolution towards a strongly keeled morphology over time, characterized by the *fohsi*, *robusta*, and *lobata* with robust imperforate keels from younger stratigraphic levels (~13.2 Ma). The divergence time of the two morphologic groups is ~13.74 Ma. The "*praefohsi*" morphotype may occur slightly earlier (~14.03 Ma) than *praefohsi* (~13.74 Ma) and become readily recognizable in samples ~13.87 Ma. For practical stratigraphic purposes, the first occurrence of "*praefohsi*" at 13.77 Ma (Wade et al., 2011) is roughly consistent to our data from Site 806.

Since we focus on the taxonomy and phylogeny of fohsellids in this study, we do not discuss the temporal and spatial patterns of other variable traits in fohsellids (e.g., depth distribution, coiling direction, size and angularity etc.). Instead, we briefly summarize the stratigraphic pattern of several other traits together with the evolution of spiral-view shape and keel growth (Fig. 9). As we show, changes in edge view from more inflated to compressed shape occur during the transition from *peripheroacuta* to later forms. All later forms have a compressed edge view (Fig. 4). Size changes, angularity changes, and changes in coiling direction are neither coupled with the keel evolution nor evolution of

lobate periphery. We addressed this mosaic pattern of evolution in fohsellids in a separate paper (Si et al., submitted to Paleobiology).

2.12 Conclusion

In the past there has been a considerable emphasis on the morphologic types of the planktonic foraminifera. However, these defined morphotypes may not represent a foraminiferal lineage with describable limits from a particular time interval of its history. In taxonomy, the ranges of variation of the population become largely matters of subjective interpretation. In this study, we combine morphologic study of type specimens together with fohsellid populations from a continuous astronomically-tuned deep-sea record in ODP Hole 806B. We find that the exclusive use of types as reference points in the reconstruction of fohsellid phylogeny has in turn led to confusion regarding taxonomy and evolutionary divergence. The dichotomy in subjective selection of primary traits in taxonomic practice (Bolli and Saunders, 1985 vs Blow and Banner, 1966) and the use of "*praefohsi*" morphotypes as representative of *praefohsi* based on a preconceived phylogenetic interpretation (Kennett and Srinivasan, 1983) are consequences of this overemphasis on the importance of type specimens in evolutionary reconstructions.

Our biometric studies using landmark-based morphometrics on the spiral view suggest that the fohsellid lineage is composed of two evolving morphologic groups of *praefohsi-lobata* and "*praefohsi*"-*fohsi-robusta* that may differ in their ontogenetic spiral growth (spiral-view morphology). Keels evolved independently in the two groups over time and became increasingly more pronounced in later forms. The stratigraphic application of

"*praefohsi*" (13.77 Ma; Wade et al., 2011) is robust. However, the use of *fohsi* (13.4 Ma) or *lobata* in biostratigraphic correlation should be carefully evaluated because there is a large variation in the keel development. Depending on sample preparation (orientation, wetting and coloring) and taxonomic interpretation of different biostratigraphers (perforate vs imperforate, partially imperforate vs complete imperforate, etc.), the lowest appearance of these index taxa could be significantly different.

2.13 Acknowledgements

We thank M.–P. Aubry and R. K. Olsson for their insightful discussion and advice on the evolution of the fohsellid lineage. D. Bord and P. N. Pearson gave advice on sample preparation and data collection techniques. Detailed comments and suggestions by P. N. Pearson, G. Scott, and an anonymous reviewer helped greatly to improve the manuscript. A. Holbourn generously shared astronomically tuned benthic foraminifera data. SEM figures of holotypes and paratypes are courtesy of A. Sanner and B. Huber at the U.S. National Museum (Smithsonian Institution), and G. Miller at the British Museum (London). This research was supported by a Rutgers Student Fellowship and Joseph A. Cushman Award for Student Research to W. Si. Samples were provided by the International Ocean Discovery Program (IODP).

2.14 Systematic taxonomy

Order FORAMINIFERA Eichwald, 1830

Superfamily GLOBOROTALIACEA Cushman 1922

Family GLOBOROTALIIDAE Cushman 1927

Fohsella peripheroacuta (Blow and Banner, 1966)

Fig. 1.1

Globorotalia (Turborotalia) peripheroacuta Blow and Banner, 1966, p. 294, pl. 1, figs. 1a–c; Holotype. [Middle Miocene, Sample RM 193667, Pozon Fm., Eastern Falcon, Venezuela].

Globorotalia fohsi peripheroacuta (Blow and Banner) – Olsson 1971, p. 431, pl. I, figs. 5; [Middle Miocene, Cipero Fm., Golconda Estate, Trinidad]. – Bolli and Saunders., 1985, p. 213, figs. 29, 13a–c, [Middle Miocene, Sample Bo 184A, Cipero Fm., Golconda Estate, Trinidad].

Globorotalia (Fohsella) peripheroacuta (Blow and Banner) – Kennett and Srinivasan 1983, p. 96, pl. 22, figs. 4–6; [Middle Miocene, DSDP Site 289–49–2, 82 cm, Pacific]. – Hodell and Vayavananda 1993, p. 283, pl. I, figs. 4–6, [Middle Miocene, DSDP Site 289, Western Pacific].

Globorotalia peripheroacuta (Blow and Banner) – Berggren 1993, p. 283, figs. 4.16–4.18; [Middle Miocene, Sample SG25, Buff Bay Secion, Jamaica]. – Zhang et al., 1993, p. 321, pl. I, figs. 13; [14, Middle Miocene, borehole E66–136, 2466 ft, Gulf of Mexico]. – Chaisson and Leckie, 1993, p. 171, pl. 3, figs. 14–15 [130–806B-52X-5,31–33cm, Western Pacific]. – Vincent and Toumarkine, 1995, p. 905,

pl. 2, figs. 4–7, [Middle Miocene, ODP 138-845A-24X-1,80–85 cm, Eastern Equatorial Pacific].

Fohsella peripheroacuta (Blow and Banner) – Pearson and Chaisson 1997, p. 68, pl. 2, figs. 22–23; [Middle Miocene, ODP Site 929A–24–6, 70–72 cm, Ceara Rise].

Remarks: Test small, ~300–400 μm. The periphery of the early chambers in the last whorl is rounded and only becomes compressed in the last two chambers, giving an acute peripheral margin but without keel development. There are 6 to 7 chambers in the last whorl and the size increase is more or less uniform.

Fohsella praefohsi Blow and Banner, 1966

Fig. 1.2

Globorotalia (Globorotalia) praefohsi Blow and Banner, 1966, p. 295, pl. 1, figs. 3–4, pl. 2, figs. 6–7, 10–11; Holotype. [Middle Miocene, Sample RM 19410, Pozon Fm., Eastern Falcon, Venezuela]. – Zhang et al., 1993, p. 321, pl. I, figs. 5–6; [5, Middle Miocene, borehole E68–136, 2467 ft, 6, Middle Miocene, borehole E66–73, 3558 ft, Gulf of Mexico] – Chaisson and Leckie, 1993, p. 171, pl. 3, figs. 5–10, [5–6, 30-806B-51X-2, 29–31 cm; 7, 130-806B-49X-CC; 8-9, 130-806B-48X-CC; 10, 130-806B-48X-CC, Western Pacific].

Globorotalia fohsi praefohsi (Blow and Banner) – Bolli and Saunders, 1985, p. 213, figs. 29, 11a–b, [Middle Miocene, Cipero Fm., Golconda Estate, Trinidad].

Fohsella lobata (Blow and Banner) – Hayashi et al. 2013, p. 100, fig 8, 2a–c, [321-U1338B-36H-7, 38–40 cm, Equatorial Pacific].

Not *Globorotalia (Fohsella) praefohsi* Kennett and Srinivasan, 1983, p. 98, pl. 22, figs. 7–9 (which represents the evolutionary transition from *peripheroacuta* Blow and Banner to *fohsi* Cushman and Ellisor)

Remarks: Morphologically similar to *F. lobata*, with seven chambers in the last whorl, increasing rapidly in size in the last two chambers, giving an elongate cockscomb shape. Weak but significant peripheral keels occur on the last two or three chambers. The lowest occurrence of this morphology is ~478 mbsf (~13.746 Ma, ODP Hole 806B).

Fohsella "praefohsi" auct.

Fig. 1.7

Globorotalia (Fohsella) praefohsi – Kennett and Srinivasan 1983, p. 98, pl. 22, figs. 7–9, [Middle Miocene, DSDP Site 289–45–6, 82 cm, Western Pacific]. – Hodell and Vayavananda 1993, p. 283, pl. I, figs. 7–9; [Middle Miocene, DSDP Site 289, Western Pacific]. – Zhang et al., 1993, p. 321, pl. I, figs. 8–9; [8–9, Middle Miocene, borehole E48–136, 2466 ft, Gulf of Mexico].

Globorotalia (Fohsella) peripheroacuta – Zhang et al., 1993, p. 321, pl. I, figs. 14–15, [14, Middle Miocene, borehole E66–73, 3598 ft; 15, E68–136, 2486 ft, Gulf of Mexico]

Fohsella praefohsi – Cifelli and Scott 1986, p.14, figs. 8f–8g; [Middle Miocene type locality *Fohsella fohsi* Zone, Trinidad]. – Hayashi et al. 2013, p. 100, fig 8, 4a–c, [321-U1338B-33H-5, 38–40 cm, Equatorial Pacific].

Remarks: By "*praefohsi*", we refer to the taxonomic concept that is widely used in biostratigraphy (Kennett and Srinivasan, 1983, Pearson and Chaisson, 1997, Wade, et al.,

2011) as a transitional form between *peripheroacuta* and *fohsi*. Diagnostic features of "*praefohsi*" in stratigraphic practice include: six chambers in the last whorl, early chambers increase slowly in size as in *peripheroacuta* but the last two chambers increase more rapidly, giving an acute and slightly lobate shape. Edge view is compressed, in contrast to the more rounded edge view of *peripheroacuta*. Some specimens seem to possess a very weak keel in the last two chambers, but most are not keeled, and therefore differ from the fully keeled *fohsi*.

Fohsella fohsi Cushman and Ellisor, 1939

Fig. 1.3

Globorotalia fohsi Cushman and Ellisor, 1939, p.12, pl. 2, figs. 6a–c, Holotype, (figured here as Fig. 9.4), [Middle Miocene, Ellender well No. 1 at 9612 feet, Terrebone Parish, Louisiana, USA]. – Berggren 1993, p. 198, figs. 4.19–4.20, [Middle Miocene, Buff Bay section, Jamaica]. – Vincent and Toumarkine, 1995, p. 905, pl. 2, figs. 11–13, [Middle Miocene, ODP 138-845A-21H-6, 143–148 cm, Eastern Equatorial Pacific].

Globorotalia fohsi fohsi (Cushman and Ellisor) – Olsson 1971, p. 431, pl. I, figs. 6, [Middle Miocene, Cipero Fm., Golconda Estate, Trinidad]. – Stainforth et al., 1975, p. 275, figs. 118, 1–9, [Middle Miocene, Cipero Fm., Trinidad] – Bolli and Saunders, 1985, p. 213, figs. 29, 12a–b, [Middle Miocene, Sample Bo 185A, Cipero Fm., Trinidad,].

Globorotalia (Fohsella) fohsi (Cushman and Ellisor) – Kennett and Srinivasan 1983, p. 100, pl. 23, figs. 1–3, [Middle Miocene, DSDP Site 289–44–2, 48 cm, Western

Pacific]. – Hodell and Vayavananda 1993, p. 284, pl. I, figs. 1–3, [Middle Miocene, SSDP Site 289, Western Pacific].

Fohsella fohsi (Cushman and Ellisor) – Cifelli and Scott 1986, p.14, figs. 8a–8c, [Middle Miocene, type locality *Fohsella lobata* Zone, Trinidad]. – Hayashi et al. 2013, p. 100, figs 8, 3a–c, [321-U1338B-34H-2, 38–40 cm, Equatorial Pacific].

Remarks: Morphologically (spiral view) not very different from "*praefohsi*". There are six to seven chambers in the last whorl, the early chambers increase slowly in size but the last two chambers increase more rapidly. Chambers in the last whorl are compressed and develop a perforate peripheral keel throughout. Examination on the holotype specimen shows that the keel on the juvenile chambers in the last whorl is faint, different from previously described (Blow and Banner, 1966, Kennett and Srinivasan 1983).

Fohsella lobata Bermúdez, 1949

Fig. 1.4

Globorotalia lobata Bermúdez, 1949, p. 286, pl. 22, figs. 15–17, Holotype (here figured in Fig. 9.5), [Middle Miocene, Bravo well No. 5, core 5, at 74–84 feet, Trinchera Fm., Trujillo Province, Dominican Republic]. – Vincent and Toumarkine, 1995, p. 905, pl. 2, figs. 14–16, [Middle Miocene, 14, 138-845A-20H-3,41 cm; 15, 18, 138-845A-19H-2,23–28 cm; 16, 138-845A-19H-CC; 17 138-845A-20H-4, 80–85 cm, Eastern Equatorial Pacific].

Globorotalia fohsi lobata (Bermúdez) – Olsson 1971, p. 431, pl. I, figs. 7, [Middle Miocene, Cipero Fm., Golconda Estate, Trinidad]. – Stainforth et al., 1975, p. 275,

figs. 117, 2–4, [Middle Miocene, Cipero Fm., Trinidad]. – Bolli and Saunders, 1985, p. 215, figs. 29, 9a–b, 10a–b, [Middle Miocene, Sample Js 32, Cipero Fm., Cipero coast, Trinidad]. – Zhang et al., 1993, p. 321, pl. I, figs. 1–2; [Middle Miocene, borehole E66–73, 3478 ft, Gulf of Mexico]

Globorotalia (Fohsella) lobata (Bermúdez) – Kennett and Srinivasan 1983, p. 100, pl. 23, figs. 4–6, [Middle Miocene, DSDP Site 289–44–6, 97 cm, Western Pacific]. – Hodell and Vayavananda 1993, p. 284, pl. I, figs. 4–9; [Middle Miocene, DSDP Site 289, Western Pacific].

Globorotalia fohsi (Bermúdez) – Chaisson and Leckie, 1993, p. 171, pl. 3, figs. 1–4, [1, 130-806B-48X-2, 34–36 cm; 2, 130-806B-47X-CC; 3 130-806B-46X-CC; 4, 130-806B-45X-5, 34–36 cm, Western Pacific].

Remarks: Test large, ~500–700 μm. Seven to eight chambers in the last whorl, increasing rapidly in size in the last two chambers, giving an elongate cockscomb shape. The holotype and specimens from DDP Hole 806B show that *lobata* developed a keel along both the peripheral margin and dorsal intercameral sutures, distinct from *praefohsi* which has only a faint keel in the last two or three chambers.

Fohsella robusta Bolli, 1950

Fig. 1.5 (holotype), 1.6 (paratype)

Globorotalia robusta Bolli, 1950, p. 89, pl. 15, figs. 2a–c. Sample JS 46, [Middle Miocene, Cipero Fm., Trinidad].

Globorotalia fohsi robusta (Bolli) – Olsson 1971, p. 431, pl. I, figs. 8; [Middle Miocene, Cipero Fm., Golconda Estate, Trinidad].

Globorotalia (Fohsella) robusta (Bolli) – Kennett and Srinivasan 1983, p. 102, pl. 23, figs. 7–9, [Middle Miocene, DSDP Site 289–40–3, 82 cm, Western Pacific].

Fohsella robusta (Bolli) – Cifelli and Scott 1986, p.14, figs. 8d–8e, [Middle Miocene, type locality *Fohsella lobata* Zone, Trinidad].

Globorotalia robusta (Bolli) – Berggren 1993, p. 198, figs. 4.24–4.26, [Middle Miocene, Buff Bay section, Jamaica]. – Vincent and Toumarkine, 1995, p. 905, pl. 2, figs. 20, [Middle Miocene, ODP 138-844B-10H-2, 79–81 cm, Eastern Equatorial Pacific].

Remarks: Test large, ~600–700 μm. *F. robusta* is very different from *lobata* in spiral view and more similar to *fohsi*. The size increases are quite uniform in the last whorl, characterized by relatively large angular growth and small radial expansion, giving rise to a more rounded and continuous peripheral margin. The taxon *robusta* also possesses pronounced imperforate keel that differs from that in *fohsi*.

2.15 References

Aubry, M.–P., 2016, Cenozoic chronostratigraphic terminology: In defense of formal subseries. Stratigraphy, v. 13, p. 1–20.

Bandy, O. L., 1972. Origin and development of *Globorotalia* (*Turborotalia*) *pachyderma* (Ehrenberg). Micropaleontology, v. 18(3), p.294–318.

Berggren, W. A., 1993, Neogene planktonic foraminiferal biostratigraphy of eastern Jamaica: Geological Society of America Memoir, v. 182, p. 179–217.

Berggren, W. A., Kent, D. V., Swisher, C. C., and Aubry, M.–P., 1995, A revised Cenozoic geochronology and chronostratigraphy, *in*: Berggren, W. A., Kent, D. V., Aubry, M.–P., Hardenbol, J. (Eds.), Geochronology, Time Scales, and Global Stratigraphic Correlation: A Unified Temporal Framework for an Historical Geology, SEPM Spec. Publ., v. 54, p. 129–212.

Blow, W. H. and Banner, F. T., 1966. The morphology, taxonomy and biostratigraphy of *Globorotalia barisanensis* LeRoy, *Globorotalia fohsi* Cushman and Ellisor, and related taxa. Micropaleontology, v. 12(3), p. 286–302.

Bolli, H. M., 1950, The direction of coiling in the evolution of some Globorotaliidae: Contributions from the Cushman Foundation Foraminifera Research, v. 1, p. 82–89.

Bolli, H. M., 1957, Planktonic foraminifera from the Oligocene-Miocene Cipero and Lengua formations of Trinidad: BWI: US National Museum Bulletin, v. 215, p. 97–123.

Bolli, H. M., 1967, The subspecies of *Globorotalia fohsi* Cushman and Ellisor and the zones based on them: Micropaleontology, v. 13, p. 502–512.

Bolli, H. M. and Saunders, J. B., 1985, Oligocene to Holocene low latitude planktic foraminifera, *in*: Bolli, H. M., Saunders, J. B., Perch–Nielsen, K. (Eds.), Plankton Stratigraphy, 1, Cambridge University Press, Cambridge, p. 155–262.

Chaisson, W. P. and Leckie, R. M., 1993, High-resolution Neogene planktonic foraminifer biostratigraphy of Site 806, Ontong Java Plateau (western equatorial Pacific), *in* Berger, W. H., Kroenke, L. W., Mayer, L. A., et al., Proc. ODP, Sci. Results, v. 130, p. 137–178.

Cifelli, R., 1968, A note on the holotype of *Globorotalia fohsi* Cushman and Ellisor: Micropaleontology, v. 14, p. 369–370.

Cifelli, R., and Scott G., 1986, Stratigraphic record of the Neogene globorotalid radiation (Planktonic Foraminiferida). Smithsonian Institution Press.

Cushman, J. A., and Stainforth, R. M., 1945, The foraminifera of the Cipero Marl Formation of Trinidad, British West Indies: Cushman Laboratory Foraminifera Research Special Publication no. 14, p. 1–75, pls. 1–16.

Eisenach, A. R., and Kelly, D. C., 2006, Coiling preferences and evolution in the middle Miocene *Fohsella* chronocline: Marine Micropaleontology, v. 60, p. 243–257.

Fleisher, R. L. 1974, Cenozoic planktonic foraminifera and biostratigraphy, Arabian Sea, Deep Sea Drilling Project, Leg 23A. Initial Reports of DSDP, v. 23: p. 1001–1072.

Hayashi, H., Idemitsu, K., Wade, B. S., Idehara, Y., Kimoto, K., Nishi, H., and Matsui, H., 2013, Middle Miocene to Pleistocene planktonic foraminiferal biostratigraphy in the eastern equatorial Pacific Ocean. Paleontological Research, v. 17(1), p. 91–109.

Holbourn, A., Kuhnt, W., Frank, M., and Haley, B. A., 2013, Changes in Pacific Ocean circulation following the Miocene onset of permanent Antarctic ice cover: Earth and Planetary Science Letters, v. 365, p. 38–50.

Holbourn, A., Kuhnt, W., Lyle, M., Schneider, L., Romero, O., and Andersen, N., 2014, Middle Miocene climate cooling linked to intensification of eastern equatorial Pacific upwelling: Geology, v. 42, p. 19–22.

Hodell, D. A., and Vayavananda A., 1993, Middle Miocene paleoceanography of the western equatorial Pacific (DSDP site 289) and the evolution of *Globorotalia* (*Fohsella*). Marine Micropaleontology, v. 22, p. 279–310.

Hull, P. M., and Norris, R. D., 2009, Evidence for abrupt speciation in a classic case of gradual evolution. Proceedings of the National Academy of Sciences v. 106, p. 21224–21229.

Kennett, J. P., and Srinivasan, M. S., 1983, Neogene Planktonic Foraminifera, A Phylogenetic Atlas. Hutchinson Ross, Stroudsburg, Pennsylvania. p. 94–101.

Leckie, R. M., Wade, B. S., Pearson, P. N., Fraass, A. J., King, D. J., Olsson, R. K., Silva, I. P., Spezzaferri, S., Berggren, W. A., Taxonomy, biostratigraphy, and phylogeny of Oligocene and Early Miocene *Paragloborotalia* and *Parasubbotina*, Cushman Foundation Special Publication, Atlas of Oligocene Planktonic Foraminifera, Wade, B. S., Olsson, R. K., Pearson, P. N., Huber, B. T., Berggren, W. A. (Editors), in press.

Malmgren, B. A., Berggren, W. A., and Lohmann, G. P., 1983, Evidence for punctuated gradualism in the Late Neogene *Globorotalia tumida* lineage of planktonic foraminifera: Paleobiology, v. 9, p. 377–389.

Norris, R. D., 1991, Parallel evolution in the keel structure of planktonic foraminifera. The Journal of Foraminiferal Research, v. 21(4), p. 319–331.

Norris, R. D., Corfield, R. M., and Cartlidge, J. E., 1993, Evolution of depth ecology in the planktic foraminifera lineage *Globorotalia* (*Fohsella*). Geology, v. 21(11), p. 975–978.

Norris, R. D., Corfield, R. M., and Cartlidge, J., 1996. What is gradualism? Cryptic speciation in globorotaliid foraminifera. Paleobiology, v. 22(3), p. 386–405.

Olsson, R. K., 1971, The logarithmic spire in planktonic foraminifera: its use in taxonomy, evolution, and paleoecology: Trans. Gulf Coast Assoc. Geol. Soc., v. 21, p. 419–432.

Pearson, P. N., and W. P. Chaisson., 1997, Late Paleocene to middle Miocene planktonic foraminifer biostratigraphy of the Ceara Rise. In Proceedings of the Ocean Drilling Program. Scientific Results, v. 154, p. 33–68.

Pearson, P. N., and Ezard, T. H. G., 2014, Evolution and speciation in the Eocene planktonic foraminifer *Turborotalia*: Paleobiology, v. 40, p. 130–143.

Si, W., Berggren W. A., and Aubry M.–P., Mosaic evolution in the planktonic foraminifera *Globorotalia fohsi* lineage, submitted to Paleobiology.

Stainforth, R. M., Lamb, J. L., Luterbacher, H., Beard, J. H. and Jeffords, R. M., 1975, Cenozoic planktonic foraminiferal zonation and characteristics of index forms. *University of Kansas Paleontological Contribution*. p. 81–82.

Tabachnick, R. E., and Bookstein, F. L., 1990, The structure of individual variation in Miocene *Globorotalia*: Evolution, v. p. 416–434.

Van Couvering, J. A., 2015, Editorial: The value of formal subseries; Stratigraphy, v.

12(2), p. 197–198.
Vincent, E. and Toumarkine, M. 1995, Data report: Miocene planktonic foraminifers from the eastern equatorial Pacific. Proceedings of the Ocean Drilling Program. Scientific results, v. 138, p. 895–907
Wade, B. S., Pearson, P. N., Berggren, W. A., and Pälike, H., 2011, Review and revision of Cenozoic tropical planktonic foraminiferal biostratigraphy and calibration to the geomagnetic polarity and astronomical time scale: Earth-Science Reviews, v. 104, p. 111–142.
Zhang, J., Miller, K. G. and Berggren. W. A., 1993, Neogene planktonic foraminiferal biostratigraphy of the northeastern Gulf of Mexico. Micropaleontology, v. 39, p. 299–326.
Zelditch, M. L., Swiderski, D. L., and Sheets, H. D., 2004, Geometric Morphometrics for Biologists: a primer: Amsterdam, Elsevier Academic. p. 1–419.

2.16 Figure Captions

Figure 1. Type specimens of fohsellid lineage; **1a**–**1c**: holotype of *F. peripheroacuta;* **2a**–**2c**: holotype of *F. praefohsi*; **3a**–**3c**: holotype of *F. fohsi;* **4a**–**4c**: holotype of *F. lobata*; **5a**–**5c**: holotype of *F. robusta*; **6a**–**6c**: paratype of *F. robusta;* **7a**–**7c**: *F. "praefohsi"* described in (Kennett and Srinivasan, 1983).

Figure 2. Phylogenetic scenarios for Middle Miocene fohsellid lineage. Note that the highest occurrences of representative species are arbitrarily drawn and carry no stratigraphic significance.

Figure 3. Comparison of different morphometric analyses. A: outline analysis on the edge-view of *F. lobata* holotype; B: an example illustrating how multivariate analysis could be performed on the *F. lobata* holotype; C: landmark-based method; red dots are landmarks; black dots are semi-landmarks.

Figure 4. Edge view analysis of holotypes and representative samples from Site 806. Outlines at the top are computed using tpsRelw (created by F. James Rohlf) with PC1 values equal to –0.1, 0 and 1, respectively. These outlines suggest that PC1 represents the change in edge view from more rounded periphery (PC1= –0.1) to acute/compressed periphery (PC1= 0.1). 1–6: holotype of *peripheroacuta*, *praefohsi*, *fohsi*, *lobata*, *robusta*, and "*praefohsi*" (from Kennett and Srinivasan) respectively. All holotype besides are *peripheroacuta* compressed in edge view. In our oldest sample (14.03 Ma), *peripheroacuta* is more dominant and therefore the PC1 is clustered to the negative end.

By 13.74 Ma, most specimens already developed a compressed periphery. Therefore, edge view can be used to differentiate *peripheroacuta* from all later forms.

Figure 5. Spiral view analysis of fohsellid type specimens and population from Hole 806B (14–12.8Ma). Black squares are type specimens. 1–6: *F. peripheroacuta* (holotype), *F. praefohsi* (holotype), *F. fohsi* (holotype), *F. lobata* (holotype), *F. robusta* (paratype) and *F.* "*praefohsi*" (Kennett and Srinivasan, 1983) respectively; Grey crosses indicate specimens from Hole 806B.

Figure 6: Distribution of types and selected specimens (illustrated in Fig. 7 and Fig. 8) and corresponding PC1 and PC2. A–C: interpretation of PC1 and PC2; arrows indicate the direction of deformation in response to changes in PC values. The magnitude of the deformation of each landmark and semi-landmark is characterized by the length of the arrows. D: Distribution of the early lobate forms (~13.746–13.46 Ma) relative to the type specimens. E: Distribution of early keeled forms (~13.98–13.45 Ma). F: Distribution of *"praefohsi"* (Kennett and Srinivasan, 1983). Orange squares are type specimens as in Fig. 5.

Figure 7. Evolution of lobate periphery and keels in fohsellids; **1**–**6**: Specimens with lobate/cockscomb-like chambers between ~13.74–13.47 Ma. (1: 806B/51/4:50–51cm, 13.74 Ma; 2: 806B/51/3:50–51cm, 13.72 Ma; 3: 806B/50/3:50–51cm, 13.52 Ma; 4: 806B/49/6:110–111cm, 13.47 Ma; 5: 806B/49/6:95–96cm, 13.47 Ma; 6: 806B/49/6:95–96cm, 13.47 Ma;); **7**–**17**: Keel growth in early forms from 14.03–13.45 Ma. Some

specimens exhibit a perforate keel throughout the entire final whorl but others have a keel developed only in the last two or three chambers. These keels are restricted along the peripheral margin and do not occur at the dorsal intercameral sutures (7: 806B/52/5:50–51cm, 14.03 Ma; 8: 806B/52/4:50–51cm, 13.97 Ma; 9: 806B/51/4:50–51cm, 13.74 Ma; 10: 806B/51/2:50–51cm, 13.68 Ma; 11: 806B/51/2:50–51cm, 13.68 Ma; 12: 806B/51/2:50–51cm, 13.68 Ma; 13: 806B/51/2:50–51cm, 13.68 Ma; 14: 806B/50/3:50–51cm, 13.52 Ma; 15: 806B/49/6:110–111cm, 13.47 Ma; 16: 806B/49/6:60–61cm, 13.47 Ma; 17: 806B/49/6:60–61cm, 13.46 Ma); **18**–**24**: *F. lobata* (18: 806B/48/3:130–131cm, 13.2 Ma; 19: 806B/48/3:130–131cm, 13.2 Ma; 20: 806B/47/5:30–31cm, 13.07 Ma; 21: 806B/46/5:20–21cm, 12.89 Ma; 22: 806B/46/2:30–31cm, 12.81 Ma; 23: 806B/46/2:30–31cm, 12.81 Ma; 24: 806B/46/2:30–31cm, 12.81 Ma); Note: there is no scale bar for these images. Because all specimens are oriented with a universal stage in this study, the distance of a foraminifera to the object lens of a microscope varies from specimen to specimen. As a result, size measurement cannot be done under the microscope. The average size of early fohsellids is ~300–400 μm (~13.9 Ma) and increase gradually to ~600–700 μm in later populations (~13 Ma).

Figure 8. **1**–**7**: selected specimens of *F. peripheroacuta* from Hole 806B (**1**–**4**: 806B/52/5:50–51cm, 14.03 Ma; **5**–**6**: 806B/52/2:51–52cm, 13.87 Ma; **7**: 806B/51/4:50–51cm, 13.74 Ma); **8**–**15**: selected specimens of *F. "praefoshi"* (8: 806B/52/5:51–52cm, 14.03 Ma; 9: 806B/50/1:89cm, 13.49 Ma; 10: 806B/49/6:110–111cm, 13.468 Ma; 11: 806B/49/6:95–96cm, 13.465 Ma; 12: 806B/49/6:66–67cm, 13.458 Ma; **13**–**15**: 806B/49/6:45–46cm, 13.455 Ma); **16**–**19**: selected specimens of *F. fohsi* (16:

806B/49/3:60–61cm, 13.37 Ma; 17: 806B/48/4:120–121cm, 13.24 Ma; 18: 806B/48/2:130–131cm, 13.18 Ma; 19: 806B/46/5:120–121cm, 12.91 Ma); There is no scale bar for all specimens.

Figure 9: Stratigraphic distribution of the evolution of various traits in *Fohsella*. Transition from more rounded *peripheroacuta* to more acute/compressed form occurs in lower part of the section, roughly synchronous with the occurrences of peripheral perforate keels and lobate adult chambers. Changes in coiling direction to dominant sinistral coiling and gradual changes in angularity of edge view (Norris et al., 1996) postdate the occurrences of keels and lobate periphery. Note: because "*praefohsi*" and *fohsi* are the dominant components of the fohsellid assemblage, changes in coiling direction ~470 mbsf primarily reflect coiling direction changes in "*praefohsi*"-*fohsi*. Lobate *praefohsi* is not abundant (a few specimens per sample on average) in lower part of the section. Therefore, it is not clear, statistically, what is the preferred coiling direction of this morphotype. Both dextral coiling and sinistral coiling occur.

2.17 Table Caption

Table 1. Placement of the lowest occurrence of fully keeled fohsellid (or *F. fohsi*, by definition) is considerably different among biostratigraphers primarily due to the subjective understanding of what is “fully” keeled. Careful examination of the specimens is required when *F. fohsi* is used for biostratigrahic purpose.

2.18 Appendix

Ages of the lower part of the record are based on astronomically tuned benthic foraminifera $\delta^{18}O$ (Holbourn et al., 2013). Miocene isotope event 3 (Mi3, 13.9 Ma) occurs at ~486 mbsf. Ages of the upper part of the records (Figure S1) are extrapolated using average sedimentation rates for the 455–480 mbsf interval. Black squares represent the benthic foraminifera isotopic data available for astronomic tuning in Holbourn et al. (2013).

The placement of landmarks and semi-landmarks is central to geometric morphometrics. Different configurations of landmarks and semi-landmarks may give different results. In this work, we follow several criteria in the placement of landmarks and semi-landmarks. First, adequate coverage of the test. One might prefer placing landmarks and semi-landmarks only in the last few chambers because they are more characteristic in terms of taxonomic subdivision. However, we believe that the adult morphology of a planktonic foraminifera being the product of its growth history, information from the juvenile chambers, at least those in the last whorl, should be included in the analysis. Furthermore, in geometric morphometrics, it is a configuration, not an individual landmark, that constitutes a datum (Zelditch et al., 2004). As an integrated entity, the test of a planktonic foraminifera should have adequate landmarks and semi-landmarks to capture the configuration of its chambers over the test.

Second, the repeatability. Landmarks and semi-landmarks should be found repeatable and reliably from sample to sample. Otherwise large sampling errors might be introduced into

the data. For example, the last chamber of the *Fohsella* lineage is often broken or deformed. Although it is characteristic in the *F. lobata* morphotype, it cannot be sampled repeatedly over the population. On the other side, the early juvenile chambers (eighth, ninth or earlier chambers) are too small to observe in our light microscope photos. Therefore, landmarks cannot be placed precisely for these structures.

Third, adequate semi-landmarks to capture curves. A sufficient number of semi-landmarks are necessary to be able to trace the curves of foraminiferal test. For example, if there are too few points to cover the last chamber of *F. lobata*, the morphometric analysis will not be accurately. On the other hand, if there are too many semi-landmarks along the suture of juvenile chambers, they are all clustered up and look uneven. Therefore, selecting an appropriate number of semi-landmarks based on the samples being analyzed is important.

Based on these criteria, we performed ten experiments for a small data set with types and selected specimens in Figure 7 and Figure 8. Different configurations of semi-landmark curves and numbers of semi-landmarks are used in each experiment. The purpose of these experiments is to figure out whether the ordination of PC1 and PC2 are stable when the configuration of semi-landmarks changes. As can be seen from Figure S2, the ordination of PC1 is very stable regardless of changes in the placement of semi-landmarks. The relative position of holotypes remains unchanged.

2.19 Appendix Figure Caption

Figure S1. Age model used in this study for Hole 806B.

Figure S2. Sensitivity test of the ordination of PC1-PC2 under different configuration of semi-landmarks. Blue curves represent the placement of semi-landmarks along sutures or peripheral margin. For example, in test 1, no semi-landmarks is placed. In test 7, there are 7 semi-landmark curves. The number of semi-landmarks of each curve is indicated by the red number next to the curve. All specimens analyzed in these trials are illustrated in Figure 7 and Figure 8. Configuration of test 10 is used in this study. From the relative position of the type specimens, it is clear that the ordination of PC1 is robust across experiments. Number **1**–**6** indicate type specimens, **1**: *F*. *peripheroacuta* (holotype); **2**: *F*. *praefohsi* (holotype); **3**: *F*. *fohsi* (holotype); **4**: *F*. *lobata* (holotype); **5**: *F*. *robusta* (paratype); **6**: *F*. *"praefohsi"* (Kennett and Srinivasan, 1983).

Figure 1

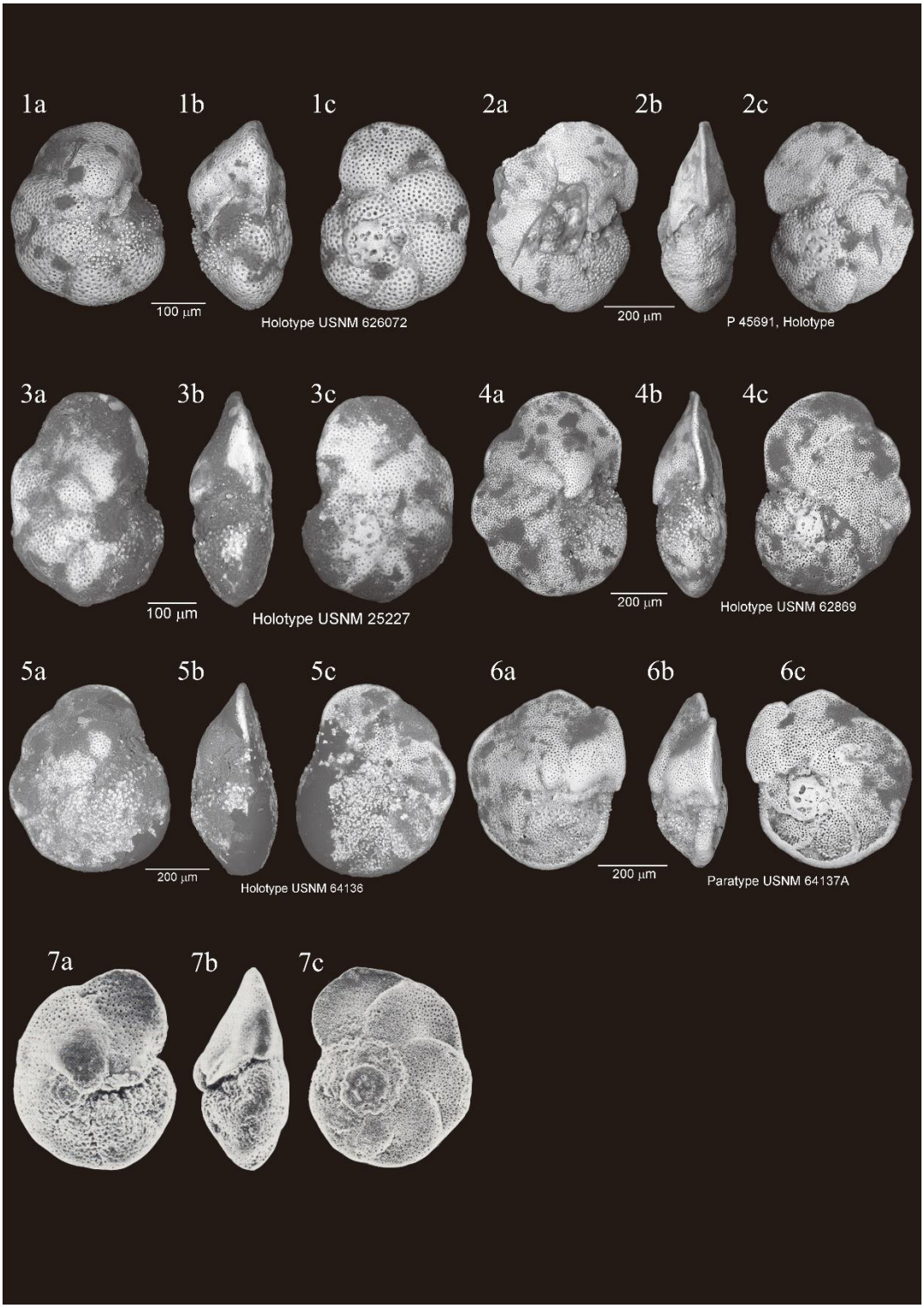
1a
1b
1c
2a
2b
2c
100 µm
Holotype USNM 626072
200 µm
P 45691, Holotype
3a
3b
3c
4a
4b
4c
100 µm
Holotype USNM 25227
200 µm
Holotype USNM 62869
5a
5b
5c
6a
6b
6c
200 µm
Holotype USNM 64136
200 µm
Paratype USNM 64137A
7a
7b
7c

Figure 2

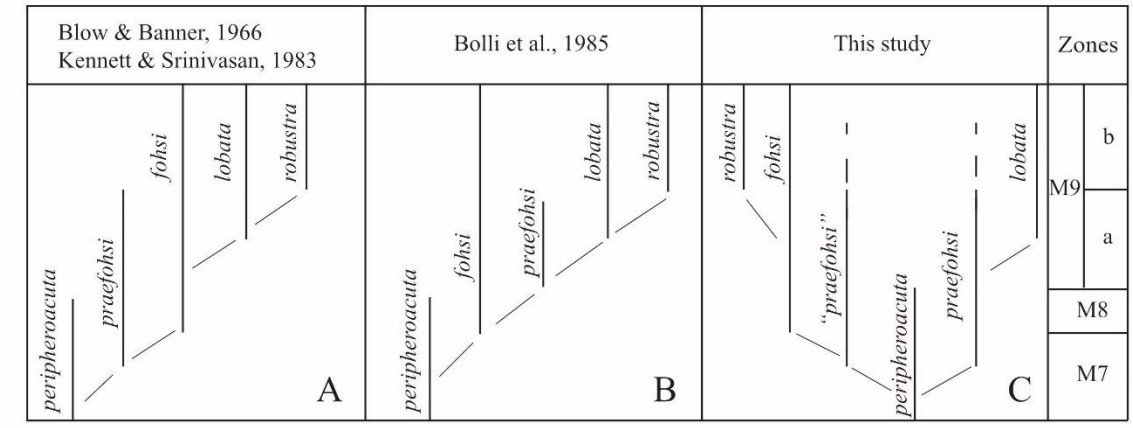
Blow & Banner, 1966
Kennett & Srinivasan, 1983
Bolli et al., 1985
This study
Zones
peripheroacuta
praefohsi
fohsi
lobata
robustra
A
peripheroacuta
fohsi
praefohsi
lobata
robustra
B
robustra
fohsi
"praefohsi"
peripheroacuta
praefohsi
lobata
C
M9
b
a
M8
M7

Figure 3

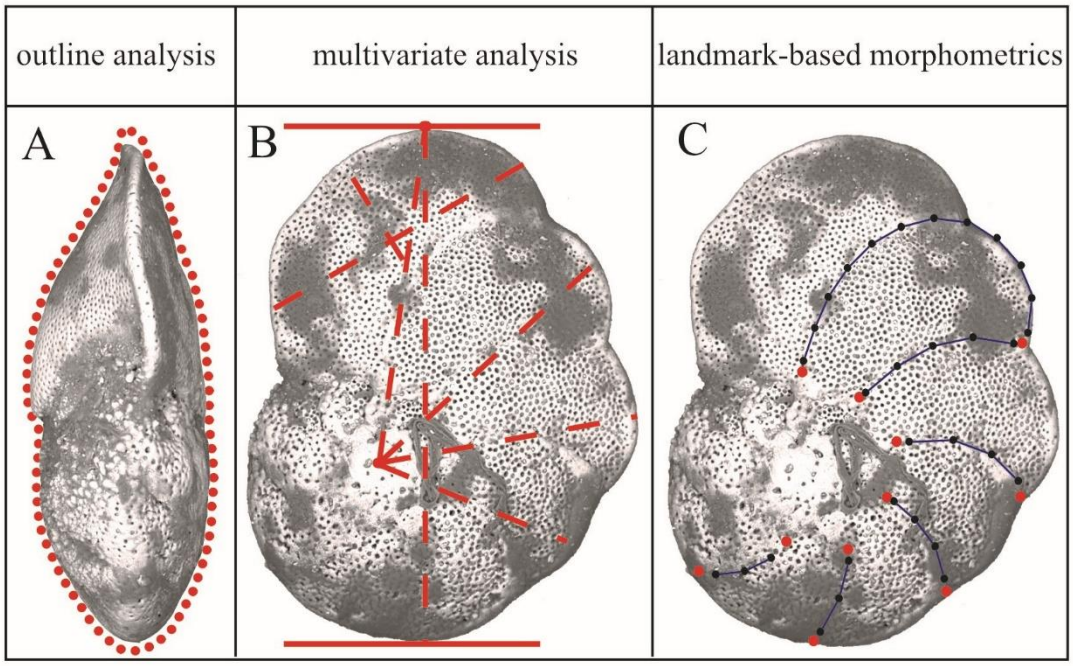
outline analysis
multivariate analysis
landmark-based morphometrics
A
B
C

Figure 4

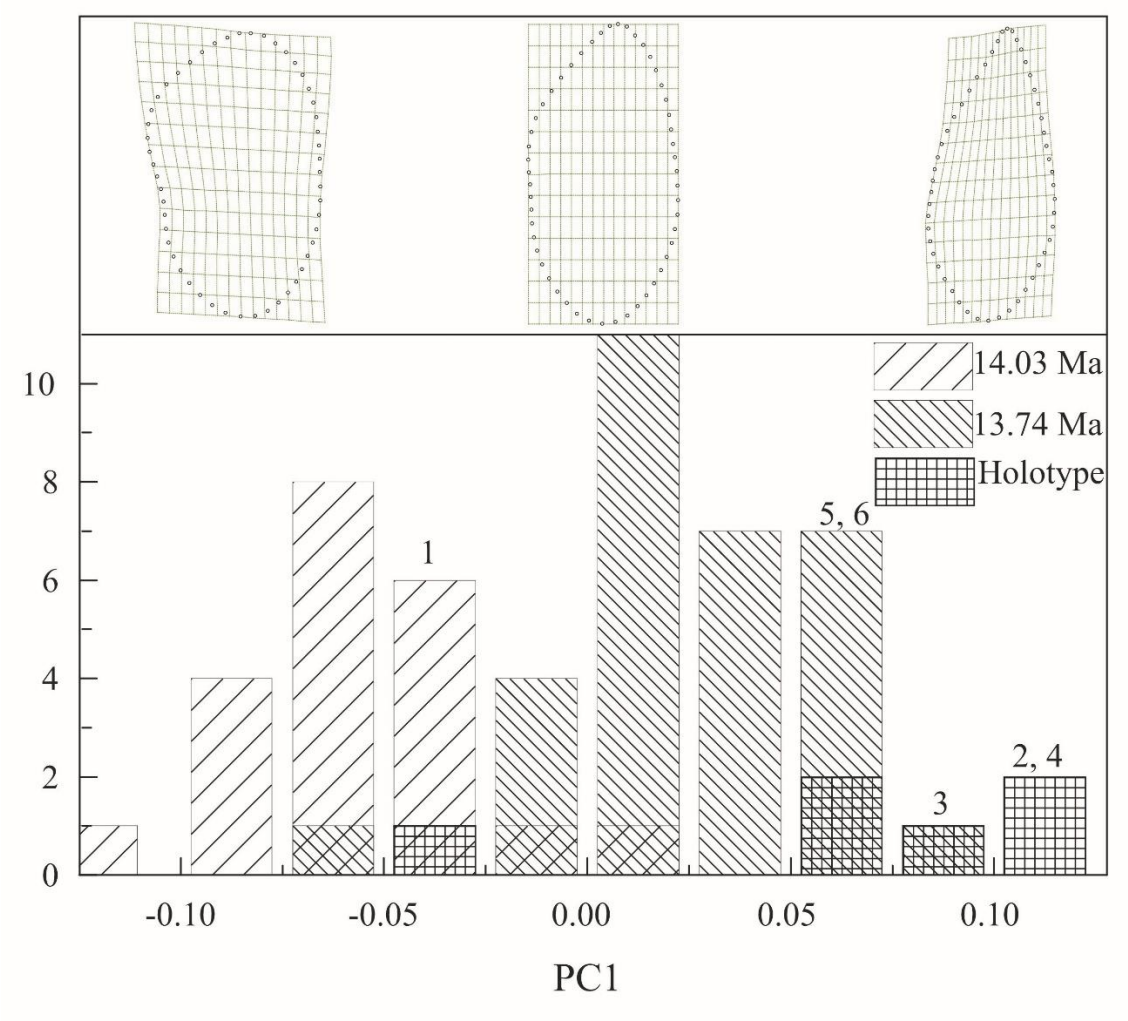
14.03 Ma
13.74 Ma
Holotype
10
8
6
4
2
0
1
5, 6
3
2, 4
-0.10
-0.05
0.00
0.05
0.10
PC1

Figure 5

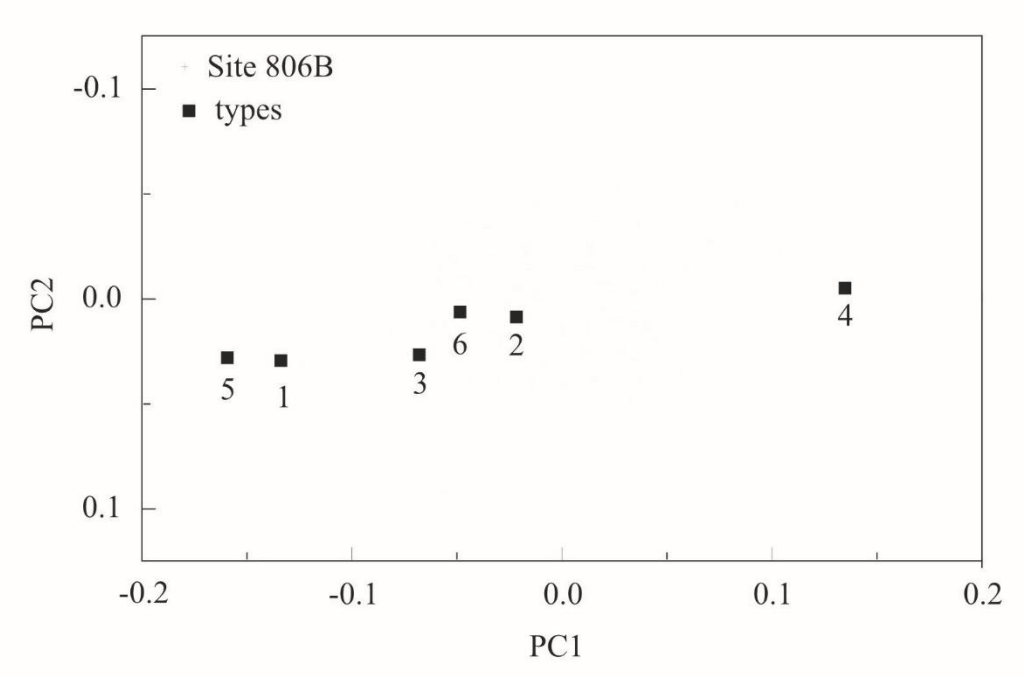

Figure 6

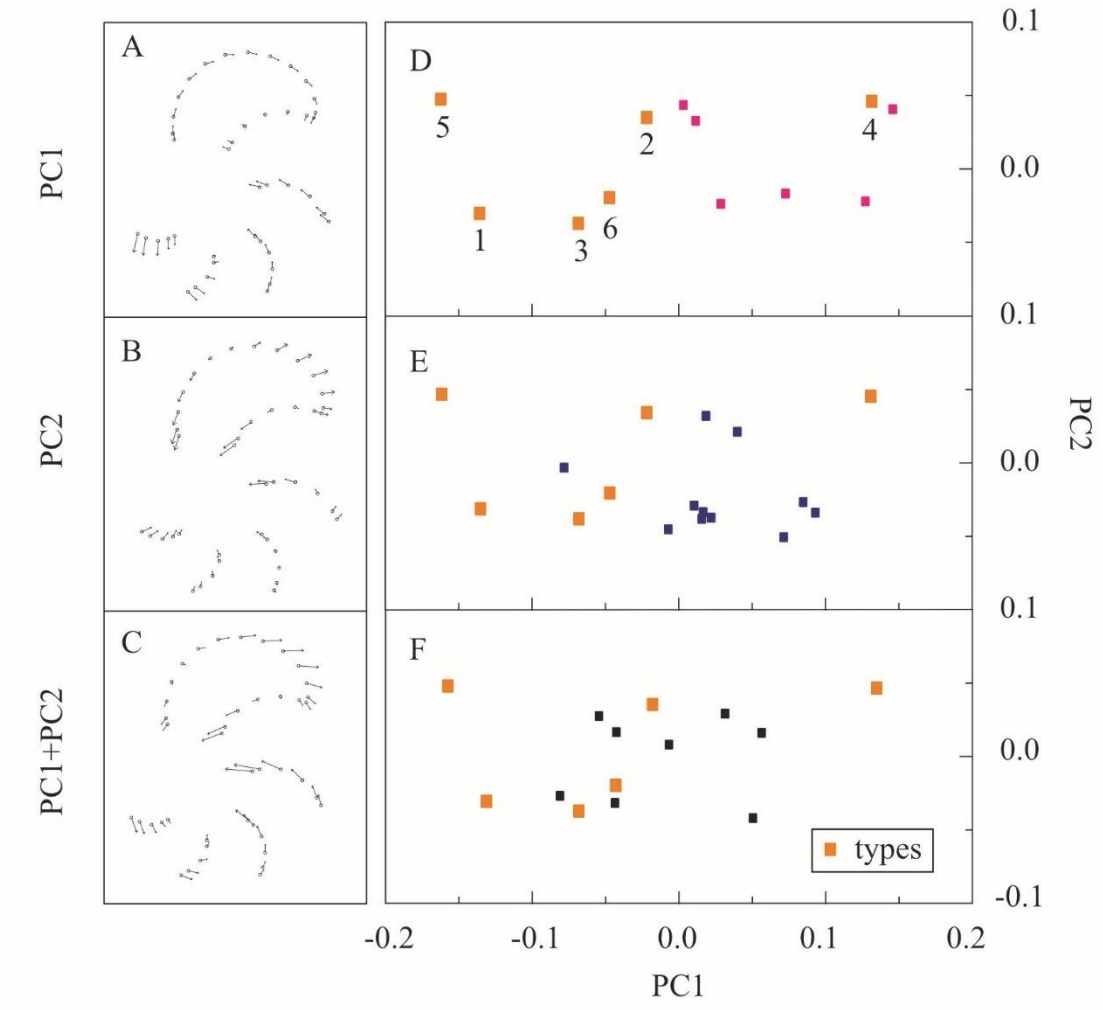
A
B
C
D
E
F
PC1
PC2
PC1+PC2
5
2
4
1
3
6
types
0.1
0.0
-0.1
-0.2
-0.1
0.0
0.1
0.2
PC1
PC2

Figure 7

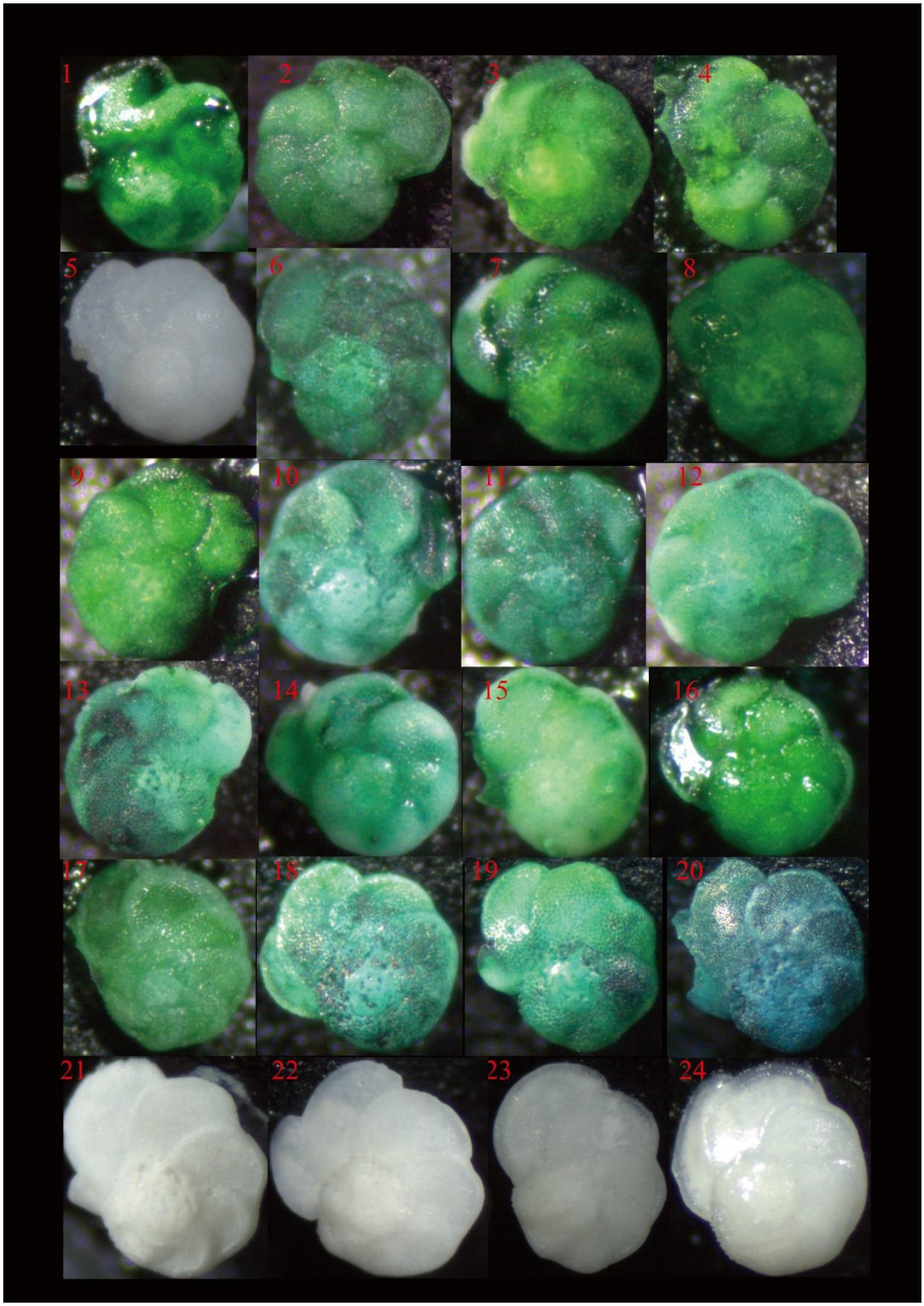

Figure 8

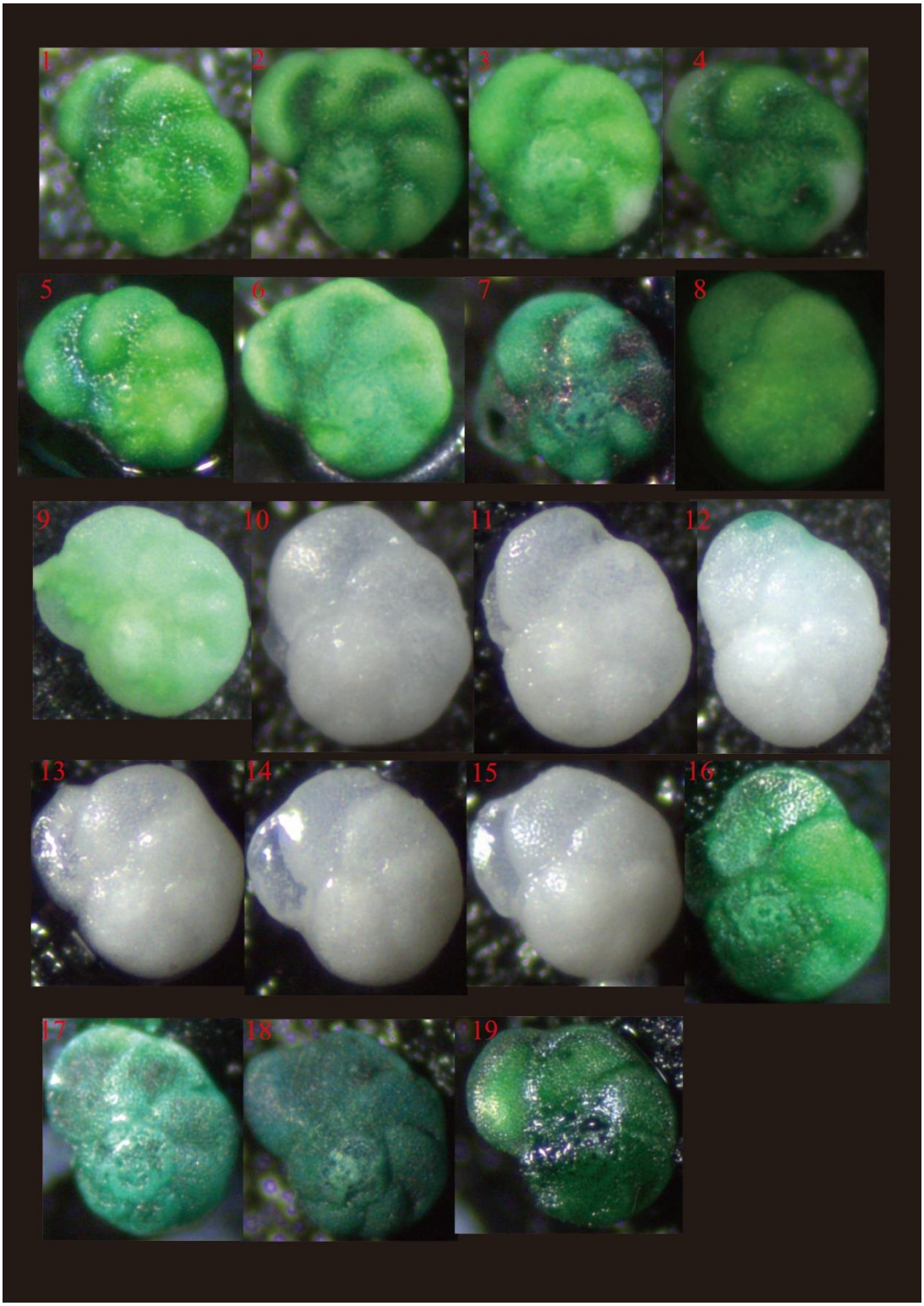

Figure 9

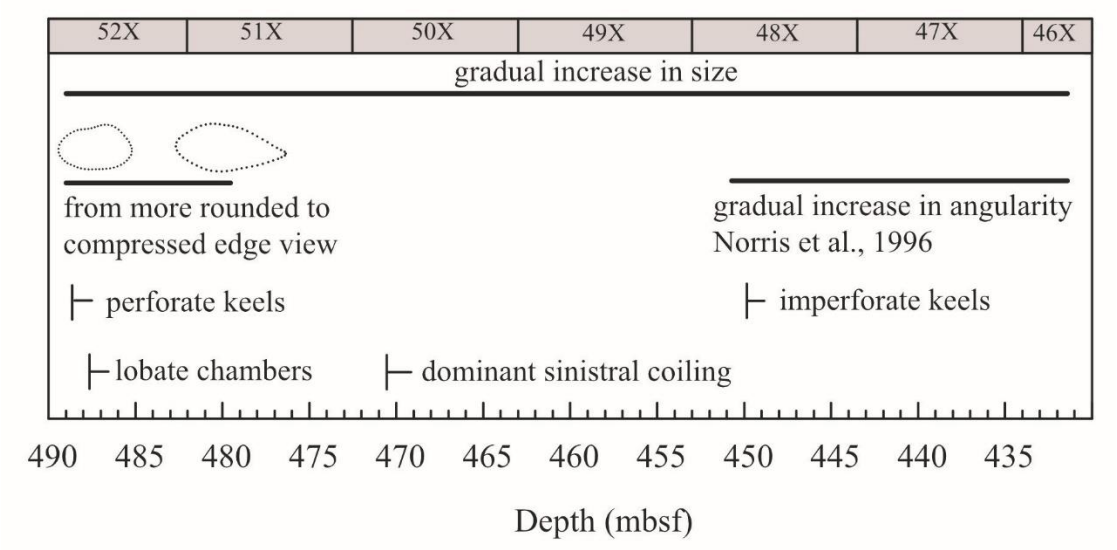
52X
51X
50X
49X
48X
47X
46X
gradual increase in size
from more rounded to
compressed edge view
gradual increase in angularity
Norris et al., 1996
perforate keels
imperforate keels
lobate chambers
dominant sinistral coiling
490
485
480
475
470
465
460
455
450
445
440
435
Depth (mbsf)

Appendix Figure S1

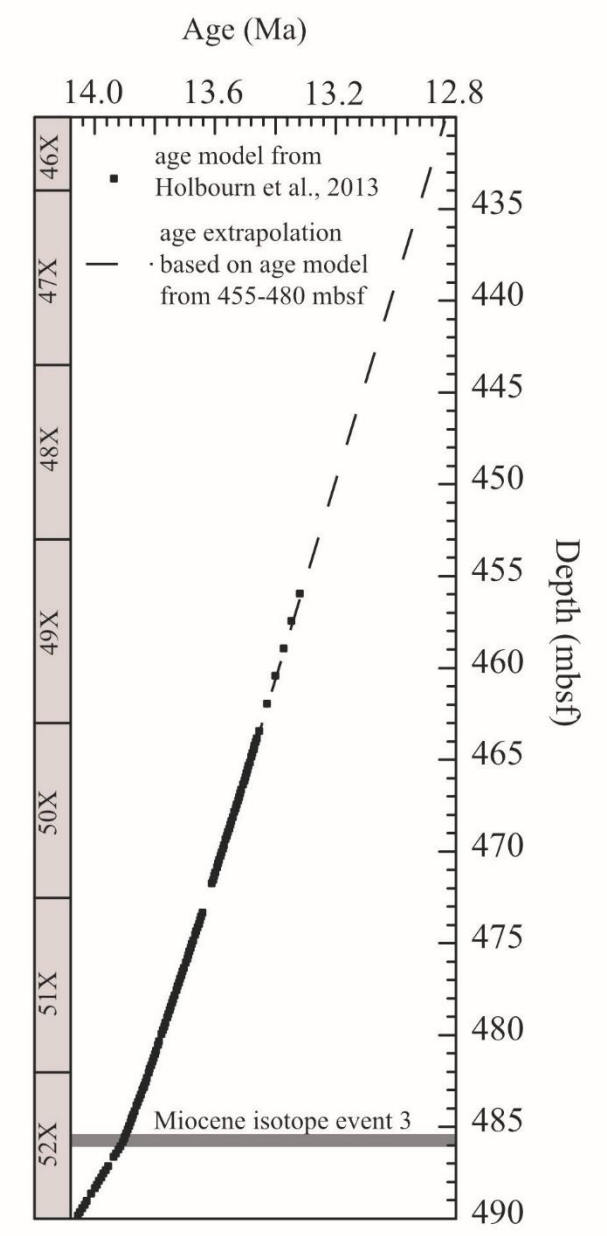

Appendix Figure S2

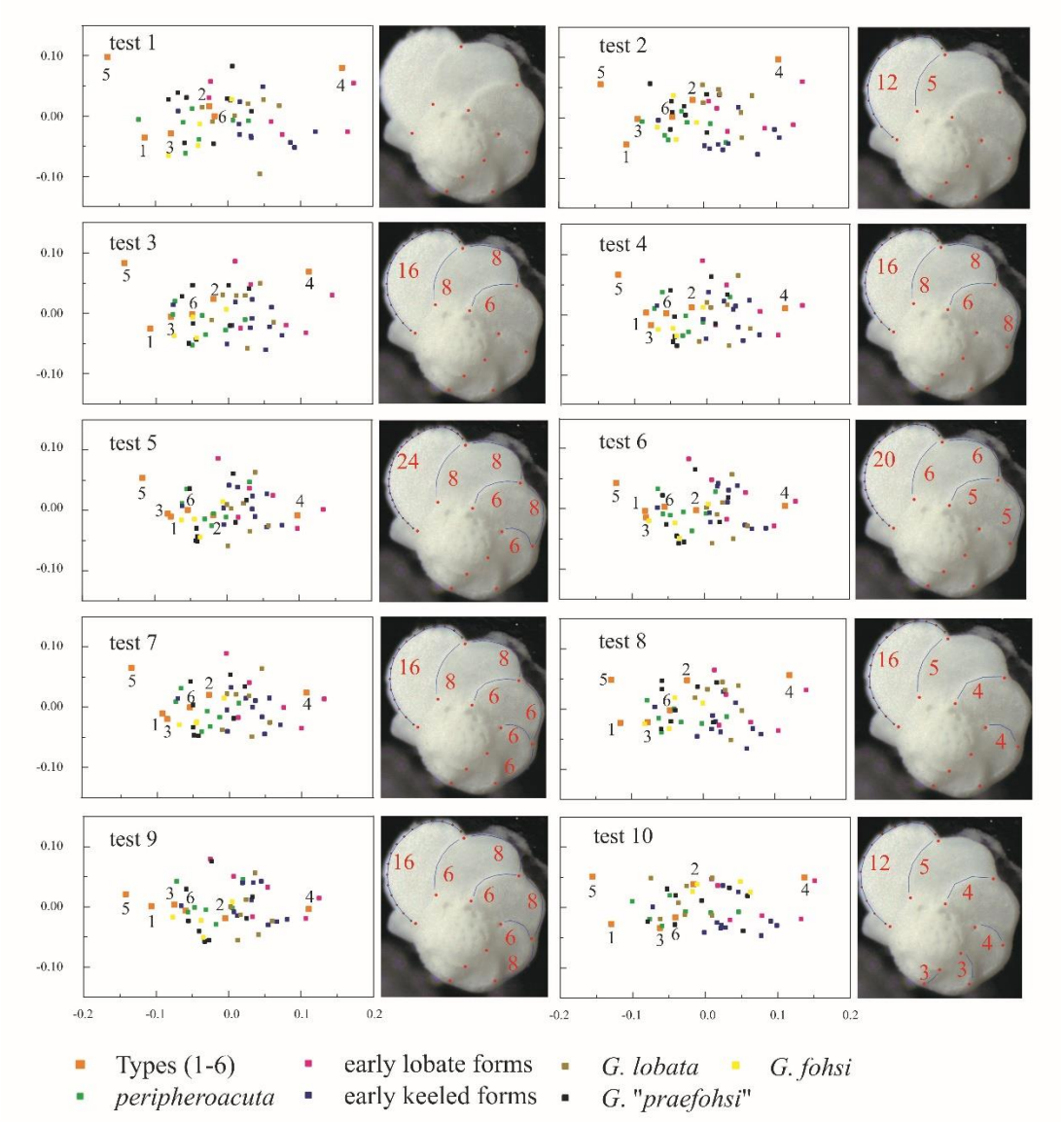

Table 1

	Chaisson and Leckie, 1993	Norris et al., 1996	Eisenach and Kelly, 2006	This study	Wade et al., 2011
Lowest occurrence of *fohsi*	~ 449.89 mbsf (between 806B/48/2:34–36 and 806B/48/5:34–36)	~450 mbsf (~13.0Ma in Norris et al., 1996)	460.21 mbsf (806B/49/6: 51cm)	fully keeled form: 487.6 mbsf, 806B/52/4:50–51cm become readily recognizable: ~460 mbsf, 806B/49/6:60–61	
Age (based on age model of this study)	~13.16–13.24 Ma	~13.2 Ma	~13.45 Ma	fully keeled form: ~13.97 Ma become readily recognizable in sample: 13.45 Ma	13.44 Ma

Chapter 3

Mosaic evolution in the middle Miocene planktonic foraminifera *Fohsella* lineage

Paper chapter

Si, W., Berggren, W. A., and Aubry, M. P. (2018). Mosaic evolution in the middle Miocene planktonic foraminifera Fohsella lineage. Paleobiology, 44(2), 263-272.

3.1 Abstract

Recent studies have shown that modes of evolution, namely directional trend, random walk, and stasis, vary across morphologic traits and over the geographic range of a taxon. If so, is it possible that our interpretation of evolutionary modes is actually driven by our selection of traits in a study? In an attempt to answer this question, we have restudied the middle Miocene planktonic foraminifera *Fohsella* lineage, an iconic example of gradual morphologic evolution. In contrast to previous studies that have focused on the gross morphology as embodied by the edge view of tests, we analyze here multiple phenotypic traits chosen because their biologic and ecologic significance is well understood in living populations. We find that traits in the lineage did not evolve in concert. The timing and geographic pattern of changes in shape, coiling direction, size, and ecology were different. The evolution of this lineage is a mosaic combination of different evolutionary modes for different traits. We suggest that overemphasis on the evolution of some single trait, such as the edge-view outline, from narrow geographic ranges, has significantly underestimated the dynamic evolutionary history of this group.

3.2 Introduction

Variances are the raw materials of evolution. Documenting temporal and spatial distribution of evolutionary variances within an ancestor-descendant lineage is important to understanding how evolution occurs (Alroy, 2000). Recent studies of fossil records have shown that patterns and modes of evolution, including directional trend, random walk and stasis, differ between morphologic traits (Hopkins and Lidgard, 2012; Hunt et al., 2015) within the geographic range of a taxon (Grey et al., 2008).

These discoveries suggest that earlier interpretations of the evolutionary patterns of some taxonomic groups may be incomplete if deduced from the analysis of a single trait and/or examined from a narrow geographic range. Interpretations of patterns of evolution may be biased by the selection of traits to be analyzed and also by the preferred morphometric methodologies used for a given taxonomic group (for example, the outline of edge-view is the most often examined in planktonic foraminifera). In addition, traits that are difficult to measure, including some ecologic and physiologic characters, are generally overlooked due to the lack of quantifiable proxies.

Finally, few evolutionary studies have compared evolutionary sequences of a lineage over broad geographic ranges with satisfactory age control. Even for Cenozoic marine microfossils that have by far the best documented continuous records, reducing uncertainties in dating and correlating multiple evolutionary records to/below ~10 kyr remains a challenge. This is because robust age control requires a significant amount of data from astrochronology, magnetostratigraphy and biostratigraphy, which are not

always available. For instance, a solid astrochronology over a 1 Myr interval requires several hundreds of stable isotope analysis.

In this study, we revisit the middle Miocene *Fohsella* lineage of planktonic foraminifera. The *Fohsella* lineage (previously referred to as the *Globorotalia fohsi* lineage, Supplementary Material) is of particular interest because it has long been considered an iconic example of gradual morphologic evolution in planktonic foraminifera, as opposed to the model of punctuated equilibrium. Its evolution between ~15–13 Ma is thought to have been gradual, as depicted by successive chronospecies linking the end members of the lineage (Kennett and Srinivasan, 1983). However, Norris et al. (1996) and Eisenach and Kelly (2006) have shown that the depth distribution of this lineage in the Western Pacific experienced a rapid shift from the surface layer to deeper depth, suggesting that the ecologic speciation was largely decoupled from the morphologic changes. Motivated by more recent studies which suggest that evolutionary changes can be introduced into an evolving lineage independently through different traits (e.g. Hopkins and Lidgard, 2012), we re-analyze the *Fohsella* lineage by incorporating multiple traits from different geographic settings. Our results show that the evolutionary history of the fohsellid lineage is very dynamic and complex. No single trait is representative of the evolutionary history in this lineage. The reconstruction of a more complete picture of the evolution of planktonic foraminifera requires consideration of multiple traits from broad geographic locations.

3.3 Phenotypic Models

Previous studies of planktonic foraminifera evolution (e.g. Malmgren et al., 1983, Norris et al., 1996; Hull and Norris, 2009; Pearson and Ezard, 2014) have focused on the changes through time of the edge view, using either outline or multivariate analysis. Although regarded as reliable proxies of the gross morphology, the biologic and/or taxonomic significance of the edge-view silhouettes is inadequately specified and difficult to interpret. Likewise, morphologic characters such as ratio of length to width have changed in fohsellids through time. While they have been extensively studied (e.g. Hodell and Vayavananda, 1993), providing a wealth of information on this group, it is not clear how they relate to biological and ecological characters of species.

Some phenotypic units in living planktonic foraminifera are better studied and their taxonomic, biologic and/or ecologic properties are better understood. Quantifying changes in these traits should provide more readily interpretable information on evolutionary patterns than unexplained characters, and sources of evolutionary variations can be more easily diagnosed. For example, although the specific adaptive function of size in planktonic foraminifera is debatable, its correlation with several environmental parameters such as water temperature in living species (Schmidt et al., 2004) make it possible for us to evaluate the size changes in fossil groups with paleoceanographic proxies. Similarly, the spiral-view morphology and coiling direction on the one hand, and the habitat ecology and size on the other hand, are characters with well specified taxonomic and ecological significance. Therefore, in this study we divide the *Fohsella* phenotype into these four subsets of characters.

Spiral-view shape: The spiral view provides information on the coiling growth of foraminiferal species (Olsson, 1971, Arnold, 1983). Its change can be explained by changes in ontogenetic spiral growth of the planktonic foraminifera (Tabachnick and Bookstein, 1990). We employ landmark-based morphometric analysis to quantify the spiral-view shape. Landmarks placed along sutures and adult test periphery (Method and Supplementary Material) help capture changes in chamber shape and sutures that cannot be effectively studied with other morphometric methods, such as outline and multivariate analysis. Theoretically, landmark deformations along principal component axes also help interpret which spiral-growth parameter(s) have generated most observed variations (Tabachnick and Bookstein, 1990). For example, adjacent chambers will overlap more when successive chambers are added to the test at a smaller angular-increment rate. As a result, more chambers will be exposed in the final whorl and each chamber will occupy less areas in the final whorl (Supplementary Material for more illustrations).

Coiling direction: genetic and paleontological studies on planktonic foraminifera suggest that heritable change in coiling direction is an important aspect of their evolution, being related in some instances to genetic-level evolution (de Vargas et al., 2001; Kučera and Kennett, 2002; Darling et al., 2004; Darling and Wade, 2008; Ujiié and Asami, 2014). In fohsellids, the coiling direction changed worldwide at ~13.6 Ma from near randomness to strong preference for sinistral coiling that persisted until the extinction of the lineage (Bolli, 1950; Blow and Banner, 1966; Bolli et al., 1985; Eisenach and Kelly, 2006). Temporal and geographic patterns of coiling direction are studied in this work.

Depth habitat ($\delta^{18}O$ of the test): planktonic foraminifera species inhabit different ecologic niches in the water column (Hemleben et al., 1988). The tests of foraminifera populations residing at different depths record $\delta^{18}O$ values that are specific of those depths due to the temperature gradient of the water column (Fairbanks et al., 1980; Birch et al, 2013). Thus $\delta^{18}O$ measurements allow reconstruction of species stratification in the past. Ecologic subdivision has been proposed as a potential mechanism for sympatric speciation in open ocean environments (Lazarus et al., 1995; Norris 2000) in the absence of geographic barriers. Previous studies have suggested that fohsellid populations globally migrated from the upper surface to the subsurface at ~13.2 Ma, probably in response to ecologic speciation (Norris et al., 1993, 1996). We generate $\delta^{18}O$ data on individual specimens of fohsellids along with *Dentoglobigerina altispira* and *D. venezuelana,* the habitats of which are believed to be, respectively, shallower and deeper than those of fohsellids (Keller, 1985; Norris et al., 1996; Stewart et al., 2012). New data are combined with previously published data (Norris et al, 1996, Eisenach and Kelly, 2006) to provide more statistically robust evidence of the divergence of fohsellid populations between 12.9 and 13.5 Ma.

3.4 Materials and Methods

Three deep-sea sites with broad geographic coverage were examined (Fig. 1). Fohsellids from Site 806 were studied previously for outline analysis on edge-view by Norris et al. (1996), for coiling direction by Eisenach and Kelly (2006), and for isotopes by both authors. It is the primary site in this investigation and it has been resampled at high

resolution. Site U1338 has been studied for coiling pattern by Hayashi et al. (2013). It has been sampled at selective intervals based on astrochronology for comparison with data from Site 806. Site 563 was previously sampled by Wright et al. (1992) and magnetostratigraphic and chemostratigraphic data are available for age correlation. We chose these sites because of their relatively good age control. More importantly, the oceanographic conditions at the three sites were very different, especially at Site U1338 with cooler upwelling in the Eastern Pacific compared with the warmer waters in the Western Pacific. We expect that these differences in temperatures, nutrient levels and/or water column structures would have affected the fohsellid populations and generated geographic variations.

Landmark morphometrics — Landmark morphometrics are used to quantify the spiral-view shape (suture, chamber and test periphery). Eleven landmarks were placed where intercameral suture and periphery meet. Given that the number of chambers in the last whorl in fohsellids varies between five and seven, eleven landmarks allow a good coverage of the chambers exposed in the last whorl. Six curves of semi-landmarks were then placed between landmarks to capture intercameral suture and chamber shape information (Fig. 2A). We follow the standard landmark method (Zelditch et al., 2004) in collecting and processing shape variables. The spiral-view shape is then summarized as the first principal component (PC1) of shape variables. Shape variations due to changes in PC1 are plotted (Fig. 2B) to help understand which growth parameters may have contributed to the observed changes (see Supplementary Materials for more illustrations).

Statistical analysis — The evolutionary modes of spiral-view shape and size evolution are evaluated with statistical models developed for random walk, directional changes and stasis (Hunt, 2006, Sheets and Mitchell, 2001). Due to uneven sampling in our study, parameters are estimated from a Bayesian approach using the Metropolis algorithm which numerically simulates the posterior distribution of parameters. Relative model support is based on calculated Deviance Information Criterion (DIC). The lower the DIC value of a model, the better the model is supported by the data relative to competing models. Details of statistical inference is presented in Supplementary Materials.

Temporal framework — All phenotypic data are combined using an integrated age framework based on correlated astrochronology, magneto- and isotope stratigraphy (Supplementary Material, Age Model). Sites 806 and U1338 records are correlated with a resolution of ~5 kyr using astronomically-tuned benthic stable isotope records (Holbourn et al., 2013; Holbourn et al., 2014). Age control of the Site 563 record is relatively poor due to the lack of high-resolution isotope astrochronology. Combined benthic foraminiferal isotope data and magnetostratigraphy, nevertheless, permit a reliable correlation of the Site 563 record to other sites (Supplementary Material).

3.5 Results

Shape — Visually, the PC1 of the spiral view at Site 806 shows little change between 14.2 and 12.9 Ma (Fig. 3A), and this is supported by the model test (Table 1), which yields lowest DIC in a simple stasis model relative to the random walk and directional evolution model. However, between ~13.41–13.44 Ma, the PC1 of two samples shows a

rapid shift in the mean values relative to adjacent samples (ANOVA, $p < 0.001$), corresponding to the rapid turnover in coiling direction (Fig. 3C). The distribution of PC1 at Sites U1338 and 563 are different and are discussed below.

Size — The mean size increases substantially at Site 806, showing an "apparent" trend from ~325 µm to ~600 µm between ~14.2–12.9 Ma (Fig. 3B). DIC values (Table 1) and provides approximately equal support to a random walk model and a directional model for size changes. The fohsellids are smaller at Sites U1338 and 563 than at Site 806, with the Site U1338 populations exhibiting the smallest average size (~280 µm) (Fig. 3B).

Coiling direction — At Site 806 the coiling direction is proportionate (~60% sinistral) prior to 13.7 Ma and then more dextrally dominant between 13.66–13.58 Ma. A shift to dominantly sinistral occurred at ~ 13.58 Ma (~360.94–361.34m; Fig. 3C). At Site U1338, the shift to dominant sinistral coiling also occurred at ~13.58 Ma (~360.94–361.34 m CCSF-A), in agreement with Hayashi et al (2013) who reported the shift at ~361 m CCSF-A. Based on our sampling resolution, we tentatively estimate that this shift took place within 11 kyr. At Site 563, the coiling direction was variable prior to 13.67 Ma but with a preference for sinistral coiling between 13.67–13.8 Ma. The change in coiling direction to sinistrally dominant may have started slightly earlier at this site (13.67 Ma) than at Site 806 and U1338. However, this discrepancy in timing may reflect weaker age control at Site 563 (Supplementary Material).

The $\delta^{18}O$ record — The composite $\delta^{18}O$ records of Site 806 (Norris et al., 1996, Eisenach and Kelly, 2006, and this study) are characterized by three intervals. Prior to 13.25 Ma fohsellid populations have $\delta^{18}O$ (-1.2±0.27‰) lighter than that of the surface species *D. altispira* (-1.0‰) and thermocline species *D. venezuelana* (-0.5~-0.75‰) (Fig. 4A, B). From ~13.25 to 12.95 Ma, the $\delta^{18}O$ of the populations is centered over -0.85±0.26‰. This interval is characterized by the occurrence of individuals with $\delta^{18}O$ heavier than *D. altispira* (Fig. 4A, B). After 12.95 Ma, there are no fohsellids with $\delta^{18}O$ lighter than *D. altispira*; only specimens with heavier $\delta^{18}O$ are present (Fig. 4A, C). Most individuals from Sites U1338 and 563 are too small to have enough mass for isotope analysis, preventing a geographic comparison of contemporary populations.

3.6 Mosaic evolution of different traits

Despite some changes in the structure of the upper water column, the warm surface waters of the Western Equatorial Pacific have been relatively stable over geologic time (Zhang et al., 2014) compared to other water masses such as upwelling zones, temperate and high latitude regions. Yet, the fohsellid populations at Site 806 exhibit a rather dynamic evolution in this geologically stable environment.

The coiling direction shows a rapid shift to permanent sinistral dominance at ~13.58 Ma within the limit of sampling resolution (~13.58–13.66 Ma), suggesting punctuated changes relative to subsequent long-term stasis. On the other hand, there is an apparent long-term trend towards larger size over the interval studied. Similar to previous research (Hunt 2006), model estimates provide about equal support to a random walk model and a

directional model for the apparent size increases, giving no definitive answer on which process is responsible for the increase. However, the geographic pattern of size distribution within the Equatorial Pacific suggests that the size increase reflects an active trend. While the size increase at Site 806 is significant, contemporary populations at Eastern Equatorial Pacific Site U1338 remain small (Fig. 3B). Given the capability of long-distance dispersal of planktonic foraminifera, the development of a geographic cline within the Equatorial Pacific, characterized by more nutrient-rich upwelling in the eastern side and a more oligotrophic and stratified water column in the western side, may have played an important role in driving and maintaining the long-term divergence in size within equatorial Pacific (see discussion below).

The $\delta^{18}O$ pattern of fohsellids at Site 806 suggests a "cladogenetic" event in habitat ecology (Norris et al., 1996) and subsequent extinction of one subpopulation. Prior to ~13.25 Ma, the consistently more negative $\delta^{18}O$ of fohsellids relative to the surface water species *D. altispira* suggests that the fohsellid populations inhabited the uppermost surface waters, recording high sea surface temperatures. Beginning ~13.25 Ma, the $\delta^{18}O$ of the fohsellid populations straddled a wider range of values towards the more positive $\delta^{18}O$ of *D. venezuelana*, implying that some fohsellids began exploring new habitats close to the shallow thermocline (Fig. 4). This expansion into a deeper habitat has been suggested as ecologic speciation through ontogenetic migration (Norris et al., 1996).

The shallower populations disappeared after ~12.95 Ma. One possible explanation for the disappearance of surface populations involves regional oceanographic changes. As an

oligotrophic warm water species, *Fohsella* may have been very sensitive to sea surface temperatures. However, Site 806 is located at the heart of the modern-day Western Pacific Warm Pool. The sea surface temperature of studied area has been proven to have been relatively stable (Zhang et al., 2014), and there is no evidence of changes in surface temperatures over the studied interval (Nathan and Leckie, 2009). Alternatively, if we accept the explanation by Norris et al. (1996) regarding the ecologic speciation through ontogenetic migration in *Fohsella*, the disappearance of the surface populations may have been ecological. Fohsellids may undergo depth migration during the ontogeny, inhabiting surface ocean during juvenile stages but calcifying and reproducing at depth during adult stage. If this is true, then the disappearance of surface populations is a pseudo-extinction. However, without isotopic studies on the ontogenetic changes of *Fohsella* and data from wider geographic coverage, the causes for habitat changes in foshellids remain undetermined.

Contrary to the dynamic changes in coiling direction, size and depth distribution, the spiral-view shape shows little change (Fig. 3). One exception is a shift in PC1 between 13.41 and 13.44 Ma (Fig. 3A, arrow indicated) that appears to be associated with the temporary reversal in coiling direction. This brief reversal in coiling direction may have affected the spiral growth in fohsellids and therefore their spiral-view shape. However, this observation on correlated changes between two traits relies only on two samples at this moment and requires further testing. Except for this brief interval, the spiral view morphology revealed in PC1 are stable over time relative to the other three traits.

Living planktonic foraminifera often harbor great genetic diversity within described morphotypes (Darling and Wade, 2008). Although these cryptic genotypic populations are difficult to distinguish based on overall morphology, detailed taxonomic work suggests that subtle but consistent differences in some traits, such as coiling pattern, test microstructure, porosity, depth distribution (as inferred from $\delta^{18}O$), among others, aid recognition of different populations (Huber et al., 1997; de Vargas et al., 1999; Darling et al., 2006). Our records from the Western Equatorial Pacific agree with observations in extant populations and they reveal that dynamic evolutionary changes occurred at subspecies levels in one of the most stable surface oceanic environments. Because the timing and modes of evolutionary changes in different traits are disassociated, the evolution of fohsellid populations at Site 806 follows a mosaic pattern.

3.7 Geographic Mosaic

In addition to the mosaic evolutionary changes of different phenotypic units at Site 806, size and spiral-view PC1 also exhibit geographic variations superimposed on synchronous coiling-direction changes in our three oceanic locations (Fig. 3), suggesting a geographic mosaic of local adaptation and coevolution among fohsellid populations. Geographic heterogeneity is particularly well marked within the Equatorial Pacific. The Eastern Pacific populations at Site U1338 stand apart from populations at Site 806 and Site 563 despite the fact that they are geographically intermediate. Since ocean currents should be able to effectively mix and disperse planktonic foraminifera populations within the Equatorial Pacific on a monthly scale (van Sebille et al., 2015), the apparent and persistent difference in shape and size may reflect faunal provincialism possibly due to

the development of environmental gradients between the Western and Eastern Equatorial Pacific as the Earth's climate transitioned from a relatively warm phase to a colder mode during the middle Miocene (Flower and Kennett, 1994).

The development of a permanent Antarctic Ice Sheet at ~13.9 Ma, for example, has been suggested to have promoted shoaling of the thermocline and intensification of upwelling within the Eastern Equatorial Pacific (Holbourn et al., 2014). The emergence of this "cold tongue" in the eastern side of the basin could have intensified the hydrologic cline within the Pacific. And the cooler, nutrient-rich waters in the Eastern Pacific may have had a negative impact on the tropical fohsellids, as indicated by their lower abundance at Site U1338 relative to Site 806 (Site 806: >100 specimens per 10-gram sample; Site U1338: ~15–30 specimens per 10-gram sample; Mass Accumulation Rates of sediments at the two sites were similar between 14–13 Ma, ~3–5 gram/cm^2 kyr). Assuming a modern-day correlation between sea-surface temperatures and foraminiferal test size (Schmidt et al., 2004), for example, the west-east oceanographic gradient may explain sustained differences in size and spiral growth (spiral-view shape) in fohsellids.

With these additional oceanographic constraints, the increase in size at Site 806 and corollary divergence between Sites 806 and U1338 were thus probably a response to environmental changes rather than simple random walk, despite the DIC values yield equal support to both modes. Our ongoing efforts in documenting more fohsellid sequences from other Eastern Equatorial Pacific sites and reconstructing regional paleoceanography and hydrology might provide further information on the coupled

relationship between high-latitude climatic changes and initiation of tropical faunal provincialism during the Neogene.

Regardless of the specific paleoenvironmental trigger for this geographic mosaic, our data agree with earlier studies that suggested that geography is crucial in understanding the modes of lineage evolution (Eldredge et al., 2005; Grey et al, 2008). Several recent studies have suggested that stasis and random walk modes are prevalent whereas directional evolution is infrequent in paleontological sequences (Hopkins and Lidgard, 2012; Hunt et al., 2015). However, evolutionary processes such as directional trend may occur only in certain geographical areas but become obscure in others. Sampling from locations peripheral to the evolutionary center of a lineage may fail to recover the critical records when lineages gain net morphologic accumulation (e.g. Site U1338 may be located at the edge of the optimal range for *Fohsella*). Therefore, a more accurate understanding of evolutionary patterns and the role of geography in generating these patterns (Kirkpatrick et al., 1997) requires detailed geographic surveys of lineages under very robust chronologic control. This has not been available in most paleontological records to date.

3.8 Evolution of other traits

So far, we have illustrated the evolutionary changes of four traits between ~14–13 Ma. However, other traits have also contributed to the total evolutionary variances of fohsellids. At Site 806, Norris et al. (1996) have shown that the angularity of the edge-view projection of fohsellids changed significantly between ~13–12 Ma in a gradual

fashion, beginning slightly before the rapid changes in depth habitat ($\delta^{18}O$). At a nearby site in Western Pacific (Site 289), Hodell and Vayavananda (1993) documented long-term increases in test area, length, breadth and ratio of length/breadth from ~15 to 11.5 Ma. They also discovered a rather rapid $\delta^{18}O$ shift in multi-specimen isotope data ~13 Ma, consistent with patterns seen at Site 806. Unfortunately, limited stratigraphic information from this site prevents us from further combining these data with ours for comparison.

The keel is another characteristic feature of *Fohsella* and it has substantially evolved. Early fohsellids are characterized by a rounded periphery without keels. Beginning ~13.9 Ma, a perforate keel (for definition, see Norris, 1991) occurred sporadically in adult chambers of fohsellid population. This perforate keel began to extend to pre-adult chambers in the last whorl and eventually (after ~13.4 Ma) evolved into an "imperforate" band covered with additional calcite on the keel surface, giving a robust and imperforate appearance.

We do not investigate further details of all traits listed above. On the one hand, the biologic/ecologic significance of these measurements are not yet well understood. For example, it is unclear what the ratio of length/width or the silhouettes of the edge view projection tells us about the physiology and/or ecology of foraminifera. On the other hand, some of these measurements may not be independent. The test area and other metric measurements may be strongly correlated with test size, in which case the multivariate dataset may include redundant measurements. Finally, the evolutionary changes of

certain traits, such as different stages of keel development, are difficult to quantify, preventing a succinct numeric summary of its temporal patterns.

Nevertheless, the diverse evolutionary patterns documented in these additional traits lend further support to the interpretation of mosaic evolution in fohsellids, which can be summarized as follows. First, the timing of these evolutionary changes are different. Chronologically, the evolution of an early keel began ~13.9 Ma and evolved into an "imperforate" band after 13.4 Ma. The changes in coiling direction occurred at ~13.58 Ma, with a rapid reversal at ~13.44 –13.41 Ma. The expansion of *Fohsella* populations into the thermocline occurred at ~13.2 Ma and the loss of surface subpopulations dated at ~12.95 Ma. Second, the evolutionary mode varies among traits and/or over time. The spiral-view PC1 remained stable while others showed intervals of rapid changes and reversals (coiling direction and depth habitat). Still other traits exhibited long-term trends (e.g. size). Even for the spiral-view shape, the stasis between ~14–13 Ma does not mean that the evolutionary mode of this trait did not change over time. As one of the anonymous reviewers pointed out "the curvature of inter-cameral sutures in spiral view has changed from being radial to curved as chamber shapes evolved from being subround to axially compressed and subacute early in the evolutionary history of the fohsellids during the transition from *Fohsella*? *kugleri* to *F. peripheroacuta* (~ late early Miocene to early middle Miocene)". Our recent sampling from Site 806 confirms this observation. However, one of the obstacles to pursue this question further is our ability to establish high resolution stratigraphic correlation over wide geographic ranges. The stratigraphy of

late early Miocene to early middle Miocene has been particularly difficult at this moment (Miller et al., 2017).

In summary, because the timing and patterns of evolution of all analyzed traits are different, and different modes may also characterize the same trait, contingent upon the particular time interval being considered (e.g. see Hopkins and Lidgard, 2012), we conclude that no single evolutionary mode is representative of the evolution of the *Fohsella* lineage. The evolution of various phenotypic units all contributed to the evolution of fohsellids.

3.9 Conclusions

Based on improved phenotypic, geographic and chronologic models, this study presents a picture different from the conventional view of phyletic gradualism in open-ocean planktonic foraminifera species. The evolutionary history of fohsellids is considerably more dynamic and complicated than thought earlier. Rather than "morphing" progressively along a global trend from ancestors to descendants as hypothesized (e.g. Bolli et al., 1985, Norris et al., 1996), the evolution of fohsellids involves stasis, long-term trends, punctuated changes, temporary reversal as well as extinction of subpopulations. These evolutionary changes did not occur in concert and were geographically independent: populations from different geographic provinces underwent divergent evolution.

Our findings highlight the fact that estimates of modes and rates of evolution are highly dependent on measured traits and geographic settings. Interpretation based on a single trait from one location will likely underestimate the evolutionary dynamics of a group, even if the lineage is capable of long-distance dispersal as is the case for the planktonic foraminifera. Also, conventional analytical procedures that overemphasize “pure” morphologic measurements and “overall shape” hinder our capability to diagnose and partition sources of variations during evolution. A more complete and accurate picture of lineage evolution may be obtained from appropriate elaboration of phenotypic models, complemented by measurements of multiple traits including ecologic characters (such as those carried by the geochemistry of skeletons) from wide geographic areas with fine chronologic controls.

3.10 Acknowledgments

We thank R. K. Olsson and D. Bord for their insightful discussion and advice on the evolution of the fohsellid lineage. A. Holbourn generously provided astronomically tuned benthic foraminifera data. J. D. Wright and K. G. Miller provided samples from Site 563 and suggestions on stratigraphic correlations. We thank two anonymous reviewers for their constructive and thoughtful comments. This research was supported by a Rutgers Student Fellowship and Joseph A. Cushman Award for Student Research to W. Si. Stable isotope measurements were provided by Rutgers University in support of research by W. A. Berggren. Samples were provided by the International Ocean Discovery Program (IODP).

3.11 References

Alroy, J. 2000. Understanding the dynamics of trends within evolving lineages. Paleobiology 26:319–329.

Arnold, J. 1983. Phyletic Evolution in the *Globorotalia crassaformis* (Galloway and Wissler) Lineage – a Preliminary-Report. Paleobiology 9:390–397.

Birch, H., H. K. Coxall, P. N. Pearson, D. Kroon, and M. O'Regan. 2013. Planktonic foraminifera stable isotopes and water column structure: Disentangling ecological signals. Marine Micropaleontology 101:127–145.

Blow, W. H., and F. Banner. 1966. The morphology, taxonomy and biostratigraphy of *Globorotalia barisanensis* LeRoy, *Globorotalia fohsi* Cushman and Ellisor, and related taxa. Micropaleontology 12:286–302.

Bolli, H. M. 1950. The direction of coiling in the evolution of some Globorotaliidae. Contributions from the Cushman Foundation for Foraminiferal Research 1:82–89.

Bolli, H. M., and J. B. Saunders. 1985. Oligocene to Holocene low latitude planktic foraminifera. In: Bolli, H. M., Saunders, J. B., Perch-Nielsen, K. (Eds.), Plankton Stratigraphy: Volume 1. Cambridge University Press, Cambridge.

Darling, K. F., M. Kucera, C. J. Pudsey, and C. M. Wade. 2004. Molecular evidence links cryptic diversification in polar planktonic protists to Quaternary climate dynamics. Proceedings of the National Academy of Sciences USA 101:7657–62.

Darling, K. F., and C. M. Wade. 2008. The genetic diversity of planktic foraminifera and the global distribution of ribosomal RNA genotypes. Marine Micropaleontology 67:216–238.

de Vargas, C., S. Renaud, H. Hilbrecht, and J. Pawlowski. 2001. Pleistocene adaptive radiation in *Globorotalia truncatulinoides*: genetic, morphologic, and environmental evidence. Paleobiology 27:104–125.

Eisenach, A. R., and D. C. Kelly. 2006. Coiling preferences and evolution in the middle Miocene *Fohsella* chronocline. Marine Micropaleontology 60:243–257.

Eldredge, N., J. N. Thompson, P. M. Brakefield, S. Gavrilets, D. Jablonski, J. B. Jackson, R. E. Lenski, B. S. Lieberman, M. A. McPeek, and W. Miller. 2005. The dynamics of evolutionary stasis. Paleobiology 31:133–145.

Fairbanks, R. G., P. H. Wiebe, and A. W. Be. 1980. Vertical distribution and isotopic composition of living planktonic foraminifera in the Western North Atlantic. Science 207:61–63.

Flower, B. P., and J. P. Kennett. 1994. The middle Miocene Climatic Transition - East Antarctic Ice-Sheet Development, Deep-Ocean Circulation and Global Carbon Cycling. Palaeogeography Palaeoclimatology Palaeoecology 108:537–555.

Grey, M., J. W. Haggart, and P. L. Smith. 2008. Variation in evolutionary patterns across the geographic range of a fossil bivalve. Science 322:1238–1241.

Hayashi, H., K. Idemitsu, B. S. Wade, Y. Idehara, K. Kimoto, H. Nishi, and H. Matsui. 2013. Middle Miocene to Pleistocene planktonic foraminiferal biostratigraphy in the eastern equatorial Pacific Ocean. Paleontological Research 17:91–109.

Hemleben, C., M. Spindler, and O. R. Anderson. 1989. Modern planktonic foraminifera. Springer-Verlag, New York.

Holbourn, A., W. Kuhnt, M. Frank, and B. A. Haley. 2013. Changes in Pacific Ocean circulation following the Miocene onset of permanent Antarctic ice cover. Earth and Planetary Science Letters 365:38–50.

Holbourn, A., W. Kuhnt, M. Lyle, L. Schneider, O. Romero, and N. Andersen. 2014. Middle Miocene climate cooling linked to intensification of eastern equatorial Pacific upwelling. Geology 42:19–22.

Hodell, D. A., and A. Vayavananda. 1993. Middle Miocene paleoceanography of the western equatorial Pacific (DSDP site 289) and the evolution of *Globorotalia* (*Fohsella*). Marine Micropaleontology 22: 279–310.

Hopkins, M. J., and S. Lidgard. 2012. Evolutionary mode routinely varies among morphological traits within fossil species lineages. Proceedings of the National Academy of Sciences USA 109:20520–20525.

Huber, B. T., J. Bijma, and K. Darling. 1997. Cryptic speciation in the living planktonic foraminifer *Globigerinella siphonifera* (d'Orbigny). Paleobiology 23:33–62.

Hull, P. M., and R. D. Norris. 2009. Evidence for abrupt speciation in a classic case of gradual evolution. Proceedings of the National Academy of Sciences USA 106:21224–21229.

Hunt, G. 2006. Fitting and comparing models of phyletic evolution: random walks and beyond. Paleobiology 32:578–601.

Hunt, G., M. J. Hopkins, and S. Lidgard. 2015. Simple versus complex models of trait evolution and stasis as a response to environmental change. Proceedings of the National Academy of Sciences 112:4885–4890.

Keller, G. 1985. Depth stratification of planktonic foraminifers in the Miocene ocean. Geological Society of America Memoirs 163:177–196.

Kennett, J. P., and M. Srinivasan. 1983. Neogene planktonic foraminifera: a phylogenetic atlas. Hutchinson Ross. Stroudsburg.

Kirkpatrick, M., and N. H. Barton. 1997. Evolution of a species' range. The American Naturalist 150:1–23.

Kucera, M., and J. P. Kennett. 2002. Causes and consequences of a middle Pleistocene origin of the modern planktonic foraminifer *Neogloboquadrina pachyderma* sinistral. Geology 30:539–542.

Lazarus, D., H. Hilbrecht, C. Spencer-Cervato, and H. Thierstein. 1995. Sympatric Speciation and Phyletic Change in *Globorotalia Truncatulinoides*. Paleobiology 21:28–51.

Malmgren, B. A., W. A. Berggren, and G. P. Lohmann. 1983. Evidence for Punctuated Gradualism in the Late Neogene *Globorotalia Tumida* Lineage of Planktonic-Foraminifera. Paleobiology 9:377–389.

Miller, K. G., R. Baluyot, J. D. Wright, R. E. Kopp, and J. V. Browning. 2017. Closing an early Miocene astronomical gap with Southern Ocean $\delta^{18}O$ and $\delta^{13}C$ records: Implications for sea level change, Paleoceanography, 32, doi:10.1002/2016PA003074.

Nathan, S. A., and R. M. Leckie. 2009. Early history of the Western Pacific Warm Pool during the middle to late Miocene (~ 13.2–5.8 Ma): Role of sea-level change and implications for equatorial circulation. Palaeogeography, Palaeoclimatology, Palaeoecology 274: 140–159.

Norris, R. D. 1991. Parallel evolution in the keel structure of planktonic foraminifera. Journal of Foraminiferal Research 21:319–331.

Norris, R. D., R. M. Corfield, and J. Cartlidge. 1996. What is gradualism? Cryptic speciation in globorotaliid foraminifera. Paleobiology 22:386–405.

Norris, R. D. 2000. Pelagic species diversity, biogeography, and evolution. Paleobiology 26:236–258.

Norris, R. D., R. M. Corfield, and J. E. Cartlidge. 1993. Evolution of Depth Ecology in the Planktic Foraminifera Lineage *Globorotalia* (*Fohsella*). Geology 21:975–978.

Olsson, R. K., 1971. The logarithmic spire in planktonic foraminifera: its use in taxonomy, evolution, and paleoecology: Gulf Coast Association of Geological Societies Transactions 21:419–432.

Pearson, P. N., and T. H. G. Ezard. 2014. Evolution and speciation in the Eocene planktonic foraminifer *Turborotalia*. Paleobiology 40:130–143.

Schmidt, D. N., S. Renaud, J. Bollmann, R. Schiebel, and H. R. Thierstein. 2004. Size distribution of Holocene planktic foraminifer assemblages: biogeography, ecology and adaptation. Marine Micropaleontology 50:319–338.

Sheets, H. D., and C. E. Mitchell. 2001. Why the null matters: statistical tests, random walks and evolution. Genetica 112:105–125.

Stewart, J. A., P. A. Wilson, K. M. Edgar, P. Anand, and R. H. James. 2012. Geochemical assessment of the palaeoecology, ontogeny, morphotypic variability and palaeoceanographic utility of "*Dentoglobigerina*" *venezuelana*. Marine Micropaleontology 84:74–86.

Tabachnick, R. E., and F. L. Bookstein. 1990. The structure of individual variation in Miocene *Globorotalia*. Evolution 44:416–434.

Ujiié, Y., and T. Asami. 2014. Temperature is not responsible for left-right reversal in pelagic unicellular zooplanktons. Journal of Zoology 293:16–24.

van Sebille, E., P. Scussolini, J. V. Durgadoo, F. J. Peeters, A. Biastoch, W. Weijer, C. Turney, C. B. Paris, and R. Zahn. 2015. Ocean currents generate large footprints in marine palaeoclimate proxies. Nature Communication 6: 6521, doi: 10.1038/ncomms7521

Wright, J. D., K. G. Miller, and R. G. Fairbanks. 1992. Early and middle Miocene Stable Isotopes: Implications for Deepwater Circulation and Climate. Paleoceanography 7:357–389.

Zelditch, M. L., D. L. Swiderski, and H. D. Sheets. 2004. Geometric morphometrics for biologists: a primer. Elsevier, Amsterdam.

Zhang, Y. G., M. Pagani, and Z. Liu. 2014. A 12-million-year temperature history of the tropical Pacific Ocean. Science 344:84–87.

3.12 Figure captions

Figure 1: Locations of sites discussed in this study. Paleo-latitude and geographic reconstruction (13.5 Ma) were generated from http://www.odsn.de/

Figure. 2A: Placement of landmarks (large red circles) and semi-landmarks (small red circles) along sutures (blue curves); specimen shown here is the holotype of *Fohsella lobata* Bermúdez; 2B: shape variations in response to changes in PC1. The arrows indicate the direction and magnitude of changes.

Figure 3. Phenotypic evolution of fohsellids (14–12.9 Ma); A: Shape (PC1), B: size, C: coiling pattern from the three studied sites. Squares in A and B are mean values of a sample with one standard deviation. Arrows indicate interval of rapid reversal in coiling direction and shift in spiral-view PC1.

Figure 4: A: Oxygen Isotopes of individual fohsellids, surface water species *D. altispira* and thermocline species *D. venezuelana* from Site 806. Red and grey squares represent individual tests $\delta^{18}O$; Purple: $\delta^{18}O$ of *D. altispira* (dot: this study; dash: data from Norris et al., 1996, fitted with a spline function); Yellow: $\delta^{18}O$ of *D. venezuelana* (dot: this study; dash: data from Norris et al., 1996, fitted with a spline function); B, C, and D: histograms of fohsellid isotopes of three intervals. Before 13.25 Ma (B), fohsellids were surface species. During 12.95–13.25 Ma (C), the fohsellids populations inhabited both surface

and thermocline depths, implying a cladogenetic event at 13.25 Ma. After 12.95 Ma (D), surface population became extinct.

3.13 Table caption

Table 1. Parameter estimates of evolutionary models for PC1 and size. Refer to supplementary material for a description of three evolutionary models and parameterization. Model selection is based on DIC values. The lower the values, the better the model is supported by the data.

3.14 Appendix

3.14.1 The Fohsella lineage

The fohsellids are often considered as a short-lived clade of the genus *Globorotalia* that is defined on the basis of apertural characteristic and includes virtually every late Neogene planktonic foraminiferal species with an extraumbilical to peripheral aperture. However, because several groups of forms referred to as *Globorotalia* have distinct ancestry (Bandy, 1972, Kennett and Srinivasan, 1983, Cifelli and Scott, 1986), the designation of these different phylogenetic lineages to *Globorotalia* is somewhat artificial. Bandy (1972) and Fleisher (1974) therefore proposed several new subgenera to represent the different globorotaliid lineages based on phylogenetic considerations. The subgenus *Fohsella* was proposed to include the *G. peripheroacuta* to *G. robusta* series (Bandy, 1972) and later included members with rounded periphery such as *G. peripheroronda* and *G. kugleri* because they represent early members of the *Fohsella* lineage (Fleisher, 1974). This subgeneric designation was adopted subsequently (Kennett and Srinivasan, 1983, Hodell and Vayavananda, 1993; Norris et al., 1996), and was further considered as a separate genus (Cifelli and Scott, 1986, Pearson and Chaisson, 1997).

3.14.2 Materials

Forty-eight, eight and eleven samples of foraminiferal-bearing nannofossil ooze from Ocean Drilling Program Site 806B, Integrated Ocean Drilling Program Site U1338B and Deep Sea Drilling Program Site 563, respectively, are analyzed. The location and water depth of the three sites are given in Table S1. Bulk samples were soaked in sodium metaphosphate overnight and then washed with tap water through a 63-μm sieve.

3.14.3 Landmark-based morphometrics

The spiral-view shape was analyzed using landmark-based morphometrics (Zelditch et al., 2004). All specimens were glued on slides with their spiral side up. A universal stage was used to ensure proper orientation of the specimens. To emphasize sutures under the binocular microscope, most specimens were colored with green food dye before photographs were taken. All dextral coiling specimens were digitally mirrored and analyzed as sinistral coiling ones.

For a combination of reasons, we did not measure the final chamber in the shape analysis this study. First, because of the bilamellar growth of foraminifera, the final chamber is thinner than previous chambers and often broken (also see Bolli and Saunders, 1985). It has been impossible to obtain a sufficient number of fohsellid specimens with a complete final chamber from our samples. Second, the final chamber forms during gametogenesis and its size and shape are of highly variable morphology, in some instances larger, in other instances smaller, and in some cases dipping towards the umbilical side. Including the shape information from the final chamber would have introduced a large amount of uncertainties in the analysis. For size measurements, final chamber is included in the measurement if it is complete. Because a much larger number of specimens are analyzed for size, we find that including some specimens with complete final chamber introduces very small variations in the results. However, it is important to note that our size data may have systematically underestimated the maximum size of the Fohsella, particularly towards the upper part of Site 806 section where most specimens are broken.

We follow standard landmark methods (Zelditch et al., 2004) in collecting and processing shape variables using available toolkits (tpsDig, tpsUtil32 and tpsRelw created by F. J. Rohlf, http://life.bio.sunysb.edu/ee/rohlf/software.html). A total of 1691 specimens were submitted to a generalized Procrustes procedure (Rohlf and Slice, 1990) with thin plate spline analysis which allows semi-landmarks to slide and therefore minimize the difference between individual shapes and the consensus form (Zelditch et al., 2004). A principal component analysis (PCA) was then carried out on the shape variables obtained. The first principle component which explains ~52.79% of the total variance was used for interpreting the spiral-view morphology.

Morphologic variations in response to changes in PC1 are illustrated in Figure S1. Each vector (arrow) indicates changes of the landmark relative to the mean shape (hollow dot) as PC values change. As PC1 decreases, landmarks and semi-landmarks on the penultimate chamber “rotate” dextrally towards the preceding chamber. Meanwhile, landmarks and semi-landmarks on the sutures of pre-adult chambers (fifth and sixth chambers in the last whorl) “rotate” sinistrally towards adult chambers. These deformations in the last whorl indicate that the angle at which chambers are added to the test decreases. As a result, more chambers are exposed in the spiral view. In addition, as PC1 decreases, the fourth and fifth chambers become smaller and “downsize” along the radial direction, probably due to increased overlap between successive chambers. These morphologic variations can also be illustrated using relative warp analysis (Rohlf and

Slice, 1990, Zelditch et al., 2004). The deformations of the green grids (Fig. S1) exhibit how chamber and sutures changes with PC1.

As we have shown in Figure 3 of the main text, the mean values of PC1 remain relatively stable over time. This observation seems to conflict with the common view that fohsellids underwent substantial morphologic changes over time. Here, we provide photographic evidence that the spiral view shape did not change over time although other phenotypic features did (Fig. S2).

In Figure S2, we have selected eight specimens spanning the studied interval. Row 1 (more positive PC1) is characterized by large angular growth rate and less number of chambers in the final whole. The increase in chamber size is more uniform. Row 2 (more negative PC1), in contrast, is characterized by small angular growth rate and more number of chambers in the final whole. Moreover, the adult chambers are larger than the pre-adult chambers. All these growth features give the spiral view of Row 2 a more lobate test shape. From ~14 Ma to 12.9 Ma, the spiral views of the selected specimens remain largely unchanged. However, the size of fohsellids increased substantially during this time. The coiling direction also changed from random to sinistral dominant. The emergence of keels from non-keeled to robustly keeled forms is also apparent (Fig. S2).

3.14.4 Sample Size

Because the landmark method is time consuming, on average ~30-50 specimens of the fohsellids were picked randomly from the >150 μm size fraction from each sample. Each

sample was split with a microsplitter to allow ~50 specimens to be picked. And these specimens were randomly arranged and glued on a slide. While photographing, some specimens may not be well oriented. If a specimen was not well oriented in the photographs, it was excluded from the analysis. By doing so, the sample size for landmark analysis was normally reduced to ~30 (on average ~27, range from 20-50). The sample size is small for Site U1338 and the upper part of Site 806. In the upper part of Site 806 record (<13 Ma), many fohsellids are broken, most likely due to their large and thin adult chamber. If more than one chamber is partially broken, the landmark analysis cannot be performed. At Site U1338, the abundance of specimens is low. Moreover, because the specimens are small on average, pre-adult chambers of the last whorl in some specimens cannot be seen clearly under binocular microscope (50X). As a result, the number of specimens available for analysis is relatively low.

Concerning size and coiling direction measurements, the sample size is not an issue for Site 806 record since a large number of specimens can be easily measured. For Site U1338, there is a concern that sample size is too small to give statistically robust estimates for coiling direction. Here, we plot the estimated ratio of sinistral coiling and corresponding standard errors (Fig. S3). On average, we have picked 26 specimens from each sample.

3.14.5 Stable isotope analysis

Individual fohsellid specimens were randomly picked from the Site 806 slides and washed in de-ionized water and 3% hydrogen peroxide in ultrasonic bath to clean them of

clay, glue and food dye contamination. For *Dentoglobigerina altispira* and *Dentoglobigerina venezuelana* isotopes, 5~6 specimens were grouped together to obtain mean isotopic values. All stable isotope analyses were performed on the Optima Mass Spectrometer housed at Rutgers University. Analytical error is ±0.05‰ for $\delta^{18}O$, and stable isotope ratios are reported using the standard δ notation relative to Vienna Pee Dee Belemnite.

3.14.6 Age model

An integrated age model for the three studied sites was developed using combined nannofossil biostratigraphy, magnetostratigraphy, and astronomically-tuned benthic foraminiferal isotope records. Planktonic foraminiferal biostratigraphy was not used in this work to ensure that the age model is independent from the fohsellid chronospecies zonation. We emphasize this independence because circular reasoning would be introduced if the stratigraphic correlation of fohsellid evolutionary sequences between sites were based on the fohsellid chronospecies zonation, which in turn relies on one's interpretation of taxonomy and evolutionary pattern of this group. Our integrated correlation between the three sites is illustrated in Figure S4.

We selected Site U1338 as the reference section in our age model given its 1) high sedimentation rate (~3-4 cm/kyr, Holbourn et al., 2014), 2) available astronomically tuned benthic stable isotope records (Holbourn et al., 2014), and 3) available paleomagnetic data (Pälike et al., 2010). Miocene Isotope Event 3 (Mi3) is dated at ~ 13.9 Ma (~368.5 CCSF-A m). The last 400 kyr carbon maximum of the ‘‘Monterey

Excursion'' [CM6, Holbourn et al., 2013] is at ~13.9-13.5 Ma (~373.5-359.7 CCSF-A m). Miocene Isotope Event 4 (Mi4) is not readily recognized at Site U1338. Using an earlier age estimate of 13.1 Ma for Mi4 (Westerhold et al, 2005), Mi4 can be potentially recognized as the positive $\delta^{18}O$ excursion at ~346 CCSF-A(m) in the lower part of magnetochron C5AAn (Figure S2). The high resolution astronomically tuned benthic isotope records (Holbourn et al., 2014) also allow us to recalibrate the numerical ages of magnetic reversals building on the shipboard stratigraphy. Ages of magnetic reversals between Chron C5ACn and Chron C5AAn at Site U1338 are summarized in Table S2.

The independently tuned Site 806 benthic isotope data (Holbourn et al., 2013) correlate well with the astronomically tuned $\delta^{18}O$ as well as $\delta^{13}C$ records from Site U1338, with Mi3 at ~486 mbsf and CM6 between ~467-484.5 mbsf at Site 806. Using this astronomically tuned age, the highest occurrence (HO) of *Sphenolithus heteromorphus* is well constrained between ~ 13.61-13.65 Ma (471.7-474.0 m, sampling resolution, mid-point age: 13.63 Ma; Fornaciari et al., 1993). Based on the correlation between Sites 806 and U1338, the HO of *S. heteromorphus* is therefore constrained within C5ABr, older than the C5ABr/C5ABn transition (~13.59 Ma, Table S2). No astronomical ages are available so far for the upper part of the section (435-455 mbsf). An average sedimentation rate of 5.5 cm/kyr based on the estimated sedimentation rate from 455-480 mbsf (Site 806B) is used to extrapolate ages above 455 mbsf (13.2-12.9 Ma).

No high resolution benthic foraminiferal isotope record is available from Site 563. Therefore, the age model of this site is based on linear interpolation of several tie-points

using nannofossil, isotope stratigraphy and paleomagnetic data (Miller et al, 1985) recalibrated in Table S2. Specifically, three normal (C5ACn, C5ABn and C5AAn) and two reversed (C5ABr and C5AAr) chrons bracketed by Mi3 (235.7 mbsf) and Mi4 (~225 mbsf) are recognized (Figure S2). Based on this paleomagnetic interpretation, the HO of *S. heteromorphus* at this site (between 231.7-232.2 m, sampling precision; Maiorano and Monechi, 1998), lies close to the top of Chron C5ACn (231.5 mbsf), slightly below C5ABr, suggesting a slightly older but nearly synchronous HO of *S. heteromorphus* relative to Site 806 (~13.63 Ma). It is important to note that the original paleomagnetic data for Site 563 is unavailable (Dennis Kent, pers. comm.), so the depths of magnetic reversals are approximated from a digital figure of an earlier publication (Khan et al., 1985). Therefore, slightly diachronous ages for the HO of *S. heteromorphus* could be due to measurement errors.

3.14.7 Evolutionary models

We follow previous studies of three classic models of evolutionary mode (Hunt, 2006; Sheets and Mitchell, 2001). For directional evolution, phenotypic changes occur through incremental evolutionary steps that are randomly drawn from a distribution with mean μ and variance σ^2. After t independent evolutionary steps, the morphologic differences between descendant and ancestral populations, $\Delta X = X_D - X_A$, have a distribution with mean $t\mu$ and variance $t\sigma^2$, where X_D and X_A are the mean trait values of the descendant and the ancestral population, respectively. If t is large, ΔX approximates normal distribution (Eq. 1) according to the Central Limit Theorem. An unbiased random walk is a special case of the directional model when μ is set to zero (Hunt, 2006).

The stasis model in Hunt (2006) follows Sheets and Mitchell (2001), assuming that trait mean is normally distributed around an optimum value, θ. Therefore, the distribution of ΔX is normal with mean of $\theta - X_A$, and variance of ω (Eq. 2), where ω indicates the magnitude of evolutionary fluctuations around the mean (Hunt, 2006).

$\Delta X \sim N(t\mu, t\sigma^2)$ (Eq. 1)

$\Delta X \sim N(\theta - X_A, \omega)$ (Eq. 2)

$\varepsilon \sim N(0, V/n)$ (Eq. 3)

Because trait means X_D and X_A are estimated from samples, sampling errors in estimating the means should be considered. Hunt (2006) assumes that the deviation of the observed mean from the true mean is normally distributed with mean of zero and variance V/n (Eq. 3), where V is the population variance and n is the number of specimens in each sample (Sokal and Rohlf, 2012).

However, population variance of each sampling horizon is also unknown and has to be estimated from the sample variance. To improve the precision of statistical inference, Hunt (2006) suggested that sample variances can be pooled over all samples unless a Bartlett's test indicates significant variance heterogeneity. For spiral-view PC1 of Site 806, Bartlett's test suggests that variances of all samples are not different ($p = 0.86$). Hence, population variance is estimated from pooled samples. We also used sample variance from each sample to estimate sampling error of each sample separately. The

results of both approaches are not different in Bayesian analysis (see below). For size data from Site 806, Bartlett's test suggests heterogeneity of variance over all samples (p<0.001). Thus, population variance of each sampling horizon is estimated separately.

After incorporating sampling errors, the distribution of evolutionary differences between adjacent ancestral-descendant populations take the form (Hunt, 2006):
for directional evolution:

$\Delta X_i \sim N (t_i\mu, t_i\sigma^2 + Va/na+Vd/nd)$ (Eq. 4)

for random walk model:

$\Delta X_i \sim N (0, t_i\sigma^2 + Va/na+Vd/nd)$ (Eq. 5)

for stasis model:

$\Delta X_i \sim N (\theta - X_A, \omega + Vd/nd)$ (Eq. 6)

, where i, ΔX_i, t_i, θ and ω represent sample i, the differences in trait mean between i and (i-1) samples, the age difference between i and (i-1) samples, optimal phenotype and corresponding variance, respectively. Va, Vd, na and nd represent the variance of ancestral and descendant populations, and number of specimens in ancestral and descendant populations, respectively.

3.14.8 Bayesian parameter estimates

The models considered in this study contain two parameters (μ and σ, or θ and ω, respectively). If all samples are collected with uniform temporal spacing and equal sampling errors, marginal posterior distribution of parameters can be derived analytically

in Bayesian analysis (e.g. Gelman et al., 2014). The route is: 1) formulating the joint posterior distribution of all unknown parameters (Eq. 7); and 2) then integrating this distribution over the unknowns that are not of immediate interest to obtain the desired marginal distribution (Eq. 8). In the simplest case, analytical form of the marginal posterior distribution is a common distribution (Gelman et al., 2014).

$p(\mu, \sigma|y) \propto p(y|\mu, \sigma)p(\mu, \sigma)$ (Eq. 7)

$p(\mu|y) = \int p(\mu, \sigma|y)\, d\sigma$ (Eq. 8)

However, we sampled Site 806 at varying temporal resolution. Therefore t_i in Equation 4 and 5 is not a constant. The absolute value of sampling errors also varies from sample to sample. In the absence of simple analytical solutions, we apply the numerical simulation to estimate parameters. A few numerical methods that belong to the family of Markov chain simulations can be employed to make Bayesian inference (Gelman et al., 2014; Kruschke 2014, Korner-Nievergelt et al., 2015). A mathematic introduction to these methods and Markov Chain Monte Carlo (MCMC) simulation is beyond the scope of this work and can be found in most Bayesian textbooks (e.g. Gelman and Hill, 2007; Gelman et al., 2014; Korner-Nievergelt et al., 2015). In general, these methods start at some arbitrary point in the parameter space and jumps to a new point in a random walk pattern. The proposed move is randomly generated, but is accepted with conditions. If the posterior density of the proposed move is higher than at the current position, then the proposed move is accepted, otherwise, it is probabilistically accepted. Because the

approximate distributions are improved at each step in the simulation, iterative samplings allow the Markov chain to converge to the target distribution (Gelman et al., 2014).

Two of these sampling methods are widely used, namely the Gibbs sampling and the Metropolis sampling. They both have pros and cons. The Gibbs sampling is a special case of the Metropolis algorithm and is efficient in multidimensional problems when the number of parameters are large. However, to perform the Gibbs sampling, we must be able to sample directly from the full conjugate conditional posterior distribution on all of each parameter (Gelman and Hill, 2007; Gelman et al., 2014; Kruschke 2014), which limits its applicability in some cases.

The Metropolis algorithm is very general and broadly applicable, but it does have drawbacks. Particularly, the proposed distribution must be properly tuned to the posterior distribution to ensure that the algorithm works well. If the proposed distribution is too narrow and the starting values are too far from the "true" posterior mean, then it may take extremely long iterations for the chain to converge. For example, using the size data of this work and given an arbitrarily large initial value for μ as well as a narrow range for the proposed distribution of μ, the MCMC are still far from steady posterior distribution (~0.23) after 300,000 iterations (Fig. S5a). Instead, using appropriate proposal distribution that has a distribution with a range on the same order of the "true" posterior distribution, the chains converge quickly and generate satisfactory results (Fig. S5b).

Because there are only a few parameters involved in the evolutionary models, we apply the Metropolis algorithm in this study. A simple metropolis algorithm (see below) can be easily performed in R (R Development Core Team, https://www.r-project.org/). After a proper proposal distribution is specified, point summary (mean) and uncertainty measurements (credible interval) for each model parameter can be obtained given enough random samples from the simulation. It is noteworthy that, different from the confidence interval in frequentist approach, the interpretation of credible interval in Bayesian analysis is straightforward. For example, the 95% credible interval is the interval within which we expect the true parameter value to be with a probability of 0.95. The larger the sample size, the narrower the interval because increasing sample size increases information about the true parameters.

Before the MCMC runs, some parameters must be specified.

First, we specify how many iterations are done (300,000 iterations in this study), how many iterations are assigned to the burn-in and, thus, how many will be discarded in each chain simulation (the first 75,000 in this study). This is because MCMC sampling often has a strong autocorrelation. The parameter value at iteration k is closer to the value at iteration k-1 than it is, for example, to the value at k-100 in a chain (Korner-Nievergelt et al., 2015). Hence, we need to run the simulations long enough with a high number of iterations to obtain a reliable sample of the distribution of the parameters (Gelman et al., 2014). We also need to determine how many chains are run in parallel (2 chains in this study) with starting points dispersed throughout parameter space. Comparing different

simulated sequences helps in assessing whether these iterative simulations have converged and well mixed (Gelman and Hill, 2007; Gelman et al., 2014), in the sense that they have converged to a common distribution.

In R, we can find indications of convergence by plotting the trace plots (Gelman and Hill, 2007; Gelman et al., 2014; Korner-Nievergelt et al., 2015) and consulting potential scale reduction factor (PSRF). In the trace plot (Fig. S6), two chain simulations of μ and σ (the directional evolutionary model), respectively, converged after ~50000 iterations although the initial values of μ and σ are generated randomly. For PSRF, a factor of 1 means that between variance and within chain variance are equal, larger values mean that there is still a notable difference between chains. If PSRF is less than 1.1 or 1.05 for all parameters, then we consider that the chains have approximately converged. The PSRF is calculated using coda package in R (Plummer et al., 2006).

Second, to start the simulation of each chain, initial values must be presented for each model parameter. Specifying initial values using random distributions ensures that different chains start at different points in the parameter space and therefore convergence of chains can be better assessed. But these initial values should not be too far away from a typical set of parameters, where posterior density is high, because the MCMC algorithms need numerous iterations before convergence if the initial values are far in the tail of the posterior distribution (e.g. Fig. S5a).

Third, a prior distribution has to be specified for each model parameter in Bayesian analysis. To play a minimal role in the inference of posterior distribution, we use non-informative prior distributions. For a prior distribution to be non-informative, its range of uncertainty should be obviously wider than the range of reasonable values of the parameters. For example, given the variation of ΔX and t is roughly of the same order of magnitude in absolute values, one would not expect to see coefficient (step mean μ in this case) much higher than 1. A standard deviation on the order of 100 would satisfy a non-informative prior. The prior distribution used in this study is seen in the code listed below.

3.14.9 Model selection

To compare which evolutionary mode better fits our size and shape data from Site 806, we have calculated Deviance information criterion (DIC). DIC is a somewhat Bayesian version of Akaike information criterion (AIC) that have been used in previous studies (Hunt, 2006) with the maximum likelihood estimate $\hat{\theta}$ replaced with the posterior mean $\hat{\theta}_{Bayes} = E(\theta|y)$ and a data-based bias correction for an effective number of parameters (Gelman et al., 2014). The lower the DIC values, the better the model is supported by the data. More discussion on this model comparison criterion can be found in most Bayesian textbooks (e.g. Gelman and Hill, 2007; Gelman et al., 2014). R code for DIC calculation is attached with the model code.

3.14.10 Results of parameter estimates

We first present the DIC values of each model for each data set (Table S3), then we illustrate details of parameter estimates from better supported model.

As can be seen, for the size data, the stasis model is significantly inferior to the directional evolution and unbiased random walk model. The DIC supports to directional evolution and unbiased random walk are about the same, with slightly better support for the directional evolution mode. For shape data, it is clear that the stasis models are better supported than the directional evolution and unbiased random walk models. Parameter estimates of each model are shown below.

3.14.11 Evolutionary models in R code

We only illustrate R code for the random walk model here. R code for the unbiased random walk model and the stasis model differ only in the likelihood function and parameterization from the directional model, and therefore can be simply modified using R code as attached below. The directional evolution model includes: likelihood function, prior function, posterior function, initial_value function, proposal_distribution function, Metropolis_algorithm function, DIC_calculate function as well as codes for convergence check and summary of posterior distribution.

```
#read data first, vector y is difference in size between ancestrial-descedant pairs; vector t
is difference in time between ancestrial-descedant pairs; vector samplingerrors is
Vd/nd+Va/na
y <-
t <-
samplingerrors <-

# likelihood function
likelihood <- function(param){
      mu=param[1]
      sigmastep=param[2]
      pred=mu*t
```

```
        sd=sqrt(sigmastep*sigmastep*t+samplingerrors)
        singlelikelihoods = dnorm(y, mean=pred, sd=sd, log=T)
        sumll = sum(singlelikelihoods)
        return(sumll)
}

# prior
prior <- function(param){
        mu = param[1]
        sigmastep=param[2]

        muprior = dnorm(mu, sd=100, log=T)
        sigmastep_prior = dunif(sigmastep, min=0, max=1, log=T)
        return(muprior+sigmastep_prior)
}

# posterior
posterior <- function(param){
        return(likelihood(param)+prior(param))
}

# metropolis algorithm
proposalfunction <- function(param){return(rnorm(2, mean = param, sd=c(0.01, 0.01)))}

run_metropolis_MCMC <- function(initials, iterations){
        chain = array(dim=c(iterations+1,2))
        chain[1,]=initials

        for(i in 1:iterations){
        proposal=proposalfunction(chain[i,])

        probability = exp(posterior(proposal)-posterior(chain[i,]))
        if(runif(1)<probability){chain[i+1,] = proposal}
        else
        {chain[i+1,] = chain[i,]}
        }
        return(mcmc(chain))
        }

# initial values to start the chain
initials = c(rnorm(1, 0, 5), runif(1, min = 0, max = 1))

# run MCMC
chain = run_metropolis_MCMC(initials, 300000)

# run another chain
```

```
initials = c(rnorm(1, 0, 5), runif(1, min = 0, max = 1))
chain2 = run_metropolis_MCMC(initials, 300000)

#convergence check
combinedchains = mcmc.list(chain, chain2)
plot(combinedchains)
gelman.diag(combinedchains)

#obtain combined of parameter after discard burnIn
> burnIn=75000
> accepted1 = chain[(burnIn+1):dim(chain)[1], ]
> accepted2 = chain[(burnIn+1):dim(chain)[1], ]
> accepted = rbind(accepted1, accepted2)

#calculate log-predictive-density and DIC
likelihood_cal <- function(post_param){
        lik_dim=dim(post_param)[1]
        lik_accepted=array(dim=c(lik_dim,1))
        for (i in 1:lik_dim){
        lik_accepted[i]=likelihood (post_param[i,])}
        return(lik_accepted)
        }

calc.dic <- function(post_param) {
        param_hat <- apply(post_param, 2, mean)
        D.hat <- -2*likelihood(param_hat)

        c<- likelihood_cal (post_param)
        D.bar <- -2*mean(c)
         pD <- D.bar - D.hat

        DIC <- D.hat + pD
        return(DIC)
}
calc.dic(accepted)

#summary
summary(accepted)

#plot histogram of posterior distribution of parameters
hist(accepted[ ,1], nclass=30, , main="posterior of μ", col="red")
hist(accepted[ ,2], nclass=30, , main="posterior of σ", col="red")
```

3.15 Appendix References

Bandy, O.L., 1972. Origin and development of *Globorotalia* (Turborotalia) *pachyderma* (Ehrenberg). Micropaleontology 18: 294–318.

Bolli, H. M., and J. B. Saunders. 1985. Oligocene to Holocene low latitude planktic foraminifera. In: Bolli, H. M., Saunders, J. B., Perch-Nielsen, K. (Eds.), Plankton Stratigraphy: Volume 1. Cambridge University Press, Cambridge.

Cifelli, R., and G. Scott G, 1986, Stratigraphic record of the Neogene globorotalid radiation (Planktonic Foraminiferida). Smithsonian Institution Press, Washington.

Fleisher, R. L. 1974, Cenozoic planktonic foraminifera and biostratigraphy, Arabian Sea, Deep Sea Drilling Project, Leg 23A. Initial Reports of Deep Sea Drilling Project 23:1001–1072.

Fornaciari, E., J. Backman, and D. Rio. 1993. Quantitative distribution patterns of selected lower to middle Miocene calcareous nannofossils from the Ontong Java Plateau. In Berger, WH, Kroenke, LW, Mayer, LA, et al., Proceedings of the Ocean Drilling Program Scientific Results 130:245-256

Gelman, A., J. B. Carlin, H. S. Stern, and D. B. Rubin. 2014. Bayesian data analysis. CRC Press, Boca Raton.

Gelman, A., and J. Hill. 2007. Data analysis using regression and multilevel/hierarchical models. Cambridge University Press, New York.

Holbourn, A., W. Kuhnt, M. Frank, and B. A. Haley. 2013. Changes in Pacific Ocean circulation following the Miocene onset of permanent Antarctic ice cover. Earth and Planetary Science Letters 365:38-50.

Holbourn, A., W. Kuhnt, M. Lyle, L. Schneider, O. Romero, and N. Andersen. 2014. Middle Miocene climate cooling linked to intensification of eastern equatorial Pacific upwelling. Geology 42:19-22.

Hodell, D. A., and A. Vayavananda. 1993. Middle Miocene paleoceanography of the western equatorial Pacific (DSDP site 289) and the evolution of *Globorotalia* (*Fohsella*). Marine Micropaleontology 22: 279-310.

Hunt, G. 2006. Fitting and comparing models of phyletic evolution: random walks and beyond. Paleobiology 32:578-601.

Kennett, J. P., and M. Srinivasan. 1983. Neogene planktonic foraminifera: a phylogenetic atlas. Hutchinson Ross. Stroudsburg.

Khan, M. J., D. V. Kent, and K. G. Miller. 1985. Magnetostratigraphy of Oligocene to Pleistocene sediments, Sites 558 and 563. Initial Reports of the Deep Sea Drilling Project 82:385-392.

Korner-Nievergelt, F., T. Roth, S. Von Felten, J. Guélat, B. Almasi, and P. Korner-Nievergelt. Bayesian data analysis in ecology using linear models with R, BUGS, and Stan. Academic Press, 2015.

Kruschke, J. 2014. Doing Bayesian data analysis: A tutorial with R, JAGS, and Stan. Academic Press, Burlington.

Miller, K. G., M.-P. Aubry, M. J. Khan, A. J. Melillo, D. V. Kent, and W. A. Berggren. 1985. Oligocene-Miocene Biostratigraphy, Magnetostratigraphy, and Isotopic Stratigraphy of the Western North Atlantic. Geology 13:257-261.

Norris, R. D., R. M. Corfield, and J. Cartlidge, 1996. What is gradualism? Cryptic speciation in globorotaliid foraminifera. Paleobiology 22:386–405.

Pälike, H., H. Nishi, M. Lyle, I. Raffi, K. Gamage, A. Klaus, and the Expedition 320/321 Scientists. 2010. Expedition 320/321summary. Proceedings of the Integrated Ocean Drilling Program. 320/321:609-614.

Pearson, P. N., and W. P. Chaisson., 1997, Late Paleocene to middle Miocene planktonic foraminifer biostratigraphy of the Ceara Rise. Proceedings of the Ocean Drilling Program. Scientific Results 154:33–68.

Plummer, M., N. Best, K. Cowles, and K. Vines. 2006. CODA: Convergence diagnosis and output analysis for MCMC. R news 6:7-11.

R Development Core Team. 2008. R: A language and environment for statistical computing. R Foundation for Statistical Computing, Vienna, Austria. ISBN 3-900051-07-0, URL http://www.R-project.org.

Rohlf, F. J., and D. Slice. 1990. Extensions of the Procrustes method for the optimal superimposition of landmarks. Systematic Biology 39: 40-59.

Shipboard Scientific Party. 1991. Site 806. In Kroenke, L.W., Berger, W.H., Janecek, T.R., et al., Proc. ODP, Init. Repts., College Station, TX (Ocean Drilling Program) 130: 291–367.

Sheets, H. D., and C. E. Mitchell. 2001. Why the null matters: statistical tests, random walks and evolution. Genetica 112–113:105–125.

Sokal, R., and F. Rohlf. 2012. Biometry: the principles and practice of statistics in biological research, 4th Edition. W.H. Freeman and Company, New York.

Westerhold, T., T. Bickert, and U. Röhl. 2005. Middle to late Miocene oxygen isotope stratigraphy of ODP site 1085 (SE Atlantic): new constrains on Miocene climate variability and sea-level fluctuations. Palaeogeography, Palaeoclimatology, Palaeoecology 217: 205-222.

Zelditch, M. L., D. L. Swiderski, and H. D. Sheets. 2004. Geometric morphometrics for biologists: a primer. Elsevier, Amsterdam.

3.16 Appendix Figure Captions

Figure S1: morphologic changes in response to PC1. Arrows indicate the direction of deformation in response to changes in PC values. The magnitude of the deformation of each landmark and semi-landmark is characterized by the length of the arrows. Figures are created using tpsRelw developed by F. J. Rohlf, http://life.bio.sunysb.edu/ee/rohlf/software.html

Figure S2: Photographic evidence illustrating how the spiral view shape did not change relative to other morphological features. Each row includes specimens with similar PC1 values. From 14-12.9 Ma, the spiral shape of each row did not change significantly. However, the coiling direction, keel growth, test size and $\delta^{18}O$ of the fohsellids all changed. It is important to note that there is no scale bar for these images (oriented spiral side). When specimens are oriented with a universal stage, the distance of a foraminifera to the object lens of a microscope varies from specimen to specimen. As a result, size measurement was not done under the microscope for these spiral-view illustrations.

Figure S3. Percentage of sinistral coiling and standard errors of Site U1338 records.

Figure S4: Stratigraphic correlation between ODP Site 806 (Western Pacific), IODP Site U1338 (Eastern Pacific) and DSDP Site 563 (North Atlantic). X axis: oxygen (black) and carbon (green) isotope data from benthic foraminifera; Y axis: compound depth (mbsf, meters below sea floor). CM6 ($\delta^{13}C$ maximum of the ‘‘Monterey Excursion’’); Mi3:

Marine Isotope Stage 3; Mi4: Marine Isotope Stage 4; Paleomagnetic data at Sites 563 and U1338 are from Miller et al. (1985) and Pälike et al. (2010), respectively.

Figure S5: Examples of how the proposal distribution and initial values may affect the MCMC simulations using size record of Site 806; a: when initial value of μ (iterations=0) is far from its "true" posterior distribution and the proposal distribution is too narrow (proposal distribution <- rnorm(mean = current values of μ in the chain, sd=0.001), the chain is still far from convergence after 300,000 iterations; b: more appropriate initial values and proposal distribution (proposal distribution <- rnorm(mean = current values of μ in the chain, sd=0.01) lead to more convergence to the steady posterior distribution.

Figure S6: a) trace plots of two chain simulations for the parameters μ of the directional model using size data from Site 806; Two chains started from very different initial values that are randomly generated but gradually converged towards a common distribution; b) trace plots and convergence of two chain simulations for the parameters σ using size data from Site 806.

Figure S7: marginal posterior distribution of: (a) μ of size evolution, (b) σ of size evolution, (c) θ of spiral-view PC1 (pooled variance), (d) ω of spiral-view PC1 (pooled variance). Credible intervals of these parameters are summarized in Table S4 and S6.

3.17 Appendix Table Captions

Table S1: geographic locations of studied sites (Miller et al., 1985; Shipboard Scientific Party, 1991; Pälike, 2010).

Table S2: Depth of magnetic reversals are from Pälike et al., 2010. Ages are estimated using astronomically-tuned benthic isotope data from Holbourn et al. (2014).

Table S3: DIC values of each model. The calculation of DIC is shown below. The lower the DIC value, the better the model is supported by the data.

Table S4: Directional model of size data (Site 806). The first seven columns of numbers give inferences for the model parameters. The parameter μ has a mean estimate of 0.231, a standard error of 0.146, and a 95% credible interval of [-0.057, 0.518]. This marginal posterior distribution of μ is also seen in Figure S7.

Table S5: Unbiased random walk model of size data (Site 806).

Table S6: Stasis model of spiral-view PC1 (Site 806).

Figure 1

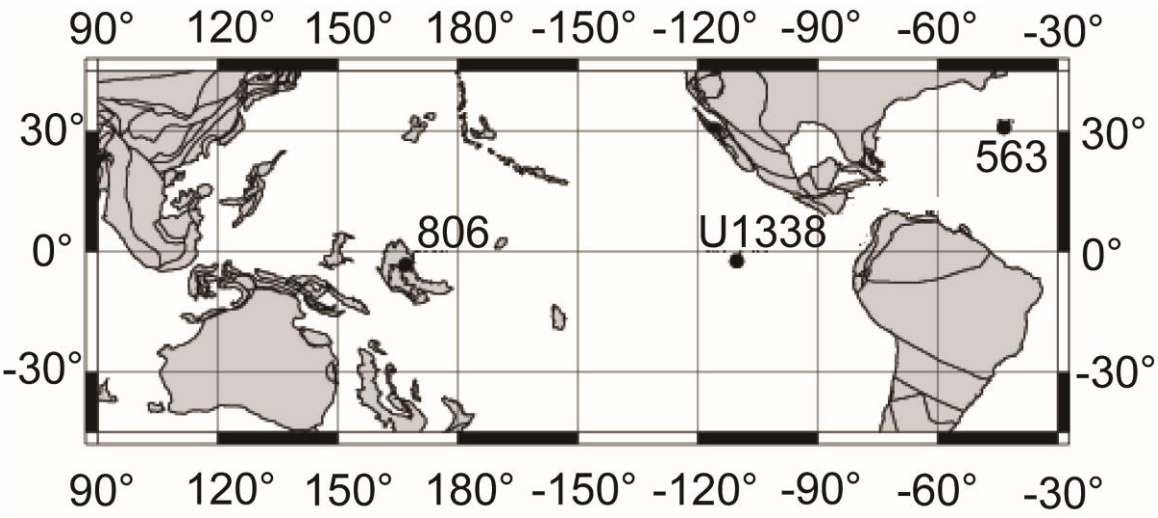
90° 120° 150° 180° -150° -120° -90° -60° -30°
30°
0°
-30°
806
U1338
563
90° 120° 150° 180° -150° -120° -90° -60° -30°

Figure 2

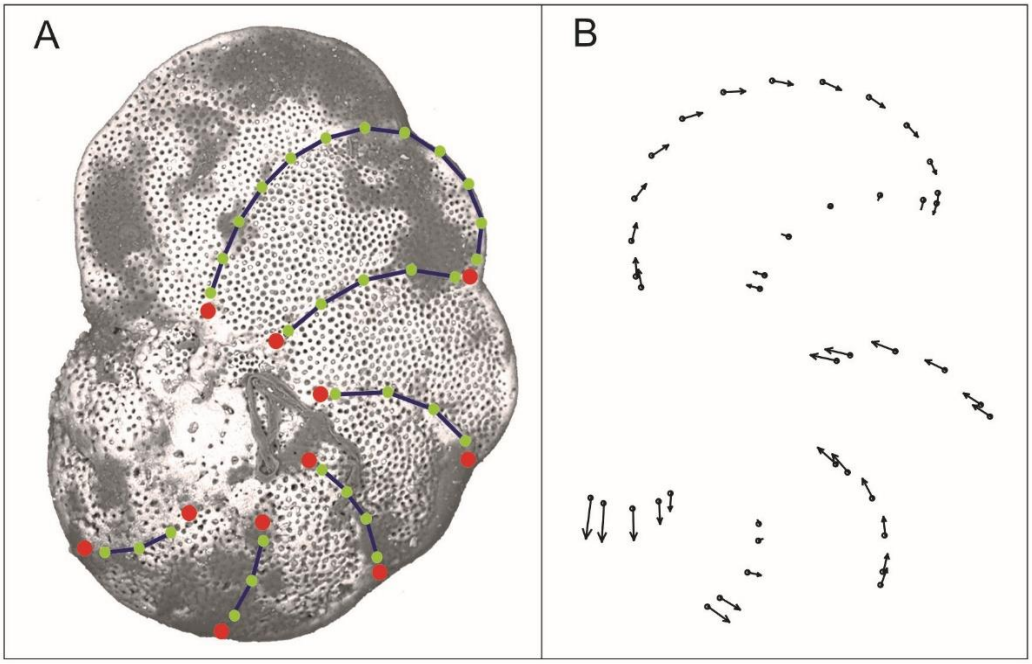

Figure 3

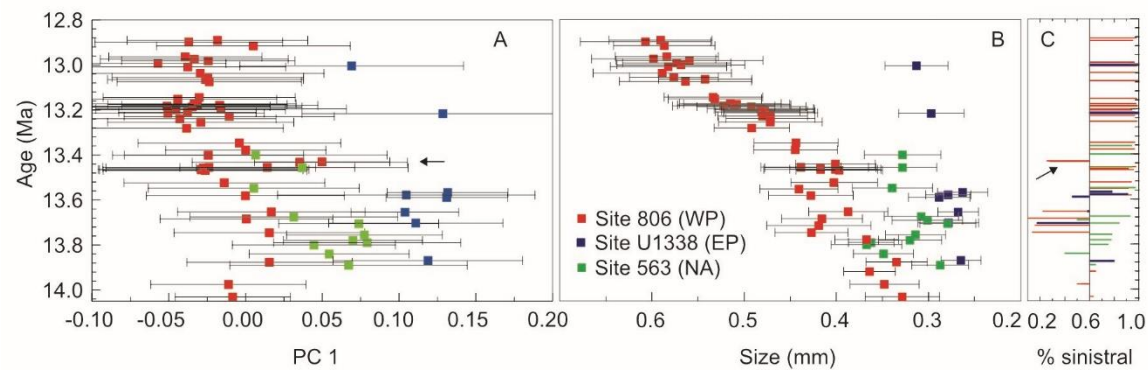
A
B
C
Age (Ma)
12.8
13.0
13.2
13.4
13.6
13.8
14.0
-0.10
-0.05
0.00
0.05
0.10
0.15
0.20
PC 1
0.6
0.5
0.4
0.3
0.2
Size (mm)
Site 806 (WP)
Site U1338 (EP)
Site 563 (NA)
0.2
0.6
1.0
% sinistral

Figure 4

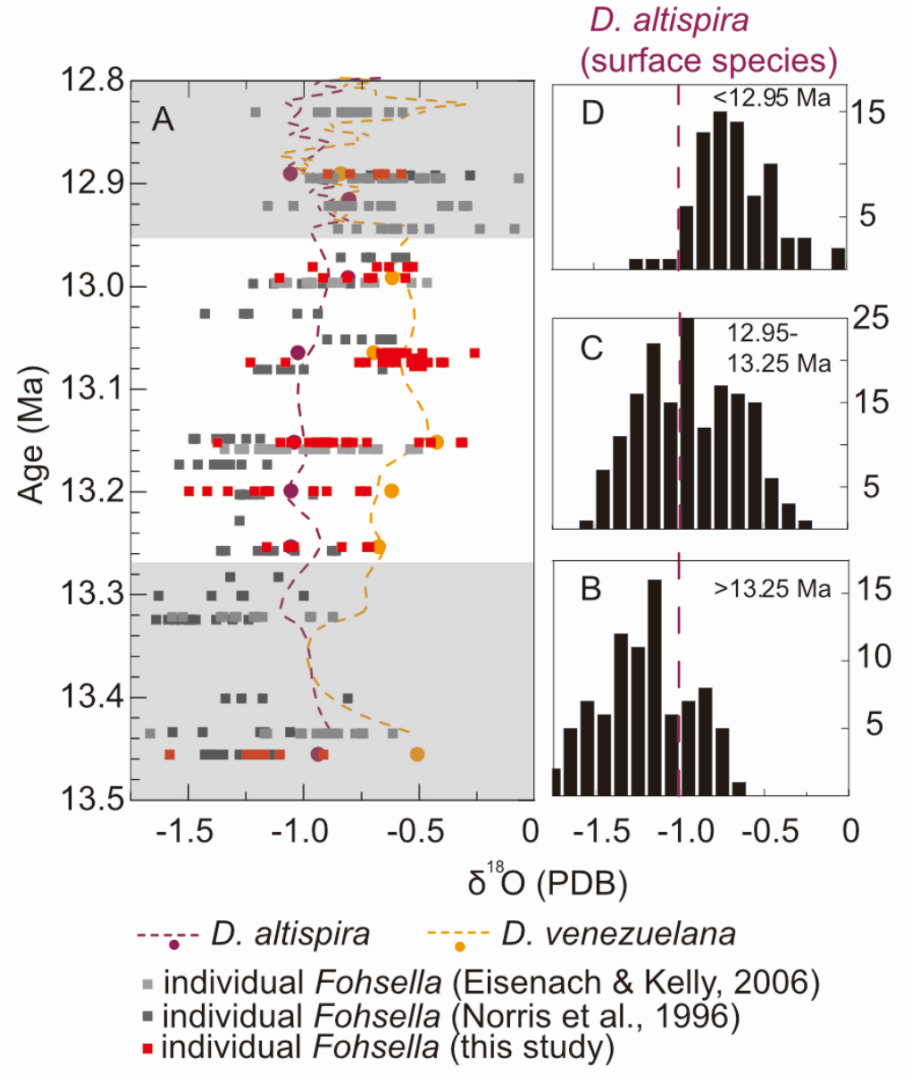
D. altispira
(surface species)
A
D
<12.95 Ma
C
12.95-
13.25 Ma
B
>13.25 Ma
Age (Ma)
12.8
12.9
13.0
13.1
13.2
13.3
13.4
13.5
-1.5
-1.0
-0.5
0
15
5
25
10
δ18O (PDB)
D. altispira
D. venezuelana
individual Fohsella (Eisenach & Kelly, 2006)
individual Fohsella (Norris et al., 1996)
individual Fohsella (this study)

Appendix Figure S1

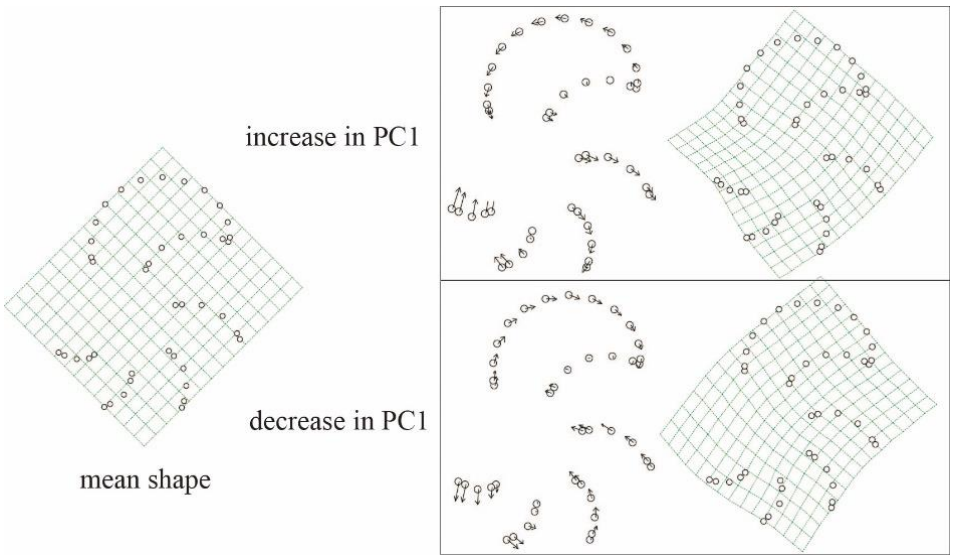

Appendix Figure S2

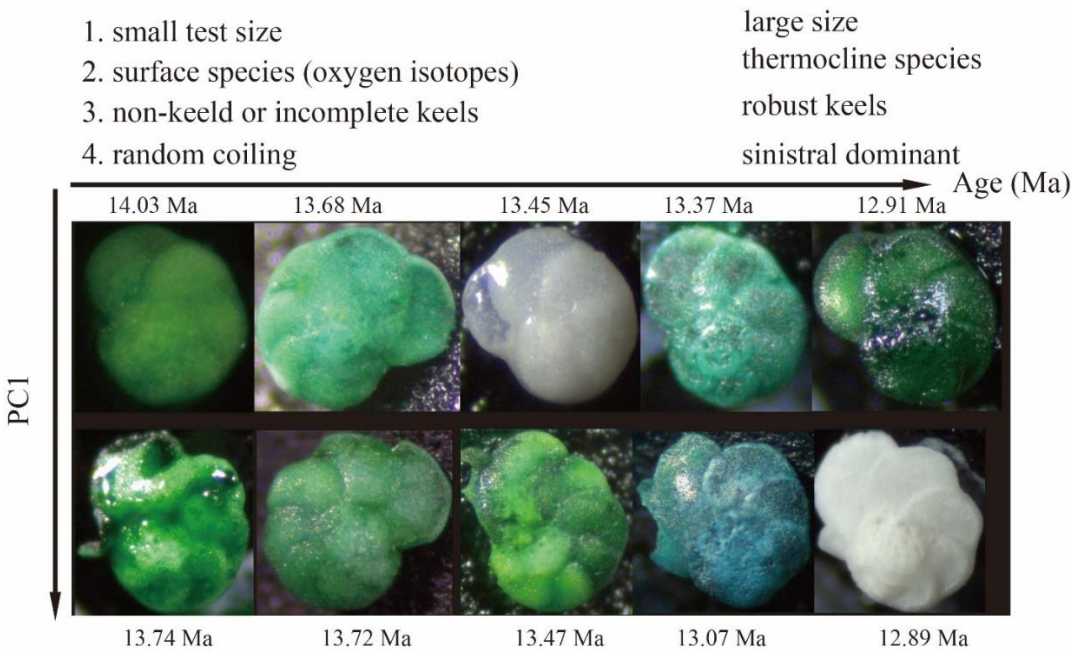

Appendix Figure S3

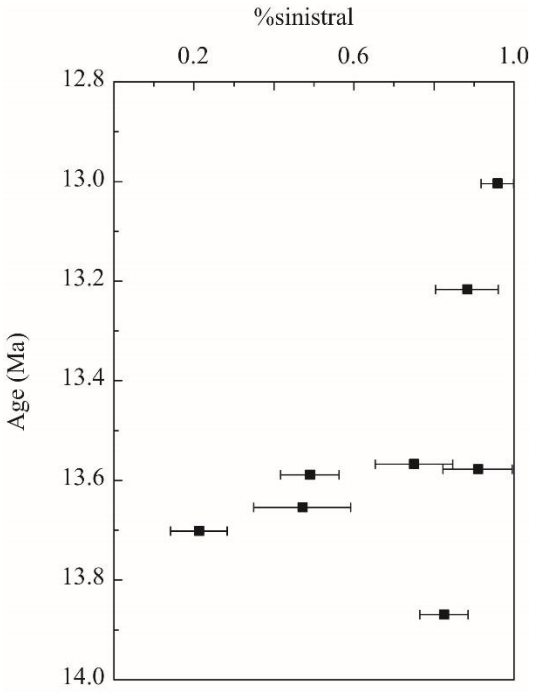

Appendix Figure S4

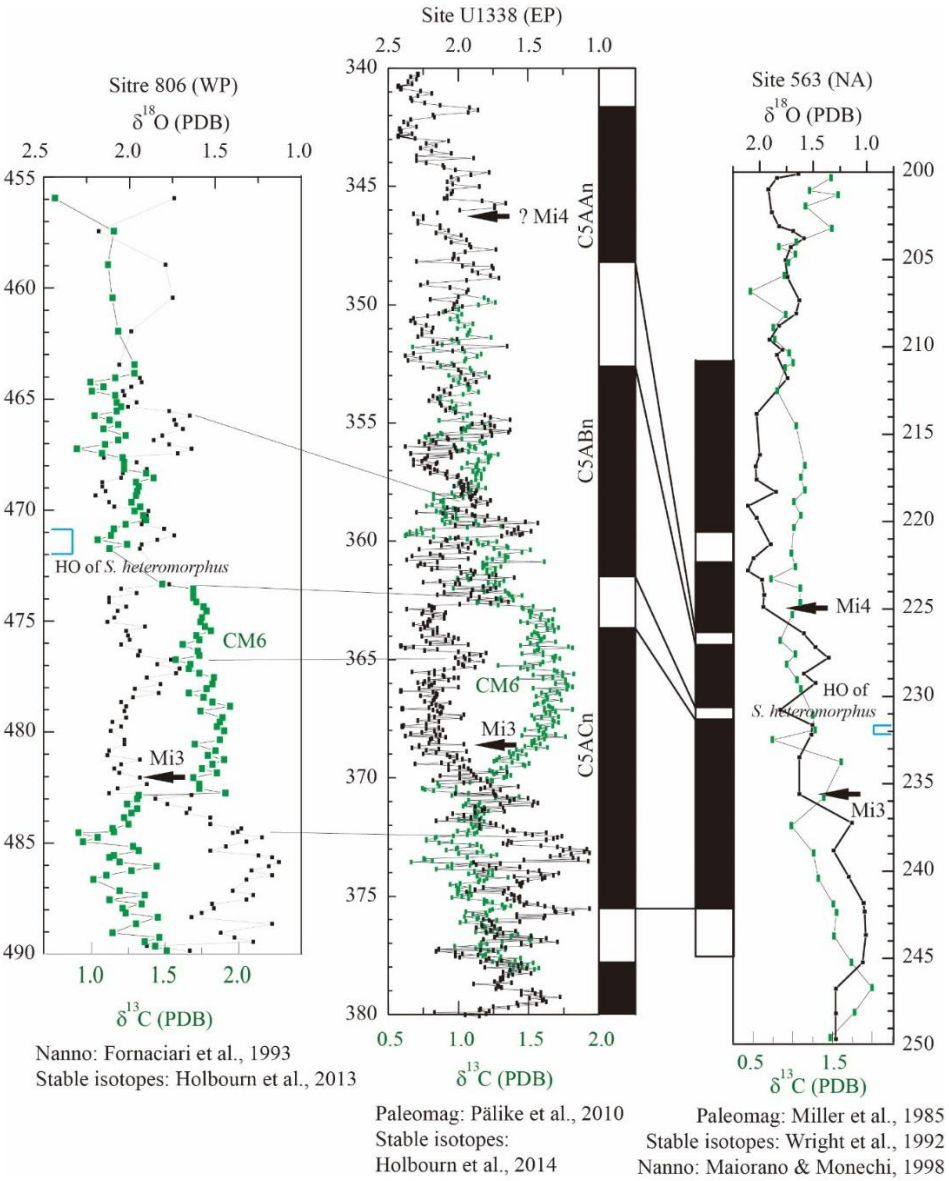

Appendix Figure S5

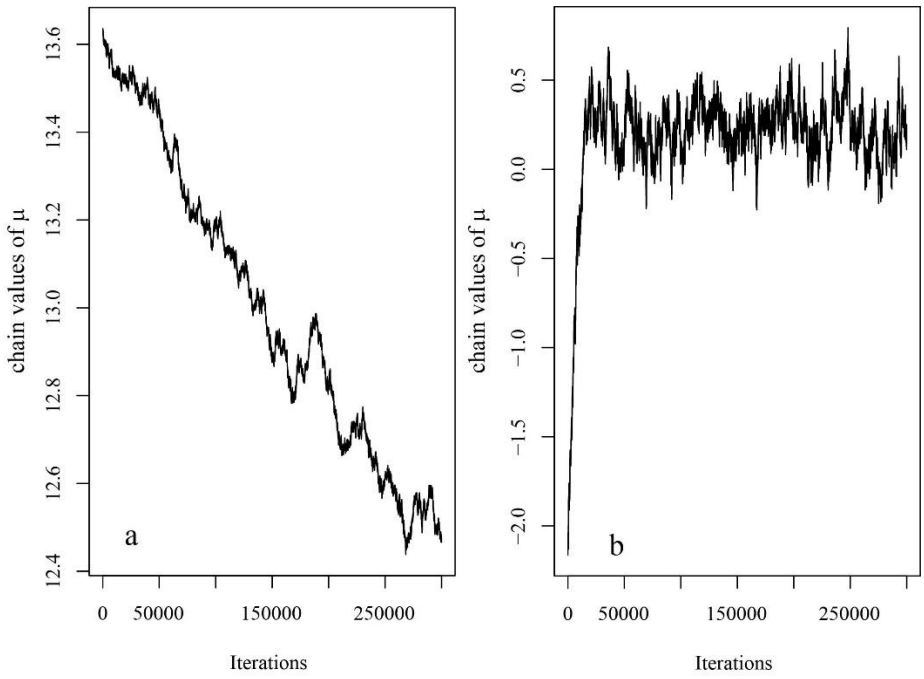

Appendix Figure S6

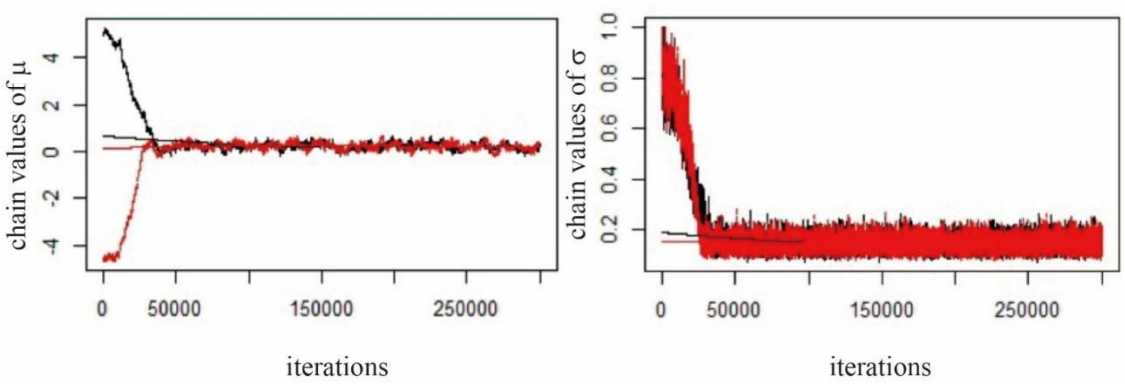

Appendix Figure S7

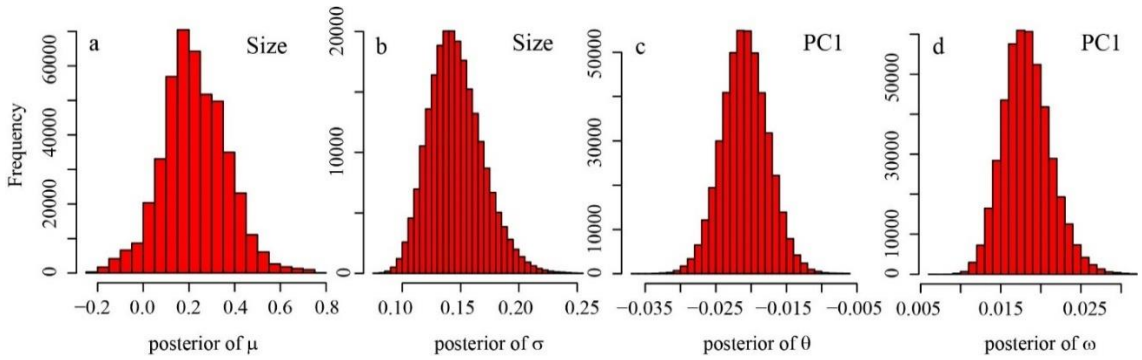

Table 1

					Model Selection (DIC)		
Trait	u_{step}	σ	θ	ω	directional	random walk	stasis
PC1	-	-	-0.021	0.018	-202.9	-204.8	-240.6
Size	0.231	0.146	-	-	-254.5	-253.9	-123.2

Appendix Table S1.

	Site 806B	Site U1338B	Site 563
Location	Western Pacific Ocean Ontong Java Plateau	Eastern Equatorial Pacific	North Atlantic Mid-Atlantic Ridge
Lat. & Long.	0˚19.11’N 159 ˚21.69’E	2°30.469′N 117°58.178′W	33 ˚39’N 43 ˚46’W
Water depth	2519 m	4200 m	3796 m

Appendix Table S2.

Hole	Core-section	Magnetic reversal	Depth CCSF-A(m)	Estimated age (Ma)
U1338B	34H-6-90	C5Ar.3r/C5AAn	341.77	13.048
U1338B	35H-3-117	C5AAn/C5AAr	348.36	13.239
U1338B	35H-6-110	C5AAr/C5ABn	352.78	13.362
U1338B	36H-6-15	C5ABn/C5ABr	361.6	13.596
U1338B	36H-7-65	C5ABr/C5ACn	363.8	13.67
U1338C	38H-4-0	C5ACr/C5ACn	375.5	13.99

Appendix Table S3.

Measurements from Site 806	Directional evolution	Unbiased random walk	Stasis
Size	-254.5	-253.9	-123.2
Spiral-view PC1	-202.9	-204.8	-240.6

Appendix Table S4.

	mean	sd	25%	50%	75%	PSRF
μ	0.231	0.146	0.135	0.23	0.32	1.001
σ	0.146	0.023	0.107	0.13	0.145	1.001

Appendix Table S5.

	mean	sd	25%	50%	75%	PSRF
σ	0.151	0.023	0.135	0.15	0.166	1.001

Appendix Table S6.

	pooled sample variance					
	mean	sd	25%	50%	75%	PSRF
θ	-0.014	0.003	-0.016	-0.014	-0.012	1.001
ω	0.018	0.002	0.016	0.018	0.020	1.001
	un-pooled sample variance					
	mean	sd	25%	50%	75%	PSRF
θ	-0.021	0.003	-0.023	-0.021	-0.019	1.001
ω	0.018	0.003	0.016	0.018	0.020	1.001

Chapter 4

Vital effects and ecologic adaptation of photosymbiont-bearing planktonic foraminifera during the Paleocene-Eocene Thermal Maximum, implications for paleoclimate

Paper chapter

Si, W., and Aubry, M. P. (2018). Vital Effects and Ecologic Adaptation of Photosymbiont-Bearing Planktonic Foraminifera During the Paleocene-Eocene Thermal Maximum, Implications for Paleoclimate. Paleoceanography and Paleoclimatology, 33(1), 112-125.

4.1 Abstract

Stable isotope-size data of four major planktonic foraminifera lineages from the Paleocene-Eocene Thermal Maximum (PETM, ca. 56 Ma) at two locations (North Atlantic New Jersey shelf and Southern Ocean) are analyzed. By comparing changes in $\delta^{13}C$/ $\delta^{18}O$-size correlation prior to and during the PETM, we present evidence of significant changes in vital effects in photosymbiont-bearing planktonic foraminifera during the PETM. The $\delta^{13}C$-size data indicate divergent changes in $\delta^{13}C$ vital effects in high-latitudes versus mid-latitude populations, due likely to different responses in photosymbiotic activities. Combined $\delta^{18}O$-size data and isotopic ranking indicates that some surface dwellers experienced changes that may be interpreted as depth migrations. Extreme temperatures (>32°C) may have exerted selective pressure and drove depth

migrations. Species with flexible depth distribution were capable of adapting to rapid warming by vertical migration in the upper ocean, while populations restricted to near surface ocean may have undergone temporal and/or regional collapse during the peak warming. From a paleo-proxy perspective, these biologic responses have the potential to obscure paleoceanographic signatures both regionally and globally.

4.2 Introduction

Although ocean warming and acidification have been recognized as major anthropogenic perturbations to impact the near future, little is known of their relative roles on species' fitness (Boyd, 2011) and the responses that can be expected in marine planktonic communities. Field observations have provided evidence of adaptation (Schlüter et al., 2014). However, how the interactions between environmental pressure and biotic adaptation may play out over long timescales (thousands to tens of thousands of years) are currently poorly known.

Studies on the Paleocene-Eocene Thermal Maximum event (PETM) may provide some insight into these concerns. The PETM is considered as a possible geologic analogue to anthropogenic climate change. It consists of an abrupt global warming of ~6˚C (Thomas et al., 2002; Zachos et al., 2007) and ocean acidification (Zachos et al., 2005) due to the rapid introduction of a large mass (>1200~4500 GtC) of greenhouse gas (Dickens et al., 1995; Zachos et al., 2005) within probably a few thousand years (Zeebe et al., 2016). Paleontological studies suggest that evolution and migrations occurred in both terrestrial and marine realms during the PETM in association with the environmental perturbations

(McInery and Wing, 2011). Radiation of land mammals (Gingerich, 2006), poleward dispersal of planktonic communities (Aubry, 1998; Bujak and Brinkhuis, 1998), as well as extinction of deep sea benthic foraminifera (Thomas, 1998) provide opportunities to evaluate the adaptive limitations and strategies of species to abrupt global warming.

In this study, we investigate changes in vital effects in planktonic foraminiferal $\delta^{18}O$ and $\delta^{13}C$ values. Elucidating the patterns and magnitudes of vital effects not only helps understand life processes that are crucial for species adaptation, it is also important for an accurate reconstruction of PETM climate, given that active adaptation of organisms may introduce large variations in proxy data. In contrast to previous studies (Thomas et al., 2002, Makarova et al. 2017) that have placed emphasis on establishing high-resolution and continuous time-series of $\delta^{18}O$ and $\delta^{13}C$ records, we focus here on analyzing multi-size fraction isotopes of different species in discrete samples from the New Jersey Coastal Plain and the Southern Ocean (Fig. 1). We show that large $\delta^{18}O$ and $\delta^{13}C$ changes in vital effects occurred in planktonic foraminifera during the PETM, which indicates rapid ecologic responses to the warming. We also point to the fact that, by their very nature, these responses may, in turn, compromise paleoenvironmental reconstructions.

4.3 Method

Geochemical vital effects in planktonic foraminifera are often due to life processes that may differ taxonomically, ontogenetically and/or physiologically. To resolve these signals from paleoclimate variations, we analyze planktonic foraminifera in five size fractions (125-150, 150-212, 212-250, 250-300, 300-355 μm). In an ideal situation, we

would have analyzed five size fractions in each sample. In practice, we could not do this consistently because the largest specimens do not always occur in sufficient numbers (materials for this study is leftover residue of several previous studies). On average, three to four size fractions were analyzed in each sample. Specimens smaller than 125 μm were excluded because small planktonic foraminifera often exhibit $\delta^{13}C$ vital effects due to the incorporation of metabolic CO_2 (Birch et al., 2013), likely complicating our interpretations.

Phylogeny — we use lineages as our operational taxonomic unit. A lineage is composed of species with morphologic and ontogenic similarities due to their evolution from a common ancestor. We use lineages because: 1) as we will demonstrate, individual lineages exhibit vital effects that are not shown when lower rank taxonomic units such as genera are used; 2) species within a lineage often show morphologic similarity on juvenile stages and when small size fractions are examined, it is difficult to identify specimens at species level. Thus, as a compromise between taxonomic precision and practical purpose, we use lineages. The four lineages studied are 1) the non-symbiotic thermocline *Subbotina* (*Subb*) lineage, and 2) the photosymbiont-bearing mixed-layer lineages of *Acarinina subsphaerica-mckannai-soldadoensis* (*Ac*), *Morozovella aequa-subbotinae* (*MAS*), and *Morozovella acuta-velascoensis* (*MAV*) (Olsson et al., 1999). Regarding the *Ac* lineage, we use *A. soldadoensis* for all PETM samples, and high-spired acarininids for pre-PETM samples from Site 689. These high-spired acarininids are identified as *A. subsphaerica* and/or *A. mckannai* (Olsson et al., 1999, Kelly, 2002). For the *MAV* and *MAS* lineages, we do not differentiate species within each lineage. For the

Subb lineage, *Subbotina roesnaesensis* is the only species used. Illustrations of selected species are included in supporting materials (Plate 1). Note that we use the term "species" occasionally in the discussion below for ease of communication although we only work at the lineage level.

In addition to the new data we present here, we have compiled previously published data to quantify the vital effects prior to the PETM. We selected the datasets that identified specimens to species level (Table S1), and lowered taxonomic resolution to lineage level so that new and old data become comparable. For instance, the δ^{13}C-size data of *M. acuta* and those of *M. velascoensis* are all considered as δ^{13}C-size data of the *MAV* lineage.

δ^{18}O vital effects — The δ^{18}O of planktonic foraminifera is controlled by the seawater temperature at the depth where they live. As different species inhabit different water depths (Birch et al., 2013), inter-species δ^{18}O gradients reflect species vertical niche partition in the water column, with lower δ^{18}O values indicating shallower and warmer habitats, and higher δ^{18}O values indicating deeper and colder habitats. In addition, the intra-species δ^{18}O-size gradient reveals the vertical migration of a species during ontogeny.

δ^{13}C vital effects — We use planktonic foraminiferal $\delta^{13}C_{planktonic}$ and bulk coccolithophore $\delta^{13}C_{bulk}$ to examine vital effects associated with photosymbiotic activities in planktonic foraminifera. Specifically, non-symbiotic $\delta^{13}C_{planktonic}$ and $\delta^{13}C_{bulk}$ are isotopically in close equilibrium with seawater ($\delta^{13}C_{sw}$) (Spero and Williams, 1988;

Bolton et al., 2012) whereas photosymbiotic $\delta^{13}C_{planktonic}$ is heavier than $\delta^{13}C_{sw}$ owing to the photosynthetic activity of the symbionts. Moreover, because symbiotic photosynthesis intensifies as a planktonic foraminifera grow (Takagi et al., 2016), there is a positive correlation between $\delta^{13}C_{planktonic}$ and test size (Shackleton et al., 1985, D'Hondt et al., 1994, Birch et al., 2012, Ezard et al, 2015). The slope of this correlation is used here to statistically estimate the magnitude of size-related vital effect in $\delta^{13}C$, which is potentially due to changes in photosynthetic activities. A small slope indicates absence of size-related vital effect, probably indicating no, or weak, photosymbiosis. Conversely, a steep slope may indicate active photosynthesis. A Bayesian hierarchical linear model was used to estimate the regression slope of $\delta^{13}C$-size prior to and during the PETM. This method allows us to evaluate the $\delta^{13}C$-size regression slope of each sample as well as the variations of estimated slopes in multiple samples. The posterior estimates of the regression slope therefore take into account both within-sample and sample-level variations. A more detailed discussion of the methodology can be found in the supporting information (Gelman and Hill, 2006, Lunn et al., 2009).

Benthic foraminifera stable isotopes — benthic isotopes were generated to constrain the isotopic signals of the deeper part of the water column in combination with *Subb* isotopes. We use *Cibicidoides* spp. and *Stensioina beccariiformis* for the pre-PETM interval, and *Anomalinoides acuta* for the PETM interval.

4.4 Stratigraphic correlation

To compare our results with previously published records and facilitate interpretations, we have established composite records for high latitude Sites 689 and 690 (689-690 record). Correlation between Sites 689 and 690 is relatively straightforward based on multiple isotopic events at both sites (Thomas et al., 2002, Zachos et al., 2007, see Supplementary Materials). Because numerical ages for the 689-690 record are controversial (e.g. Farley and Eltgroth, 2003, Röhl et al., 2007), we describe data in terms of depths rather than ages.

The correlation of the Atlantic coastal margin Millville record (Figure 1b) to 689-690 records is hampered by the truncation of the Millville record ~10 m above the onset of the CIE (Sugarman et al., 2005), and it is unclear how much of the PETM has been preserved. The highest occurrences (HOs) of planktonic foraminifera excursion taxa *Acarinina sibaiyaensis* at ~263 m and *Ac. africana* at ~262.4 m (Fig. 2a), respectively, suggest that the uppermost part of the Millville record may have entered the "recovery" phase. Unfortunately, because of the absence of these excursion taxa at high latitude Sites 689-690, the application of these two datums for stratigraphic correlation is limited. Nevertheless, age uncertainties do not compromise our study since we primarily focus on changes in vital effects in response to the CIE onset, which can be correlated unambiguously using $\delta^{13}C_{bulk}$ (Fig. 2a) and constrained by the appearance of the excursion taxa.

4.5 Results

4.5.1 Changes in $\delta^{18}O$-size vital effects

Prior to the PETM, inter-species $\delta^{18}O$ gradients from both the Millville and 689-690 records show lower $\delta^{18}O$ values in *Ac*, *MAS* and/or *MAV* relative to higher values in *Subb* (Figs. 2b-c, 3a). This suggests that the depth distribution of these lineages prior to the PETM is consistent with the conventional paleo-ecology model (Shackleton et al., 1985, D'Hondt et al., 1994, Birch et al., 2012), with *Ac*, *MAS*, and *MAV* inhabiting surface water and *Subb* residing deeper close to the thermocline. However, we observe significant changes in $\delta^{18}O$ vital effects during the PETM.

PETM Millville record — interspecies gradients between $\delta^{18}O_{Ac}$, $\delta^{18}O_{Subb}$ and $\delta^{18}O_{benthic}$ collapsed (MV 273.6-267m, Fig. 2b, 2d). This was followed by a two-step recovery (Fig. 2b, 2e, 2f). The first step (MV 265-263 m, Fig. 2e) is characterized by the establishment of a $\delta^{18}O_{Ac}$-size gradient (more negative $\delta^{18}O_{Ac}$ in large specimens) and the second step (MV 262-261 m, Fig. 2f) is characterized by increasingly heavier $\delta^{18}O_{Subb}$. Among the morozovellids, the $\delta^{18}O$ of the *MAS* lineage mirrored the $\delta^{18}O_{Ac}$, whereas a divergent pattern occurs in the sister lineage *MAV* with constant $\delta^{18}O$ of ~-4.2‰ in the largest size fraction (Fig. 2b). These observations broadly agree with time-series data from Millville (Makarova et al., 2017) and Bass River (John et al., 2007) albeit with some critical differences (see discussion below).

The 689-690 record — The $\delta^{18}O$ gradients between *Ac* and *Subb* collapsed at the CIE onset, and was followed by a recovery ~70 cm above the onset (Fig. 3a) characterized by

the appearance of a $\delta^{18}O_{Ac}$-size gradient (lighter $\delta^{18}O_{Ac}$ in large-sized *Ac*). Interestingly, the *MAS* lineage (Fig. 3a Green triangles) occurred briefly following the CIE onset with heavier $\delta^{13}C$ (~1.5‰) and lighter $\delta^{18}O$ (~1‰) relative to *Ac* and *Subb* in the same sample. Note that the preservation of planktonic foraminifera is moderate at Site 689-690 in contrast to the glassy foraminifera from Millville and Bass River. Overgrowth of secondary calcite may have biased the isotopic signals to more positive values (Pearson et al., 2001).

4.5.2 Changes in $\delta^{13}C$-size vital effects

Statistical estimates of compiled pre-PETM $\delta^{13}C$-size data (Shackleton et al., 1985, D'Hondt et al., 1994, Norris, 1996, Quillévéré et al., 2001) indicate a ~0.5-0.6‰ increase in $\delta^{13}C$ for every 100 µm increase in size in *Ac, MAS,* and *MAV* (Fig. 4a). In other words, *Ac, MAS,* and *MAV* of 300-355 µm are, on average, ~1‰ higher isotopically than those from the 125-150 µm fraction. These abstract summary statistics are also illustrated qualitatively in Figure 4b. In this figure, we plot several $\Delta\delta^{13}C_{Ac}$-size series from pre-PETM intervals. Each $\delta^{13}C_{Ac}$-size series is moved arbitrarily along the Y axis to line up with other pre-PETM $\delta^{13}C_{Ac}$-size series. By doing so, we reduce the between-sample offsets (the intercepts) but retain the within-sample information (the slope). This procedure is analogous to the hierarchical lineage regression.

Significant changes occurred at both Sites 689/690 and on the New Jersey Margin during the PETM. At Millville, the $\delta^{13}C$-size gradients increased significantly in all photosymbiont-bearing lineages following the CIE onset (MV 273.6-263 m). Regression

analyses on the $\delta^{13}C$-size data suggest that the slope of the $\delta^{13}C$-size regression increased by 60%, 50% and 100% in *Ac*, *MAS* and *MAV*, respectively, compared to the pre-CIE background values (Fig. 4a). As a result, the large specimens of *Ac*, *MAS* and *MAV* (300-355 μm) are significantly enriched (by ~2‰) in $\delta^{13}C$ relative to 125-150 μm fractions (Figure 4b).

The 689-690 record exhibited dynamic changes in inter- and intra- species $\delta^{13}C$ gradient (Fig. 3c-d). The $\delta^{13}C$ gradients between *Ac* and *Subb* first collapsed at the CIE onset in all size fractions (Fig. 3b, d). Regression analyses show that the $\delta^{13}C_{Ac}$-size gradient is ~0 (Fig. 4a-b). However, about 70 cm above the onset (207.3 mbsf at Site 689), a clear $\delta^{13}C_{Ac}$-size gradient reappears, causing a positive $\delta^{13}C$ shift in the large specimens of *Ac* (Fig. 3b, e). These observations suggest geographically different changes in $\delta^{13}C$ vital effects at southern high latitudes and the mid latitudes.

4.6 Discussion

4.6.1 Possible causes for changes in $\delta^{18}O$ vital effects

There are a couple of possible explanations to the changes in $\delta^{18}O$ in the planktonic foraminifera. As shown in Figure 2b-d, the gradient collapse during the PETM between planktonic *Ac* and thermocline (*Subb*)/benthics is the result of changing benthic (and *Subb*) isotopes rather than $\delta^{18}O_{Ac}$. If it is assumed that *Ac* was the surface dweller during the PETM, it may be concluded that the thermocline structure of the water column had changed. The warm surface water may have expanded deeper following the CIE onset,

reducing the $\delta^{18}O$ gradients between deep dwellers (*Subb* and shelf benthic foraminifera) and surface *Ac* species (e.g. Makarova et al., 2017).

However, our data do not support this hydrologic scenario. First, the isotopic gradients between $\delta^{18}O_{benthic}$, $\delta^{18}O_{Subb}$ and large-sized $\delta^{18}O_{MAV}$ was approximately 1.5‰ prior to and during the PETM (Fig. 2b-e), implying that changes in the thermal gradient of the water column was small, or at least that it was not a dominant factor in shaping the isotopic signatures. Makarova et al. (2017) reached a different conclusion suggesting greater warming in the thermocline ($\Delta\delta^{18}O$ = -1.75 ‰ in thermocline and benthic taxa) relative to mixed layer ($\Delta\delta^{18}O$ = -1 ‰ in surface taxa). We suspect that separation of the *Morozovella* lineages in our work explains the differences between the results in the two studies. Makarova et al. (2017) used *Morozovella* spp. to infer changes in sea surface temperatures (SST). However, as we show, more than half of the PETM morozovellids (species of *MAS* lineage) yielded $\delta^{18}O$ values similar to *Subb* and benthic foraminifera. Consequently, their data may be biased and likely cannot provide reliable estimates of SST during the PETM. Makarova et al. (2017) also suggest that $\delta^{18}O$ changes in *Morozovella* and *Acarinina* were the same ($\Delta\delta^{18}O$ = -1 ‰, see Figure 5 in Makarova et al. 2017). However, this is not the case. The magnitude of warming recorded in *Ac* and *MAV* are different (Fig. 2b, orange and grey dash lines emphasize $\delta^{18}O$ changes in *MAV* and *Ac*, respectively). A plot of their data against ours (supplementary material Fig. S3) shows that their *Morozovella* $\delta^{18}O$ is consistently higher than the $\delta^{18}O_{MAV}$ of large specimens in our study, implying a mixture of different lineages in their geochemical analysis.

Another possible explanation for the changes in $\delta^{18}O$ vital effects involved changes in the seasonality of planktonic foraminifera (personal communication of J. D. Wright). For example, if *MAV* and *Ac* were both seasonal planktons during the PETM, being dominant in the warm and cool seasons, respectively, then the isotopic gradient between *MAV* and *Ac* in large specimens may reflect seasonal changes in the SST. However, there is not sufficient independent evidence about the seasonal flux of Paleogene planktonic foraminifera or about the seasonality of the PETM SST to assert a seasonal effect.

Based on changes in inter-species gradients (between *MAV*, *Ac*, *Subb* and benthics) and $\delta^{18}O$-size gradient in *Ac*, we suggest that changes in habitat depths of *Ac* are responsible for the observed changes in $\delta^{18}O$ vital effects. This idea is not new, and several authors have proposed a similar idea based on studies of equatorial Pacific Site 865 (Kelly et al., 1998, Dunkley Jones et al., 2013). In our records, *Ac* experienced three phases of habitat distribution during the PETM at Millville. Firstly, following the CIE onset, it descended into the thermocline, as indicated by the overlap of $\delta^{18}O_{Ac}$, $\delta^{18}O_{Subb}$ and $\delta^{18}O_{benthic}$ (Fig. 2b, d). Subsequently (MV ~265-263m), *Ac* began to re-populate the mixed layer during part of its life cycle by ascending from the thermocline into warmer, shallower depths as they grew to adult stage, resulting in more depleted $\delta^{18}O$ (-3.5‰) in adult specimens (Fig.2b, e). In the last phase (above 262m), *Ac* no longer experienced significant ontogenetic changes in depth habitat and permanently resided in the mixed layer, as suggested by the divergence of $\delta^{18}O_{Ac}$ from $\delta^{18}O_{Subb}$ and $\delta^{18}O_{benthic}$ (Fig. 2b, f). The $\delta^{18}O_{MAS}$ suggests that the *MAS* lineage behaved like *Ac* and went through similar depth shifts during the PETM. *MAV*, however, resided in the shallowest and warmest water

mass alone (in adult stage) and shows no depth changes during the PETM, continuing to carry the lightest $\delta^{18}O$ among all lineages.

At Sites 689-690, changes in inter-species and $\delta^{18}O$-size gradients between *Ac*, *MAS* and *Subb* also suggest a deeper habitat of *Ac* after the PETM onset, followed by migration back to a shallower habitat (as shown by arrow in Fig 3a). In fact, if we only considered the $\delta^{18}O_{Ac}$ records while ignoring the ontogenetic migration of *Ac*, we would alternatively suggest that there was a sudden "warming" ~70 cm above the onset (Fig. 3a) without realizing that this is simply an artifact of changes in vital effects.

It is important to point out that our interpretation of size of planktonic foraminifera as ontogenic stage is a simplified view of what different sizes of foraminifera in the fossil record may reflect. The size distribution of a fossil assemblage can be interpreted alternatively as due to: 1) ontogeny, or 2) environmental control. In the latter case, the size of foraminifera is affected by environmental conditions such as temperature, salinity, food availability etc. Growth under unfavorable conditions for instance result in small size of the population. With regard to this study, if temperature (or any other environmental factor) strongly controlled the growth of foraminifera, changes in $\delta^{18}O_{Ac}$-size can be explained alternatively as follows: *Ac* was able to grow at a relatively wide range of water depths prior to the PETM, recording relatively scattered $\delta^{18}O_{Ac}$ (Fig. 2c). During the PETM, *Ac* could only grow at the thermocline. As a result, the $\delta^{18}O_{Ac}$ in all size fractions became tightly constrained (Fig. 2d). Up-section (Fig. 2e), *Ac* began to re-populate a wider depth range, particularly at shallow depth where optimum growth

occurred, resulting in more negative $\delta^{18}O$ in the large fractions. This alternative interpretation, although different from the ontogenic-based explanation, does not change our inference on the causes of changes in $\delta^{18}O_{Ac}$ during the PETM (section 5.2, possible hostile conditions at sea surface). It also does not affect our discussion of paleoceanographic implications in section 6. Hence, we adopt the size-ontogeny model in this paper although recognizing that both ontogeny and environmental conditions can affect the size distribution of a fossil assemblage.

4.6.2 Possible causes of changes in $\delta^{13}C$ vital effects

Depth migration of *Ac* may explain several $\delta^{13}C$ features in the 689-690 record. First, the inter-species $\delta^{13}C$ gradient disappeared in all size fractions between *Ac* and *Subb* right above the CIE onset (Fig. 3c VS 3d). This disappearance of between-species $\delta^{13}C$ gradient in small size fractions suggests a deeper habitat of *Ac* (thermocline), where remineralization of organic materials depletes the $\delta^{13}C_{sw}$ relative to the mixed layer. In addition, a deeper habitat of *Ac* may have suppressed photosymbiosis, causing symbionts loss/bleaching (Edger et al., 2013) and therefore diminished $\delta^{13}C_{Ac}$-size gradients (compare the slope of $\delta^{13}C_{Ac}$-size in Fig. 3c, d, and e). *MAS* would still have harbored photosymbionts (~1.5‰ heavier in large fraction, Fig. 3b, d) probably due to their slightly shallower habitat as inferred from $\delta^{18}O_{MAS}$. *Ac* began to repopulate the surface water later (Fig. 3a), and it resumed photosymbiosis, as indicated by the reestablishment of $\delta^{13}C_{Ac}$-size gradients (Fig. 3e).

The $\delta^{13}C$-size gradients in *Ac*, *MAS* and *MAV* increased significantly during the PETM at Millville, possibly due to enhanced photosymbiontic activity (Figure 4a, b). However, it is unclear why photosymbiontic activities in *Ac* have increased. Warming may have directly impacted photosynthetic physiology and growth rates in temperate regions (Boyd et al., 2013), enhancing the productivity of symbionts. Additionally, a deeper habitat close to the nutricline may also have increased the productivity of their symbionts.

We acknowledge that our interpretation of changes in photosymbiontic activities using $\delta^{13}C$ relies on the conventional model of $\delta^{13}C$-size correlation (Shackleton et al., 1985, D'Hondt et al., 1994, Birch et al., 2012). Studies on core top materials, however, suggest that some living non-symbiotic planktonic foraminifera also exhibit a $\delta^{13}C$-size correlation (Elderfield et al., 2002, Friedrich et al., 2012), possibly due to the incorporation of metabolic CO_2 even in moderate size (~300 μm). In a recent compilation and statistical analysis of stable isotopes-size data of extant planktonic foraminifera, Ezard et al., (2015) suggest that multiple factors (locations, live/dead assemblages, and depth habitats etc.) all have the potential to complicate the regression analysis. Therefore, changes in photosymbiontic activity as a possible explanation of changes in $\delta^{13}C$ vital effects should be taken cautiously, and alternative interpretations are possible.

4.6.3 Causes of the depth migration

If our interpretation of depth migration in *Ac* (and *MAS*) is correct, a further question is why these near surface dwellers preferred a deeper habitat during the PETM. We consider two possibilities here, the biotic versus abiotic forcing.

Species of *MAV* may have been well adapted to the mixed layer and its competitive advantages over *Ac* and *MAS* may have driven them to migrate to a deeper habitat during the PETM. Were this the case, we should expect that *MAV* species to be abundant in the foraminiferal assemblages. However, *MAV* (particularly large individuals) is far from abundant at Millville and Bass River. At other locations, *MAV* is either absent throughout the PETM (Thomas et al., 2002, Aze et al., 2014) or during the peak of the PETM (Kelly et al., 1998), suggesting that species of this lineage were poorly adapted. Therefore, it is unlikely that the changes in habitat in *Ac*/*MAS* is due to the ecologic success of *MAV* lineage.

Alternatively, abiotic forcing such as extreme warming could have created a vertical selective gradient for depth migrations of *Ac* and *MAS* during the PETM. Temperature has long been recognized as the main environmental parameter controlling the physiology (Thomas et al., 2012) and geography (Rutherford et al., 1999) of marine planktonic communities. Most living marine plankton, including planktonic foraminifera (Bijma et al., 1990), phytoplankton (Breitbarth et al., 2007, Boyd et al., 2013), and photosynthetic symbionts (Tchernov et al., 2004, Schmidt et al., 2011) experience significant decline in fitness when environmental temperature increases above their thermal optima. Culturing experiments show that in living tropical symbiotic planktonic foraminifera with optimum temperatures of ~26°C (*Trilobatus sacculifer*, *Globigerinoides ruber*, *Globigerinella siphonifera*, *Orbulina universa* and *Neogloboquadrina dutertrei*), food acceptance, chamber formation and reproduction

(gametogenesis) rarely occur when temperatures rise above ~32°C, even though their lower-temperature tolerances could be as low as ~14°C (Bijma et al., 1990).

As a cautious, exploratory exercise, we take the upper limit of ~32°C and calculate the corresponding $\delta^{18}O$ value (using Kim and O'Neil, 1997, for temperature estimates and assuming $\delta^{18}O_{sw}$ = -1‰). The reason for this is that we want to know what $\delta^{18}O$ might be if we *assume* that ancient planktonic foraminifera share similar thermal tolerance with modern species. Interestingly, we obtain a $\delta^{18}O$ value of -4.5‰ for PETM planktonic foraminifera. This estimate is very close to the lowest $\delta^{18}O$ values (~-4.2‰) obtained from PETM Millville, which leads us to suspect that the abrupt warming at the PETM onset, especially in the tropics and subtropics, may have stressed planktonic foraminifera and initiated the migration of *Ac* and *MAS* to deeper water depth.

While there may not be firm reason to assume that Holocene and Paleogene planktonic foraminifera share the same thermal tolerance, several independent observations support our argument. At equatorial Site 865, Kelly et al. (1998) noticed that the true mixed-layer dweller *M. velascoensis* (*MAV*) occurring just above the PETM onset are exclusively reworked from older sediments, suggesting a selective temporal disappearance of this species immediately following the onset. The first PETM *M. velascoensis* (*MAV*) occurred 11 cm above the PETM onset (102.87 mbsf) and they recorded the lowest PETM $\delta^{18}O_{MAV}$ value of -4.47‰ (Kozdon et al., 2011) when SST may have had already dropped below the species' thermal threshold of ~32°C (-4.5‰ $\delta^{18}O$). Based on the Millville records, the *MAV* lineage seems to have been restricted mixed-layer dwellers.

As obligate mixed dwellers, their lack of flexibility to live at deeper depth, unlike *Ac* and *MAS*, may have caused their selective disappearance during the peak warming.

At Millville, the first ~30 cm of the PETM is characterized by a "barren zone" with abrupt drop in $CaCO_3$ percentage to ~0% (Wright and Schaller, 2013), just as it does at the PETM GSSP section in Egypt (Aubry et al., 2007). Moreover, the true surface lineage *MAV* did not reappear until ~90 cm above the onset at MV (Fig. 2b, Fig. 5a). Oceanic acidification cannot explain the absence of biogenic carbonates in these shallow water settings because the upper surface ocean should have remained supersaturated during the PETM (Zeebe and Zachos, 2007). Although dissolution due to increased terrigenous inputs or bacterial activity in suboxic sediments may account for the disappearance of biogenic calcite within the barren zone, it still does not explain the absence of mixed-layer dwellers *MAV* (Fig. 5a) up-section given the occurrences of other species (*Ac* and benthic foraminifera) with excellent preservation. Therefore, it is likely that high SST (e.g. >32°C, -4.5‰ $\delta^{18}O$) at the PETM onset may have stressed many planktonic communities, causing the temporary reduction/collapse of populations in the mixed layer on the New Jersey Margin during peak warmth.

A recent study from the Equatorial Atlantic (Nigeria) finds a decrease from 10^5 to less than 10^2 dinocysts per gram of dry sediment immediately above the PETM (Frieling et al., 2017). Planktonic foraminifera seem to be absent from that record (see Fig. S6 in Frieling et al., 2017) during the CIE. Modeling suggests that the Nigeria Basin represented some of the warmest open ocean temperatures in the Early Paleogene world (Frieling et al.,

2017) and pre-PETM temperatures may have had already reached the upper-thermal limit of planktonic foraminifera. PETM warming may have stressed the planktonic foraminifera and even dinoflagellate populations which are among the most temperature-resilient planktonic groups (Frieling et al., 2017).

Note that our argument also assumes that $\delta^{18}O_{sw}$ was approximately -1‰ prior to and during the PETM for Millville records. Using multi-proxies, previous studies have suggested that $\delta^{18}O_{sw}$ may have changed during the PETM, especially on continental shelves where enhanced hydrologic cycles and riverine inputs may have depleted $\delta^{18}O_{sw}$ (Zachos et al., 2006). However, Zachos et al. (2006) presented no $\delta^{18}O_{MAV}$ from the pre-PETM interval, and their argument relies on changes in $\delta^{18}O_{Ac}$. The one pre-PETM $\delta^{18}O_{Ac}$ data point in their work is quite positive (approximately -1.7‰) relative to the thermocline $\delta^{18}O_{Subb}$ (approximately -2‰). Given the large spread of $\delta^{18}O_{Ac}$ from pre-PETM interval (Fig. 2c), we suggest that the pre-PETM $\delta^{18}O_{Ac}$ data should be used with caution. Although we do not rule out the possibility of a change in $\delta^{18}O_{sw}$, as we will illustrate below, we suggest that discrepancies in different proxies may be largely attributable to changes in inter- and intra-species vital effects during the PETM. If we assume that TEX_{86}^{H} estimates from Bass River (~6°C warming) are representative of regional temperature changes during the PETM, then a 5°C warming in $\delta^{18}O_{MAV}$ (average -3.2‰ in pre-PETM and average -4.2‰ during the PETM) at Millville suggests that changes in regional $\delta^{18}O_{sw}$ are small.

4.7 Paleoclimatic significance

The observation of large changes in vital effects in foraminiferal $\delta^{18}O$ and $\delta^{13}C$ and the interpretation from a biologic perspective suggest caution on some inferences from proxy data. Paleoceanographic studies assume that *Ac*, *MAV*, and *MAS* are mixed-layer photosymbiont-bearing populations. Changes in shell chemistry are primarily interpreted in the context of paleoceanography. Instead, we show here that vital effects can be significantly large relative to the PETM signal in both the $\delta^{18}O$ and $\delta^{13}C$ signatures. Paleoclimatic interpretations may be biased if these biologic complications are overlooked.

4.7.1 The magnitude of the CIE

Changes in the $\delta^{13}C$ vital effects may bias estimates of the magnitude of the CIE. In the 689-690 record, the $\delta^{13}C_{Ac}$-size correlation has diminished and interspecies gradients between *Ac* and *Subb* have disappeared above the onset (Fig. 3b, d, Fig. 4b). In contrast, adult *MAS* is isotopically ~1.5‰ heavier than *Ac* and *Subb* (Fig. 3d). The estimates of the magnitude of the CIE from Site 689/690 based on *Acarinina* (*Ac*), therefore, should be overestimated. Assuming 3.5-4‰ $\delta^{13}C$ for pre-PETM mixed layer dwellers (*Ac*) and 1-1.5‰ for PETM mixed layer dwellers (*MAS*), the magnitude of CIE at Site 689/690 preserved in photosymbiont-bearing planktonic foraminifera is approximately 2.5‰.

At Millville, the apparent magnitude of CIE is ~4‰ in *Ac* and *MAV*, 3.5‰ in *Subb* (Fig. 2c-d), and ~2.6‰ in benthics. However, estimates of changes in $\delta^{13}C_{sw}$ are complicated by at least two factors. First, the PETM $\delta^{13}C$ of bulk, benthic foraminifera, *Subb*, small-

sized *Ac*, *MAS* and *MAV* are all depleted relative to pelagic 689-690 records by ~-2‰. Second, increased $\delta^{13}C$-size gradients in *Ac, MAS,* and *MAV* add further uncertainty to the estimate of the magnitude of the CIE in seawater (Fig. 4). A steeper gradient of the $\delta^{13}C_{Ac}$-size correlation implies that the Millville *Ac* population had stronger vital effects and likely recorded more positive $\delta^{13}C$ values relative to the seawater $\delta^{13}C$ (Fig. 4b). Because we do not have a satisfactory explanation for the possible cause(s) of enhanced vital effects for these shelf populations at this moment, estimates of the magnitude of the CIE based on these records should be considered with caution.

In summary, size-related vital effects alone could potentially introduce large uncertainties in the estimates of $\delta^{13}C_{sw}$ even in the same species (Fig. 4b). Therefore, when $\delta^{13}C$ from remote sites are compared, vital effects of foraminifera should be evaluated first.

4.7.2 The temperature hiatus

A further implication raised by our data concerns the completeness of the temperature records preserved in PETM foraminiferal records both regionally and globally.

Regionally, our $\delta^{18}O$-size data suggest that only large (>300 μm) *MAV* have recorded SST following the PETM onset (Fig. 2b). As a result, estimates of the magnitude of warming can be significantly biased if 1) large *MAV* specimens are sparse/absent in foraminiferal assemblages, and 2) other species are used. For example, a close inspection shows that the "surface" species *Ac* recorded little temperature changes across the PETM onset at MV (273.2-274.4 m) despite the fact that the $\delta^{18}O_{benthic}$ recorded a significant

temperature rise (from -1.5‰ to -3‰ in *Anomalinoides acuta*, Fig. 5). Rather than being indicative of a lack of temperature changes, the relatively small changes in $\delta^{18}O_{Ac}$ and $\delta^{18}O_{MAS}$ provides evidence of species' adaptations to rapid environmental changes by tracking their optimal habitats – one cost-efficient strategy for survival under rapid climate changes. Similarly, the SST may remain indeterminate at Sites 689-690 due to the depth migration of *Ac*. We propose that this lineage lived at depth following the CIE onset, and therefore does not record SST. Lower $\delta^{18}O_{MAS}$ (-2‰, 208 m, Site 689) and $\delta^{18}O_{Ac}$ (~-2.35‰, 170-170.2 m, Site 690) together suggest that SST following the CIE onset were warmer than that recorded in $\delta^{18}O_{Ac}$.

We also compared TEX_{86}^{H} records with $\delta^{18}O$ data from Bass River (Sluijs et al., 2006) and Wilson Lake (Zachos et al., 2006), respectively. ΔSST estimated from TEX_{86}^{H} and $\delta^{18}O_{MAV}$ from Wilson Lake shows significant discrepancies, in contrast to the estimates from Bass River (Fig. 6a vs 6b). In shallow water setting (Wilson Lake), the large pelagic species would have been absent due to environmental and ecologic factors unrelated to temperatures, e.g. relatively shallow thermocline nearshore (Castelao et al., 2008). The absence of large *MAV* in Wilson Lake, therefore, prevents accurate reconstructions of PETM SST and results in systematic discrepancies between TEX_{86}-based and $\delta^{18}O$ calibrations (Fig. 6a). In more offshore sections (Bass River and Millville), the occurrences of large forms allow us to reconstruct the full range of vital effects as well as paleoclimatic signals (Fig. 6b).

Globally, adaptation and maladaptation of planktonic foraminifera may have systematically biased our paleotemperature records. A compilation of several of the best PETM $\delta^{18}O$ records shows that the all highest SST estimates fall close to the same threshold of -4.5‰ (Fig. 7). The convergence of the lowest $\delta^{18}O$ from different locations may suggest diminished latitudinal gradients and uniform warming during the PETM (Zachos et al., 2007). However, this may indeed reflect a hiatus in temperature records due to the absence of planktonic foraminifera in warmer waters (significantly above 32°C). During the peak warming, the tropics and subtropics surface ocean may have experienced regionally and/or temporally high temperatures that were inimical to planktonic organisms. Foraminifera are unable to provide us with a record of these hostile SST if they were not able to maintain a sizable local population and contribute to a significant proportion of the fossil assemblages. As a result, the highest SST determined from planktonic foraminifera would likely converge at the upper thermal limit of foraminifera. Regional or temporal variations in SST above this threshold may not be recorded.

Therefore, we speculate here that there might be a temperature ceiling (or more accurately, the $\delta^{18}O$ ceiling) in the planktonic foraminifera fossil records, with most negative $\delta^{18}O$ approximately -4.5‰ assuming $\delta^{18}O_{sw}$=-1‰ in an ice free world. To test this idea, we compiled planktonic foraminifera $\delta^{18}O$ from another example of extreme warmth — the Late Cretaceous greenhouse climate. We have selected only data with excellent preservation and glassy appearance of planktonic foraminifera, and we have tried to cover a wide range of latitudes. The compiled Late Cretaceous data (Fig. 8) show

similarity to the PETM (Fig. 7). The lowest $\delta^{18}O$ were largely topped at approximately -4.5‰ except for the Tanzanian sites where both PETM and Late Cretaceous records show values between -4.5~-5‰ in some species (average -4.6±0.2‰ in *Whiteinella* spp, Fig. 8). These more negative values suggest a few possibilities. First, some species may have managed to adapt to warmer SST (e.g. ~35°C) and were capable of recording higher SST. Given the prolonged Late Cretaceous extreme warmth (from late Albian to Turonian, Fig. 8), it is possible that some species somehow managed to increase their thermal tolerance by a few degrees. Moreover, the thermal threshold values do not have to be a global clear cut. Changes in vital effects from Millville to Sites 689/690 already suggest that adaptation of foraminifera can be site specific. Therefore, it would not be surprising that foraminifera showed regional variances in terms of thermal tolerance. The distribution of the thermal tolerance may vary around ~32°C and as high as indicated by the Tanzanian populations. Another possibility is change in $\delta^{18}O_{sw}$. We assumed a value of -1‰ $\delta^{18}O_{sw}$ for all PETM and Late Cretaceous records. However, $\delta^{18}O_{sw}$ may have changed, leading to different calculated SST. Ideally, other proxies such as Mg/Ca would be helpful to address this issue. However, vital effects in PETM Mg/Ca data are not well understood yet, and published Mg/Ca data may suffer from problems such as mixing of different species of *Morozovella* for analysis. Future studies on the vital effects of trace metal data may help constrain the $\delta^{18}O_{sw}$ and provide better temperature estimates.

4.7 Conclusion

We find evidence of significant changes in vital effects in photosymbiont-bearing planktonic foraminifera during the PETM. The $\delta^{13}C$-size correlation disappeared

following the CIE onset in 689-690 records, whereas it increased in Millville records. Based on the conventional model for $\delta^{13}C$-size correlation, these changes in $\delta^{13}C$ vital effects likely indicate divergent changes in photosymbiotic activities between sites, and have complicated our estimates of the magnitude of the CIE. On the other hand, combined $\delta^{18}O$-size data and isotopic ranking suggest that depth migration may have occurred in some (*Ac* and *MAS*) but not all planktonic foraminifera. Species of the *MAV* lineage remained in the surface ocean, recording SST until the upper thermal limit for foraminifera (~32 °C) was reached. Our capability of reconstructing the full magnitude of the PETM warming may have also been compromised by the biologic and physiologic limitations of species.

4.8 Acknowledgments

The data and supporting tables and figures are in the supporting information. We thank J. D. Wright and K. G. Miller for providing samples from Millville; J. Browning and C. Lombardi for sampling Bass River; R. K. Olsson and W. A. Berggren for taxonomic guidance. J. D. Wright and K. G. Miller provided insightful discussion and advice on an earlier version of this manuscript. We thank three anonymous reviewers for their constructive and thoughtful comments. This study would not have been possible without the help of R. Mortlock and J. D. Wright on stable isotope analysis. This research was supported by a Rutgers Student Fellowship to W. Si. Samples were provided by the International Ocean Discovery Program (IODP).

4.8 References

Aubry, M.-P. (1998), Early Paleogene calcareous nannoplankton evolution: a tale of climatic amelioration: in M.-P. Aubry, S. G. Lucas, and W. A. Berggren (Eds.), *Late Paleocene Early Eocene climatic and biotic events in the marine and terrestrial records* (pp. 158–203), Columbia University Press, New York.

Aubry, M.-P., K. Ouda, C. Dupuis, W. A. Berggren, and J. A. Van Couvering (2007), The Global Standard Stratotype-section and Point (GSSP) for the base of the Eocene Series in the Dababiya section (Egypt). *Episodes*, 30, 271–286.

Aze, T., P. N. Pearson, A. Dickson, M. Badger, P. Bown, R. Pancost, S. Gibbs, S., B. Huber, M. Leng, M., and A. Coe (2014), Extreme warming of tropical waters during the Paleocene–Eocene Thermal Maximum. *Geology*, 42, 739–742.

Bains, S., R. M. Corfield, and R. D. Norris (1999), Mechanisms of climate warming at the end of the Paleocene. *Science*, 285, 724–727.

Bice, K. L., B. T. Huber, and R. D. Norris (2003), Extreme polar warmth during the Cretaceous greenhouse? Paradox of the late Turonian $\delta^{18}O$ record at Deep Sea Drilling Project Site 511. *Paleoceanography* 18, doi/10.1029/2002PA000848

Bijma, J., W. W. Faber, and C. Hemleben (1990), Temperature and Salinity Limits for Growth and Survival of Some Planktonic Foraminifers in Laboratory Cultures. *Journal of Foraminiferal Research*, 20, 95–116.

Birch, H. S., H. K. Coxall, and P. N. Pearson (2012), Evolutionary ecology of Early Paleocene planktonic foraminifera: size, depth habitat and symbiosis. *Paleobiology*, 38, 374–390.

Birch, H. S., H. K. Coxall, P. N. Pearson, D. Kroon and M. O'Regan (2013), Planktonic foraminiferal stable isotopes and water column structure: Disentangling ecological signals. *Marine Micropaleontology*, 101, 127–143.

Bolton, C. T., H. M. Stoll, and A. Mendez-Vicente (2012), Vital effects in coccolith calcite: Cenozoic climate-pCO_2 drove the diversity of carbon acquisition strategies in coccolithophores. *Paleoceanography*, 27, 1–16.

Boyd, P. W. (2011), Beyond ocean acidification. *Nature Geoscience*, 4, 273–274.

Boyd, P. W., T. A. Rynearson, E. A. Armstrong, F. Fu, K. Hayashi, Z. Hu, D. A. Hutchins, R. M. Kudela, E. Litchman, M. R. Mulholland, U. Passow, R. F. Strzepek, K. A. Whittaker, E. Yu, and M. K. Thomas (2013), Marine phytoplankton temperature versus growth responses from polar to tropical waters--outcome of a scientific community-wide study. *PLoS One*, 8, e63091.

Breitbarth, E., A. Oschlies, and J. LaRoche (2007), Physiological constraints on the global distribution of Trichodesmium? effect of temperature on diazotrophy. *Biogeosciences*, 4, 53–61.

Bujak, J. P., and H. Brinkhuis (1998), Global warming and dinocyst changes across the Paleocene/Eocene Epoch boundary: Late Paleocene-early Eocene climatic and biotic events in the marine and terrestrial records, in M. -P. Aubry, S. G. Lucas, and W. A. Berggren (Eds.), *Late Paleocene Early Eocene climatic and biotic events in the marine and terrestrial records* (pp. 277–295), Columbia University Press, New York.

Castelao, R., S. Glenn, O. Schofield, R. Chant, J. Wilkin, and J. Kohut (2008), Seasonal evolution of hydrographic fields in the central Middle Atlantic Bight from glider observations. *Geophysical Research Letters* 35, doi:10.1029/2007GL032335

Dickens, G. R., M. M. Castillo, and J. C. G. Walker (1997), A blast of gas in the latest Paleocene: Simulating first-order effects of massive dissociation of oceanic methane hydrate. *Geology* 25, 259–262.

D'Hondt, S., J. C. Zachos, and G. Schultz (1994), Stable isotopic signals and photosymbiosis in late Paleocene planktic foraminifera. *Paleobiology*, 20, 391–406.

Edgar, K. M., S. M. Bohaty, S. J. Gibbs, P. F. Sexton, R. D. Norris, and P. A. Wilson (2013), Symbiont 'bleaching'in planktic foraminifera during the Middle Eocene Climatic Optimum. *Geology*, 41, 15–18.

Elderfield, H., M. Vautravers, and M. Cooper (2002), The relationship between shell size and Mg/Ca, Sr/Ca, $\delta^{18}O$, and $\delta^{13}C$ of species of planktonic foraminifera. *Geochemistry, Geophysics, Geosystems*, 3, 1–13.

Erbacher, J., O. Friedrich, P. A. Wilson, J. Lehmann, and W. Weiss (2011), Short-term warming events during the boreal Albian (mid-Cretaceous). *Geology* 39, 223–226.

Ezard, T. H. G., K. M. Edgar, and P. M. Hull (2105), Environmental and biological controls on size-specific $\delta^{13}C$ and $\delta^{18}O$ in recent planktonic foraminifera. *Paleoceanography* 30, 151–173.

Farley, K. A., and S. F. Eltgroth (2003), An alternative age model for the Paleocene–Eocene thermal maximum using extraterrestrial ^{3}He. *Earth and Planetary Science Letters*, 208, 135–418.

Friedrich, O., R. Schiebel, P. A. Wilson, S. Weldeab, C. J. Beer, M. J. Cooper and J. Fiebig (2012), Influence of test size, water depth, and ecology on Mg/Ca, Sr/Ca, $\delta^{18}O$ and $\delta^{13}C$ in nine modern species of planktic foraminifers. *Earth and Planetary Science Letters*, 319, 133–145.

Frieling, J., H. Gebhardt, M. Huber, O. A. Adekeye, S. O. Akande, G. Reichart, J. J. Middelburg, S. Schouten, and A. Sluijs (2017), Extreme warmth and heat-stressed plankton in the tropics during the Paleocene-Eocene Thermal Maximum. *Science advances*, 3, e1600891.

Gelman, A., and J. Hill (2006), Data analysis using regression and multilevel/hierarchical models, Cambridge University Press, New York, NY, USA

Gingerich, P. D. (2006), Environment and evolution through the Paleocene-Eocene thermal maximum. *Trends* in *Ecology and Evolution*, 21, 246–253.

Huber, B. T., D. A. Hodell, and C. P. Hamilton (1995), Middle–Late Cretaceous climate of the southern high latitudes: stable isotopic evidence for minimal equator-to-pole thermal gradients. *Geological Society of America Bulletin*, 107, 1164–1191.

John, C. M., S. M. Bohaty, J. C. Zachos, A. Sluijs, S. Gibbs, H. Brinkhuis, and T. J. Bralower (2008), North American continental margin records of the Paleocene-Eocene thermal maximum: Implications for global carbon and hydrological cycling. *Paleoceanography*, 23, doi:10.1029/2007PA001465

Denkley Jones, T., D. J. Lunt, D. N. Schmidt, A. Ridgwell, A. Sluijs, P. J. Valdes, and M. Maslin (2013), Climate model and proxy data constraints on ocean warming across the Paleocene–Eocene Thermal Maximum. *Earth-Science Reviews*, 125, 123–145.

Kelly, D. C. (2002), Response of Antarctic (ODP Site 690) planktonic foraminifera to the Paleocene–Eocene thermal maximum: faunal evidence for ocean/climate change. *Paleoceanography*, 17, doi: 10.1029/2002PA000761

Kelly, D. C., T. J. Bralower, and J. C. Zachos (1998), Evolutionary consequences of the latest Paleocene thermal maximum for tropical planktonic foraminifera. *Palaeogeography Palaeoclimatology Palaeoecology*, 141, 139–161.

Kozdon, R., Kelly, D. C., Kita, N. T., Fournelle, J. H., and Valley, J. W. (2011), Planktonic foraminiferal oxygen isotope analysis by ion microprobe technique suggests warm tropical sea surface temperatures during the Early Paleogene. *Paleoceanography*, 26, doi:10.1029/2010PA002056

Lunn, D., D. Spiegelhalter, A. Thomas, and N. Best (2009) The BUGS project: Evolution, critique and future directions (with discussion). *Statistics* in *Medicine*, 28, 3049–3082.

MacLeod, K. G., B. T. Huber, Á. J. Berrocoso, and I. Wendler (2013), A stable and hot Turonian without glacial $\delta^{18}O$ excursions is indicated by exquisitely preserved Tanzanian foraminifera. *Geology*, 41, 1083–1086.

Makarova, M., J. D. Wright, K. G. Miller, T. L. Babila, Y. Rosenthal, and J. I. Park (2017), Hydrographic and ecologic implications of foraminiferal stable isotopic response across the US mid-Atlantic continental shelf during the Paleocene-Eocene Thermal Maximum. *Paleoceanography*, 32, 56–73.

McInerney, Francesca A., and S. L. Wing (2011), The Paleocene-Eocene Thermal Maximum: a perturbation of carbon cycle, climate, and biosphere with implications for the future. *Annual Review of Earth and Planetary Sciences*, 39, 489–516.

Miller, K. G., P. J. Sugarman, J. V. Browning, M. -P. Aubry, G. J. Brenner, D. Bukry, L. D. Burkle, B. S. Cramer, J. Curran, R. F. Dalton, M. Feigenson, R. P. Lawrence, J. M. Metzger, R. K. Olsson, S. F. Pekar, T. J. Reilly, M. Stewart, J. Uptegrove, and J. D. Wright (1997), Bass River site report. In K.G. Miller, P.J. Sugarman, J.V. Browning et al., *Initial Reports New Jersey Coastal Plain, Proceedings of the Ocean Drilling Program*, v. 174X: College Station (Ocean Drilling Program), 5–43.

Moriya, K., P. A. Wilson, O. Friedrich, J. Erbacher, and H. Kawahata (2007), Testing for ice sheets during the mid-Cretaceous greenhouse using glassy foraminiferal calcite from the mid-Cenomanian tropics on Demerara Rise. *Geology*, 35, 615–618.

Norris, R. D. (1996), Symbiosis as an evolutionary innovation in the radiation of Paleocene planktic foraminifera. *Paleobiology*, 22, 461–480.

Olsson, R. K., C. Hemleben, and W. A. Berggren (eds.) (1999), Atlas of Paleocene Planktonic Foraminifera, Smithsonian Contributions to Paleobiology, 85, 1–25.

Pearson, P. N., P. W. Ditchfield, J. Singano, K. G. Harcourt-Brown, C. J. Nicholas, R. K. Olsson, N. J. Shackleton, and M. A. Hall, (2001), Warm tropical sea surface temperatures in the Late Cretaceous and Eocene epochs. *Nature*, 413, 481–487.

Quillévéré, F., R. D. Norris, I. Moussa, and W. A. Berggren (2001), Role of photosymbiosis and biogeography in the diversification of early Paleogene acarininids (planktonic foraminifera). *Paleobiology*, 27, 311–326.

Rohl, U., T. Westerhold, T. J. Bralower, and J. C. Zachos (2007), On the duration of the Paleocene-Eocene thermal maximum (PETM). *Geochemistry Geophysics Geosystems*, 8, doi:10.1029/2007GC001784

Rutherford, S., S. D'Hondt, and W. Prell (1999), Environmental controls on the geographic distribution of zooplankton diversity. *Nature*, 400, 749–753.

Schlüter, L., K. T. Lohbeck, M. A. Gutowska, J. P. Gröger, U. Riebesell, and T. B. Reusch (2014), Adaptation of a globally important coccolithophore to ocean warming and acidification. *Nature Climate Change*, 4, 1024–1030.

Schmidt, C., P. Heinz, M. Kucera, and S. Uthicke (2011), Temperature-induced stress leads to bleaching in larger benthic foraminifera hosting endosymbiotic diatoms. *Limnology and Oceanography*, 56, 1587–1602.

Shackleton, N. J., R. M. Corfield and M. A. Hall (1985), Stable Isotope Data and the Ontogeny of Paleocene Planktonic-Foraminifera. *Journal of Foraminiferal Research*, 15, 321–336.

Sluijs, A., S. Schouten, M. Pagani, M. Woltering, H. Brinkhuis, J. S. Sinninghe Damste, G. R. Dickens, M. Huber, G. J. Reichart, R. Stein, J. Matthiessen, L. J. Lourens, N. Pedentchouk, J. Backman, K. Moran and Expedition 302 Scientists (2006), Subtropical Arctic Ocean temperatures during the Palaeocene/Eocene thermal maximum. *Nature*, 441, 610–613.

Spero, H. J., and D. F. Williams (1988), Extracting environmental information from planktonic foraminiferal $\delta^{13}C$ data. *Nature*, 335, 717–719.

Sugarman, P.J., K. G. Miller, J. V. Browning, P. P. McLaughlin, G. J. Jr. Brenner, B. Buttari, B. S. Cramer, A. Harris, J. Hernandez, M. E. Katz, B. Lettini, S. Misintseva, D. H. Monteverde, R. K. Olsson, L. Patrick, E. Roman, M. J. Wojtko, M. –P. Aubry, M. D. Feigenson, J. A. Barron, S. Curtin, G. Cobbs, G. III Cobbs, D. Bukry, and B. Huffman (2005), Millville site. In K.G. Miller, P.J. Sugarman, J.V. Browning et al., *Initial Reports New Jersey Coastal Plain, Proceedings of the Ocean Drilling Program*, v. 174X: College Station (Ocean Drilling Program), 1-94. doi:10.2973/odp.proc.ir.174axs.106.2005

Takagi, H., K. Kimoto, T. Fujiki, A. Kurasawa, K. Moriya, and H. Hirano (2016), Ontogenetic dynamics of photosymbiosis in cultured planktic foraminifers revealed by fast repetition rate fluorometry. *Marine Micropaleontology*, 122, 44–52.

Tchernov, D., M. Y. Gorbunov, C. de Vargas, S. Narayan Yadav, A. J. Milligan, M. Haggblom, and P. G. Falkowski (2004), Membrane lipids of symbiotic algae are diagnostic of sensitivity to thermal bleaching in corals. *Proceedings of the National Academy of Sciences*, 101, 13531–13535.

Thomas, D. J., J. C. Zachos, T. J. Bralower, E. Thomas, and S. Bohaty (2002), Warming the fuel for the fire: Evidence for the thermal dissociation of methane hydrate during the Paleocene-Eocene thermal maximum. *Geology*, 30, 1067–1070.

Thomas, E. (1998), Biogeography of the late Paleocene benthic foraminiferal extinction: Late Paleocene-Early Eocene climatic and biotic events in the marine and terrestrial records, in M. -P. Aubry, S. G. Lucas, and W. A. Berggren (Eds.), *Late Paleocene Early Eocene climatic and biotic events in the marine and terrestrial records* (pp. 214–243), Columbia University Press, New York.

Thomas, M. K., C. T. Kremer, C. A. Klausmeier and E. Litchman (2012), A global pattern of thermal adaptation in marine phytoplankton. *Science*, 338, 1085–1088.

Wright, J. D., and M. F. Schaller (2013), Evidence for a rapid release of carbon at the Paleocene-Eocene thermal maximum. *Proceedings of the National Academy of Sciences,* 110, 15908–15913.

Zachos, J. C., U. Röhl, S. A. Schellenberg, A. Sluijs, D. A. Hodell, D. C. Kelly, and E. Thomas et al. (2005), Rapid acidification of the ocean during the Paleocene-Eocene thermal maximum. *Science,* 308, 1611–1615.

Zachos, J. C., S. M. Bohaty, C. M. John, H. McCarren, D. C. Kelly, and T. Nielsen (2007), The Palaeocene-Eocene carbon isotope excursion: constraints from individual shell planktonic foraminifer records. *Philosophical Transactions of the Royal Society of London A*,365, 1829–1842.

Zachos, J. C., S. Schouten, S. Bohaty, T. Quattlebaum, A. Sluijs, H. Brinkhuis, S. J. Gibbs and T. J. Bralower (2006), Extreme warming of mid-latitude coastal ocean during the Paleocene-Eocene Thermal Maximum: Inferences from TEX_{86} and isotope data. *Geology*, 34, 737–740.

Zeebe, R. E., A. Ridgwell, and J. C. Zachos (2016), Anthropogenic carbon release rate unprecedented during the past 66 million years. *Nature Geoscience*, 9, 325–329.

Zeebe, R. E., and J. C. Zachos (2007), Reversed deep-sea carbonate ion basin gradient during Paleocene-Eocene thermal maximum. *Paleoceanography*, 22, doi:10.1029/2006PA001395

4.9 Figure Captions

Figure 1: a. Late Paleocene geographic reconstruction (from Ocean Drilling Stratigraphic Network) and location of the sites studied herein; b. Location map of the PETM sections on the New Jersey coastal plain (modified after Miller et al. 1996).

Figure 2. (a) Planktonic foraminiferal $\delta^{13}C$-Size, and (b) $\delta^{18}O$-size data from the Millville PETM section. Bulk $\delta^{13}C_{bulk}$ are from Wright and Schaller (2013). Size related isotopic changes from selected intervals are plotted in c-f.

Figure 3. (a-b) Planktonic foraminiferal stable isotopes from Sites 689-690. The correlation of these two records are based on (Zachos et al., 2007). In c-e, $\delta^{13}C$-size data from Site 689 show changes in vital effects during the PETM "core" interval. Bulk $\delta^{13}C$ data are from Bains et al. (1999).

Figure 4. (a) Estimates of the slope of $\delta^{13}C$-size data in three studied lineages prior to and during the PETM. Pre-PETM $\delta^{13}C$-size measurements are compiled from multiple sites (Supplementary Material). Error bar indicates 1 standard error of the slope. (b) These changes in slope of $\delta^{13}C$-size regression are qualitatively illustrated. For instance, vital effect in *Ac* is ~1‰, ~2‰ and ~0‰ over the size range in pre-PETM, Millville (PETM) and Site 689 (PETM), respectively.

Figure 5. Zoom-in of $\delta^{18}O$-size data from the onset of the CIE at Millville (see Figure 2). The isotopic gradient between *Ac* and *Subb* (and benthic foraminifera) disappears across the CIE onset, suggesting the adaptation of *Ac* during initial warming.

Figure 6. Compared TEX_{86}^{H} records with $\delta^{18}O$-size data from Wilson Lake and Bass River, respectively. At each site, ΔT is centered at the pre-PETM means so that the magnitudes of ΔT based on TEX_{86}^{H} and $\delta^{18}O$ calibrations can be compared. At Wilson Lake (a), due to the absence of large *MAV* in this shallow water setting, TEX_{86}^{H} and $\delta^{18}O$ calibrations show consistent discrepancies. On the other hand (b), the Bass River record shows a good TEX_{86}^{H}-$\delta^{18}O_{MAV}$ agreement and illustrates changing ontogenetic signals in *MAV*, *MAS* and *Ac* over depth.

Figure 7: Oxygen isotope distributions from selected locations suggest potentially incomplete warming records of the PETM. Temperature is calculated assuming $\delta 18O_{sw}$ = -1‰.

Figure 8. Late Cretaceous planktonic foraminifera oxygen isotope distributions.

4.10 Appendix

4.10.1 Materials

The geographic location of the data discussed in this paper are summarized in Figure S1. Pre-PETM (Late Paleocene) δ^{13}C-size measurements for photosymbiont-bearing planktonic foraminifera were compiled from Bass River, Site 384, Site 758, Site 761 and Site 577. In total 128 pairs of size- δ^{13}C measurements were collected from publications (Table S1) in addition to eight pairs of new measurements from Site 384 and Bass River. For the PETM δ^{13}C-size measurements, 400 pairs of size-δ^{18}O-δ^{13}C data were generated from five samples from Bass River, 19 from Millville, and six from Site 689. The data sources of δ^{13}Cbulk, δ^{13}C and δ^{18}O on individual planktonic foraminifera, and TEX_{86} data are summarized in Table S2.

4.10.2 Stratigraphic correlation

Data from Sites 689 and 690 are compiled together ("Sites 689-690"). Composite records allow us to make full use of data from previous studies and facilitate comparison with earlier studies. Three event horizons recognized at both Site 689 and Site 690 (Zachos et al., 2007) are used for stratigraphic correlation between the two sites (Fig. S2). They are (1) the onset of the carbon isotope excursion in *Acarinina* at 208.22 mbsf (Site 689) and at 170.78 mbsf (Site 690); (2) the benthic foraminifera extinction (BFE) at 208 mbsf (Site 689) and at ~170.65 mbsf (Site 690); and (3) the negative excursion in $\delta^{18}O_{Ac}$ at ~207.3 mbsf (Site 689) and at ~170.25 mbsf (Site 690). We have assumed constant sedimentation rates between tie points at Site 689.

4.10.3 Stable isotope analysis and diagenesis

Planktonic foraminifera specimens were picked and washed in de-ionized water and then ultrasonically cleaned in 3% hydro-peroxide. Five or six specimens from the large size fractions (>300, 250-300 µm) and 10 to 15 specimens from the small size fractions (125-150 µm) were grouped together for isotopic analysis. For Benthic foraminifera, specimens >250 µm are picked and identified. About 3 to 8 specimens of each species are grouped for analysis. All analyses were conducted at the Stable Isotope Laboratory at Rutgers University on a Micromass Optima Mass Spectrometer with an attached multi-prep device. Approximately 100 µg of sample were reacted in 100% phosphoric acid at 90°C for 10 minutes and the evolved CO_2 was collected in a liquid nitrogen cold finger. Ratios are reported in standard delta notation in parts per thousand (per mil, ‰) $\delta = ((R_{sample}/R_{standard}) - 1) \times 1000$ where $R = {}^{13}C/{}^{12}C$ or ${}^{18}O/{}^{16}O$, relative to Vienna-Pee Dee Belemnite ($\delta^{13}C$ and $\delta^{18}O_{VPDB}$) through the analysis of an in–house laboratory standard (RGF1). This standard is routinely calibrated to NBS–19 to insure consistency in reported values. Analytical error (1-sigma) is ± 0.05‰ and ± 0.08‰ for $\delta^{13}C$ and $\delta^{18}O$, respectively.

The preservation of planktonic foraminifera from Millville, Bass River and Wilson Lake is excellent. The “glassy” appearance and thin transparent test suggest that these specimens underwent little or no diagenetic alternation. Preservation of planktonic foraminifera from Sites 689-690 is generally poor in comparison to those from Millville and Bass River. Due to dissolution, many specimens were cemented together by foraminifera fragments. In addition, calcite infillings (mostly coccoliths) within the test

might also bias the isotopic composition of the planktonic foraminifera. To remove potential contamination, individual specimens were cracked with a needle and placed in an ultrasonic bath for ~1-2 min until the test fragments became semi-translucent. However, this procedure could not be applied to the small size fractions (125-150 μm) because of the overall weight loss in this cleaning procedure. Therefore, specimens from the small size fractions were simply ultrasonically cleaned for ~5 min under low ultrasonic frequency.

4.10.4 Taxonomy

We use lineages as the operational taxonomic unit in our isotope analysis. The four lineages studied are 1) the non-symbiotic thermocline *Subbotina* (*Subb*) lineage, and 2) the photosymbiont-bearing mixed-layer lineages of *Acarinina subsphaerica-mckannai-sodadoensis* (*Ac*), *Morozovella aequa-subbotinae* (*MAS*), and *Morozovella acuta-velascoensis* (*MAV*) (Olsson et al., 1999). For *Ac* lineage, we use *A. soldadoensis* for all sites, except for pre-PETM samples from Site 689 where high-spired acarininids are used instead. These high-spired acarininids are identified as *A. subsphaerica* and/or *A. mckannai* (Olsson et al., 1999, Kelly, 2002). For the *MAV* and *MAS* lineages, we did not differentiate species in all size fractions within each lineage. For *Subb* lineage, *Subbotina roesnaesensis* is the only species used. In Plate I, we use SEM figures from Olsson et al. (1999) and light microscope photos of our specimens to illustrate our taxonomic work.

4.10.5 Comparing new (this study) and published (Makarova et al., 2017) isotopic data from Millville

We suggest in the main text that critical differences in the planktonic foraminiferal isotopes between our work and a previous study are most likely due to grouping of different species in Makarova et al., (2017). Our study shows that 1) more than half of the PETM morozovellids (species of *MAS* lineage) give $\delta^{18}O$ not different from *Subb* and benthic foraminifera, and 2) on the other hand, *MAV* gives consistently the most negative $\delta^{18}O$. If different species (or different sizes) of *Morozovella* are used for isotopic analysis, the $\delta^{18}O$ values become more positive than the $\delta^{18}O_{MAV}$. Figure S3 shows that *Morozovella* $\delta^{18}O$ (Makarova et al., 2017) is consistently higher than the $\delta^{18}O_{MAV}$ of large specimens in our study, and intermediate between the end values of $\delta^{18}O_{MAV}$ and $\delta^{18}O_{MAS}$, suggesting a mixture of different species (or different sizes) in their geochemical analysis.

4.10.6 Statistic estimates of the regression slope of the $\delta^{13}C$-size data

4.10.6.1 $\delta^{13}C$-size regression as a proxy of photosynthetic "activity"

The symbiotic photosynthetic activity of PF can be studied by examining the intra-species $\delta^{13}C$ gradients in different size fractions. In photosymbiont-bearing planktonic foraminifera, symbiotic photosynthesis increases as planktonic foraminifera grow. The increased photosynthesis in large adult planktonic foraminifera results in their heavier $\delta^{13}C$ relative to small juvenile tests (D'Hondt et al., 1994) and therefore leads to a positive $\delta^{13}C$-size correlation (Birch et al., 2012; D'Hondt et al., 1994) (Fig. S4, a).

For planktonic foraminifera of the same size, the stronger the symbiotic photosynthesis is, the heavier the $\delta^{13}C$ of the test is expected to be. Hence, if photosynthesis in species A is more active than in species B species, A will have a steeper slope of $\delta^{13}C$-size regression

relative to species B, so that the slope (or correlation coefficient) of the δ^{13}C-size regression can be used as a "proxy" of the photosynthetic "activity", with a ~0 indicating weak/non-symbiotic activity and a steep slope indicating strong photosynthesis activity (Fig. S4, b).

For a given planktonic foraminiferal species or lineage, a simple linear regression analysis of the δ^{13}C-size measurements helps illustrate the changes in photosynthetic activities prior to and during the PETM. As shown in Fig. S4, c, the slope of the *Acarinina mckannai-sodadoensis* (*Ac*) lineage are significantly different between two samples from the PETM (Millville vs Site 689). The slope is very steep during the PETM at Millville but reduced to ~0 at Sites 689-690.

The method we described above is visually straightforward and simple. However, it has very low statistic power. For example, it cannot help determining how robust the estimate of the pre-PETM δ^{13}C-size slope is if more samples from different geographic settings or different ages are included, or whether the pre-PETM slope is statistically different from the PETM slope?

4.10.6.2 Simple complete-pooling linear regression analysis

To address above question and give statistical estimates of the δ^{13}C-size regression, numerous δ^{13}C-size measurements are compiled from pre-PETM and PETM samples. One simple way of making a statistical estimate of the δ^{13}C-size slope is to use a complete-pooling regression analysis (Gelman and Hill, 2006) for pre-PETM and PETM

data, respectively. For example, all pre-PETM $\delta^{13}C$ of *Ac* are pooled into 6 different size fractions (125-150, 150-180, 180-212, 212-250, 250-300, 300-355 μm) regardless of their age and geographic locations (Fig. S4, d). A simple linear regression is then fitted with this pooled dataset. Similar procedures can be applied for PETM *Ac* data. The two regression coefficients (pre-PETM and PETM) obtained in these regression analyses can be compared to infer changes in photosynthetic "activity".

For PETM $\delta^{13}C$-size measurements from Site 689, only two samples were analyzed above the CIE between 207.9 and 208 mbsf; therefore, we used the complete pool method to estimate the slopes of $\delta^{13}C_{Ac}$-size and $\delta^{13}C_{MAS}$-size. The results are shown in Table S3.

However, this method fails to take into account the sampling procedures that generated the data and lose statistic power when more samples are considered. Specifically, $\delta^{13}C$-size measurements are structured in groups/samples according to their geography and ages. Regression coefficients (both slope and intercept) can vary by sample due to various uncertainties such as geographic heterogeneity or simple sampling errors. Simply ignoring this sample-level variation and pooling all data into one regression analysis prevent us from accurately estimating the parameters we are interested in (e.g. in Fig. S4, d, two samples have similar slope but different intercepts, pooling those data together would significantly compromise the estimate of slope).

4.10.6.3 A hierarchical linear model for the estimate of slope of $\delta^{13}C$-size data

To make statistically robust estimates of the δ^{13}C-size slopes when multiple samples over wide geographic ranges or time intervals are included, we used a hierarchical linear model to take into account both within-sample and sample-level variations in estimating the correlation coefficient, and summarize the photosynthetic "activity" as the Bayesian posterior distribution of the hyperparameters of the regression coefficient. We use a varying-intercept and varying-slope model to account for the variances in the regression coefficients among samples:

$$\delta^{13}C_i = a_{j(i)} + b_{j(i)}size_i + \varepsilon_i$$

where j represents sample j from a given geographic location and time period;

$\delta^{13}C_i$ is the δ^{13}C of $size_i$ in sample j, a_j and b_j are the regression coefficients of sample j;

In this simple hierarchical model, the slope b_j is the δ^{13}C-size regression of sample j. Because each sample is collected from different locations or of different ages, b_j is expected to vary from sample to sample and all b_j are different. For example, for the 14 pairs of δ13C-size measurements of pre-PETM *Ac*, each b_j estimate can be affected by many local effects such as difference in hydrology, productivity or other poorly known processes. However, we are not particularly interested in the differences among those b_j. Instead, we are interested in estimating the symbiotic-photosynthesis "activity" of pre-PETM *Ac* populations as a whole and quantify how variable it is when samples from different regions are included. To this end, we assume that the symbiotic-photosynthesis "activity" of each pre-PETM *Ac* sample, b_j, is a sample of the distribution $N(u_b, \sigma_b^2)$ which characterizes the photosynthesis "activity" of the pre-PETM *Ac* population:

$$b_j \sim N(u_b, \sigma_b^2)$$

where u_b is the hyperparameter that represents the symbiotic-photosynthesis "activity" of pre-PETM *Ac* population; σ_b is the sample-level variability, indicating variations in b_j among samples.

The intercepts of δ^{13}C-size regression, a_j, also vary by sample. Assuming two *Ac* samples from two different locations with the same symbiotic-photosynthesis "activity" but with primary productivities different at the two sites, then b_j estimated from each sample will be the same but the intercept a_j will be different. Nevertheless, we are not interested in a_j in this study, and therefore, a vague prior distribution is given to a_j as follows:

$$a_j \sim N(0, 100)$$

In summary, our hierarchical linear model is as follow:

$$\delta^{13}C_i = a_{j(i)} + b_{j(i)} size_i + \varepsilon_i$$

$$b_j \sim N(u_b, \sigma_b^2)$$

$$a_j \sim N(0, 100)$$

where j represents sample j from a given geographic location and time period;

$\delta^{13}C_i$ is the δ^{13}C of $size_i$ in sample j, a_j and b_j are the regression coefficients of sample j;

u_b and σ_b are the mean and variability of a normal distribution.

We write the Bayes's rule for this model:

$$p(\theta|size, d13C) \sim p(size, d13C|\theta)P(\theta)$$

The vector θ represents the regression coefficients a_j, b_j, ε_i, as well as hyperparameter u_b, σ_b.

The model specification in BUG (Bayesian using Gibbs Sampling) language and prior distribution are illustrated as below for thirteen pre-PETM *Ac* samples. We used weak prior information to allow the data to "speak" for themselves. Markov chain Monte Carlo (MCMC) is simulated in OPENBUGS (Lunn et al., 2009) in R for 30000 iterations and the first 15000 iterations are discarded. The posterior distribution of parameters for pre-PETM *Ac* is summarized in Table S3 and Figure S5:

```
Model {
        for (i in 1:n) {
                y(i) ~ dnorm(y.hat(i), tau.y)
                y.hat(i) <- a(sampleID(i)) + b(sampleID(i))*x(i)
                }

tau.y <- pow(sigma.y, -2)
sigma.y ~ dunif(0, 100)

for (j in 1:13) {
                a(j) ~ dnorm(0, 0.0001)
                b(j) ~ dnorm(mu.b, tau.b)
                }
        mu.b ~ dnorm(0, 0.0001)
        tau.b <- pow(sigma.b, -2)
        sigma.b ~ dunif(0, 100)
}
```

4.11 Appendix References

Bains, S., R. M. Corfield, and R. D. Norris (1999), Mechanisms of climate warming at the end of the Paleocene. *Science*, 285, 724-727.

Birch, H. S., H. K. Coxall, and P. N. Pearson (2012), Evolutionary ecology of Early Paleocene planktonic foraminifera: size, depth habitat and symbiosis: Paleobiology, 38, 374-390.

D'Hondt, S., J. C. Zachos, and G. Schultz (1994), Stable isotopic signals and photosymbiosis in late Paleocene planktic foraminifera. *Paleobiology*, 20, 391-406.

Gelman, A., and Hill J., 2006, Data analysis using regression and multilevel/hierarchical models, Cambridge University Press, New York, NY, USA

Lunn, D., D. Spiegelhalter, A. Thomas, and N. Best (2009) The BUGS project: Evolution, critique and future directions (with discussion). *Statistics* in *Medicine*, 28, 3049--3082.

Makarova, M., J. D. Wright, K. G. Miller, T. L. Babila, Y. Rosenthal, and J. I. Park (2017), Hydrographic and ecologic implications of foraminiferal stable isotopic response across the US mid-Atlantic continental shelf during the Paleocene-Eocene Thermal Maximum. *Paleoceanography* 32, 56-73.

Norris, R. D. (1996), Symbiosis as an evolutionary innovation in the radiation of Paleocene planktic foraminifera. *Paleobiology*, 22, 461-480.

Quillévéré, F., R. D. Norris, I. Moussa, and W. A. Berggren (2001), Role of photosymbiosis and biogeography in the diversification of early Paleogene acarininids (planktonic foraminifera). *Paleobiology*, 27, 311-326.

Rohl, U., T. Westerhold, T. J. Bralower, and J. C. Zachos (2007), On the duration of the Paleocene-Eocene thermal maximum (PETM). *Geochemistry Geophysics Geosystems*, 8, doi:10.1029/2007GC001784

Shackleton, N. J., R. M. Corfield and M. A. Hall (1985), Stable Isotope Data and the Ontogeny of Paleocene Planktonic-Foraminifera. *Journal of Foraminiferal Research*, 15, 321-336.

Sluijs, A., S. Schouten, M. Pagani, M. Woltering, H. Brinkhuis, J. S. Sinninghe Damste, G. R. Dickens, M. Huber, G. J. Reichart, R. Stein, J. Matthiessen, L. J. Lourens, N. Pedentchouk, J. Backman, K. Moran and Expedition 302 Scientists (2006), Subtropical Arctic Ocean temperatures during the Palaeocene/Eocene thermal maximum. *Nature*, 441, 610-613.

Thomas, D. J., J. C. Zachos, T. J. Bralower, E. Thomas, and S. Bohaty (2002), Warming the fuel for the fire: Evidence for the thermal dissociation of methane hydrate during the Paleocene-Eocene thermal maximum. *Geology*, 30, 1067-1070.

Wright, J. D., and M. F. Schaller (2013), Evidence for a rapid release of carbon at the Paleocene-Eocene thermal maximum. *Proceedings of the National Academy of Sciences*, 110, 15908-15913.

Zachos, J. C., S. M. Bohaty, C. M. John, H. McCarren, D. C. Kelly, and T. Nielsen (2007), The Palaeocene-Eocene carbon isotope excursion: constraints from individual shell planktonic foraminifer records. *Philosophical Transactions of the Royal Society of London A*, 365, 1829-1842.

Zachos, J. C., S. Schouten, S. Bohaty, T. Quattlebaum, A. Sluijs, H. Brinkhuis, S. J. Gibbs and T. J. Bralower (2006), Extreme warming of mid-latitude coastal ocean

during the Paleocene-Eocene Thermal Maximum: Inferences from TEX_{86} and isotope data. *Geology*, 34, 737-740.

4.12 Appendix Figure Captions

Figure S1. Late Paleocene geographic reconstruction showing the location of the sites discussed in this study (from Ocean Drilling Stratigraphic Network).

Figure S2: stratigraphic correlation between Site 689 and Site 690. Tie points A, B and C are from (Rohl et al., 2007).

Figure S3: Comparison of isotope data between this study and Makarova et al. (2017) emphasizing the importance of appropriate taxonomic practice in understanding the sources of variations in the isotopic data. Symbols: this study; solid lines: Makarova et al. (2017). For $\delta^{18}O$, the solid lines (orange and grey) are plotted in-between the envelope of our data and show large variations of ~1‰ (e.g. grey line between 262-264 m, orange line between 267-269 m).

Figure S4. Statistic estimates of photosynthetic "activity": a) positive $\delta^{13}C$-size correlation in photosymbiont-bearing PF; b) comparing the $\delta^{13}C$-size correlation of non-symbiotic (*Subb*) and symbiotic (*Ac*) PF. Asymbiotic planktonic foraminifera show no $\delta^{13}C$-size correlation (MV= Milville); c) For a given planktonic foraminifera species or lineage (*Ac*), a simple linear regression analysis of the $\delta^{13}C$-size regression helps illustrates the differences in photosynthetic activities; pooling all pre-PETM $\delta^{13}C_{Ac}$-size measurements into one regression analysis. This complete pooling method ignores the sample-level variations and therefore gives poor estimates of the parameters we are interested in. For example, two samples in our figure have very similar slopes but

different intercept. A complete pooling of these two samples would incorporate sample-level variation into slope estimate, giving biased estimate.

Figure S5: Posterior distribution of parameters estimates for $\delta^{13}C$-size slope (MV-BR: PETM samples from Millville and Bass River).

4.13 Appendix Plate Caption

Plate 1: taxonomic illustration used in this study. 1) *Morozovella acuta*, Zone P4, Velasco Fm., Tamaulipas, Mexico. (Olsson et al., 1999), 2) *Morozovella acuta*, Zone P4, Velasco Fm., Tamaulipas, Mexico. (Olsson et al., 1999), 3) *Morozovella velascoensis*, Zone P4, ODP Hole 758A/28/1: 50-52 cm. (Olsson et al., 1999), 4) *MAV* (this study), *Morozovella acuta*, Millville 881 ft, 5) *MAV* (this study), *Morozovella acuta*, Millville 881 ft, 6) *MAV* (this study), *Morozovella velascoensis*, DSDP 384/61/1/89-91 cm, 7) *Morozovella aequa*, Zone P4, DSDP Site 465/3/3: 98-100 cm. (Olsson et al., 1999), 8) *Morozovella subbotinae*, Zone P5, DSDP Site 213/16/1: 104-106 cm. (Olsson et al., 1999), 9) *Morozovella subbotinae*, Zone P5, DSDP Site 213/16/1: 104-106 cm. (Olsson et al., 1999), 10) *MAS* (this study), *Morozovella aequa*, Millville 895.1 ft, 11) *MAS* (this study), *Morozovella subbotinae*, Millville 886.5 ft, 12) *MAS* (this study), *Morozovella gracilis*, Millville 895.1 ft, 13) *Acarinina soldadoensis*, Zone P6a, DSDP Hole 20C/3/1: 1-19 cm. (Olsson et al., 1999), 14) *Ac* (this study), *Acarinina soldadoensis*, Bass River, 1177.15 ft, 15) *Subbotina roesnaesensis*, Bass River Borehole, New Jersey, ODP 174AX, 1150.0-.1 ft. (Olsson et al., 1999), 16) *Subb* (this study), *Subbotina roesnaesensis*, Bass River, 1177.15 ft.

4.14 Appendix Table Captions

Table S1: $\delta^{13}C$-size data combined from upper Paleocene records to characterize the "activity" of symbiontic photosynthesis.

Table S2: PETM data discussed in this study.

Table S3: Estimates of the slope of $\delta^{13}C$-size measurements. Note that the PETM data from Site 689 are analyzed with a simple complete pooling regression analysis using two samples above the CIE (207.9 and 208 mbsf). The PETM MV-BR data are analyzed with the hierarchical linear model developed in this study.

Figure 1

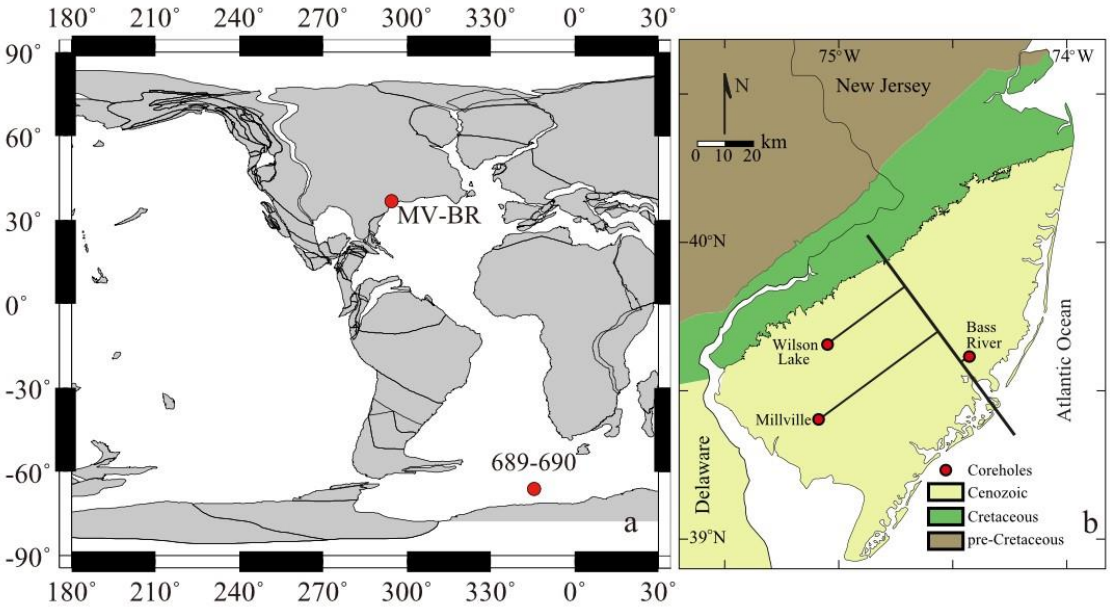
180° 210° 240° 270° 300° 330° 0° 30°
90°
60°
30°
0°
-30°
-60°
-90°
MV-BR
689-690
a
75°W
74°W
N
New Jersey
km
0 10 20
40°N
39°N
Wilson Lake
Bass River
Millville
Delaware
Atlantic Ocean
Coreholes
Cenozoic
Cretaceous
pre-Cretaceous
b

Figure 2

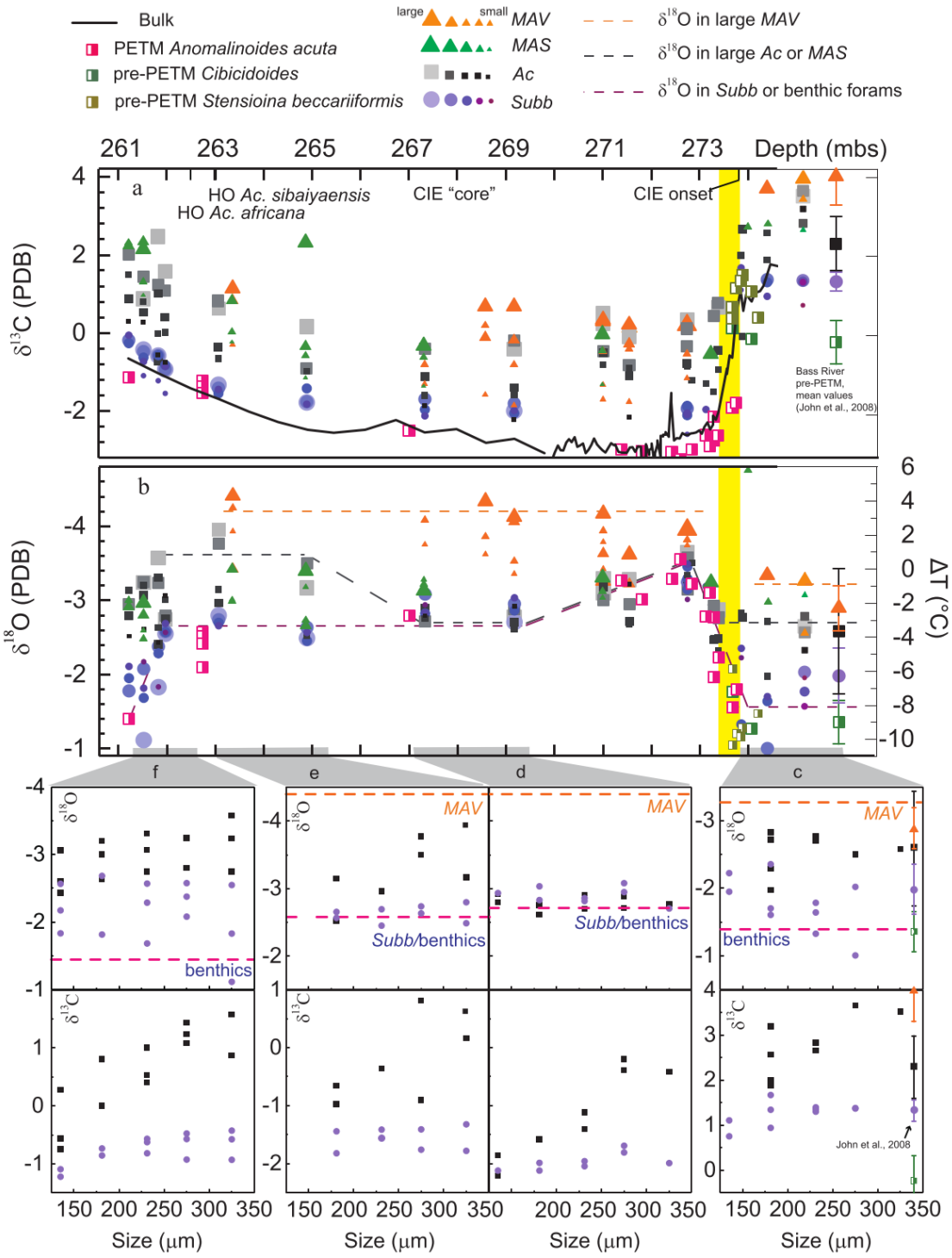
Bulk
PETM Anomalinoides acuta
pre-PETM Cibicidoides
pre-PETM Stensioina beccariiformis
large
small
MAV
MAS
Ac
Subb
δ18O in large MAV
δ18O in large Ac or MAS
δ18O in Subb or benthic forams
Depth (mbs)
HO Ac. sibaiyaensis
HO Ac. africana
CIE "core"
CIE onset
Bass River pre-PETM, mean values (John et al., 2008)
δ13C (PDB)
δ18O (PDB)
ΔT (°C)
Subb/benthics
benthics
John et al., 2008
Size (μm)

Figure 3

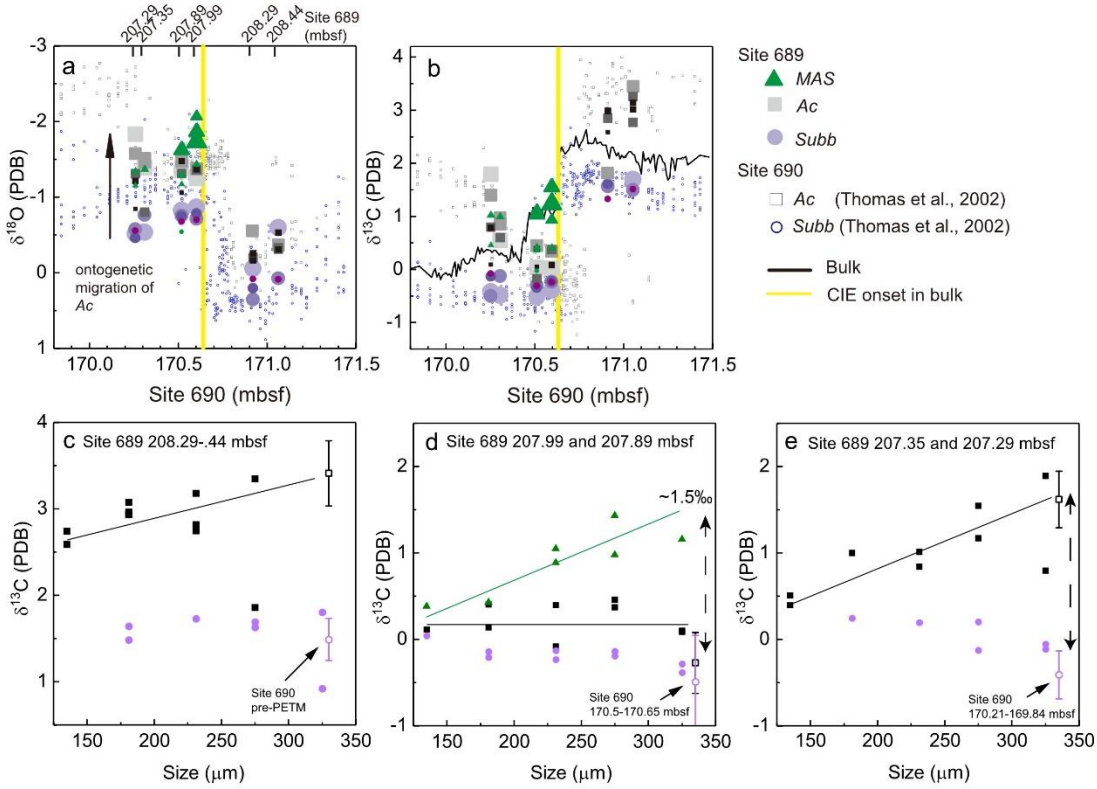
207.29
207.35
207.89
207.99
208.29
208.44
Site 689 (mbsf)
a
b
δ18O (PDB)
δ13C (PDB)
ontogenetic migration of Ac
Site 690 (mbsf)
Site 689
MAS
Ac
Subb
Site 690
Ac (Thomas et al., 2002)
Subb (Thomas et al., 2002)
Bulk
CIE onset in bulk
c Site 689 208.29-.44 mbsf
d Site 689 207.99 and 207.89 mbsf
e Site 689 207.35 and 207.29 mbsf
Site 690 pre-PETM
~1.5‰
Site 690 170.5-170.65 mbsf
Site 690 170.21-169.84 mbsf
Size (μm)

Figure 4

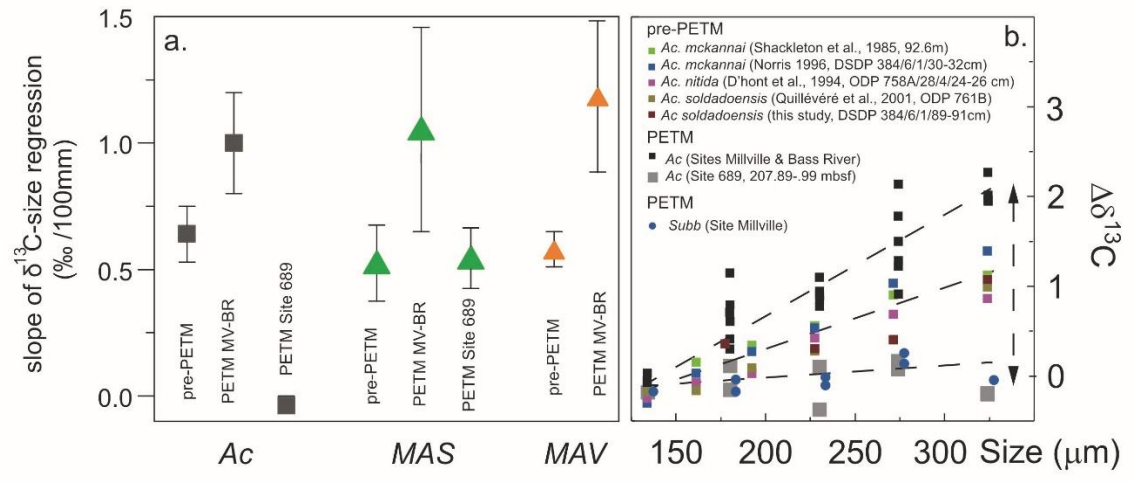
a.
b.
slope of δ13C-size regression (‰ /100mm)
1.5
1.0
0.5
0.0
pre-PETM
PETM MV-BR
PETM Site 689
pre-PETM
PETM MV-BR
PETM Site 689
pre-PETM
PETM MV-BR
Ac
MAS
MAV
pre-PETM
Ac. mckannai (Shackleton et al., 1985, 92.6m)
Ac. mckannai (Norris 1996, DSDP 384/6/1/30-32cm)
Ac. nitida (D'hont et al., 1994, ODP 758A/28/4/24-26 cm)
Ac. soldadoensis (Quillévéré et al., 2001, ODP 761B)
Ac soldadoensis (this study, DSDP 384/6/1/89-91cm)
PETM
Ac (Sites Millville & Bass River)
Ac (Site 689, 207.89-.99 mbsf)
PETM
Subb (Site Millville)
3
2
1
0
Δδ13C
150
200
250
300
Size (μm)

Figure 5

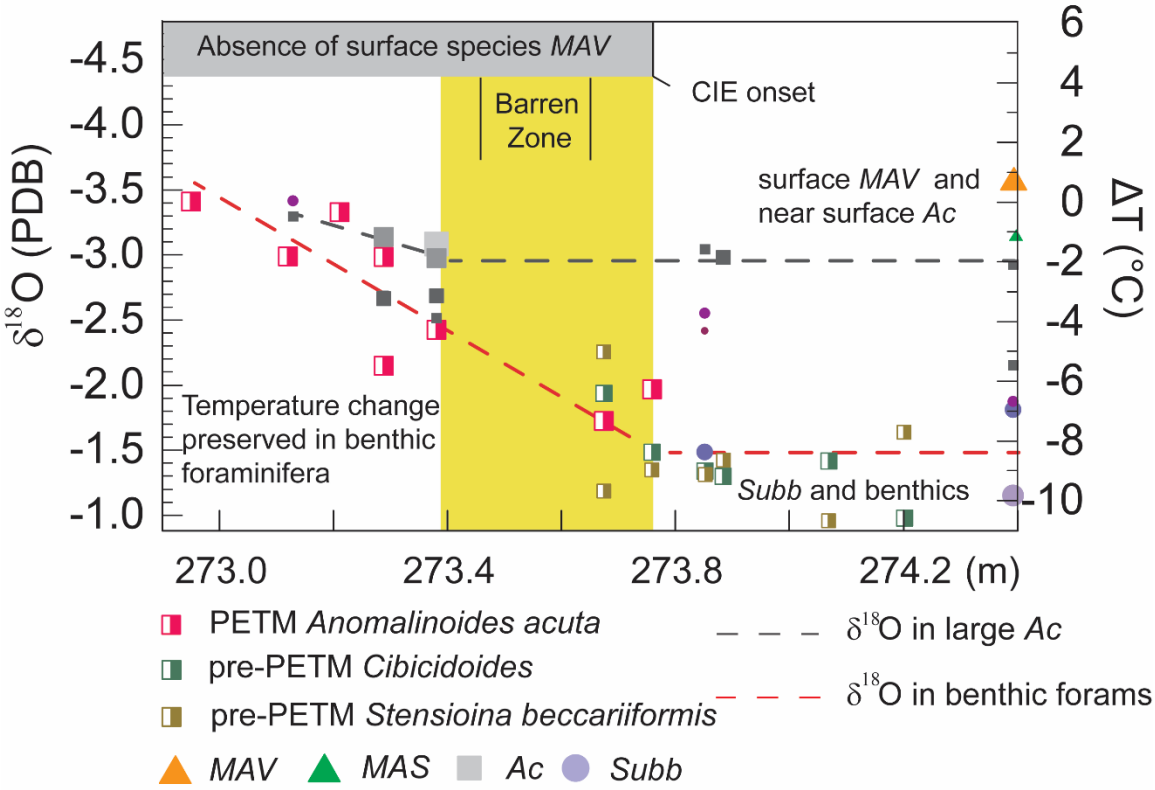
Absence of surface species MAV
CIE onset
Barren Zone
surface MAV and near surface Ac
Temperature change preserved in benthic foraminifera
Subb and benthics
δ18O (PDB)
ΔT (°C)
-4.5
-4.0
-3.5
-3.0
-2.5
-2.0
-1.5
-1.0
6
4
2
0
-2
-4
-6
-8
-10
273.0
273.4
273.8
274.2 (m)
PETM Anomalinoides acuta
pre-PETM Cibicidoides
pre-PETM Stensioina beccariiformis
δ18O in large Ac
δ18O in benthic forams
MAV
MAS
Ac
Subb

Figure 6

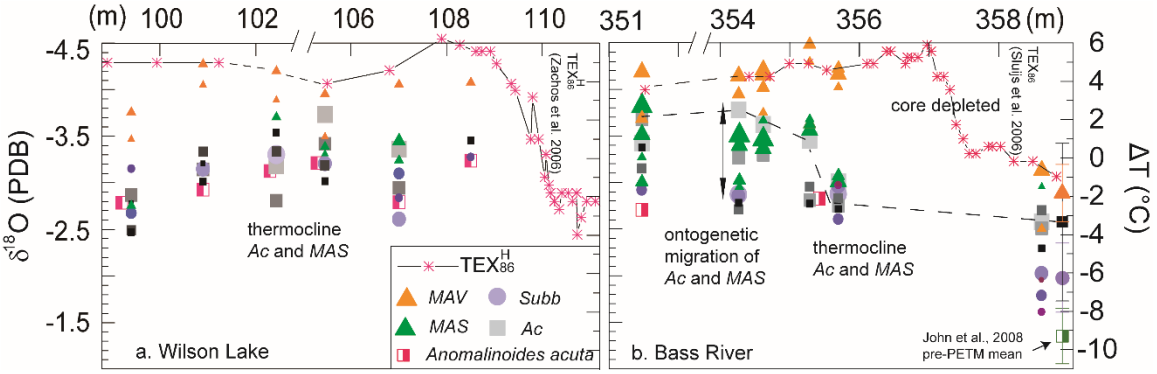
(m) 100 102 106 108 110 351 354 356 358 (m)
-4.5
-3.5
-2.5
-1.5
δ18O (PDB)
6
4
2
0
-2
-4
-6
-8
-10
ΔT (°C)
TEX86H (Zachos et al. 2006)
TEX86 (Sluijs et al. 2006)
thermocline
Ac and MAS
ontogenetic
migration of
Ac and MAS
thermocline
Ac and MAS
core depleted
TEX86H
MAV
Subb
MAS
Ac
Anomalinoides acuta
a. Wilson Lake
b. Bass River
John et al., 2008
pre-PETM mean

Figure 7

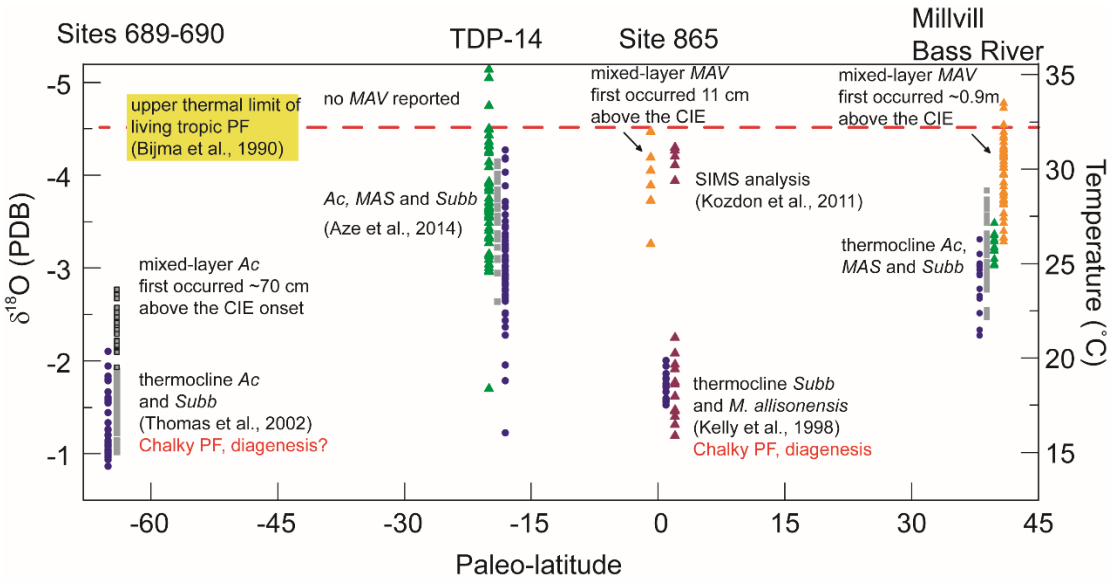
Sites 689-690
TDP-14
Site 865
Millvill
Bass River
upper thermal limit of
living tropic PF
(Bijma et al., 1990)
no MAV reported
mixed-layer MAV
first occurred 11 cm
above the CIE
mixed-layer MAV
first occurred ~0.9m
above the CIE
Ac, MAS and Subb
(Aze et al., 2014)
SIMS analysis
(Kozdon et al., 2011)
thermocline Ac,
MAS and Subb
mixed-layer Ac
first occurred ~70 cm
above the CIE onset
thermocline Ac
and Subb
(Thomas et al., 2002)
Chalky PF, diagenesis?
thermocline Subb
and M. allisonensis
(Kelly et al., 1998)
Chalky PF, diagenesis
δ18O (PDB)
Temperature (°C)
Paleo-latitude
-5
-4
-3
-2
-1
35
30
25
20
15
-60
-45
-30
-15
0
15
30
45

Figure 8

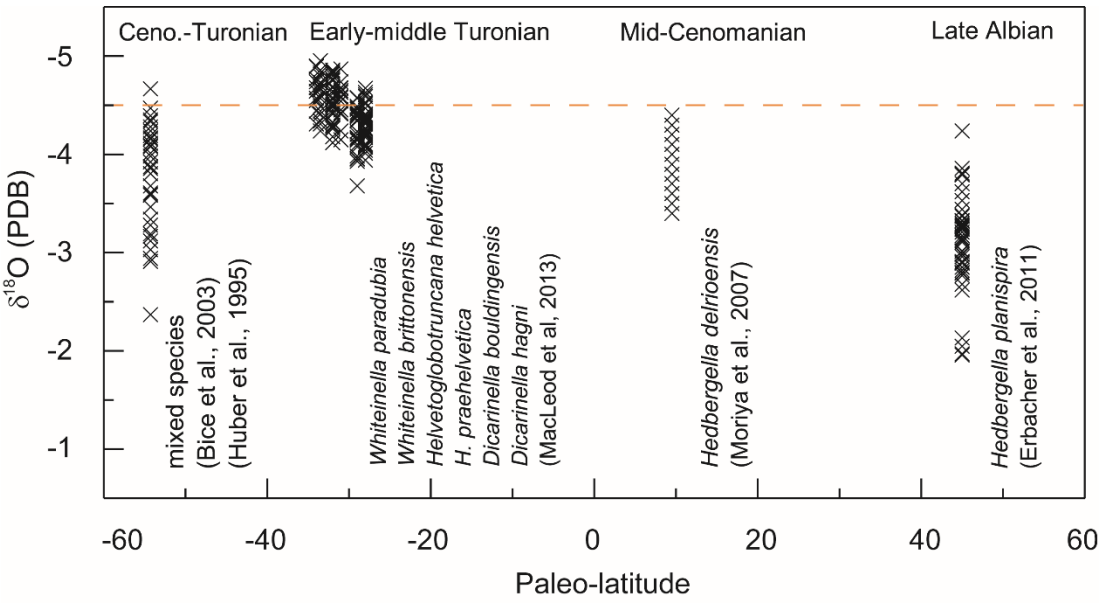
Ceno.-Turonian
Early-middle Turonian
Mid-Cenomanian
Late Albian
δ18O (PDB)
-5
-4
-3
-2
-1
-60
-40
-20
0
20
40
60
Paleo-latitude
mixed species
(Bice et al., 2003)
(Huber et al., 1995)
Whiteinella paradubia
Whiteinella brittonensis
Helvetoglobotruncana helvetica
H. praehelvetica
Dicarinella bouldingensis
Dicarinella hagni
(MacLeod et al, 2013)
Hedbergella delrioensis
(Moriya et al., 2007)
Hedbergella planispira
(Erbacher et al., 2011)

Appendix Figure S1

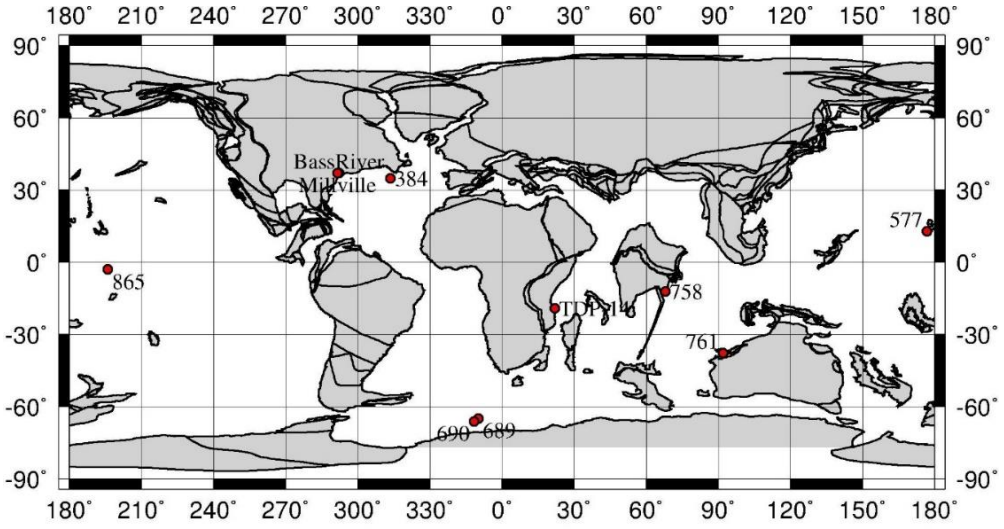

Appendix Figure S2

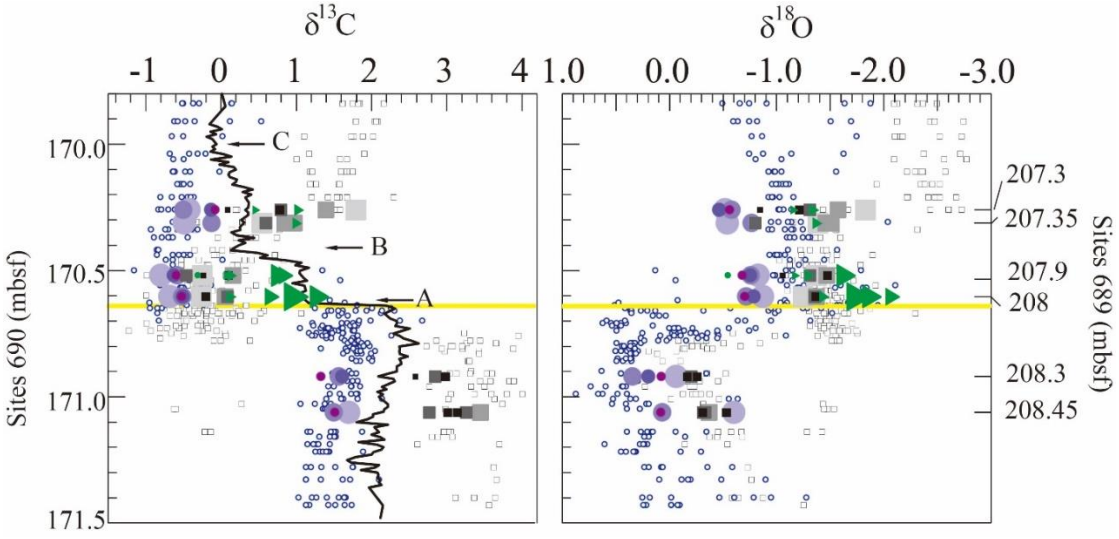

Appendix Figure S3

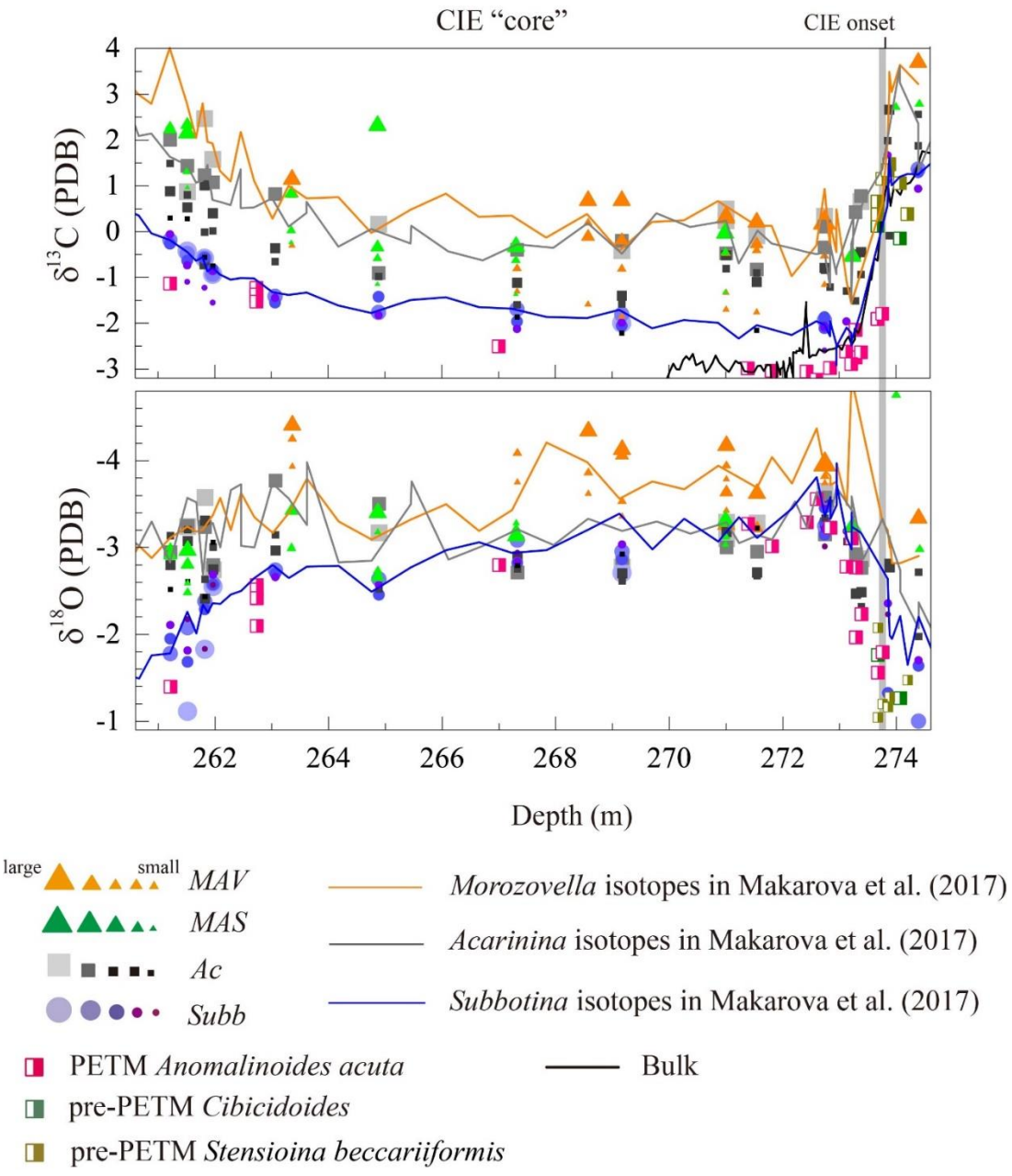

Appendix Figure S4

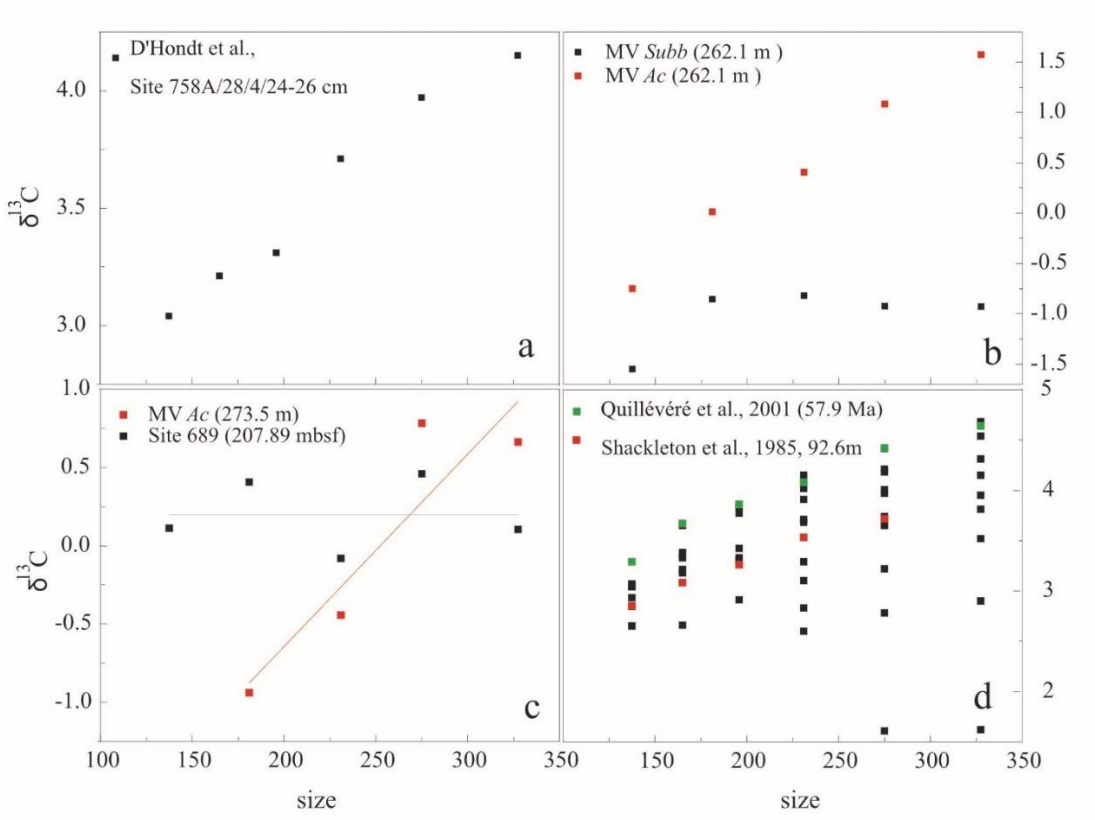

Appendix Figure S5

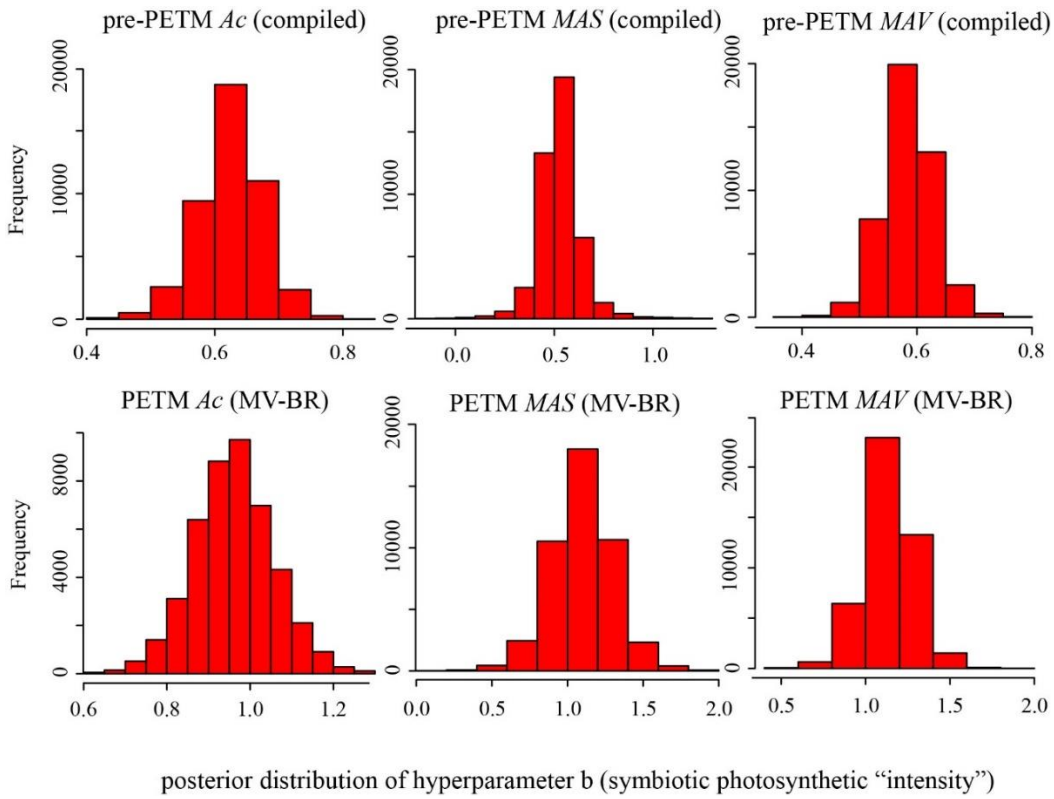

Appendix Plate 1

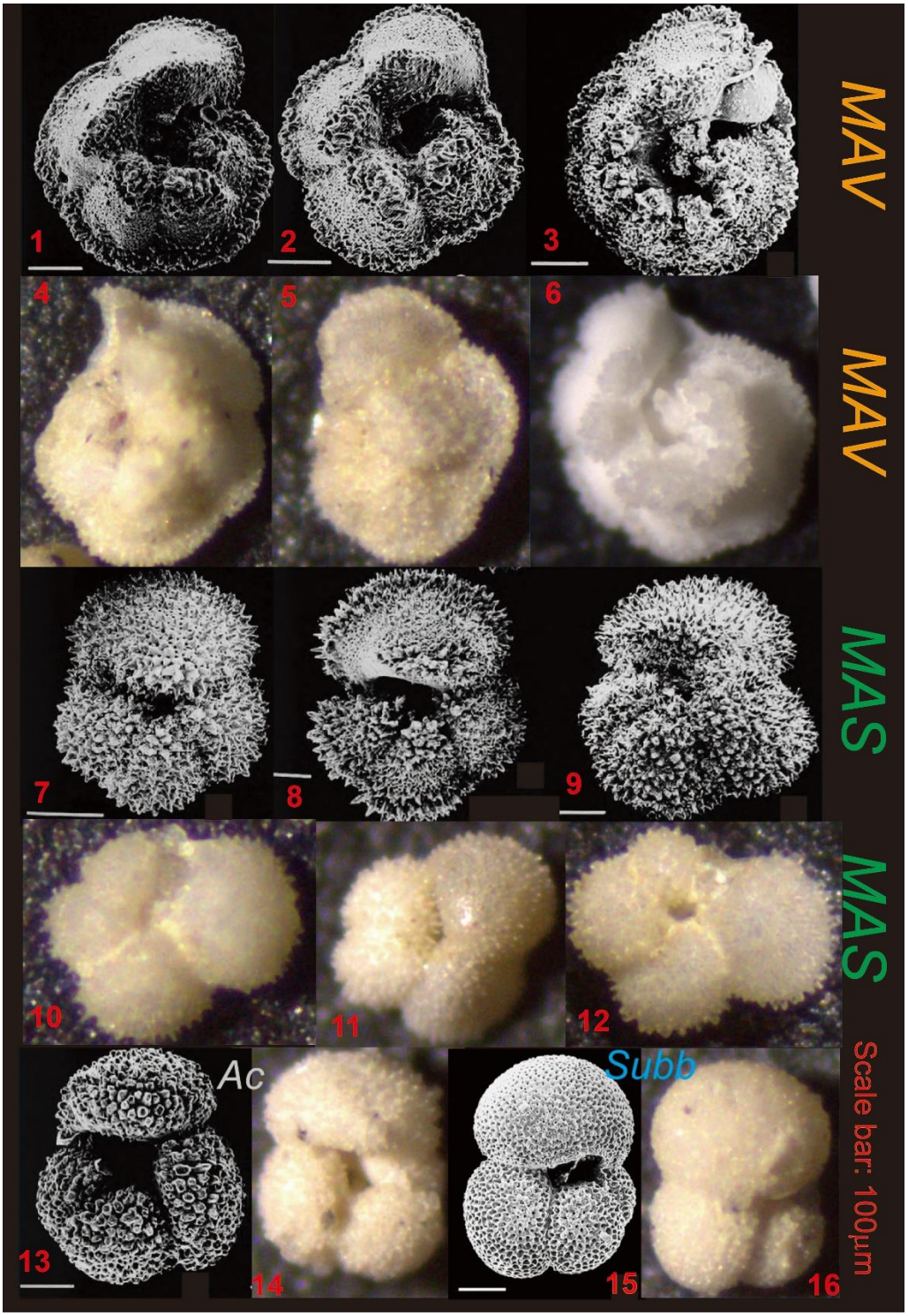

Appendix Table S1

	Location	Sources of isotopic data
Bass River	39.6°N 74.43°W	This study
Site 384	40.36°N 51.63°W	(Norris, 1996) and this study
Site 758	5.38°N 90.36°E	(D'Hondt et al., 1994)
Site 761	16.73°S 115.53°E	(Quillévéré et al., 2001)
Site 577	32.44°N 157.72°E	(Shackleton et al., 1985)

Appendix Figure S2

	Location	Sources of isotopic data
Millville	39.4°N 75.08°W	Planktonic foraminifera: this study; $\delta 13C_{bulk}$: (Wright and Schaller, 2013))
Bass River	39.6°N 74.43°W	Planktonic foraminifera: this study; TEX_{86} (Sluijs et al., 2006)
Wilson Lake	39°39'N, 75°03'W	TEX_{86} (Zachos et al., 2006)
Site 689	64.01°S 3.09°E	This study
Site 690	65.16°S 1.2°E	Planktonic foraminifera (Thomas et al., 2002); $\delta^{13}C_{bulk}$: (Bains et al., 1999)

Appendix Table S3

	Slope	std
Pre-PETM *Ac*	0.64	0.11
PETM *Ac* (MV-BR)	1	0.2
PETM *Ac* (Site 689)	0	0.001
Pre-PETM *MAS*	0.526	0.15
PETM *MAS* (MV-BR)	0.89	1.3
PETM *MAS* (Site 689)	0.545	0.12
Pre-PETM *MAV*	0.58	0.069
PETM MAV (MV-BR)	1.2	0.37

Chapter 5

Decreased coccolith carbonate production and accumulation during the late Neogene, Implication for continental weathering

Paper chatper

Si, W., and Rosenthal, Y. A less chalky ocean and its implication for continental weathering since 15 Ma. *In preparation.*

5.1 Abstract

The globally-averaged Calcite Compensation Depth (CCD) has deepened by several hundred meters in the last 15 Myr. This deepening has been interpreted as increased alkalinity input to the sea due to enhanced continental weathering driven by active tectonic orogeny. By examining Mass Accumulation Rate of pelagic carbonate (MARc), however, we find that accumulation of pelagic carbonates has decreased from Miocene to Pleistocene even though its preservation, as indicated by foraminiferal fragmentation, has improved. Comparison of MARc from shallow sites, where minimum dissolution is expected, to deep sites, where dissolution has taken its toll, suggests that a substantial decline in coccolith production in the euphotic zone is responsible for the decreased pelagic carbonate accumulation. The MARc reconstruction indicates that the pelagic carbonate accumulation has declined from Miocene to Pleistocene, suggesting reduced weathering alkalinity input to the ocean as the climate cooled.

5.2 Introduction

The history of Neogene climate is characterized by successive cooling steps that culminated with the Quaternary glaciations (Zachos et al., 2001). The origin of this long-term cooling remains debatable. On geological timescales, atmospheric pCO_2 is regulated though the balance between volcanic/metamorphic outgassing, silicate weathering and organic burial (Berner et al., 1983). In the Neogene, seafloor spreading rates (and hence rates of outgassing) appear to have been relatively constant (Rowley, 2002). It is therefore proposed that active orogeny, characterized by the uplift of the Himalayas, has enhanced rock weathering and lowered atmospheric pCO_2 (Raymo et al., 1988). The weathering hypothesis is however controversial because it argues that weathering processes can act as a forcing, rather than a negative stabilizing feedback of the Earth's thermostat (Berner and Caldeira, 1997; Walker et al., 1981).

5.3 Reconstructing ocean's alkalinity budget

In a steady-state ocean, weathering fluxes of dissolved solutes to the sea must be balanced by output fluxes, primarily through sedimentation and chemical reactions at the ridge axes. With regard to the ocean's carbonate alkalinity budget, the balance between riverine alkalinity input and $CaCO_3$ burial is, somewhat counterintuitively, achieved through $CaCO_3$ dissolution. Today, planktonic foraminifera and coccolithophores "manufacture" ~50 Tmol/yr carbonates in the upper ocean (Berelson et al., 2007; Dunne et al., 2012; Milliman, 1993), consuming about three times the alkalinity that is made available to the ocean from rivers (33Tmol/yr, (Cai et al., 2008)). To keep ocean's alkalinity budget at balance, dissolution of these overproduced $CaCO_3$ takes place in the

deepsea and manifests itself in the Calcite Compensation Depth (CCD) (Broecker, 1971), below which seawater is sufficiently undersaturated to dissolve all $CaCO_3$ rains.

For the last 15 Myr, the globally-averaged CCD has deepened by ~500 m (Van Andel, 1975). This deepening has been interpreted as increased carbonate burial fluxes in response to higher riverine alkalinity input as a result of enhanced chemical weathering from mountain building (Raymo, 1991; Raymo et al., 1988). However, the CCD-based interpretation relies critically on the assumption of constant carbonate production. Were the strength of carbonate (alkalinity) pump different in the past, the CCD alone, as we will demonstrate below, is insufficient to constrain the pelagic carbonate budget.

To improve our understanding of the late Neogene (0-15 Ma) carbonate cycle, we reconstruct histories of pelagic carbonate accumulation, production and dissolution through Mass Accumulation Rates of carbonate (MARc) from 30 deepsea cores (Figure 1, Figure S1-S6). We focus on open ocean sites from mid- and low-latitudes that are ecologically favored by planktonic calcifiers (coccolithophores and planktonic foraminifera) and where the seafloor is above the CCD. Pelagic settings that satisfy both criteria have high $CaCO_3$ content and account for most pelagic carbonate accumulation (Archer, 1996).

5.4 Calculate Mass Accumulation Rates of carbonates, foraminifera and coccolithophores

Mass Accumulation Rates of bulk samples (MAR-bulk) and carbonates (MARc) were calculated using: 1) linear sedimentation rates (LSRs) derived from age-depth models; 2)

dry bulk density calculated from shipboard moisture and density analyses, and 3) carbonate weight percent (%CaCO3 wt). Specifically, MAR-bulk = linear sedimentation rate (cm/kyr) × dry bulk density (g/cm3), and MARc = MAR-bulk × CaCO3 (wt%).

Dry bulk density was calculated from porosity and wet-bulk density data based on the following relationship: Dry bulk density = wet-bulk density – porosity × 1.025

Calculated dry density data were then averaged over 0.5 Myr intervals. Although bulk-density data were collected at high resolution in most downcore records, we have used calculated mean values because LSRs can only be calculated at a much lower resolution. Multiplying low resolution LSRs with high resolution bulk density data may give a false impression that the MAR variations are known at a high resolution, when, in fact, LSR variations on the first order determine the trends.

In addition to %CaCO3 data from ODP initial report, 500 data were generated using Inductively Coupled Plasma Optical Emission Spectrometry (ICP-OES) at the Department of Marine and Coastal Sciences, Rutgers University. Bulk samples were oven dried and ground into a fine powder. About 0.5-0.8 mg powder was then weight with an accuracy of 0.01 mg before being dissolved in 300 ml of 0.5% acetic acid over 12 hours. After centrifugation, 100 ml solution was further diluted with HNO_3 to 400 ml for [Ca] analysis on ICP-OES. Scandium was used as the internal standard for calibration. Calculated [Ca] is then converted into %CaCO3 of the bulk sample.

To calculate MAR of foraminifera (MAR-foraminifera), bulk samples were washed through a 20 μm sieve and the weight percent of >20 μm was calculated. In the <20 μm fraction, coccoliths are dominant, with only very minor fraction of planktonic foraminiferal fragments. The >20 μm fraction, on the other hand, capture foraminifera and some other minor components (diatom and radiolarian). Because siliceous microfossils account for less than 5% of the >20 μm residues in most samples, MAR-foram was calculated by multiplying weight percent of foraminifera (>20 μm) with MAR-bulk:

MAR-foram = MAR-bulk × foraminifera (wt%).

MAR of coccoliths (MAR-coccolith) was then calculated as:

MAR-coccolith = MARc - MAR-foraminifera.

MAR-bulk, MARc, MAR-foraminifera are summarized in **Figure S2-6**. The offset between MARc and MAR-foraminifera are MAR-coccolith.

5.5 Result

MARc are summarized for three evenly spaced intervals, i.e. Pleistocene, 0-2.5 Ma, Late Miocene, 5.3-7.5 Ma, and Middle Miocene 11.5-13.5 Ma (Figure 2). Multi-Myr averages are used because they supposedly reflect long-term steady states. Because a range of processes can affect local carbonate accumulation, temporal behaviors of MARc from Middle-Late Miocene to Pleistocene are expected to be spatially heterogeneous. Two global features, however, stand out.

First, MARc have decreased significantly in relatively shallow sites but show little variations at depth. This is best illustrated by two depth transects in the western and central equatorial Pacific (Figures 2a-b). At the shallowest site (Site 806), MARc show a maximum decrease from >4 g/cm^2 kyr in the Miocene to ~1.7 g/cm^2 kyr in the Pleistocene. In contrast, MARc from both transects show little variations at ~4 km water depth, consistent with a previous reconstruction suggesting relatively constant CCD in the Pacific since 15 Ma (Palike et al., 2012).

Second, large decreases in MARc have occurred over the late Neogene in regions where today's carbonate production and burial potentials are high (Figure 2a-d), such as the central Pacific, southwest Pacific and North Atlantic (Dunne et al., 2007). In North Atlantic, MARc of Site 982 (1.1 km water depth) decreased from >5 to ~1.5 g/cm^2 kyr. Decreases of similar are also seen at western Pacific Site 590 at 1.5 km water depth. Interestingly, MARc in this region increased in tropical and mid-latitude divergence zones, whereas it decreased in subtropical and high latitudes (Figure S7), exhibiting a latitudinal pattern that resembles the productivity gradients in the modern ocean (Dunne et al., 2007). Despite these latitudinal variations, the Miocene MARc are consistently higher than the Pleistocene MARc.

The temporal pattern of decreasing MARc are less apparent in the equatorial and South Atlantic. At Site 925, MARc have remained mainly constant, decreasing only by ~1 g/cm^2 kyr in the Late Pleistocene (Figure 2d, Figure S4). In the South Atlantic, MARc of Site 1264 have a temporal pattern that is more similar to nearby continental margin Site

1085 (Diester-Haass et al., 2004), high in the Late Miocene, but low in the Middle Miocene and the Pleistocene (Figure S4). In the deep South Atlantic, MARc of Sites 928 and 1266 show some increases over time, consistent with previous CCD reconstruction of a deepening towards the Pleistocene (Van Andel, 1975). Higher Pleistocene MARc at Site 1266, however, may be partially due to winnowing and redeposition (Supporting Information).

The Indian Ocean exhibits the lowest pelagic MARc (<1.5 g/cm2 kry) and the smallest variations (<0.5 g/cm^2 kyr) of all basins throughout the late Neogene (Figure S1b, S6-7). Hence, the MARc history of this ocean is not further discussed.

5.6 Dissolution of deepsea carbonate during the last 15 Myr

Late Neogene decreases in MARc in the Pacific and Atlantic can be due to either increased dissolution or decreased production. Here, we examine carbonate preservation along a depth transect in the western equatorial Pacific (Sites 806-804) where the deep water likely represents the mean ocean. The %$CaCO_3$ along this transect show a decrease during the last 15 Myr (Figure 3a). Given relatively constant non-carbonate MAR (~0.2-0.4 g/cm^2 kyr, Figure S10), this decrease seems to indicate increased dissolution over time, particularly at deepest Site 804 (3.8 km water depth). The preservation of the planktonic foraminifera, however, indicates the opposite.

We applied a coccolith-free size index (hence force CF-size index) to qualitatively evaluate the preservation of planktonic foraminifera (Supporting information). The idea

is that fragmentation of foraminiferal tests will move materials from the coarse fraction (>60 μm) into the fine fraction (20-60 μm), lowering the CF-size index (weight ratio of >60 μm versus >20 μm). The high (low) index values, therefore, indicate high (low) degree of foraminiferal test preservations. The CF-size indices from Sites 806-804 show generally increasing trends throughout the past ~14 My (Figure 3b), which suggests improved foraminiferal preservation over time. The progressively enhanced trend in test preservation is only interrupted at ~10 Ma when a minimum CF-size index indicates that about half of the foraminiferal tests in the oozes are in the form of fine fragments (20-60 μm). These changes in preservation can also be visually recognized under the light microscope, which shows increasing abundance of whole-shell planktonic foraminifera in washed residues over time (Figure S11).

MAR-foraminifera from this depth transect further support higher dissolution in the Middle Miocene. In the Pleistocene, average MAR-foraminifera are ~0.45 and ~0.27 g/cm^2 kyr at Site 806 and 803, respectively, suggesting minimal dissolution between 2.5-3.4 km water depth. This estimate is close to Holocene estimates based on radiocarbon ages of coretop materials, which suggests ~0.4 g/cm^2 kyr foraminiferal dissolution over this depth interval (Table S3). Between 11.5-13.5 Ma, however, the MAR-foraminifera were ~1.5 g/cm^2 kyr at Site 806 and ~0.25 g/cm^2 kyr at Site 803 indicating that more than 1 g/cm^2 kyr of planktonic foraminifera had dissolved over the same depth interval (Figure S13).

Away from the equatorial Pacific, we find an overall increase in the CF-size index in the south-west Pacific, tropical Indian Ocean, South Atlantic, and equatorial Atlantic, even though the timing and patterns vary from site to site (Figure S12). Taken together, these data indicate that the deepsea has become more saturated since the Middle Miocene.

5.7 Cause of decreases in MARc

The apparently paradoxical evidence of decreasing pelagic carbonate accumulation in a more saturated ocean would indicate that carbonate production has decreased during the late Neogene. In the modern ocean, sedimentary traps show that the median of carbonate production in mid- and low-latitudes (60°S-60°N) is ~1.2 g/cm^2 kyr (Honjo et al., 2008), a value close to our averaged Pleistocene MARc (Figure S14). In contrast, MARc from relatively shallow sites where the dissolution effect is insignificant show much higher carbonate production in the Middle and Late Miocene (Figure 4).

Because pelagic carbonates are mainly precipitated from coccolithophores and planktonic foraminifera, we calculated MAR-foraminifera and MAR-coccolith to investigate their relative contributions to higher Miocene MARc (Figure 4, Figure S2-S5). The calculation shows that MAR-foraminifera remained nearly constant over time, whereas MAR-coccolith has decreased significantly over the course of the late Neogene. As preservation has improved during this interval, we conclude that decreasing carbonate production from coccolithophores is responsible for the decreased MARc.

5.8 Changes in carbonate budgets

When carbonate production is constant, the correlation between dissolution and carbonate accumulation is straightforward. More dissolution implies less burial, and vice versa. A deeper CCD, for instance, increases carbonate preservation and therefore is interpreted as increased carbonate burial (Figure S15a). Carbonate dissolution can also be affected by the thickness of the transition zone, which is defined as the depth interval between the calcite saturation horizon and the CCD. If the transition zone becomes thicker, dissolution increases even though the CCD remains constant (Figure S15b). Variations in the thickness of the transition zone, therefore, has also been invoked to explain changes in carbonate burial.

In contrast to these "preservation-driven" setups, we find antagonistic correlation between the dissolution and the accumulation for late Neogene carbonate records, namely high dissolution associated with high accumulation, and vice versa (Figure 5). In this scenario, enhanced Miocene carbonate production "outcompetes" high dissolution and results in higher carbonate burial. The CCD is able to remain relatively constant over time, e.g. in the equatorial Pacific, due to the covariation between deepsea undersaturation and carbonate production.

Essential to our model is the enhanced coccolith carbonate production in the Middle-Late Miocene and subsequent decreases in the Pleistocene. The cause(s) for this Pleistocene decline is unclear. Evolutionary changes in coccolithophores including decreasing size associated with taxonomic turnover (Aubry, 2007), weakened calcification (Bolton et al.,

2016; Suchéras-Marx and Henderiks, 2014) and waning ecologic dominance (Cermeno et al., 2015) may have contributed to this long-term weakening of the carbonate pump.

5.9 Implication for continental weathering

Although MARc suggest decreased carbonate burial in the Pleistocene relative to the Middle-Late Miocene, the compensation effects due to a deeper Pleistocene CCD also needs to be considered in order to constrain the changes in carbonate budget. In the North Atlantic, the CCD has likely deepened from ~4 km to ~5 km from Miocene to Pleistocene, introducing a compensation effect on the order of ~1.2 g/cm^2 kyr (based on MARc estimates for the modern ocean, (Dunne et al., 2012), Figure S16). Observed decreases in MARc, however, vary from ~1.2-4 g/cm^2 kyr. Thus, deeper Pleistocene CCD has partially compensated for the decreased MARc, but smaller in magnitude. On the other hand, carbonate burial in the equatorial Pacific (Palike et al., 2012) has most likely experienced net decreases given the relatively constant CCD since 15 Ma. A recent study suggests that the CCD may have deepened by ~500m in this region (Campbell et al., 2018). However, this only introduces a compensation effect of <0.5 g/cm^2 kyr (Figure S16), negligible relative to the reduced carbonate production (2~3 g/cm^2 kyr). Given these constrains and the hypsometry of the ocean, a Pleistocene compensation should unlikely account for the observed large decreases in MARc.

In addition to mid- and low-latitude pelagic oceans, MARc have also decreased in subpolar regions where coccolith ooze were replaced by diatoms in Pleistocene sediments (e.g. ODP 747, (Schlich et al., 1989)). On continental shelves and slopes, carbonate

accumulation is also believed to have been higher in the Miocene due to higher sea-levels (Holland, 2005). Taken together, the global carbonate burials should have decreased since 15 Ma, implying that the weathering alkalinity input to the ocean was also reduced as the climate cooled.

Although contradictory to the weathering hypothesis, our argument is supported by both regional and global proxies indicating changes in chemical weathering. In the South China Sea and the Indian Ocean, chemical and mineralogical indices that have been used to monitor the intensity of chemical weathering suggest a wet climate and strong chemical weathering in the Himalayas during the Middle Miocene, followed by a long, steady decline in wetness and weathering after ~10 Ma (Clift et al., 2008). Globally, seawater δ^7Li began to increase at ~15 Ma (Misra and Froelich, 2012). This increase has been interpreted as increasingly incongruent weathering that is characteristic of weathering-limited regime. Under weathering-limited regime, weatherable materials such as fresh rocks are in sufficient supply. Weathering rates are limited by climatic factors such as temperature and precipitation (Kump and Arthur, 1997). Increasingly cooling in the late Neogene thus should have decreased rock weathering, reducing the alkalinity input to the ocean. Marine δ^7Li isotope records, therefore, support our interpretation of decreased chemical weathering in a cooling climate.

In conclusion, we find that the ocean became less “chalky” during the late Neogene — in both the sunlit zone and the abyss. In the surface ocean, coccolith production (and the carbonate pump) has significantly weakened. In the deep ocean, carbonate accumulation

has also decreased despite improved preservation. Decreased carbonate accumulation indicate reduced weathering alkalinity input to the ocean, suggesting weaker chemical weathering as the climate cooled during the late Neogene.

5.10 References

Archer, D. E., 1996, An atlas of the distribution of calcium carbonate in sediments of the deep sea: Global Biogeochemical Cycles, v. 10, no. 1, p. 159-174.

Aubry, M. P., 2007, A major Pliocene coccolithophore turnover: Change in morphological strategy in the photic zone: Large Ecosystem Perturbations: Causes and Consequences, v. 424, p. 25-51.

Berelson, W. M., Balch, W. M., Najjar, R., Feely, R. A., Sabine, C., and Lee, K., 2007, Relating estimates of CaCO3 production, export, and dissolution in the water column to measurements of CaCO3 rain into sediment traps and dissolution on the sea floor: A revised global carbonate budget: Global Biogeochemical Cycles, v. 21, no. 1.

Berner, R. A., and Caldeira, K., 1997, The need for mass balance and feedback in the geochemical carbon cycle: Geology, v. 25, no. 10, p. 955-956.

Berner, R. A., Lasaga, A. C., and Garrels, R. M., 1983, The Carbonate-Silicate Geochemical Cycle and Its Effect on Atmospheric Carbon-Dioxide over the Past 100 Million Years: American Journal of Science, v. 283, no. 7, p. 641-683.

Bolton, C. T., Hernández-Sánchez, M. T., Fuertes, M.-A., González-Lemos, S., Abrevaya, L., Mendez-Vicente, A., Flores, J.-A., Probert, I., Giosan, L., and Johnson, J., 2016, Decrease in coccolithophore calcification and CO 2 since the middle Miocene: Nature communications, v. 7, p. 10284.

Broecker, W. S., 1971, A kinetic model for the chemical composition of sea water: Quaternary Research, v. 1, no. 2, p. 188-207.

Cai, W.-J., Guo, X., Chen, C.-T. A., Dai, M., Zhang, L., Zhai, W., Lohrenz, S. E., Yin, K., Harrison, P. J., and Wang, Y., 2008, A comparative overview of weathering intensity and HCO3− flux in the world's major rivers with emphasis on the Changjiang, Huanghe, Zhujiang (Pearl) and Mississippi Rivers: Continental Shelf Research, v. 28, no. 12, p. 1538-1549.

Campbell, S. M., Moucha, R., Derry, L. A., and Raymo, M. E., 2018, Effects of dynamic topography on the Cenozoic carbonate compensation depth: Geochemistry, Geophysics, Geosystems, v. 19, no. 4, p. 1025-1034.

Cermeno, P., Falkowski, P. G., Romero, O. E., Schaller, M. F., and Vallina, S. M., 2015, Continental erosion and the Cenozoic rise of marine diatoms: Proc Natl Acad Sci U S A, v. 112, no. 14, p. 4239-4244.

Clift, P. D., Hodges, K. V., Heslop, D., Hannigan, R., Van Long, H., and Calves, G., 2008, Correlation of Himalayan exhumation rates and Asian monsoon intensity: Nature Geoscience, v. 1, no. 12, p. 875-880.

Diester-Haass, L., Meyers, P. A., and Bickert, T., 2004, Carbonate crash and biogenic bloom in the late Miocene: Evidence from ODP Sites 1085, 1086, and 1087 in the Cape Basin, southeast Atlantic Ocean: Paleoceanography, v. 19, no. 1, p. n/a-n/a.

Dunne, J. P., Hales, B., and Toggweiler, J. R., 2012, Global calcite cycling constrained by sediment preservation controls: Global Biogeochemical Cycles, v. 26, no. 3.

Dunne, J. P., Sarmiento, J. L., and Gnanadesikan, A., 2007, A synthesis of global particle export from the surface ocean and cycling through the ocean interior and on the seafloor: Global Biogeochemical Cycles, v. 21, no. 4, p. n/a-n/a.

Holland, H. D., 2005, Sea level, sediments and the composition of seawater: American Journal of Science, v. 305, no. 3, p. 220-239.

Honjo, S., Manganini, S. J., Krishfield, R. A., and Francois, R., 2008, Particulate organic carbon fluxes to the ocean interior and factors controlling the biological pump: A synthesis of global sediment trap programs since 1983: Progress in Oceanography, v. 76, no. 3, p. 217-285.

Kump, L. R., and Arthur, M. A., 1997, Global chemical erosion during the Cenozoic: Weatherability balances the budgets, Tectonic Uplift and Climate Change, Springer, p. 399-426.

Milliman, J. D., 1993, Production and Accumulation of Calcium-Carbonate in the Ocean - Budget of a Nonsteady State: Global Biogeochemical Cycles, v. 7, no. 4, p. 927-957.

Misra, S., and Froelich, P. N., 2012, Lithium isotope history of Cenozoic seawater: changes in silicate weathering and reverse weathering: Science, v. 335, no. 6070, p. 818-823.

Palike, H., Lyle, M. W., Nishi, H., Raffi, I., Ridgwell, A., Gamage, K., Klaus, A., Acton, G., Anderson, L., Backman, J., Baldauf, J., Beltran, C., Bohaty, S. M., Bown, P., Busch, W., Channell, J. E., Chun, C. O., Delaney, M., Dewangan, P., Dunkley Jones, T., Edgar, K. M., Evans, H., Fitch, P., Foster, G. L., Gussone, N., Hasegawa, H., Hathorne, E. C., Hayashi, H., Herrle, J. O., Holbourn, A., Hovan, S., Hyeong, K., Iijima, K., Ito, T., Kamikuri, S., Kimoto, K., Kuroda, J., Leon-Rodriguez, L., Malinverno, A., Moore, T. C., Jr., Murphy, B. H., Murphy, D. P., Nakamura, H., Ogane, K., Ohneiser, C., Richter, C., Robinson, R., Rohling, E. J., Romero, O., Sawada, K., Scher, H., Schneider, L., Sluijs, A., Takata, H., Tian, J., Tsujimoto, A., Wade, B. S., Westerhold, T., Wilkens, R., Williams, T., Wilson, P. A., Yamamoto, Y., Yamamoto, S., Yamazaki, T., and Zeebe, R. E., 2012, A Cenozoic record of the equatorial Pacific carbonate compensation depth: Nature, v. 488, no. 7413, p. 609-614.

Raymo, M. E., Ruddiman, W. F., and Froelich, P. N., 1988, Influence of Late Cenozoic Mountain Building on Ocean Geochemical Cycles: Geology, v. 16, no. 7, p. 649-653.

Rowley, D. B., 2002, Rate of plate creation and destruction: 180 Ma to present: Geological Society of America Bulletin, v. 114, no. 8, p. 927-933.

Schlich, R., Wise, S. W., Jr., Palmer Julson, A. A., Aubry, M.-P., Berggren, W. A., Bitschene, P. R., Blackburn, N. A., Breza, J., Coffin, M. F., Harwood, D. M., Heider, F., Holmes, M. A., Howard, W. R., Inokuchi, H., Kelts, K., Lazarus, D. B., Mackensen, A., Maruyama, T., Munschy, M., Pratson, E., Quilty, P. G., Rack, F., Salters, V. J. M., Sevigny, J. H., Storey, M., Takemura, A., Watkins, D. K., Whitechurch, H., and Zachos, J., 1989, Site 747: Central Kerguelen Plateau; covering Leg 120 of the cruises of the drilling vessel JOIDES Resolution, Fremantle, Australia, to Fremantle, Australia, Sites 747-751, 20 February to 30 April 1988, v. 120, p. 89.

Suchéras-Marx, B., and Henderiks, J., 2014, Downsizing the pelagic carbonate factory: impacts of calcareous nannoplankton evolution on carbonate burial over the past 17 million years: Global and Planetary Change, v. 123, p. 97-109.

Van Andel, T. H., 1975, Mesozoic/Cenozoic calcite compensation depth and the global distribution of calcareous sediments: Earth and Planetary Science Letters, v. 26, no. 2, p. 187-194.

Walker, J. C., Hays, P., and Kasting, J. F., 1981, A negative feedback mechanism for the long-term stabilization of Earth's surface temperature: Journal of Geophysical Research: Oceans, v. 86, no. C10, p. 9776-9782.

Zachos, J., Pagani, M., Sloan, L., Thomas, E., and Billups, K., 2001, Trends, rhythms, and aberrations in global climate 65 Ma to present: Science, v. 292, no. 5517, p. 686-693.

5.11 Figure Caption

Figure 1: ODP sites plotted with gridded seafloor %$CaCO_3$ (Archer, 1996).

Figure 2: Changes in MARc in the Pacific and Atlantic Oceans. Grey dash lines represent hypsometry. Because of the large productivity gradient across the eastern equatorial Pacific (Supporting Information), plate movement and ridge subsidence can complicate the temporal trend of MARc at a single site. A composite MARc based on multiple sites is used in Figure 2b.

Figure 3. a) bulk %$CaCO_3$ from the western Equatorial Pacific; b) Coccolith-free size index showing changes in fragmentation of planktonic foraminiferal test over the last 15 Myr.

Figure 4. Changes in MARc, MAR-foraminifera and MAR-coccolith from six sites where dissolution is not significant.

Figure 5. Figure 5. Proposed model for changes in carbonate production, dissolution and accumulation during the Late Neogene and its relation to the transition zone and the CCD. The model is also constrained by the data from the depth transect Site 806-804.

5.12 Appendix

5.12.1 Site locations and water depths

Miocene paleolatitudes of studied sites were plotted in Figure S1. For most sites, changes in paleo-depth are small. For instance, ODP 1264 and 1266 from Walvis Ridge have potentially deepened by ~300 m since Middle Miocene (Zachos et al., 2004a). This deepening had only minor effects on dissolution and therefore does not compromise our discussion. However, this is not the case for sites from the eastern Equatorial Pacific where significant changes in latitude and depth have occurred. For instance, ODP U1338 has potentially deepened by 800 m (see discussion below) and this deepening may have significantly affected the carbonate preservation.

5.12.2 Age-depth model

The age model is based primarily on nannofossil stratigraphy in combination with other available data including paleomagnetic and isotopic records for the Pleistocene and isotope stratigraphy for the Middle Miocene intervals. All data are from published work and a list of references consulted for this work is given in Table S2.

When building age-depth model, various smoothing methods (i.e. the midpoints of the age intervals, spline functions, etc.) are often used to eliminate punctuated changes in sedimentation rates with more continuous age-depth function. For this work, we have preferred the step plot because it illustrates clearly the selected age resolution that are considered reasonable and conservative. Given the age-depth model, sample ages were interpolated linearly between two age control points.

5.12.3 Latitudinal variations in MARc in the west Pacific

In the western Pacific, MARc from relative shallow sites (from 50°S to equator, ODP 1171, ODP 593, ODP 590, ODP 588) show latitudinal variations that are similar to productivity gradient in the modern ocean (Dunne et al., 2007), higher in tropical/mid-latitude divergence zones and lower in subtropics and high latitudes

5.12.4 Composite MARc from eastern Equatorial Pacific

Sediment trap data show that there is a sharp productivity gradient across the equator in the eastern Equatorial Pacific (Honjo et al., 1995). Productivity is high at the equator but decreases significantly a few degrees off it (Figure S8a). Moreover, carbonate dissolution increases with water depth. As a result of both changes in productivity and dissolution, MARc show large spatial variations in the eastern Equatorial Pacific (Figure S8b).

Over the last 15 Myrs, sites in the eastern Equatorial Pacific have experienced large changes in paleodepths as well as paleo-latitudes (Figure S8c). Plate movement and ridge subsidence may have complicated the MARc history of a single site. For instance, changes in MARc from ODP U1338 (Figure S3) cannot be simply explained as changes in either productivity or dissolution. In order to better constrain changes in MARc in this region, we have reconstructed a composite MARc (Figure S9).

5.12.5 Size index and planktonic foraminiferal preservation

To measure the size index of foraminifera, we removed the coccolith fraction with a 20 μm sieve. Because most Neogene coccoliths have a dimension of <20 μm, this procedure can effectively separate the coccoliths from the foraminiferal shells. In the fraction of >20 μm, we further separate the 20-60 μm and the >60 μm fractions. The weight ratio of >60 μm/>20 μm is then calculated.

Changes in the size index along the Western Equatorial Pacific depth transect (Figure 3, main text) suggest that the preservation of planktonic foraminifera was particularly poor ~10 Ma but improved increasingly over time. This improvement is visible under the light microscope (Figure S11). In ODP 803 (3.4 km), whole shell foraminifera are nearly absent in the >60 μm fraction at ~10 Ma. In contrast, siliceous shells and heavily encrusted foraminiferal fragments are abundant, suggesting that most foraminifera have been dissolved, left only recalcitrant fractions. In the same core, the numbers of whole shell foraminifera have clearly increased a ~6 Ma. More soluble species such as Globigerinoides spp. occur in the residues. In Pleistocene, the preservation of foraminiferal assemblages is as good as at shallower depth ODP 806 (2.5 km), show minor sign of dissolution.

In addition to the equatorial Pacific, we also generated planktonic foraminifera size index from other sites in order to obtain a global coverage (Figure S12). As discussed in the main text, although the timing and pattern differ from site to site, all locations show improved preservation towards Pleistocene.

In equatorial Indian Ocean (ODP 758), foraminifera preservation was generally good in the Middle Miocene and Pleistocene, but poor in the Late Miocene (5-10 Ma). In the southwest Pacific (ODP 590), size index shows two-step improvements in foraminifera preservation at ~13-14 Ma and ~2.7 Ma, which are coincident with Mi3 glaciation and Northern Hemisphere Glaciation, respectively. In Caribbean Sea, size index was low until ~3 Ma. Increased size index in Pleistocene corresponds to increased MAR-foraminifera (Figure S4), suggesting improved preservation of planktonic foraminifera. In equatorial Atlantic, size index from ODP 667 (3.5 km) and ODP 928 (4 km) suggest that dissolution was particularly strong in Miocene. Most foraminifera became dissolved at/below 3.5 km. Foraminifer preservation, however, significantly improved above the Miocene/Pliocene boundary. As a result, MAR-foraminifera from these two sites also increased after ~5 Ma (Figure S5). In South Atlantic, size index from ODP 1266 suggests that dissolution was strong at ~3.5 km prior to 13 Ma. During ~13-14 Ma (~94-99 mcd), foraminifer preservation significantly improved. This change corresponds to an increase in B/Ca in benthic foraminifera, which has been interpreted as an increase in $[CO_3]_{sw}$ by more than 60 µmol/kg (Kender et al., 2014).

5.12.6 Dissolution rates of foraminifera in Miocene, Pleistocene and Holocene sediments

Here, we calculated the changes in MAR-foraminifera along the Ontong-Java depth transect. In Middle Miocene (~13 Ma), MAR-foraminifera from Sites 806 and 807 are similar. In contrast, a large decrease in MAR-foraminifera occurs between ODP 807 and 803 (Figure S13), suggesting that significant dissolution (>1 g/cm^2 kyr) have occurred

between 2.7 and 3.4 km. In the Pleistocene, MAR-foraminifera become very similar across the depth transect, indicating smaller dissolution rates of foraminifera (~0.2 g/cm^2 kyr) over the depth range (Figure S13).

Using carbon-14 age from (Broecker, 2003), MAR for Holocene samples can be calculated independently of the Pleistocene bio-magnetic-stratigraphy (Table S3). The calculation indicates dissolution rate of ~0.44 g/cm^2 kyr over the depth range of 2.3-3.4 km, which is higher but of the same magnitude as our Pleistocene average.

5.12.7 Hypothetical scenarios of changes in carbonate production, dissolution and accumulation

In scenario 1 and 2 (Figure S15a-b), carbonate production in the surface ocean is assumed to be constant. In scenario 1, the thickness of the transition zone is also assumed to be constant. The CCD, however, has deepened from Miocene to Pleistocene. In scenario 2, the CCD remains relatively constant. The transition zone, however, is thinner in the Miocene than in the Pleistocene. In this case, we would expect less dissolution in the Miocene and therefore more burial, as indicated by the hypothetical curves of the %$CaCO_3$. In scenario 3, the transition zone is thicker in the Miocene and the dissolution is higher. The MARc, however, is also higher. Large decreases in MARc from Miocene to Pleistocene is not due to dissolution but to decreased production.

5.13 Appendix References

Berger, W., Leckie, R., Janecek, T., Stax, R., and Takayama, T., Neogene carbonate sedimentation on Ontong-Java-Plateau highlights and open questions, *in* Proceedings Proc ODP Sci Res1993a, Volume 130, p. 711-744.

Berger, W. H., Bickert, T., Schmidt, H., and Wefer, T., 1993b, Quaternary oxygen isotope record of pelagic foraminifers; Site 806, Ontong Java Plateau: Proceedings of the Ocean Drilling Program; Ontong Java Plateau, covering Leg 130 of the cruises of the drilling vessel JOIDES Resolution, Apra Harbor, Guam, to Apra Harbor, Guam, Sites 805-807, 18 January-26 March 1990, v. 130, p. 381.

Bougault, H., Cande, S. C., Brannon, J. C., Christie, D. M., Clark, M., Curtis, D. M., Drake, N., Echols, D. J., Hill, I. A., Khan, M. J., Mills, W. G., Neuser, R., Rideout, M. L., and Weaver, B. L., 1985, Site 558: Initial reports of the Deep Sea Drilling Project; covering Leg 82 of the cruises of the Drilling Vessel Glomar Challenger; Ponta Delgada, Azores, to Balboa, Panama; September-November 1981, v. 82, p. 127.

Bralower, T. J., Premoli Silva, I., Malone, M. J., Arthur, M. A., Averyt, K., Bown, P. R., Brassell, S. C., Channell, J. E. T., Clarke, L. J., Dutton, A., Eleson, J. W., Frank, T. D., Gylesjo, S., Hancock, H., Kano, H., Leckie, R. M., Marsaglia, K. M., McGuire, J., Moe, K. T., Petrizzo, M. R., Robinson, S. A., Röhl, U., Sager, W. W., Takeda, K., Thomas, D., Williams, T., and Zachos, J. C., 2002, Site 1208: Proceedings of the Ocean Drilling Program, initial reports, extreme warmth in the Cretaceous and Paleogene; a depth transect on Shatsky Rise, Central Pacific; covering Leg 198 of the cruises of the drilling vessel JOIDES Resolution; Yokohama, Japan, to Honolulu, Hawaii; sites 1207-1214; 27 August-23 October 2001, v. 198, p. 93.

Broecker, W., 2003, The oceanic CaCO3 cycle: Treatise on Geochemistry, v. 6, p. 625.

Broecker, W., and Clark, E., 1999, CaCO3 size distribution: A paleocarbonate ion proxy?: Paleoceanography, v. 14, no. 5, p. 596-604.

Catubig, N. R., Archer, D., Francois, R., DeMenocal, P., Howard, W., and Yu, E. F., 1998, Global deep-sea burial rate of calcium carbonate during the Last Glacial Maximum: Paleoceanography, v. 13, no. 3, p. 298-310.

Curry, W. B., Shackleton, N. J., Richter, C., Backman, J. E., Bassinot, F., Bickert, T., Chaisson, W. P., Cullen, J. L., deMenocal, P., Dobson, D. M., Ewert, L., Grützner, J., Hagelberg, T. K., Hampt, G., Harris, S. E., Herbert, T. D., Moran, K., Murayama, M., Murray, D. W., Pearson, P. N., Raffi, I., Schneider, D. A., Tiedemann, R., Valet, J.-P., Weedon, G. P., Yasuda, H., and Zachos, J. C., 1995a, Site 925: Proceedings of the Ocean Drilling Program; initial reports; Ceara Rise; covering Leg 154 of the cruises of the drilling vessel JOIDES Resolution, Bridgetown, Barbados, to Bridgetown, Barbados, sites 925-929, 24 January-25 March 1994, v. 154, p. 55.

Curry, 1995b, Site 928: Proceedings of the Ocean Drilling Program; initial reports; Ceara Rise; covering Leg 154 of the cruises of the drilling vessel JOIDES Resolution, Bridgetown, Barbados, to Bridgetown, Barbados, sites 925-929, 24 January-25 March 1994, v. 154, p. 281.

Dunne, J. P., Hales, B., and Toggweiler, J. R., 2012, Global calcite cycling constrained by sediment preservation controls: Global Biogeochemical Cycles, v. 26, no. 3.

Dunne, J. P., Sarmiento, J. L., and Gnanadesikan, A., 2007, A synthesis of global particle export from the surface ocean and cycling through the ocean interior and on the seafloor: Global Biogeochemical Cycles, v. 21, no. 4, p. n/a-n/a.

Evans, H. F., 2006, Magnetic stratigraphy and environmental magnetism of oceanic sedimentsPh. D.]: University of Florida, 204 p.

Exon, N. F., Kennett, J. P., Malone, M. J., Brinkhuis, H., Chaproniere, G. C. H., Ennyu, A., Fothergill, P., Fuller, M. D., Grauert, M., Hill, P. J., Janecek, T. R., Kelly, D. C., Latimer, J. C., Nees, S., Ninnemann, U. S., Nürnberg, D., Pekar, S. F., Pellaton, C. C., Pfuhl, H. A., Robert, C. M., Roessig, K. L. M., Röhl, U., Schellenberg, S. A., Shevenell, A. E., Stickley, C. E., Suzuki, N., Touchard, Y., Wei, W., and White, T. S., 2001, Site 1171: Proceedings of the Ocean Drilling Program, initial reports, the Tasmanian Gateway, Cenozoic climatic and oceanographic development; covering Leg 189 of the cruises of the drilling vessel JOIDES Resolution; Hobart, Tasmania, to Sydney, Australia; sites 1168-1172, 11 March-6 May 2000, v. 189, p. 176.

Farrell, J. W., Murray, D. W., McKenna, V. S., and Ravelo, A. C., 1995, Upper ocean temperature and nutrient contrasts inferred from Pleistocene planktonic foraminifer δ¹⁸O and δ¹³C in the eastern Equatorial Pacific: Proceedings of the Ocean Drilling Program; scientific results; eastern Equatorial Pacific, covering Leg 138 of the cruises of the drilling vessel JOIDES Resolution, Balboa, Panama, to San Diego, California, Sites 844-854, 1 May-4 July 1991, v. 138, p. 289.

Gersonde, R., Hodell, D. A., Blum, P., Andersson, C., Austin, W. E. N., Billups, K., Channell, J. E. T., Charles, C. D., Diekmann, B., Filippelli, G. M., Flores, J. A., Hewitt, A. T., Howard, W. R., Ikehara, M., Janecek, T. R., Kanfoush, S. L., Kemp, A. E. S., King, S. L., Kleiven, H. F., Kuhn, G., Marino, M., Ninnemann, U. S., O'Connell, S., Ortiz, J. D., Stoner, J. S., Sugiyama, K., Warnke, D. A., and Zielinski, U., 1999, Site 1088: Proceedings of the Ocean Drilling Program; initial reports; Southern Ocean paleoceanography; covering Leg 177 of the cruises of the drilling vessel JOIDES Resolution; Cape Town, South Africa, to Punta Arenas, Chile; sites 1088-1094; 9 December 1997-5 February 1998, v. 177, p. 66.

Hodell, D. A., Charles, C. D., Curtis, J. H., Mortyn, P. G., Ninnemann, U. S., and Venz, K. A., 2003, Oxygen isotope stratigraphy of ODP Leg 177 sites 1088, 1089, 1090, 1093, and 1094: Proceedings of the Ocean Drilling Program, scientific results; Southern Ocean paleoceanography; covering Leg 177 of the cruises of the drilling vessel JOIDES Resolution; Cape Town, South Africa, to Punta Arenas, Chile; sites 1088-1094; 9 December 1997-5 February 1998, v. 177, p. 26.

Holbourn, A., Kuhnt, W., Frank, M., and Haley, B. A., 2013, Changes in Pacific Ocean circulation following the Miocene onset of permanent Antarctic ice cover: Earth and Planetary Science Letters, v. 365, p. 38-50.

Honjo, S., Dymond, J., Collier, R., and Manganini, S. J., 1995, Export Production of Particles to the Interior of the Equatorial Pacific-Ocean during the 1992 Eqpac Experiment: Deep-Sea Research Part Ii-Topical Studies in Oceanography, v. 42, no. 2-3, p. 831-870.

Honjo, S., Manganini, S. J., Krishfield, R. A., and Francois, R., 2008, Particulate organic carbon fluxes to the ocean interior and factors controlling the biological pump: A

synthesis of global sediment trap programs since 1983: Progress in Oceanography, v. 76, no. 3, p. 217-285.

Jansen, E., Raymo, M. E., Blum, P., Andersen, E. S., Austin, W. E. N., Baumann, K.-H., Bout-Roumazeilles, V., Carter, S. J., Channell, J. E. T., Cullen, J. L., Flower, B., Higgins, S., Hodell, D. A., Hood, J. A., Hyun, S. M., Ikehara, M., King, T., Larter, R., Lehman, B., Locker, S., McIntyre, K., McManus, J., Meng, L. B., O'Connell, S., Ortiz, J. D., Rack, F. R., Solheim, A., and Wei, W., 1996, Site 982: Proceedings of the Ocean Drilling Program; initial reports; North Atlantic-Arctic gateways II; covering Leg 162 of the cruises of the drilling vessel JOIDES Resolution, Edinburgh, United Kingdom, to Málaga, Spain, Sites 980-987, 7 July-2 September 1995, v. 162, p. 91.

Kender, S., Yu, J., and Peck, V. L., 2014, Deep ocean carbonate ion increase during mid Miocene CO 2 decline: Scientific reports, v. 4, p. 4187.

Kennett, J. P., von der Borch, C. C., Baker, P. A., Barton, C. E., Boersma, A., Caulet, J. P., Dudley, W. C., Jr., Gardner, J. V., Jenkins, D. G., Lohman, W. H., Martini, E., Merrill, R. B., Morin, R. H., Nelson, C. S., Robert, C., Srinivasan, M. S., Stein, R., and Takeuchi, A., 1986a, Site 588; Lord Howe Rise, 26°S: Initial reports of the Deep Sea Drilling Project covering Leg 90 of the cruises of the drilling vessel Glomar Challenger; Noumea, New Caledonia, to Wellington, New Zealand, December 1982-January 1983; Part 1, v. 90, p. 139.

Kennett, 1986b, Site 590; Lord Howe Rise, 31°S: Initial reports of the Deep Sea Drilling Project covering Leg 90 of the cruises of the drilling vessel Glomar Challenger; Noumea, New Caledonia, to Wellington, New Zealand, December 1982-January 1983; Part 1, v. 90, p. 263.

Kennett, 1986c, Site 593; Challenger Plateau: Initial reports of the Deep Sea Drilling Project covering Leg 90 of the cruises of the drilling vessel Glomar Challenger; Noumea, New Caledonia, to Wellington, New Zealand, December 1982-January 1983; Part 1, v. 90, p. 551.

Kroenke, L. W., Berger, W. H., Janecek, T. R., Backman, J., Bassinot, F., Corfield, R. M., Delaney, M. L., Hagen, R. A., Jansen, E., Krisek, L. A., Lange, C., Leckie, R. M., Lind, I. L., Lyle, M. W., Mahoney, J. J., Marsters, J. C., Mayer, L. A., Mosher, D. C., Musgrave, R., Prentice, M. L., Resig, J. M., Schmidt, H., Stax, R., Storey, M., Takahashi, K., Takayama, T., Tarduno, J. A., Wilkens, R. H., and Wu, G., 1991a, Site 806: Proceedings of the Ocean Drilling Program, Ontong Java Plateau, covering Leg 130 of the cruises of the drilling vessel JOIDES Resolution, Apra Harbor, Guam, to Apra Harbor, Guam, sites 803-807, 18 January 1990-26 March 1990, v. 130, p. 291.

Kroenke, L. W., Berger, W. H., Janecek, T. R., Backman, J., Bassinot, F., Corfield, R. M., Delaney, M. L., Hagen, R. A., Jansen, E., Krissek, L. A., Lange, C., Leckie, R. M., Lind, I. L., Lyle, M. W., Mahoney, J. J., Marsters, J. C., Mayer, L. A., Mosher, D. C., Musgrave, R., Prentice, M. L., Resig, J. M., Schmidt, H., Stax, R., Storey, M., Takahashi, K., Takayama, T., Tarduno, J. A., Wilkens, R. H., and Wu, G., 1991b, Site 803: Proceedings of the Ocean Drilling Program, Ontong Java Plateau, covering Leg 130 of the cruises of the drilling vessel JOIDES Resolution, Apra Harbor, Guam, to Apra Harbor, Guam, sites 803-807, 18 January 1990-26 March 1990, v. 130, p. 101.

Kroenke, 1991c, Site 804: Proceedings of the Ocean Drilling Program, Ontong Java Plateau, covering Leg 130 of the cruises of the drilling vessel JOIDES Resolution, Apra Harbor, Guam, to Apra Harbor, Guam, sites 803-807, 18 January 1990-26 March 1990, v. 130, p. 177.

Kroenke, 1991d, Site 807: Proceedings of the Ocean Drilling Program, Ontong Java Plateau, covering Leg 130 of the cruises of the drilling vessel JOIDES Resolution, Apra Harbor, Guam, to Apra Harbor, Guam, sites 803-807, 18 January 1990-26 March 1990, v. 130, p. 369.

Kroenke, L. W., Berger, W. H., and Janecek, T. R., et al.,, 1991e, Proc. ODP, Init. Repts., 130: College Station, TX (Ocean Drilling Program). doi:10.2973/odp.proc.ir.130.1991.

Lawrence, K. T., Bailey, I., and Raymo, M. E., 2013, Re-evaluation of the age model for North Atlantic Ocean Site 982 - arguments for a return to the original chronology: Climate of the Past, v. 9, no. 5, p. 2391-2397.

Lisiecki, L. E., and Raymo, M. E., 2005, A Pliocene-Pleistocene stack of 57 globally disturbed benthic δ¹⁸O records: Paleoceanography, v. 20, no. 1, p. 17.

Littke, R., Rullkötter, J., and Schaefer, R. G., 1991, Organic and carbonate carbon accumulation on Broken Ridge and Ninetyeast Ridge, central Indian Ocean: Proceedings of the Ocean Drilling Program, Broken Ridge and Ninetyeast Ridge; covering Leg 121 of the cruises of the drilling vessel JOIDES Resolution, Fremantle, Australia, to Port of Singapore, Singapore, sites 752-758, 30 April to 28 June 1988, v. 121, p. 467.

Lohman, W. H., 1986, Calcareous nannoplankton biostratigraphy of the southern Coral Sea, Tasman Sea, and southwestern Pacific Ocean, Deep Sea Drilling Project Leg 90; Neogene and Quaternary: Initial reports of the Deep Sea Drilling Project covering Leg 90 of the cruises of the drilling vessel Glomar Challenger, Noumea, New Caledonia, to Wellington, New Zealand, December 1982-January 1983, v. 90, p. 763.

Lopes, C., Kucera, M., and Mix, A. C., 2015, Climate change decouples oceanic primary and export productivity and organic carbon burial: Proc Natl Acad Sci U S A, v. 112, no. 2, p. 332-335.

Lyle, M., 2003, Neogene carbonate burial in the Pacific Ocean: Paleoceanography, v. 18, no. 3.

Mayer, L. A., Pisias, N. G., Janecek, T. R., Baldauf, J. G., Bloomer, S. F., Dadey, K. A., Emeis, K.-C., Farrell, J., Flores, J. A., Galimov, E. M., Hagelberg, T. K., Holler, P., Hovan, S. A., Iwai, M., Kemp, A. E. S., Kim, D. C., Klinkhammer, G., Leinen, M., Levi, S., Levitan, M. A., Lyle, M. W., MacKillop, A. K., Meynadier, L. M., Mix, A. C., Moore, T. C., Jr., Raffi, I., Ravelo, C., Schneider, D., Shackleton, N. J., Valet, J.-P., and Vincent, E., 1991a, Site 846: Proceedings of the Ocean Drilling Program; Initial reports; Part 1, Eastern Equatorial Pacific; covering Leg 138 of the cruises of the drilling vessel JOIDES Resolution, Balboa, Panama, to San Diego, California, sites 844-854, 6 May 1991-5 July 1991, v. 138, p. 265.

Mayer, 1991b, Site 847: Proceedings of the Ocean Drilling Program; Initial reports; Part 1, Eastern Equatorial Pacific; covering Leg 138 of the cruises of the drilling

vessel JOIDES Resolution, Balboa, Panama, to San Diego, California, sites 844-854, 6 May 1991-5 July 1991, v. 138, p. 335.

Mayer, 1991c, Site 849: Proceedings of the Ocean Drilling Program; Initial reports; Part 1, Eastern Equatorial Pacific; covering Leg 138 of the cruises of the drilling vessel JOIDES Resolution, Balboa, Panama, to San Diego, California, sites 844-854, 6 May 1991-5 July 1991, v. 138, p. 735.

Mayer, 1991d, Site 850: Proceedings of the Ocean Drilling Program; Initial reports; Part 1, Eastern Equatorial Pacific; covering Leg 138 of the cruises of the drilling vessel JOIDES Resolution, Balboa, Panama, to San Diego, California, sites 844-854, 6 May 1991-5 July 1991, v. 138, p. 809.

Mix, A. C., Pisias, N. G., Rugh, W., Wilson, J., Morey, A., and Hagelberg, T. K., 1995, Benthic foraminifer stable isotope record from Site 849 (0-5 Ma); local and global climate changes: Proceedings of the Ocean Drilling Program; scientific results; eastern Equatorial Pacific, covering Leg 138 of the cruises of the drilling vessel JOIDES Resolution, Balboa, Panama, to San Diego, California, Sites 844-854, 1 May-4 July 1991, v. 138, p. 371.

Mix, A. C., Tiedemann, R., Blum, P., Abrantes, F. F., Benway, H., Cacho-Lascorz, I., Chen, M.-T., Delaney, M. L., Flores, J.-A., Giosan, L., Holbourn, A. E., Irino, T., Iwai, M., Joseph, L. H., Kleiven, H. F., Lamy, F., Martinez, P., McManus, J. F., Ninnemann, U. S., Pisias, N. G., Robinson, R. S., Stoner, J. S., Sturm, A., Wara, M. W., and Wei, W., 2003, Site 1237: Proceedings of the Ocean Drilling Program, initial reports, Southeast Pacific paleoceanographic transects; covering Leg 202 of the cruises of the drilling vessel JOIDES Resolution; Valparaiso, Chile, to Balboa, Panama; sites 1232-1242, 29 March-30 May 2002, v. 202, p. 107.

Pälike, H., Lyle, M. W., Nishi, H., Raffi, I., Ridgwell, A., Gamage, K., Klaus, A., Acton, G., Anderson, L., and Backman, J., 2012, A Cenozoic record of the equatorial Pacific carbonate compensation depth: Nature, v. 488, no. 7413, p. 609.

Pälike, H., Nishi, H., Lyle, M., Raffi, I., Gamage, K., Klaus, A., and the Expedition 320/321 Scientists, 2010, Expedition 320/321summary: Proc. IODP, 320/321: Tokyo (Integrated Ocean Drilling Program Management International, Inc.). , v. 320/321.

Peirce, J. W., Weissel, J. K., Taylor, E., Dehn, J., Driscoll, N., Farrell, J., Fourtanier, E., Frey, F. A., Gamson, P. D., Gee, J. S., Gibson, I. L., Janecek, T. R., Klootwijk, C., Lawrence, J. R., Littke, R., Newman, J. S., Nomura, R., Owen, R. M., Pospichal, J. J., Rea, D. K., Resiwati, P., Saunders, A. D., Smit, J., Smith, G. M., Tamaki, K., Weis, D., and Wilkinson, C., 1989a, Site 754: Broken Ridge and Ninetyeast Ridge; covering Leg 121 of the cruises of the drilling vessel JOIDES Resolution, Fremantle, Australia, to Port of Singapore, sites 752-758, 30 April to 28 June 1988, v. 121, p. 191.

Peirce, 1989b, Site 758: Broken Ridge and Ninetyeast Ridge; covering Leg 121 of the cruises of the drilling vessel JOIDES Resolution, Fremantle, Australia, to Port of Singapore, sites 752-758, 30 April to 28 June 1988, v. 121, p. 359.

Peterson, L., and Backman, J., 1990, Late Cenozoic carbonate accumulation and the history of the carbonate compensation depth in the western equatorial Indian Ocean, Proc., scientific results, ODP, Leg 115, Mascarene Plateau, ODP, Texas

AandM University, College Station; UK distributors, IPOD Committee, NERC, Swindon.

Ruddiman, W., Sarnthein, M., Baldauf, J., Backman, J., Bloemendal, J., Curry, W., Farrimond, P., Faugeres, J. C., Janacek, T., Katsura, Y., Manivit, H., Mazzullo, J., Mienert, J., Pokras, E., Raymo, M., Schultheiss, P., Stein, R., Tauxe, L., Valet, J.-P., Weaver, P., and Yasuda, H., 1988, Site 667: Proceedings of the Ocean Drilling Program, eastern tropical Atlantic, covering Leg 108 of the cruises of the drilling vessel JOIDES Resolution, Marseille, France, to Dakar, Senegal, sites 657-668, 18 February 1986-17 April 1986, v. 108, p. 833.

Ruddiman, W. F., Kidd, R. B., Baldauf, J. G., Clement, B. M., Dolan, J. F., Eggers, M. R., Hill, P. R., Keigwin, L. D., Jr., Mitchell, M., Philipps, I., Robinson, F., Salehipour, S. A., Takayama, T., Thomas, E., Unsold, G., and Weaver, P. P. E., 1987a, Site 607: Initial reports of the Deep Sea Drilling Project covering Leg 94 of the cruises of the drilling vessel Glomar Challenger, Norfolk, Virginia, to St. John's, Newfoundland, June-August 1983, v. 94, no. 1, p. 75.

Ruddiman, 1987b, Site 608: Initial reports of the Deep Sea Drilling Project covering Leg 94 of the cruises of the drilling vessel Glomar Challenger, Norfolk, Virginia, to St. John's, Newfoundland, June-August 1983, v. 94, no. 1, p. 149.

Shackleton, N. J., Crowhurst, S., Hagelberg, T., Pisias, N. G., and Schneider, D. A., 1995, A new late Neogene time scale; application to Leg 138 sites: Proceedings of the Ocean Drilling Program; scientific results; eastern Equatorial Pacific, covering Leg 138 of the cruises of the drilling vessel JOIDES Resolution, Balboa, Panama, to San Diego, California, Sites 844-854, 1 May-4 July 1991, v. 138, p. 73.

Sigurdsson, H., Leckie, R. M., Acton, G. D., Abrams, L. J., Bralower, T. J., Carey, S. N., Chaisson, W. P., Cotillon, P., Cunningham, A. D., D'Hondt, S. L., Droxler, A. W., Galbrun, B., Gonzalez, J., Haug, G., Kameo, K., King, J., Lind, I. L., Louvel, V., Lyons, T. W., Murray, R. W., Mutti, M., Myers, G., Pearce, R. B., Pearson, D. G., Peterson, L. C., and Röhl, U., 1997, Site 999: Proceedings of the Ocean Drilling Program; Initial reports; Caribbean ocean history and the Cretaceous/Tertiary boundary event; covering Leg 165 of the cruises of the Drilling Vessel JOIDES Resolution, Miami, Florida, to San Juan, Puerto Rico, sites 998-1002, 19 December 1995-17 February 1996, v. 165, p. 131.

Takayama, T., Notes on Neogene calcareous nannofossil biostratigraphy of the Ontong Java Plateau and size variations of Reticulofenestra coccoliths, *in* Proceedings Proc. ODP, Sci. Res.1993, Volume 130, Ocean Drilling Program, p. 179-230.

Wilkens, R., Drury, A. J., Westerhold, T., Lyle, M., Gorgas, T., and Jun, T., 2017, Revisiting the Ceara Rise, Equatorial Atlantic ocean; isotope stratigraphy of ODP Leg 154, European Geosciences Union general assembly 2017, Volume 19: Katlenburg-Lindau, Germany, Copernicus GmbH on behalf of the European Geosciences Union (EGU).

Zachos, J., Kroon, D., Blum, P., Bowles, J., Gaillot, P., Hasegawa, T., and Hathorne, E., 2004a, Proceedings of the Ocean Drilling Program, Initial Reports, Volume 208.

Zachos, J. C., Kroon, D., Blum, P., Bowles, J., Gaillot, P., Hasegawa, T., Hathorne, E. C., Hodell, D. A., Kelly, D. C., Jung, J.-H., Keller, S. M., Lee, Y. S., Leuschner, D. C., Zhifei, L., Lohmann, K. C., Lourens, L., Monechi, S., Nicolo, M. J., Raffi, I., Riesselman, C., Röhl, U., Schellenberg, S. A., Schmidt, D., Sluijs, A., Thomas, D.

J., Thomas, E., and Vallius, H., 2004b, Site 1264: Proceedings of the Ocean Drilling Program; initial reports; early Cenozoic extreme climates; the Walvis Ridge Transect; covering Leg 208 of the cruises of the drilling vessel JOIDES Resolution; Rio de Janeiro, Brazil, to Rio de Janeiro, Brazil; sites 1262-1267, 6 March-6 May 2003, v. 208, p. 73.

Zachos, 2004c, Site 1266: Proceedings of the Ocean Drilling Program; initial reports; early Cenozoic extreme climates; the Walvis Ridge Transect; covering Leg 208 of the cruises of the drilling vessel JOIDES Resolution; Rio de Janeiro, Brazil, to Rio de Janeiro, Brazil; sites 1262-1267, 6 March-6 May 2003, v. 208, p. 79.

5.14 Appendix Figure Caption

Figure S1. a) Locations of the sites discussed in this study. Paleo-latitude and geographic reconstruction (13.5 Ma) were generated from http://www.odsn.de/; b) Summary of MARc of studied sites. Sites that do not extend back to 15 Ma (ODP 667 and ODP 607) are not included. SP: southwest Pacific; WP: western Equatorial Pacific; CP: central Pacific; NA: North Atlantic; EA: equatorial Atlantic; SA: South Atlantic.

Figure S2. MAR of bulk samples (solid line), MARc (black squares) and MAR-foraminifera (blue dots) from Pacific ODP 806, 807, 803, 804, 590 and 1171. Note that sedimentation rates were particularly high between ~8-10 Ma at ODP 804. This anomalous MARc (~4 g/cm^2 kyr) of the lower upper Miocene section at ODP 804 is especially striking when compared to more normal sedimentation rates. The presence of turbidites was noted in the core descriptions (Kroenke et al., 1991e), suggesting redeposition during this time interval (Berger et al., 1993a).

Figure S3. MAR of bulk samples (solid line), MARc (black squares) and MAR-foraminifera (blue dots) from Pacific ODP U1338, 846, 1208, and Caribbean Sea ODP 999.

Figure S4. MAR of bulk samples (solid line), MARc (black squares) and MAR-foraminifera (blue dots) from Atlantic sites. Note that the sedimentation rate was particularly high at ODP 608 between 2.5 and 4 Ma. Visual observation of the core photos suggests numerous slumps during the deposition of this interval. Similarly, slumps

occurred in cores 15 to 18 in ODP 667. Therefore, MAR was not calculated for sediments older than 8 Ma at this site.

Figure S5. MAR of bulk samples (solid line), MARc (black squares) and MAR-foraminifera (blue dots) from Indian Ocean sites ODP 754 and 758.

Figure S6. MAR of bulk samples (solid line), MARc (black squares) and MAR-foraminifera (blue dots) of the western equatorial Indian Ocean. Data are from (Peterson and Backman, 1990). Although the dataset includes ODP 707-711, the shallowest ODP 707 was not considered here. Carbonate content of this site is particularly low, possibly due to strong dissolution associated with local circulation effect (Peterson and Backman, 1990).

Figure S7. Latitudinal variations in MARc in Middle Miocene, Late Miocene and Pleistocene, respectively, in southwest Pacific.

Figure S8. a) sediment trap showing latitudinal variations with decreasing values off the equator in the eastern Equatorial Pacific; b) Pleistocene MARc. Age model are based on paleomagnetic and biostratigraphy data from ODP initial report. MARc of ODP 70, 573 and 574 data are from (Lyle, 2003). MARc of ODP U1331, U1332, U1334, U1335 and U1337 are from (Pälike et al., 2012); c) Changes in paleo-latitude and paleodepth of selected sites in the eastern equatorial Pacific. Data are from (Pälike et al., 2012).

Figure S9. Composite MARc of Eastern Equatorial Pacific.

Figure S10. Mass Accumulation Rates of non-carbonate (MAR-noncarb) from western equatorial Pacific depth transect ODP 806-804.

Figure S11. light microscope study of ODP 803 (3.4 km) planktonic foraminifera in the >60 μm residues.

Figure S12. Size index of planktonic foraminifera from equatorial Indian Ocean (ODP 758, 2.9 km), southwest Pacific (ODP 590, 1.3 km), Caribbean Sea (ODP 999, 2.8 km), equatorial Atlantic (ODP 667, 3.5 km, ODP 925, 3.0 km, and ODP 928, 4.0 km), and South Atlantic (ODP 1264, 2.5 km, ODP 1266, 3.8 km).

Figure S13. MAR-foraminifera from the Ontong-Java depth transect. The yellow arrow indicates a decrease in MAR-foraminifera between 2.7 and 3.4 km.

Figure S14. Carbonate fluxes at 2 km based on sedimentary trap (Honjo et al., 2008) indicate $CaCO_3$ fluxes with a median value ~1.2 g/cm^2 kyr.

Figure S15. Three hypothetical scenarios of changes in carbonate production, dissolution and accumulation. Grey lines in b) indicate hypothetical %$CaCO_3$ decrease with increasing water depth (undersaturation). Grey lines in c) indicate changes in MARc that are constrained by the data from western equatorial Pacific.

Figure 16S. MARc estimates of modern ocean based on model output (Dunne et al., 2012) which was optimized to fit the observed Holocene carbonate burial fluxes. These estimates help constrain the compensation effects due to a deeper Pleistocene CCD. In the North Atlantic, deepening of the CCD from 4 to 5 km increased carbonate accumulation. by ~1.2 g/cm^2 kyr below the Miocene CCD. In the equatorial Pacific, deepening CCD by ~500 m in the Pleistocene had negligible effect on carbonate budget.

5.15 Appendix Table Caption

Table S1: modern longitudes, latitudes and water depths of studied sites

Table S2: data source for age control points and %CaCO3 data.

Table S3. Estimates of Mass Accumulation Rates in Ontong-Java coretop samples.

Figure 1

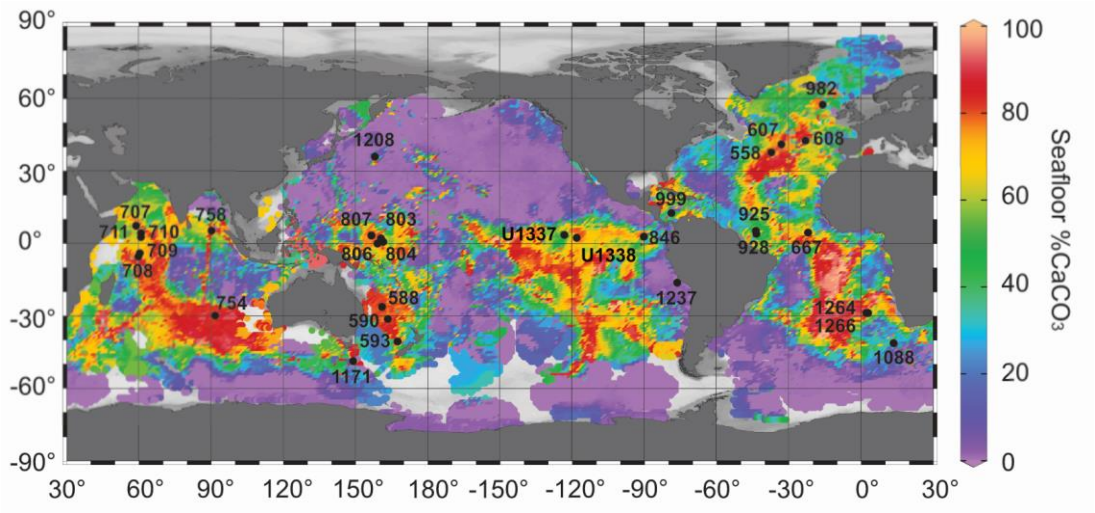
90°
60°
30°
0°
-30°
-60°
-90°
30°
60°
90°
120°
150°
180°
-150°
-120°
-90°
-60°
-30°
0°
30°
982
607
608
558
1208
999
925
928
667
707
711
710
709
708
758
807
803
806
804
U1337
846
U1338
1237
588
590
593
754
1171
1264
1266
1088
100
80
60
40
20
0
Seafloor %CaCO3

Figure 2

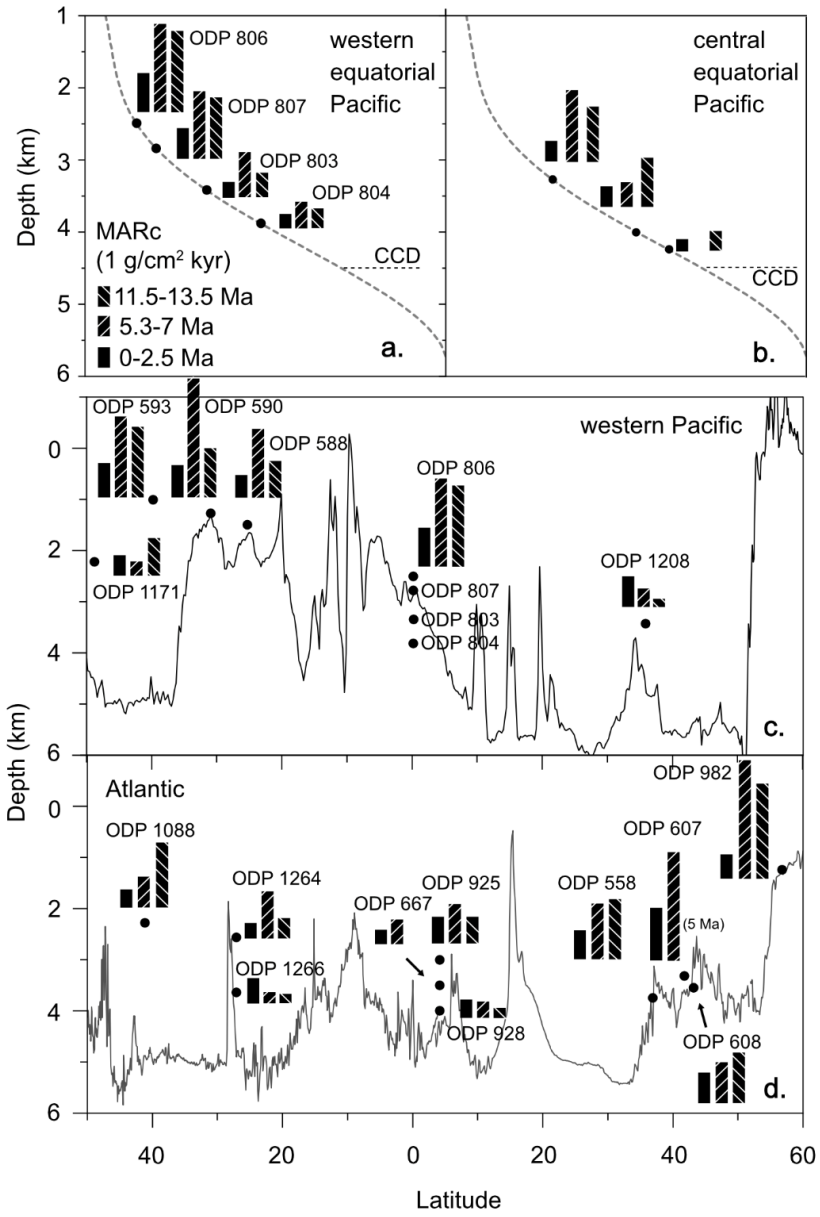
ODP 806
western
equatorial
Pacific
ODP 807
ODP 803
ODP 804
MARc
(1 g/cm² kyr)
11.5-13.5 Ma
5.3-7 Ma
0-2.5 Ma
CCD
a.
central
equatorial
Pacific
CCD
b.
Depth (km)
ODP 593
ODP 590
ODP 588
ODP 806
ODP 1208
ODP 1171
ODP 807
ODP 803
ODP 804
western Pacific
c.
Atlantic
ODP 982
ODP 1088
ODP 607
ODP 1264
ODP 925
ODP 667
ODP 558
(5 Ma)
ODP 1266
ODP 928
ODP 608
d.
Depth (km)
Latitude

Figure 3

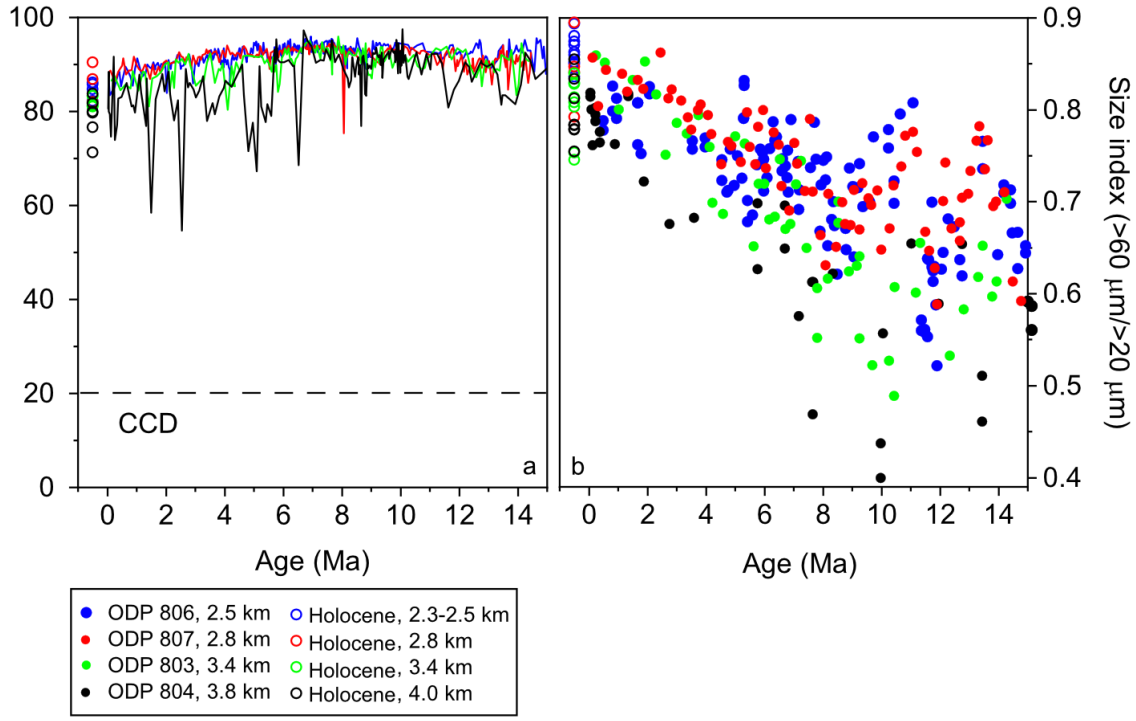
100
80
60
40
20
0
CCD
a
0 2 4 6 8 10 12 14
Age (Ma)
b
0 2 4 6 8 10 12 14
Age (Ma)
0.9
0.8
0.7
0.6
0.5
0.4
Size index (>60 µm/>20 µm)
ODP 806, 2.5 km
ODP 807, 2.8 km
ODP 803, 3.4 km
ODP 804, 3.8 km
Holocene, 2.3-2.5 km
Holocene, 2.8 km
Holocene, 3.4 km
Holocene, 4.0 km

Figure 4

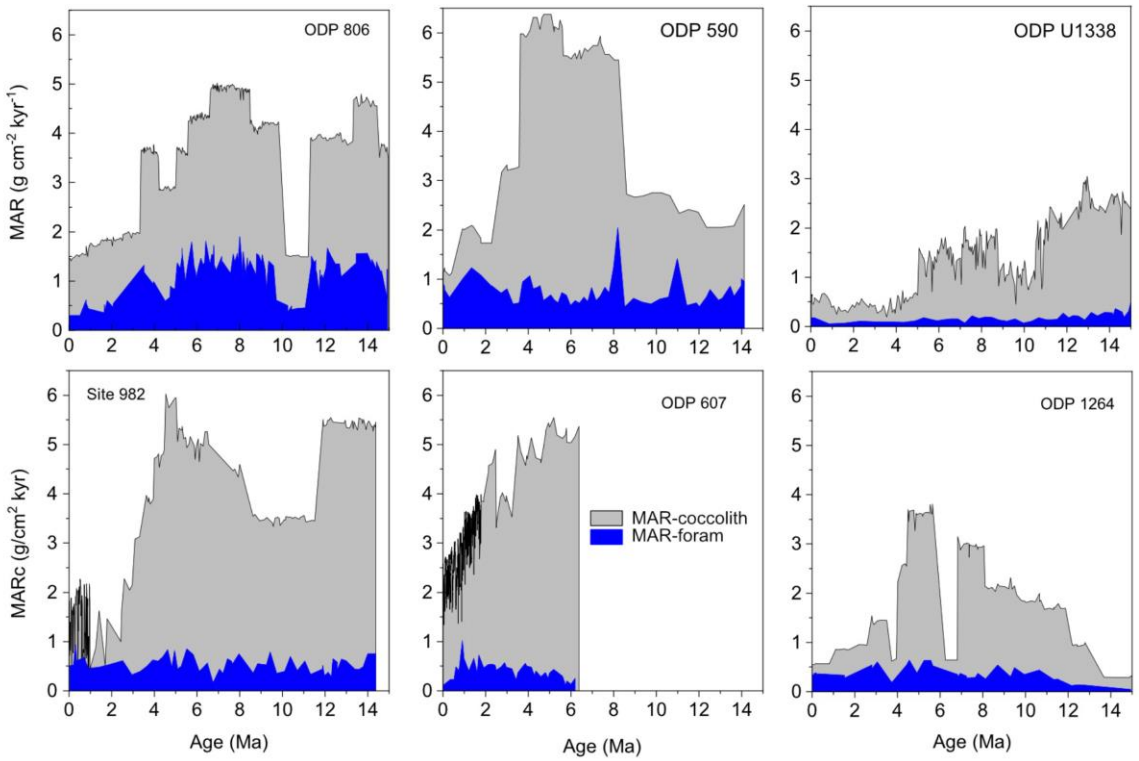
ODP 806
ODP 590
ODP U1338
Site 982
ODP 607
ODP 1264
MAR (g cm-2 kyr-1)
MARc (g/cm2 kyr)
MAR-coccolith
MAR-foram
Age (Ma)
Age (Ma)
Age (Ma)

Figure 5

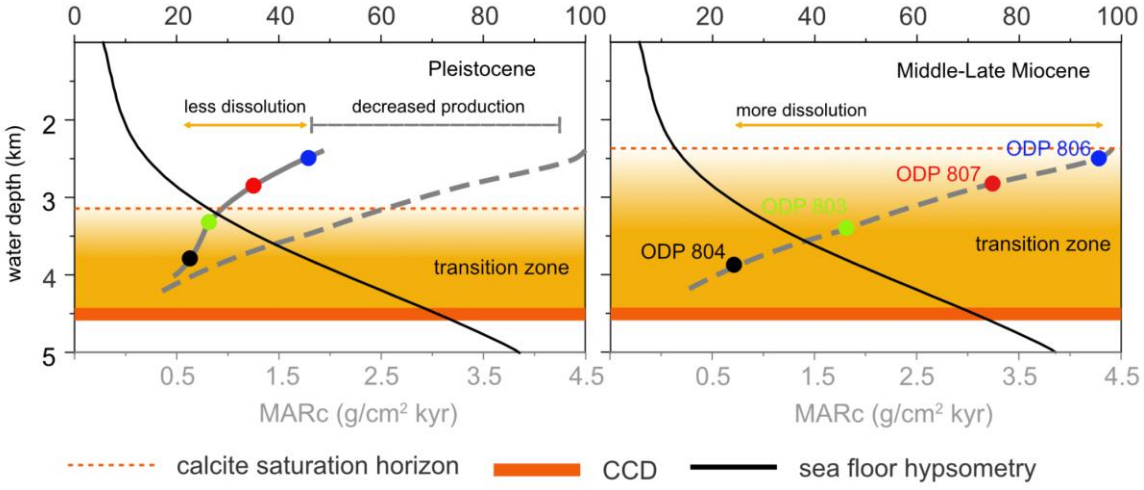
0
20
40
60
80
100
Pleistocene
less dissolution
decreased production
transition zone
water depth (km)
2
3
4
5
0.5
1.5
2.5
3.5
4.5
MARc (g/cm² kyr)
20
40
60
80
100
Middle-Late Miocene
more dissolution
ODP 806
ODP 807
ODP 803
ODP 804
transition zone
0.5
1.5
2.5
3.5
4.5
MARc (g/cm² kyr)
calcite saturation horizon
CCD
sea floor hypsometry

Appendix Figure S1

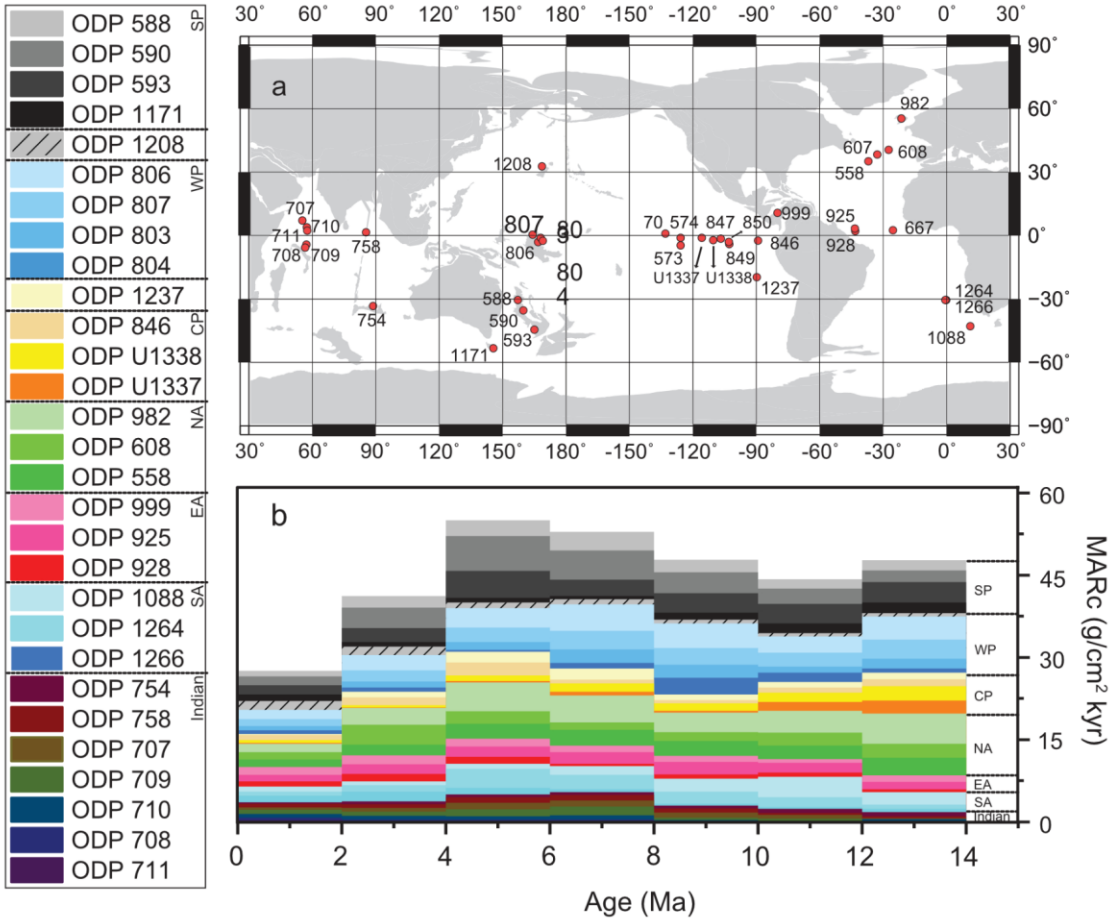

Appendix Figure S2

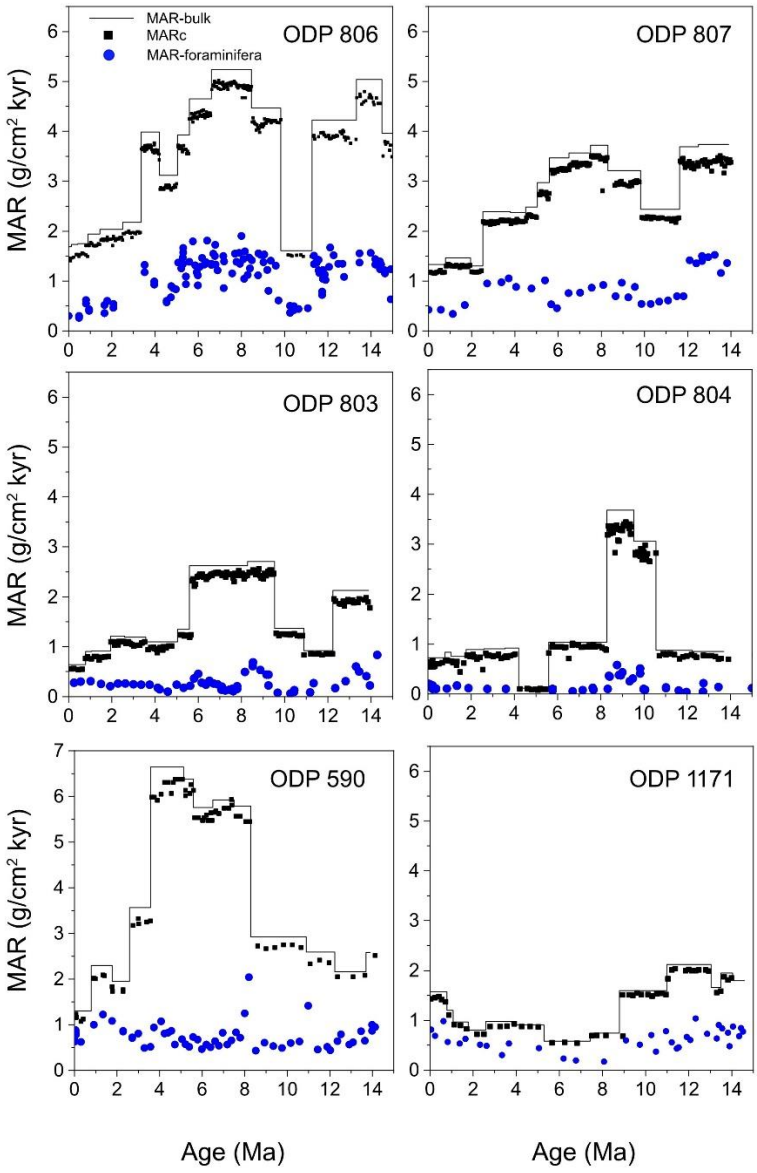

Appendix Figure S3

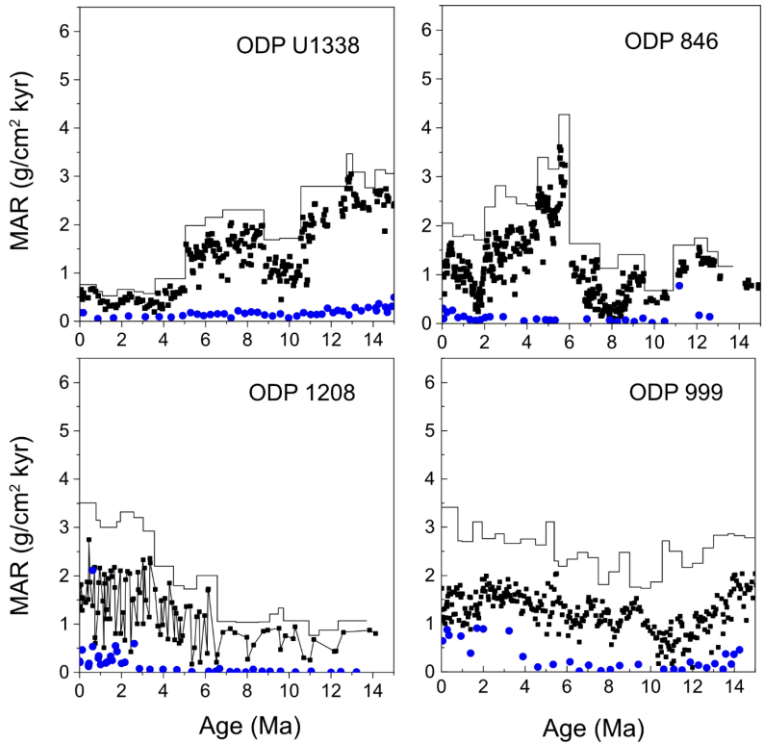

Appendix Figure S4

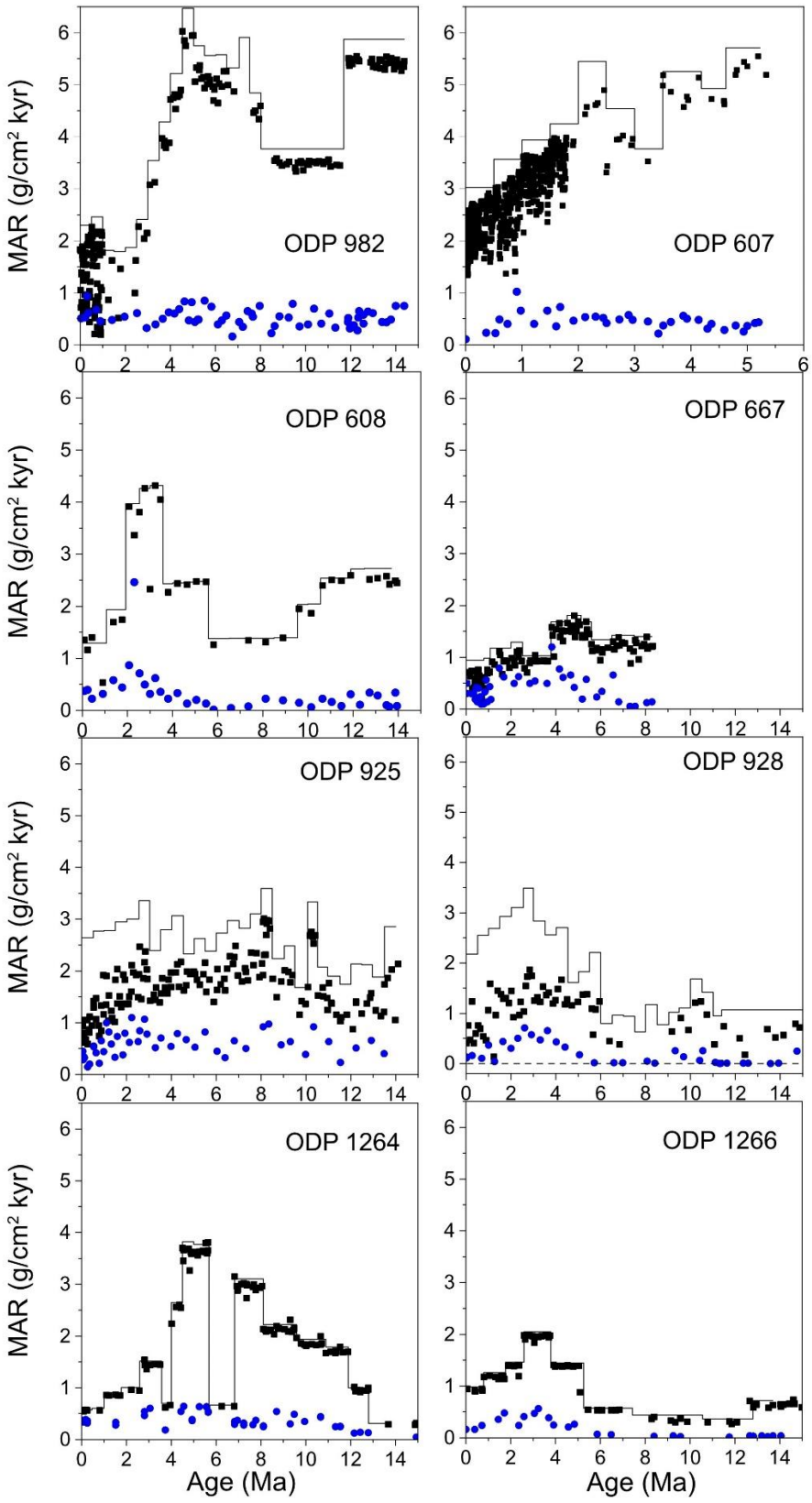

Appendix Figure S5

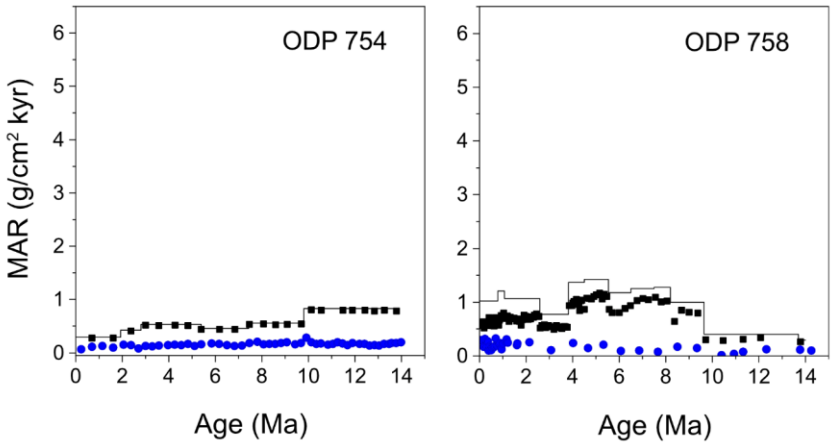

Appendix Figure S6

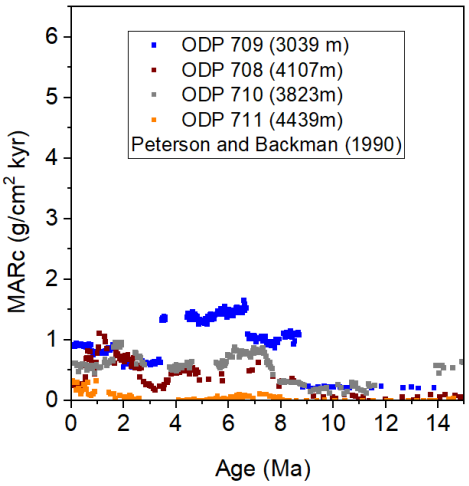

Appendix Figure S7

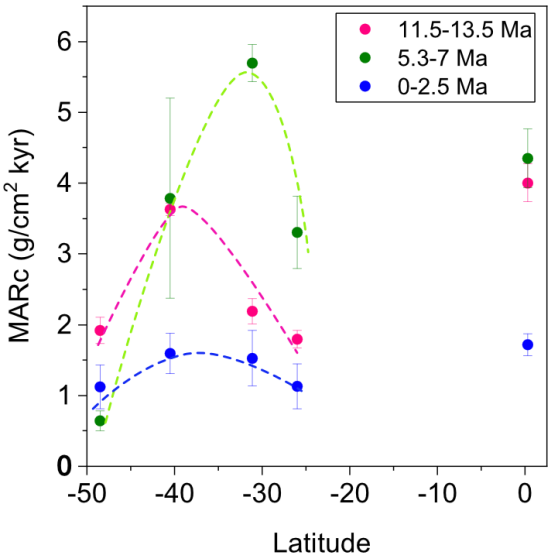

Appendix Figure S8

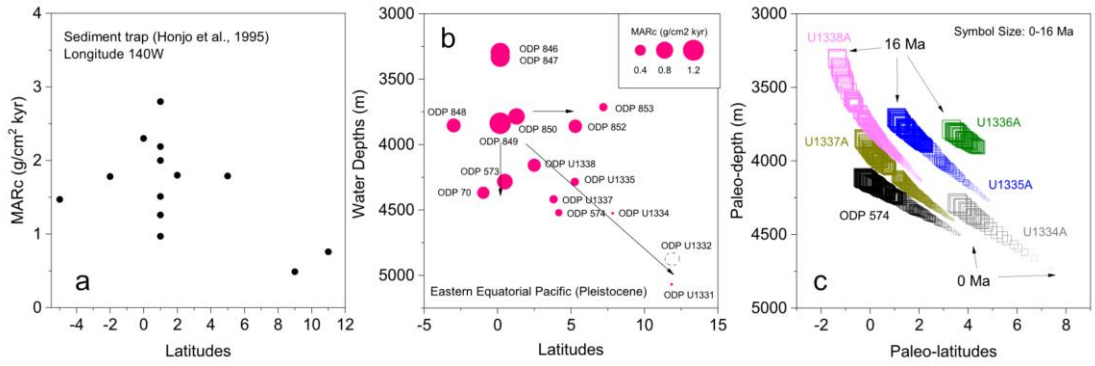

Appendix Figure S9

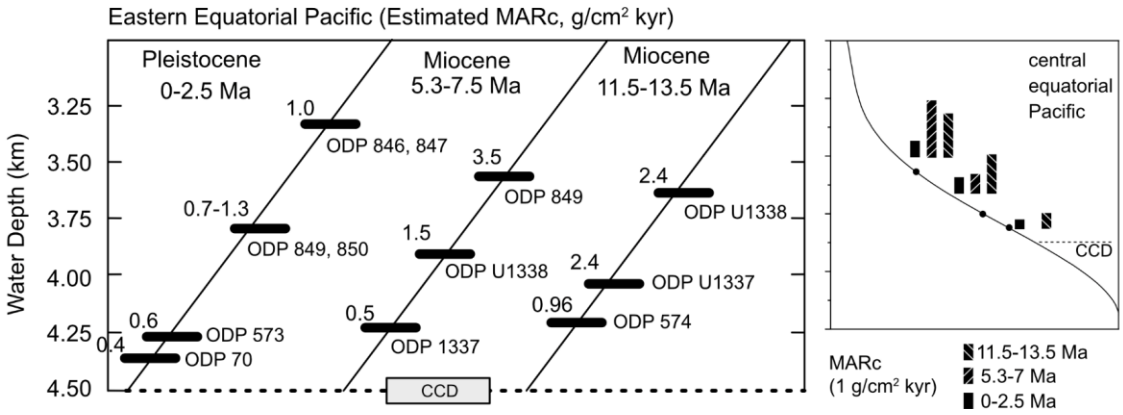

Appendix Figure S10

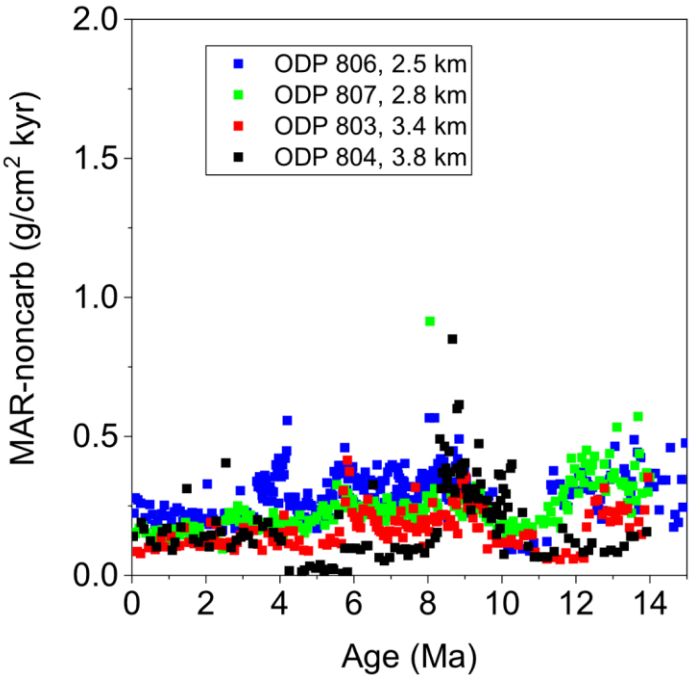

Appendix Figure S11

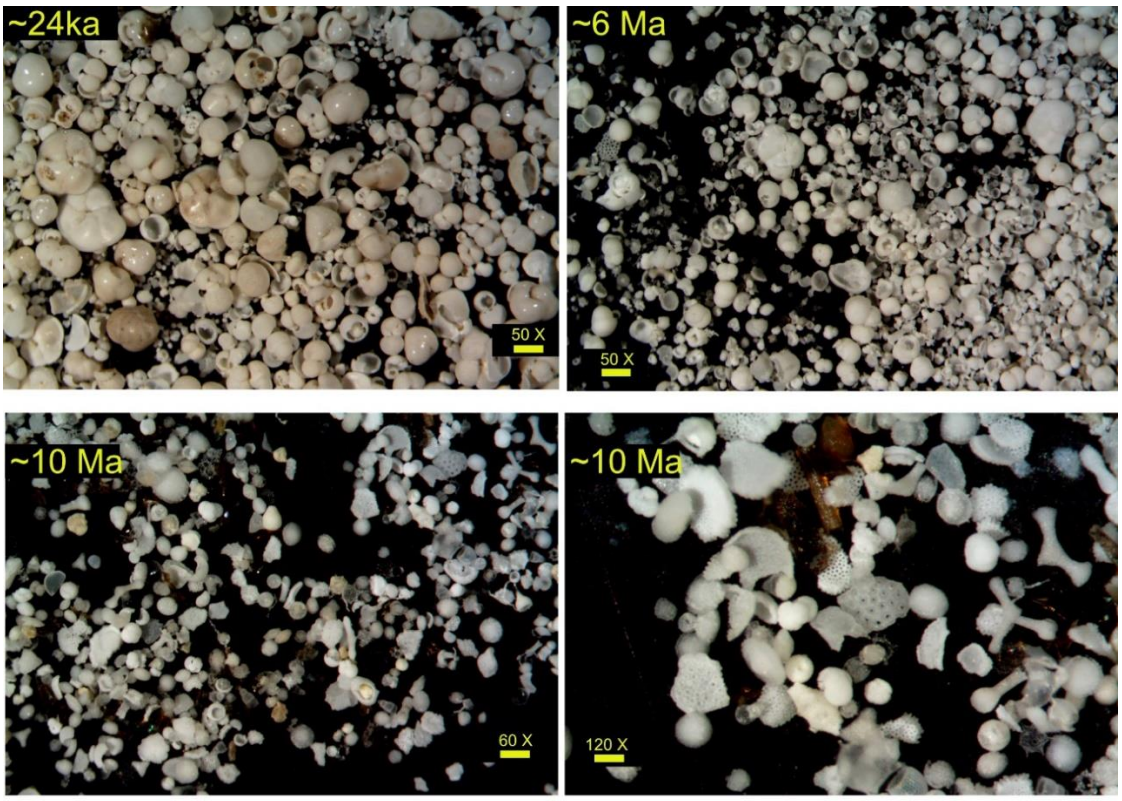

Appendix Figure S12

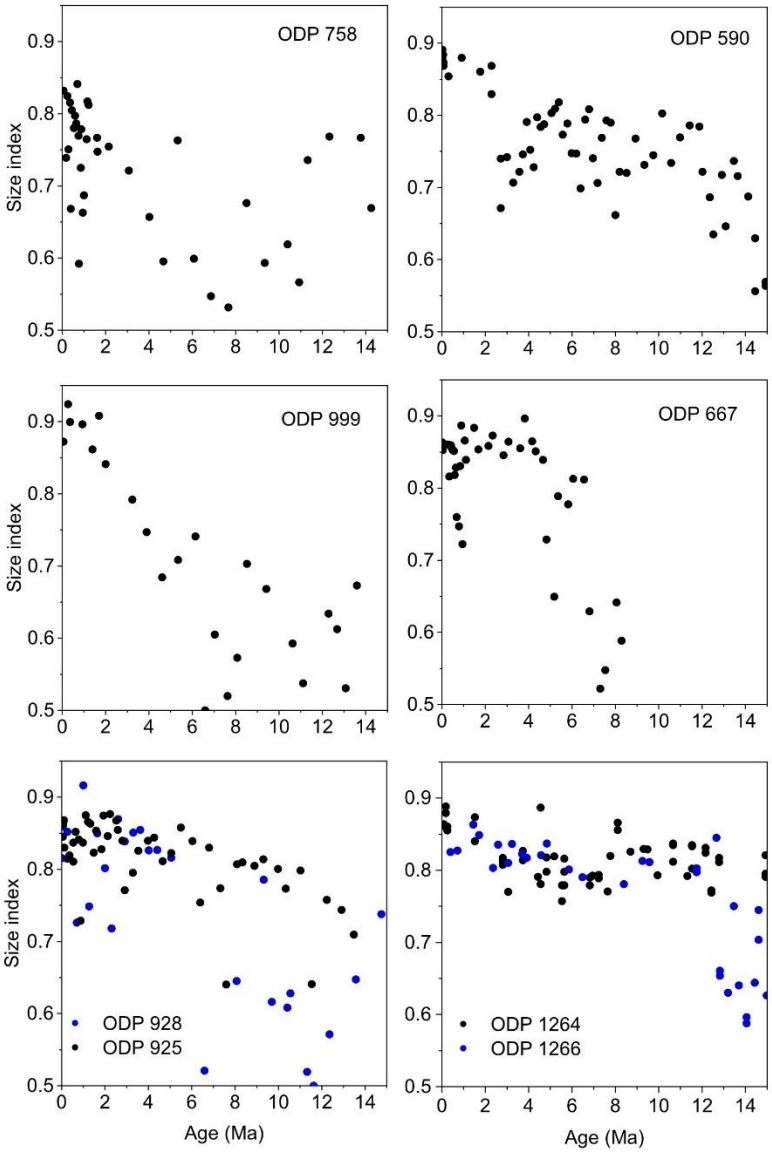

Appendix Figure S13

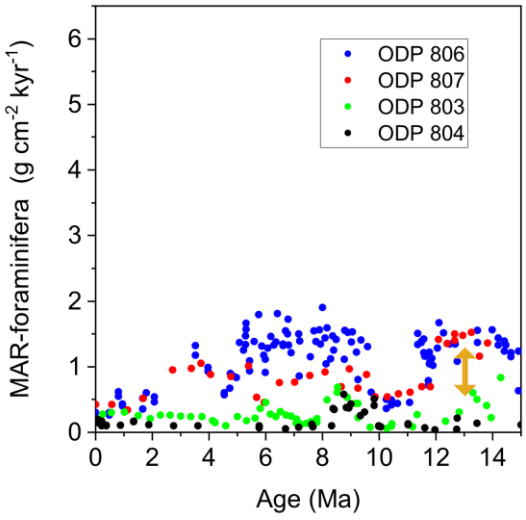

Appendix Figure S14

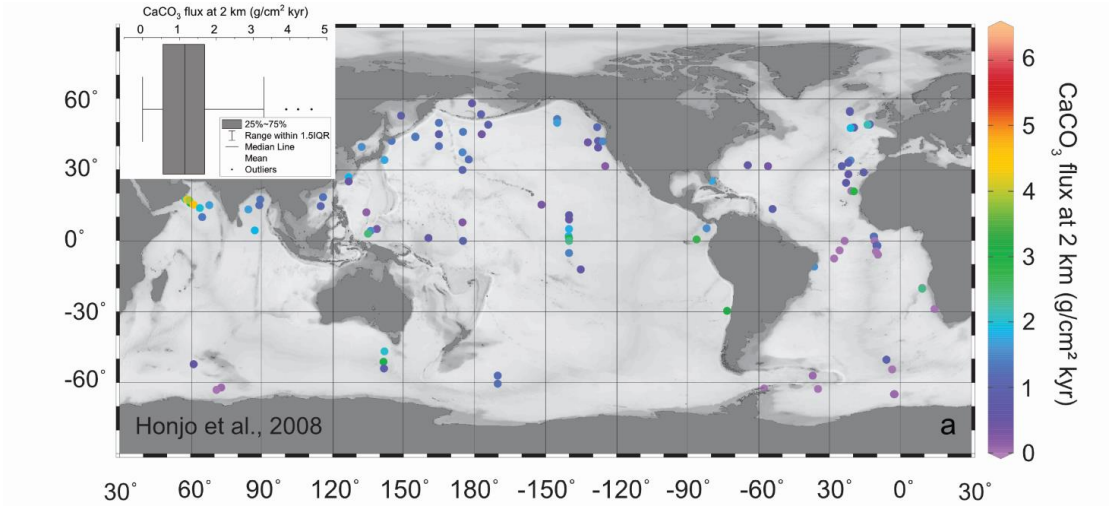

Appendix Figure S15

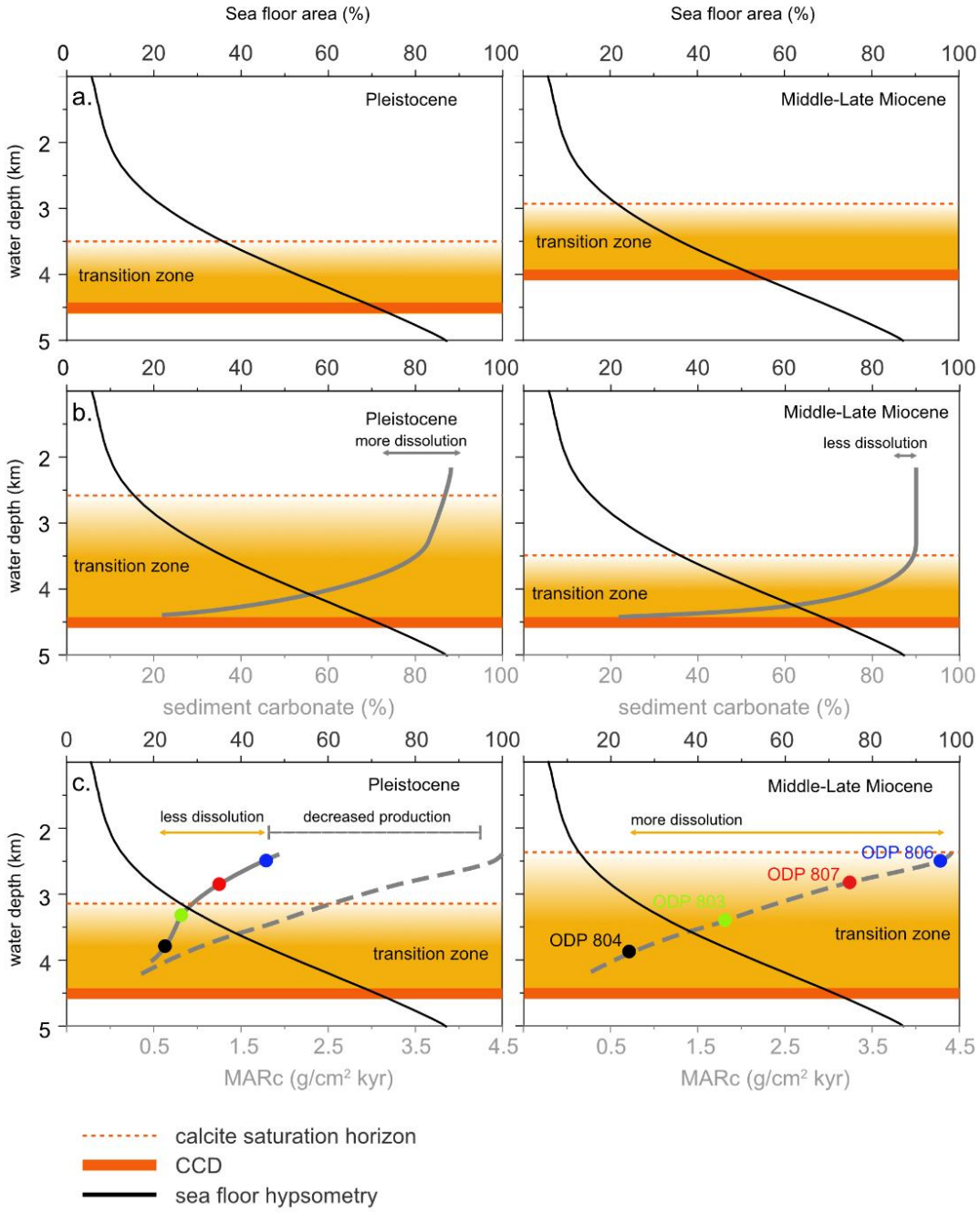

Appendix Figure S16

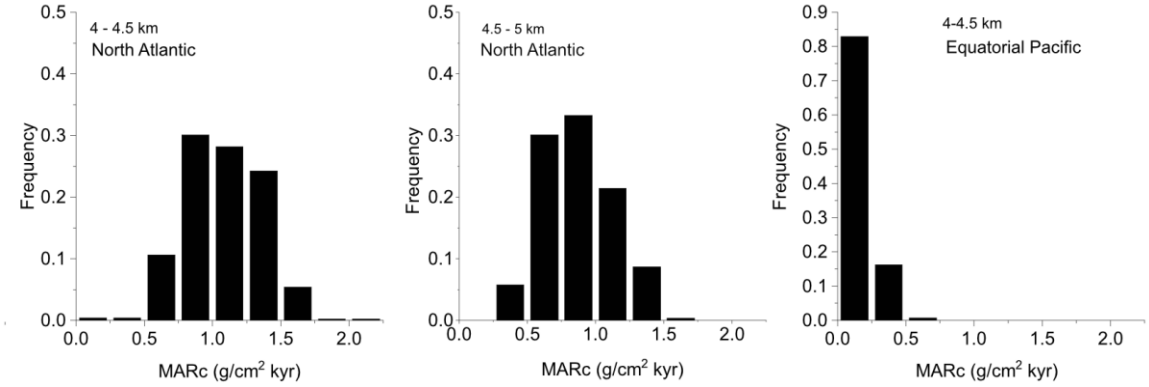

Appendix Table S1

	Latitude and longitude	Water depth (m)
ODP 806	0° 19.11'N, 159° 21.68' E	2521
ODP 807	3° 36.42'N, 156°37.49' E	2804
ODP 803	2° 25.98'N, 160° 32.40'E	3410
ODP 804	1° 00.28'N, 161° 35.62' E	3862
ODP 1208	36°7.6301´N, 158°12.0952´E	3346
ODP 588	26°06.7'S, 161°13.6'E	1533
ODP 590	31°10.02'S, 163°21.51'E	1299
ODP 593	40°30.47'S, 167°40.47'E	1068
ODP 1171	48°29.9960´S, 149°6.6901´E	2150
ODP U1337	3°50.009′N, 123°12.352′W;	4463
ODP U1338	2°30.469′N, 117°58.178′W	4200
ODP 1237	16°0.421´S, 76°22.685´W	3212
ODP 846	3° 5.70'S, 90° 49.08'W	3296
ODP 847	0° 11.593'N, 95° 19.22'W	3334
ODP 849	0°10.983'N, 110°31.183'W	3837
ODP 850	1°17.837'N, 110°31.283'W	3786
ODP 573	0°29.91'N, 133°18.57'W	4301
ODP 574	04°12.52'N, 133° 19.81'W	4561
ODP 70	6° 20.08'N, 140°21.72'W	5059
ODP 982	57°31.002'N, 15°51.993'W	1145
ODP 607	41°00.068'N, 32°57.438'W	3426
ODP 608	42°50.21'N, 23°05.25'W	3526
ODP 558	37°46.2'N, 37°20.61'W	3754
ODP 667	4°34.15'N, 21°54.68'W	3539
ODP 999	12°44.639'N, 78°44.360'W	2838
ODP 925	4°12.249'N, 43°29.334'W	3053
ODP 928	5°27.320'N, 43°44.884'W	4022
ODP 1264	28°31.95´S, 2°50.73´E	2507
ODP 1266	28°32.55´S, 2°20.61´E	3798
ODP 1088	41° 8.163'S, 13° 33.770'E	2250
ODP 758	5°23.052'N, 90°21.672'E	2923
ODP 707	7°32.718'S, 59° 1.008'E	1553
ODP 708	05°27.35'S, 59°56.63'E	4109
ODP 709	3°54.900'S, 60°33.102'E	3040
ODP 710	04°18.7'S, 60°58.8'E	3824
ODP 711	02°44.56'S, 61°09.78'E	4429
ODP 758	5°23.049'N, 90°21.673'E	2923
ODP 754	30°56.439'S, 93°33.991'E	1074

Appendix Table S2

	Biostratigraphy, Paleomagnetic data, and Isotope stratigraphy	%$CaCO_3$
ODP 806	(Berger et al., 1993b; Holbourn et al., 2013; Kroenke et al., 1991a; Takayama, 1993)	(Kroenke et al., 1991a)
ODP 807	(Kroenke et al., 1991d; Takayama, 1993)	(Kroenke et al., 1991d)
ODP 803	(Berger et al., 1993a; Kroenke et al., 1991b)	(Kroenke et al., 1991b)
ODP 804	(Kroenke et al., 1991c; Takayama, 1993)	(Kroenke et al., 1991c)
ODP 1208	(Bralower et al., 2002; Evans, 2006)	(Bralower et al., 2002)
ODP 588	(Kennett et al., 1986a; Lohman, 1986)	(Kennett et al., 1986a)
ODP 590	(Kennett et al., 1986b; Lohman, 1986)	(Kennett et al., 1986b)
ODP 593	(Kennett et al., 1986c; Lohman, 1986)	(Kennett et al., 1986c)
ODP 1171	(Exon et al., 2001)	(Exon et al., 2001)
ODP U1337	(Pälike et al., 2012)	(Pälike et al., 2012)
ODP U1338	(Pälike, 2010)	(Pälike, 2010)
ODP 1237	(Mix et al., 2003)	(Lopes et al., 2015)
ODP 846	(Mayer et al., 1991a; Shackleton et al., 1995)	(Mayer et al., 1991a)
ODP 847	(Farrell et al., 1995; Mayer et al., 1991b)	(Mayer et al., 1991b)
ODP 849	(Mayer et al., 1991c; Mix et al., 1995)	(Mayer et al., 1991c)
ODP 850	(Mayer et al., 1991d)	(Mayer et al., 1991d)
ODP 982	(Jansen et al., 1996; Lawrence et al., 2013)	(Jansen et al., 1996)
ODP 607	(Lisiecki and Raymo, 2005; Ruddiman et al., 1987a)	(Ruddiman et al., 1987a)
ODP 608	(Ruddiman et al., 1987b)	(Ruddiman et al., 1987b)
ODP 558	(Bougault et al., 1985)	(Bougault et al., 1985)
ODP 667	(Ruddiman et al., 1988)	(Ruddiman et al., 1988)
ODP 999	(Sigurdsson et al., 1997)	(Sigurdsson et al., 1997)
ODP 925	(Curry et al., 1995a; Wilkens et al., 2017)	(Curry et al., 1995a)
ODP 928	(Curry et al., 1995b; Wilkens et al., 2017)	(Curry et al., 1995b)
ODP 1264	(Zachos et al., 2004b)	(Zachos et al., 2004b)
ODP 1266	(Zachos et al., 2004c)	(Zachos et al., 2004c)
ODP 1088	(Gersonde et al., 1999)	(Gersonde et al., 1999; Hodell et al., 2003)
ODP 758	(Peirce et al., 1989b)	(Peirce et al., 1989b)
ODP 754	(Peirce et al., 1989a)	(Littke et al., 1991; Peirce et al., 1989a)

Appendix Table S3

Core ID	Depth (km)	%CaCO3	Sampling depth (cm)	MAR-bulk (g cm^{-2} kyr^{-1}) (Broecker, 2003)	MAR-foraminifera (g cm^{-2} kyr^{-1})	MAR-coccolith (g cm^{-2} kyr^{-1})
GGC15	2.31	84	5-6	1.84 (based on BC-36)	0.98	0.55
BC-51	3.39	75	5-6	1.61	0.55	0.65